Capturing Photosynthetic Traits from the Progenitors of Wheat.

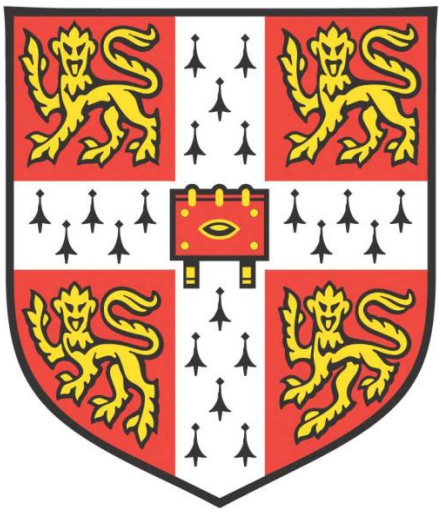

Tally Wright

Darwin College

NIAB

and the

Department of Plant Science

University of Cambridge

This dissertation is submitted for the degree of Doctor of Philosophy

September 2018

To Mollie.

DECLARATION

This dissertation is the result of my own work and includes nothing, which is the outcome of work done in collaboration except where specifically indicated in the text (see: Appendix 6). It has not been previously submitted, in part or whole, to any university of institution for any degree, diploma, or other qualification.

It is not substantially the same as any that I have submitted, or, is being concurrently submitted for a degree or diploma or other qualification at the University of Cambridge or any other University or similar institution except as declared in the Preface and specified in the text. I further state that no substantial part of my dissertation has already been submitted, or, is being concurrently submitted for any such degree, diploma or other qualification at the University of Cambridge or any other University or similar institution except as declared in the Preface and specified in the text.

It does not exceed the prescribed word limit for the relevant Degree Committee.

Signed:_____

Date:_____

Tally Wright

SUMMARY

Bottlenecks exist in raising wheat yield, which are associated with the constriction of available genetic diversity in the modern wheat gene pool and difficulties in improving photosynthesis during the growing season. Using a range of phenotyping techniques including portable infrared gas analysers, a collection of field grown progenitor wheat species and modern wheat varieties were screened for traits linked to the supply and demand components of flag leaf photosynthesis.

Two *Triticum dicoccoides* (AABB) individuals had high rates of flag leaf photosynthesis, driven by enhanced characteristics that facilitated the supply of CO_2 to the sites of carboxylation, including high stomatal and mesophyll conductance. Progeny formed through tetraploid and hexaploid crossing carried introgressions from these *T. dicoccoides* and were screened in a subsequent field trial. Although per unit CO_2 assimilation was increased in the progeny, flag leaf area was decreased, leading to an overall lower CO_2 assimilation per flag leaf. The results highlighted the negative trade-off between flag leaf area and CO_2 assimilation rate. Furthermore, a yield penalty was observed in the progeny associated with linkage drag from the wild progenitors. The progenitor individuals had higher CO_2 assimilation per ear than cultivated bread wheat, most likely driven by awn presence.

These findings led to an investigation of how awn presence influences ear and flag leaf photosynthesis, and thus overall grain yield, using pairs of awned and unawned Near Isogenic Lines derived from Synthetic Hexaploid Wheat (SHW NILs). Results showed that while awn presence is linked to increased ear photosynthesis, in some SHW NIL pairs there was a trade-off with flag leaf CO_2 assimilation. During this field trial, 4 of the 5 unawned counterparts of each SHW NIL pair had higher grain yield than the awned individuals. However, this trend was not consistent over multiple years and locations. A genome-wide association study (GWAS) was used to identify Single Nucleotide Polymorphisms (SNPs) strongly linked to the presence of awns in a larger panel of SHW.

Based on these results and examples in literature, theoretical ideotypes were formed for targeted environments. To map proxies for ideotype traits, a novel mapping population was created from two tetraploid *Triticum dicoccum* lines. The population was genotyped using a high density SNP array and a new genetic linkage map was created. Quantitative trait loci were identified and mapped, to aid the introgression of desirable traits from a tetraploid background into hexaploid wheat.

ACKNOWLEDGEMENTS

This project would not have been possible without the continued support, guidance and reassurance from Fiona Leigh, who I will always be grateful to for rescuing a stranded marine biologist. Secondly, the direction, knowledge and equipment provided by Howard Griffiths has been paramount to this investigation. Howard has also provided me with some good memories from the Portugal field-courses.

I would like to thank Phil Howell for is help and advice throughout the project, and for providing me with my first opportunity at NIAB in the pre-breeding team. Maxime Kadner played an important role in the 2017 field trial period, I am very grateful for his help and really enjoyed working with him. I would also like to thank Luis Robledo-Arratia for his help and advice with the mesophyll conductance analysis and cross sectioning. Jamie Males also played a key role in helping me get started with the physiology. Thank you to Stéphanie Swarbreck for her advice and to Alison Bentley and the CINTRIN project for the opportunity to go to India. I would also like to thank the NIAB Ornamental Crop team for providing me with field space for my trials. I owe a large thank you to Jacob Lage, and team at KWS, for growing the Chapter 2 field trial. David Evershed, and team, provided with an ideal field lab for my experiments and I enjoyed their company during the summer periods. Thank you to Kayla Friedman and Malcolm Morgan of the Centre for Sustainable Development, University of Cambridge, UK for producing the Microsoft Word thesis template used to produce this document. Thank you to Greg Reeves for providing useful R Script and for some more good times on the Portugal trips. Thank you to John Andralojc for the use of his leaf area calculator. Thank you to Hugo Oliveira and the University of Manchester for providing funding for the genotyping. I am indebted to Ian Mackay who has provided a wealth of knowledge and advice on the genetic components of the project. I would also like to thank Keith Gardner for his time and direction with the association mapping. I am extremely grateful to Jessica Royles for the time she gave in reading my drafts and for her help during some stressful fieldwork periods. I am indebted to Tony Barber and Richard Horsnell who both have played major roles in my enjoyment at NIAB, I hope I repaid them with the ping-pong tutorials. I would again like to thank Razzle, for some enjoyable lunchtime walks and for sitting faithfully by my side whilst I've been writing. Thank you to my parents for their continued support. Lastly, a colossal thank you to Mollie, who has taken care of me during my PhD.

CONTENTS

LIST OF TABLES

LIST OF FIGURES

LIST OF ABBREVIATIONS AND ACRONYMS

% Airspace: Percentage intercellular airspace

A (flag leaf^{-1}): CO_2 assimilation per leaf

A: Per unit net CO_2 assimilation

A_L : Awn length

A_{low} : CO_2 assimilation under low O_2

A_{MAX}: Maximum photosynthetic rate

BBSRC: Biotechnology and Biological Sciences Research Council

C_a: External CO_2 concentration

CBC: Calvin Benson Cycle

CE_{amb}: Carboxylation efficiency

Chl: Flag leaf chlorophyll content

C_i : Intercellular CO_2 concentration

CIM: Composite interval mapping

DQC: Dish quality control

DW : Leaf core dry weight

E: Transpiration

E_{CA} : Calculated ear area

E_L: Ear length

EN: Ear number per plant

E_W: Ear width

FL_A : Flag leaf area

FL_L: Flag leaf length

FL_{LONG} : Leaf longevity score

FL_{THICK}: Flag leaf thickness

FL_W: Flag leaf width

F_m': Maximal fluorescence

F_s : Steady-state fluorescence

f-s: Days from flowering to 80% flag leaf senescence

F_T: Flowering time

FW : Leaf core fresh weight

GA: Gross assimilation

GAR: Gross assimilation rate

g_m : Mesophyll conductance

GS: Growth stage

g_s: Stomatal conductance

GWAS: Genome-wide association study

H^2: Broad sense heritability

HI: Harvest Index

IRGA: Infrared gas analyser

J: Rate of electron transport

J_{CAL}: Calibrated rate of electron transport

LC_{area} : Area of leaf core

LCF: Leaf chamber fluorometer

LD: Linkage disequilibrium

LDMC: Leaf dry matter content

LI: Light interception

LI-COR CC : LI-COR 6400XT combined with a 6400-22 Opaque Conifer Chamber and the 6400-18A RGB Light Source

LMA: Leaf mass area

LOD: Logarithm of odds

MAF: Minor allele frequency

MAS: Marker assisted selection

$N_{\%}$: Percentage nitrogen content

NILs: Near Isogenic Lines

PPFD: Photosynthetic photon flux density

PS1: A tetraploid mapping population

QTL: Quantitative Trait Loci

R_{DARK} : Respiration in the dark

$R_{L:}$ Respiration in the light

RuBP: Ribulose-1,5-Bisphosphate

RUE: Radiation use efficiency

RWC: Relative water content

S.D: Standard deviation

$S_{C/O:}$ Rubisco specificity factor

$S_{D:}$ Stomatal density

s-f: Days from sowing to flowering (anthesis)

SHW NILs: Synthetic hexaploid wheat near isogenic lines

SHW: Synthetic hexaploid wheat

SLA: Specific Leaf Area

SNP: Single nucleotide polymorphism

SSD: Single seed decent

SW : Leaf core saturated weight

TGW: Thousand grain weight

TPU: Triose Phosphate Use

TxH: Tetraploid and hexaploid crossing

$V_{c:}$ Rubisco carboxylation

$V_{e:}$ Environmental variance

$V_{g:}$ Genetic variance

$V_{o:}$ Rubisco oxygenation

V_p: Phenotypic variance

WISH: Wheat Improvement from Synthetic Hexaploids

WISP: Wheat Strategic Improvement Program

WUE: Water Use Efficiency

$Y(II)_{amb}$: Quantum Yield of photosystem II under an ambient O_2 concentration

$Y(II)_{low}$: Quantum Yield of photosystem II under low O_2 concentration

YE: Grain yield per ear

YP: Grain yield per plant

Γ^*: CO_2 compensation point in the absence of respiration in the light

$\Delta^{13}C$: Carbon isotope discrimination

$\delta^{13}C$: Carbon isotope composition

Φ_{PSII}: Quantum yield of photosystem II

List of Appendices

INTRODUCTION

Food security, the growing population and wheat production.

With the exponential growth in the human population, the threat of changing climates and finite land available for agricultural expansion, progress in crop breeding over the next 50 years will be paramount to global food security. Food security is achieved when all people have access to adequate nutrition for maintaining a healthy lifestyle (FAO 1996). The global hunger epidemic is rising, in 2016 there were 815 million chronically undernourished (FAO 2017). This humanitarian crisis is likely to intensify over the coming decades, as global populations rise to 9.1 billion by 2050, with the majority of increases in developing countries (Diouf 2009). Global food security rests on a few major crops utilised as crucial food sources, of which wheat is one of most valuable and productive (Curtis & Halford 2014). Globally, wheat was the second most productive crop in 2016 (749.5 million tonnes), behind maize (1060.1 million tonnes) and slightly higher than rice (741.0 million tonnes, FAO, www.fao.org/faostat). Wheat was the crop grown over most agricultural land (220.1 million ha) and provides 20% of daily protein and 18% of daily calorie supply globally. The figures highlight the urgent obligation for the wheat breeding and agricultural industries to increase production proportionately to the growing population.

During the 1960s a phenomenon termed the 'green revolution' began, involving dramatic increases in cereal yields brought about by advances in genetics and agronomy (Figure I, Khush 2001). The 'green revolution' was responsible for a narrow avoidance of mass famine in developing countries (Khush 1995) and provides a first-hand example of how plant breeding, genetic improvement and plant physiology, can influence the lives of millions.

a).

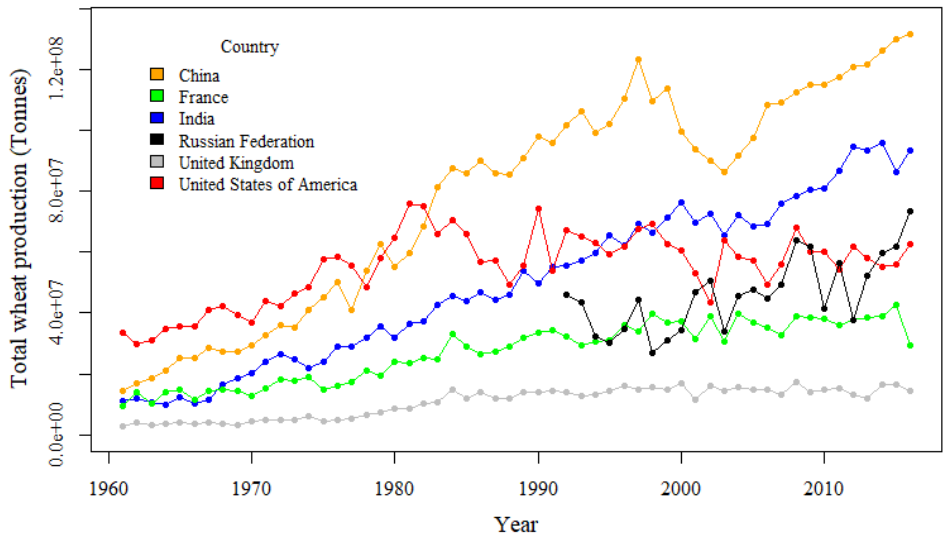

b).

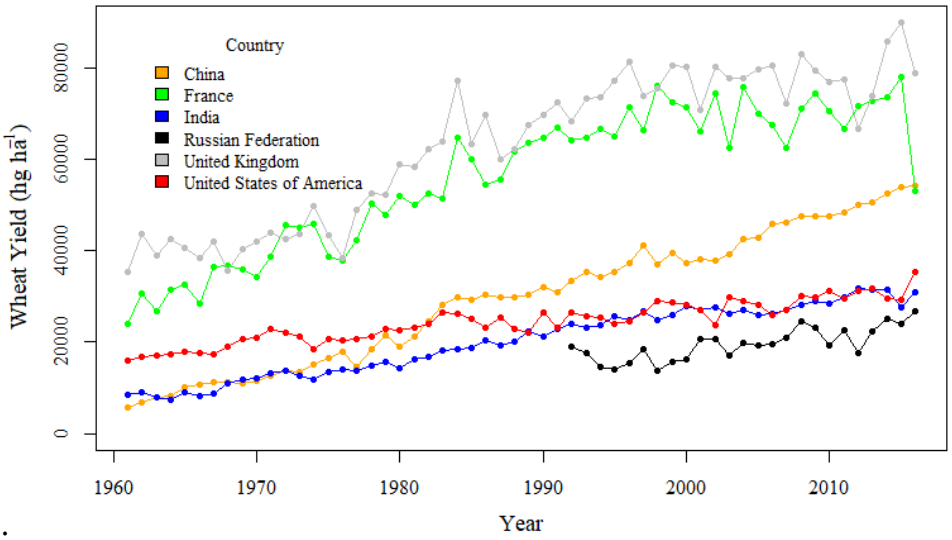

c).

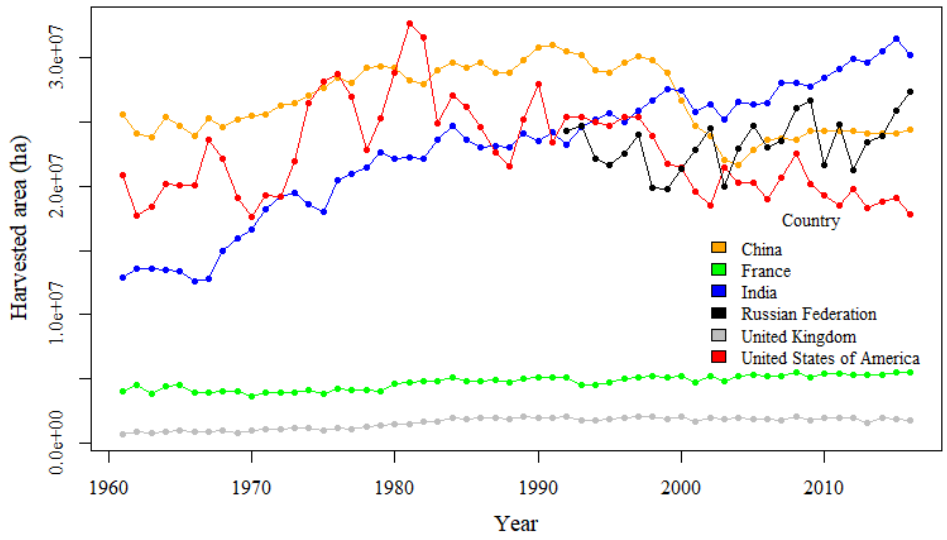

Figure I - The progression of the total production of wheat (a), wheat yield (b) and area of wheat harvested (c) in the current top 5 largest wheat producing countries (with the addition of the UK) over the last 6 decades. Graphs were produced using data from the Food and Agriculture Organisation of the United Nations (available from: www.fao.org/faostat).

Despite advances in science and technology since the 1960s, yield increases have slowed, leading to a second phenomenon termed the 'yield plateau'. There has been a substantial decrease in yield gain in the regions that account for 31% of the global wheat, rice and maize supplies; in particular severe plateaus have been observed in wheat production in northwest Europe and rice production in Eastern Asia (Grassini *et al.* 2013). Wheat yields in the UK since 1961 provide a suitable example of both the yield increases associated with the 'green revolution' and the stagnation connected with the 'yield plateau' (Figure I). For instance, between 1961 and 2000 wheat yield in the UK increased by 126%, but between 2000 and 2016 yield has actually decreased by 1% (FAO, www.fao.org/faostat). There was a 1.4% decrease estimated in global wheat production from 2017 to 2018 (FAO 2018a), therefore, the 'yield plateau' is currently a worrying concern, but as projections of yield advancement in several major crops are insufficient to keep up with the projected global population growth, the yield plateau becomes alarming.

Global demands for crop protein and calories are predicted to increase by around 110% and 100%, respectively, between 2005 and 2050 (Tilman *et al.* 2011). Furthermore, the demand for the coarse grains used in biofuels is also on the rise (Diouf 2009), adding further pressure for the increased production of main cereals. Ray *et al.* (2013) calculated that global wheat yields are only increasing at a rate of 0.9% per year, whereas an increase of 2.4% is required to meet the proposed projections. These projections suggest that if significant yield gains are not achieved over the coming decades, there could be insufficient production to meet demand. Regardless of the projections, even this year the production of wheat globally is forecasted to be short of the required demand (FAO 2018b) and as the population increases the situation will undoubtedly worsen. Ultimately, a second, more sustainable 'green revolution' is required to ensure future food security (Beddington 2010). As it did during the first green revolution, the responsibility to increase yields to feed a hungry world rests on the shoulders of plant breeders.

Yield potential, photosynthesis and the diversity bottleneck.

The genetic yield potential of a crop reflects the yield of a cultivar grown under optimum conditions in the absence of stress (Evans & Fisher 1999). Following Reynolds *et al.* (2009), yield potential can be simplified to:

$$Yield\ Potential = LI \times RUE \times HI$$

Where yield potential is the product of light interception (*LI*), radiation use efficiency (*RUE*) and harvest index (*HI*).Therefore, breeding targets to increase yield potential can focus on increasing these defining components. Past advances in yield potential, observed during the green revolution, were associated with increases in the proportion of grain yield to biomass, termed *HI* (Austin *et al.* 1980). In wheat, the introduction of semi-dwarfing genes from a Japanese wheat called 'Norin 10' contributed to the large increases in yield potential observed during the 'green revolution' (Borlaug 1968). These semi-dwarf varieties revolutionised wheat breeding by elevating *HI*, due to an increase in grain yield caused by reduced straw biomass (Milach & Federizzi 2001). However, *HI* in wheat and rice is now close to optimisation and future advancements via this avenue are unlikely (Long *et al.* 2006; Parry *et al.* 2011; Richards 2000). Improvements in *LI* have been driven by genetic selection, conventional breeding and improved agronomy, which has led to increased light capture and duration of the canopy (Richards 2000). Again, *LI* is approaching theoretical maximum (Long *et al.* 2006), as leaf area per unit ground cover is already high in most crops and canopies can be fully saturated by irradiance (Horton 2000).

Improvements in *RUE* may be the most profitable avenue for raising yield potential (Long *et al.* 2006; Murchie *et al.* 2009; Parry *et al.* 2011; Reynolds *et al.* 2009, 2011, 2012; Richards 2000). *RUE* is the slope of correlation between dry matter content at harvest and total intercepted solar radiation (Murchie *et al.* 2009). Total dry matter is the product of carbohydrates produced over the growing season through photosynthesis (Thorne 1974), so selection for photosynthetic improvement in wheat is a viable route for increasing yield potential. Ultimately, *RUE* is determined by the absolute photosynthetic rate of the crop canopy, minus respiratory losses (Long *et al.* 2006). Targets for improvements in *RUE* have been identified, including improving the efficiency of light capture and use (Horton 2000) and optimising downstream photosynthetic enzyme activity (Parry *et al.* 2011). In C3 plants, the observed *RUE* potential is 70% of the theoretical maximum (Long *et al.* 2006), suggesting ample room for improvements. A strong argument that improvements in *RUE* will have a direct positive influence on yield potential in wheat is provided by CO_2 enrichment studies. Under artificially elevated CO_2, higher leaf photosynthesis is observed (Mitchell *et al.* 1999; Thilakarathne *et al.* 2013), caused by increased CO_2 at the sites of carboxylation and inhibition of counterproductive oxygenation by photosynthetic enzymes (Drake *et al.* 1997). The higher CO_2 fixation has been linked to increased yield and biomass (Bender *et al.* 1999; Thilakarathne *et al.* 2013). If variation in *RUE* exists in

the genepool of wheat, selection could be implemented in breeding programs to target improvements.

During the green revolution, increases in yield potential were achieved by the incorporation of genetic diversity into the wheat genepool, which is still a conceivable avenue for future advances (Evans & Fisher 1999). However, there is a genetic diversity bottleneck in modern wheat varieties (Figure II). During the domestication of wheat the continued selection and propagation of lines which possessed favourable alleles narrowed the genepool; this constriction was tightened further via continuous breeding between genetically similar varieties (Tanksley & McCouch 1997). This diversity bottleneck limits potential trait and yield improvements when breeding within the existing bread wheat genepool. Furthermore, an earlier genetic bottleneck was created during the chance hybridisation events between the tetraploid and diploid progenitors which formed the modern wheat we grow today and would have only captured a small proportion of the diversity available from those genepools (Lopes *et al.* 2015).

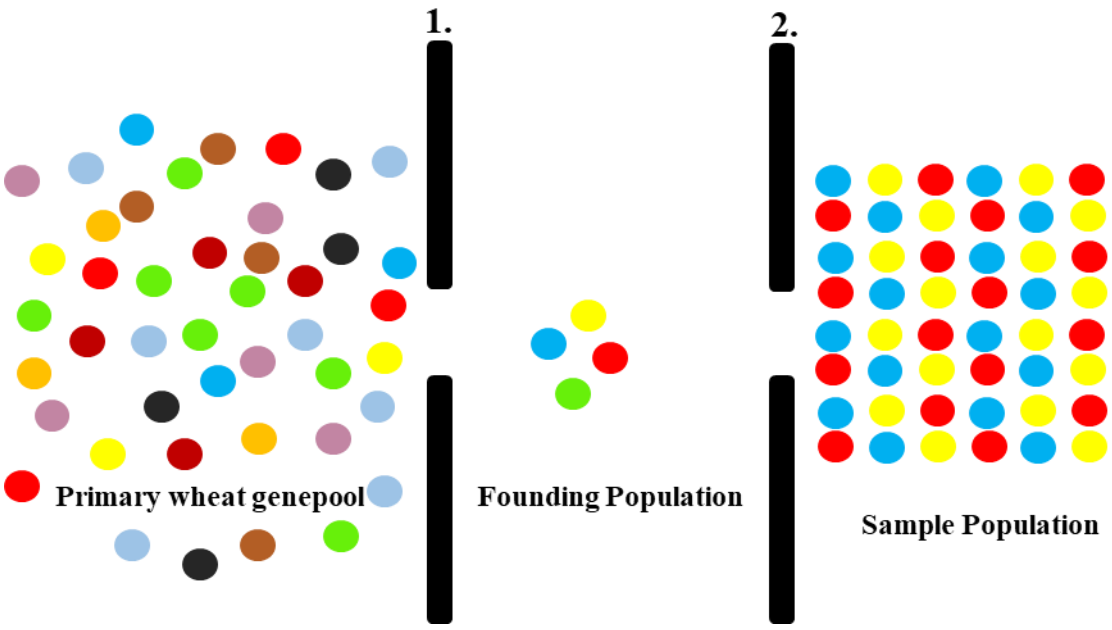

Figure II - A schematic showing the genetic diversity bottlenecks caused by the domestication of wheat from the primary genepool, where the most varied colours represent the greatest diversity present. The first bottleneck (1.) reflects the constriction of available diversity in the primary gene pool caused by the chance hybridisation of only a few representatives of that pool. The second bottleneck (2.) shows a second constriction of genetic diversity, caused by the continued propagation of only a few representatives of the founding population due to the possession of favourable characteristics.

The origin, domestication and progenitors of bread wheat.

Modern wheat grown today mainly belongs to two species: the hexaploid *Triticum aestivum* (2*n*, 6*x*, 42 chromosomes) and the tetraploid *Triticum turgidum* subspecies *durum* (2*n*, 4*x*, 28 chromosomes) commonly known as bread and macaroni wheats respectively (Nevo *et al.* 2002). Bread wheat (*T. aestivum*) is an allohexaploid, meaning it is the product of natural hybridisations of multiple genomes from different homozygous species (Cox 1997, Figure III).

a).

b).

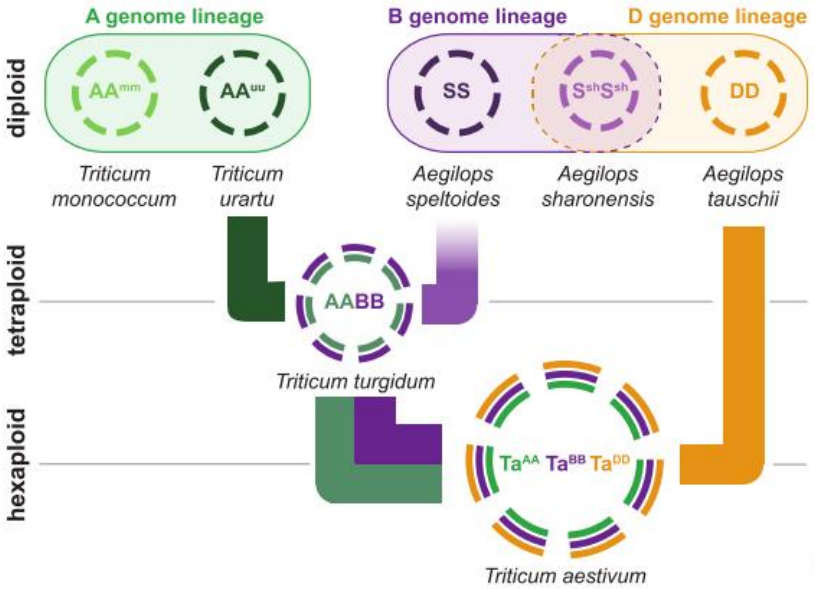

Figure III – Images adapted from International Wheat Genome Sequencing Consortium (IWGSC) (2014). a). Photographs of mature ears of *Triticum turgidum* subspecies: durum wheat (*Triticum durum*), wild emmer (*Triticum dicoccoides*) and cultivated emmer (*Triticum dicoccum*). b). A schematic showing the hybridisation, and progenitor species, involved in the evolution of allohexaploid bread wheat (*Triticum aestivum*).

The generally acknowledged view is that *T. aestivum* was formed through a chance hybridisation between a cultivated form of the tetraploid wild emmer (*Triticum turgidum* subsp. *dicoccoides*, AABB) and *Aegilops tauschii* (DD) the diploid wild goatgrass (Cox 1997; McFadden & Sears 1946; Petersen *et al.* 2006). The allotetraploid *T. dicoccoides* (Figure III) originated from a much earlier chance hybridisation of two diploid grasses: *Triticum urartu* (AA, Dvorák *et al.* 1993) and *Aegilops speltoides* (BB, Petersen *et al.* 2006).

The discovery of ancient farming villages and the earliest evidence of domesticated crops has shown that the Fertile Crescent was the site of wheat domestication and the cradle of agriculture (Nesbitt & Samuel 1996). The Fertile Crescent is:

> *"a region that spans modern-day Israel, Jordan, Lebanon and western Syria, into southeast Turkey and, along the Tigris and Euphrates rivers, into Iraq and the western flanks of Iran"(Salamini et al. 2002).*

Domestication took place around 12,000 BP and although diploid wheat was the first cultivated, it was subsequently replaced by domesticated forms of *T. dicoccoides*, predominately *Triticum turgidum* subsp. *dicoccum* commonly known as emmer wheat (Salamini *et al.* 2002). Although not free-threshing, *T. dicoccum* was domesticated by selection against a brittle rachis to prevent ear shattering (Özkan *et al.* 2002) and was the most important Neolithic crop (Zohary *et al.* 2000). At some point, pollen transferred from the wild *Ae. tauchii* to emmer wheat grown in fields by early Neolithic farmers (Cox 1997), which ultimately gave rise to cultivated hexaploid wheat. At the same time, emmer wheat was gradually replaced by the free-threshing *T. durum* wheat (Haudry *et al.* 2007).

A small number of genes played important roles in the domestication of wheat, including: the brittle rachis (*Br*) spike gene (Peleg *et al.* 2011); threshability genes including the *Qgene* (Simons *et al.* 2006) and the genes linked to the soft glume phenotype (*sog, Tg*, Sood *et al.* 2009). The continued selection for individuals with these desirable alleles, would have contributed to narrowing of the genepool of domesticated wheat. Therefore, throughout the existence of *T. aestivum* there has been a constriction of genetic diversity (Cox 1997). Fortunately potential avenues for widening the genepool of modern wheat do exist.

If suitable sources can be identified (Figure IV), the introduction of diversity is the obvious solution to the bottlenecks in wheat breeding as it could broaden the genepool and provide potential opportunities for substantial gains in yield. The primary gene pool

of wheat includes some species in which direct crossing is easily achieved (Skovmand *et al.* 2001) via hybridisation and backcrossing methods (Chaudhary *et al.* 2014). Species in this group include landraces of *T. durum* and *T. dicoccum,* and wild tetraploids such as *T. dicoccoides*. Species such as *Ae. tauschii* fall into the category of the secondary gene pool: additional techniques are required for direct hybridisation when crossing bread wheat with these materials (Skovmand *et al.* 2001). The tertiary gene pool is comprised of related grasses with genomes that are non-homologous to the wheat A, B and D genomes, including Rye and other Triticeae (Chaudhary *et al.* 2014). Lastly are completely unrelated species that are only a source of improvement through genetic engineering and manipulation, recent advances in technology have provided opportunities for incorporating favourable characteristics from a completely different domain (see: Lin *et al.* 2014; Occhialini *et al.* 2016). The cost and difficulty of incorporating diversity into the breeding gene pool, increases in relation to the genetic distance between the donor and the primary gene pool.

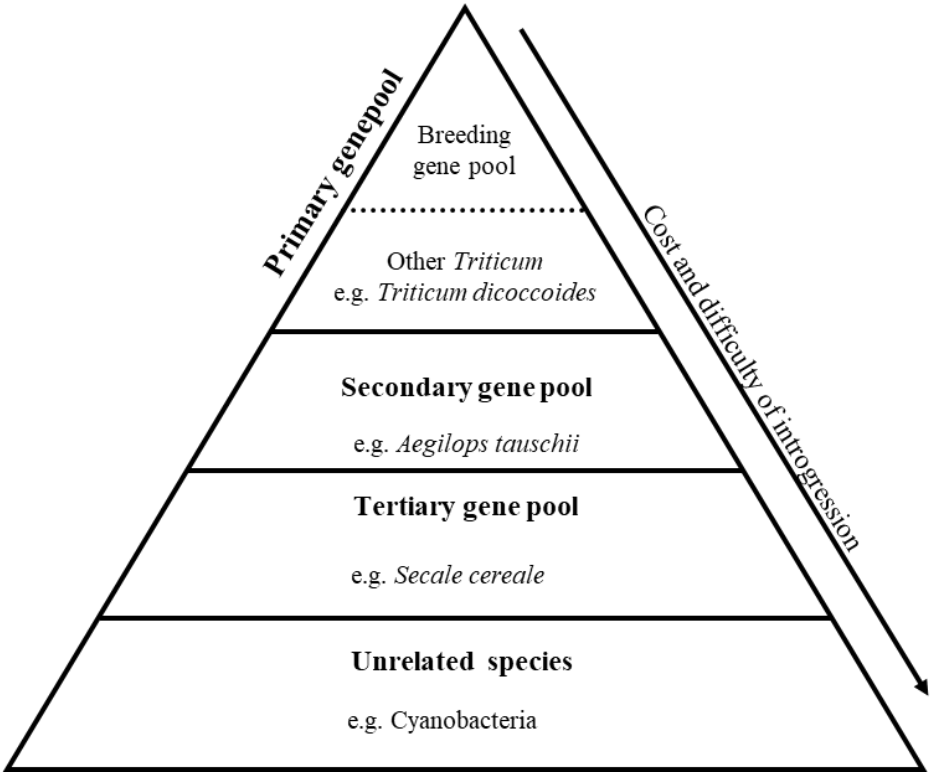

Figure IV – A schematic showing the potential sources for incorporating diversity into modern wheat to make crop improvements. The top of the triangle reflects the current breeding genepool and other species in the primary genepool of wheat. Moving down the triangle, the cost and difficulty of capturing the diversity increases from the secondary and tertiary gene pool, eventually increasing to completely unrelated species.

Wild ancestors of the primary genepool have already been tapped for certain traits as a genetic resource for modern wheat, in particular for disease resistance. For example, diversity has been utilised in breeding for stripe rust resistance (Marais *et al.* 2005; Peng *et al.* 2000, 2012), powdery mildew resistance (Xie & Nevo 2008) and resistance to bleaching caused by Fusarium head blight (Ban & Watanabe 2001). However, as Reynolds *et al.* (2009) highlighted, breeders have focused heavily on incorporating disease resistance through wide crossing, but have not explored well the potential diversity for physiological trait improvement. Progenitor wheats such as *T. dicoccoides* are typically environmental specialists that are adapted to a broad range of environments (Nevo 2014). Therefore, it is unsurprising that wild ancestors are a useful genetic resource for improvements in abiotic stress tolerance; in particular drought and salinity tolerance (Ergen *et al.* 2009; Nevo *et al.* 1992; Peng *et al.* 2012). The success of modern bread wheat cultivars which contain introgressions from *T. dicoccoides* also highlights the merit of the primary genepool as a source of diversity. Robigus was a very successful Group 3 bread wheat and is in the pedigree of many recent varieties (Figure V, AHDB 2017; HGCA 2013). Robigus is thought to have an unknown *T. dicoccoides* introgression in its pedigree (Gardner *et al.* 2016; Kumar & Rustgi 2014). The non-glaucous variety Shamrock was a Group 1 bread wheat which also contained introgressions from wild emmer, although slightly lower yielding than some contemporaries, it possessed environmental stability qualities typical of *T. dicoccoides* (Simmonds *et al.* 2008).

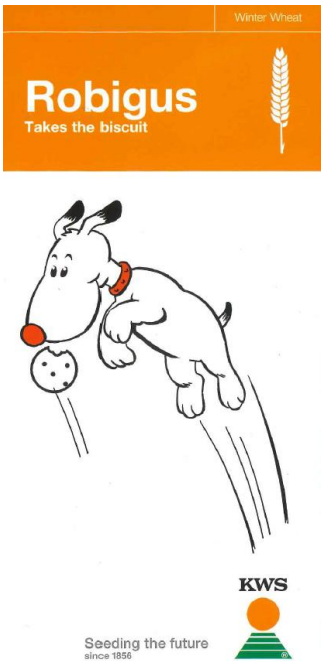

Figure V – An advert for the Robigus winter wheat variety that is suspected to contain an introgression from the tetraploid progenitor of modern wheat: *T. dicoccoides* (KWS UK LTD, Thriplow, UK).

Diversity is also being utilised from the secondary gene pool in the form of Synthetic Hexaploid Wheats (SHW). These advancements were made in Mexico in the 1980s where durum cultivars were crossed with *Ae. tauchii* lines to exploit novel diversity of the D genome donor (Mujeeb-Kazi *et al.* 2013). Improvements in yield potential have been observed in SHW in comparison to modern hexaploids, highlighting the impact of genetic improvement (Li *et al.* 2014).

A number of authors have emphasised that targeting crop photosynthetic improvements by the replacement of key enzymes in the Calvin-Benson Cycle (CBC) from alien sources could be important for yield improvement (see: Parry *et al.* 2013, 2011; Sharwood 2017; Sharwood *et al.* 2016). Strategies to improve Rubisco through direct engineering and manipulation are underway, although development is not finished and technical challenges still need to be overcome (Sharwood 2017; Sharwood *et al.* 2016). A more accessible and readily available source of diversity may already be present in the primary genepool of wheat.

Wild ancestors and landraces could hold the key to improving yield potential in the breeding gene pool (Skovmand *et al.* 2001). High photosynthetic rates have been identified in progenitor wheat species (Austin *et al.* 1982; Dunstone *et al.* 1973; Evans & Dunstone 1970; Johnson *et al.* 1987b; Khan & Tsunoda 1970), highlighing a potential source of modern wheat improvement. Since these investigations there has been a reduced focus in literature on capturing photosynthetic diversity from ancestral wheats. One of the exceptions is a study conducted by Parmer (2015), which was an investigation into radiation and water use efficiency in cultivated ancient wheat types: cultivated emmer, spelt and einkorn. These ancient wheats demonstrated high water use efficiency through a number of different mechanisms, including increased photosynthetic rates or a conservative stomatal conductance. This study highlighted the potential diversity available in ancestral cultivated wheats, but there could still be a plethora of diversity present in wild progenitor populations.

Populations of *T. dicoccoides* still exist in the wild, in a region that forms a rough arc across Israel, Lebanon, Syria, Turkey, Iraq and Iran (Luo *et al.* 2007). These natural reserves, and accessions in gene banks, are pools of readily available, untapped diversity that may be the key to modern wheat improvement. However, introgressions of beneficial traits from a wild background, can also include the unintentional ‘linkage drag’ of genes linked to undesirable characteristics (Haggard *et al.* 2013; Reynolds *et al.* 2009; Summers & Brown 2013). The incorporation of novel diversity into modern varieties should not be

at the expense of elite performance (Moose & Mumm 2008). The advances made in genetic investigation over recent decades has provided the breeding industry with tools to more accurately incorporate diversity from different backgrounds into modern varieties.

Advances in genetic and physiological investigation.

Characteristics of the wheat genome have hindered the progress of genomic investigations. These features include a large genome size (17 Gb), high frequency of repeated sequences (more than 85%) and the complex polyploidy nature (IWGSC 2018; Uauy 2017). The allohexaploid *T. aestivum* (AABBDD) has 21 pairs of homologous chromosomes separated into 7 groups, each group consists of 6 chromosomes, aligned in pairs from the 3 distinct ancestral genomes (Figure VI, Martinez-Perez *et al.* 2003). The tetraploids *T. durum*, *T. dicoccum* and *T. dicoccoides* do not have the ancestral D genome, so possess 14 pairs of homologous chromosomes separated into 7 groups, each group consists of 4 chromosomes from the 2 diploid ancestral genomes discussed earlier (Figure VI). The hybridisation of related species during the formation of an allopolyploid leads to sets of similar (but not identical) chromosomes which are termed homoeologous (Glover *et al.* 2016; Martinez-Perez *et al.* 2003). For instance, the pairs 1A, 1B and 1D in *T. aestivum* are part of homoeologous group 1 (Feldman *et al.* 1997). Each pair from the same ancestral genome is termed homologous (e.g. pair 1A). While homologous chromosomes will contain the same order of genes and repetitive content (although not necessarily the same alleles), homoeologous chromosomes will possess a similar order of genes but differ in repetitive content (Martinez-Perez *et al.* 2003). Only the homologous chromosomes will pair during meiotic pairing, leading to disomic inheritance (Chapman & Riley 1970).

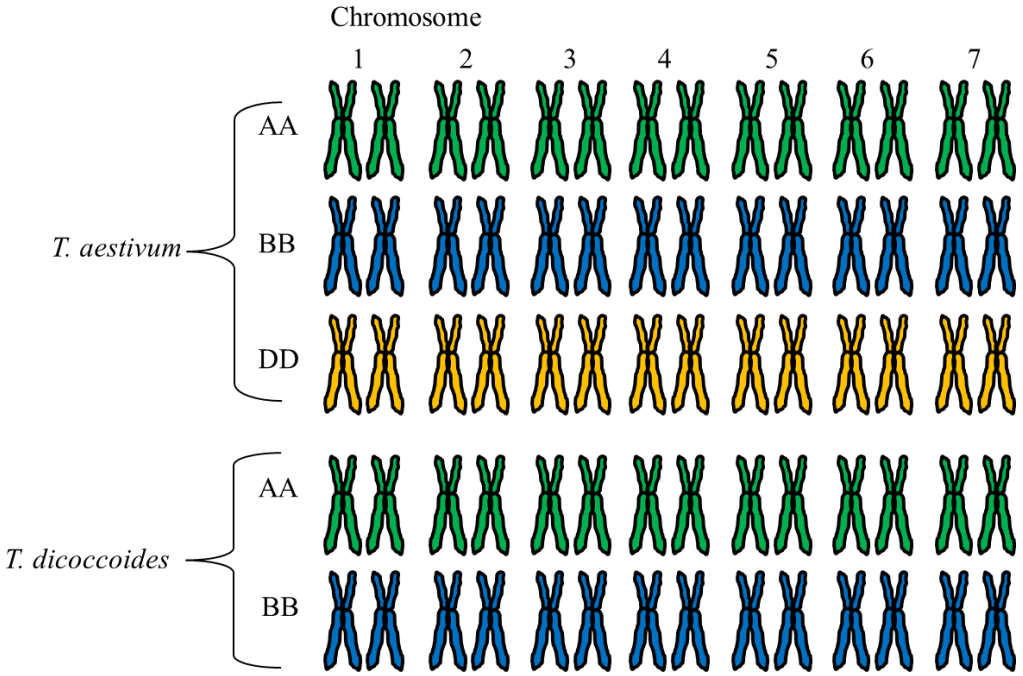

Figure VI - Chromosome number and genome structure in modern hexaploid wheat (*T. aestivum*) and the wild tetraploid wheat (*T. dicoccoides*). The genome of *T. aestivum* originates from 3 ancestral genomes (AA, BB and DD) and consists of 21 homologous pairs of chromosomes groups. The *T. dicoccoides* genome is formed from 2 ancestral genomes (AA and BB) and consists of 14 pairs of homologous chromosomes.

The complex nature of the wheat genome has also hindered gene identification and marker development (Ribaut *et al.* 2001). However, genetic investigation was accelerated during the 1980s by the development of molecular markers (Collard *et al.* 2005; Nadeem *et al.* 2017). These markers are fundamentally landmarks in the DNA sequence across the genome, which act as guides to the locations of genes when used in parallel to genetic linkage maps (Acquaah 2012). Marker discovery has facilitated the identification of genetic regions linked to quantitatively inherited traits (Moose & Mumm 2008). Quantitatively inherited traits are non-binary complex traits such as height or yield which are polygenetic and not inherited in a typical Mendelian fashion (Hill 2010). The individual loci linked to regions controlling quantitative traits are termed quantitative trait loci (QTL, Tanksley 1993). The identification of numerous QTL in crop species has facilitated the development of markers for selection using the knowledge of the marker-trait associations (Collard & Mackill 2008). The use of marker assisted selection (MAS) offers a high-throughput and low cost tool for breeders to make indirect selections of phenotypes based on genotype, without the requirement for field trials or mature plants, which has been a limitation of traditional phenotypic selection (Reynolds *et al.* 2011).

Although MAS promises to be a useful tool for the breeding industry (Gupta *et al.* 2010; Koebner & Summers 2003), progress has been slow (Collard & Mackill 2008) with limited application so field based phenotypic selection is still the dominant method in modern cultivar breeding. The recent development of high density single nucleotide polymorphism (SNP) genotyping platforms (e.g. Allen *et al.* 2017; Semagn *et al.* 2014; Wang *et al.* 2014; Winfield *et al.* 2016), may address the limitations to marker development for MAS. Due to their abundance, SNPs are powerful tools in genotyping (Rimbert *et al.* 2018). If progress in MAS is limited by the polymorphism observed in the breeding genepool of modern wheat, an incorporation of diversity from the extended genepools could address these restrictions.

Use of MAS can avoid the undesirable linkage drag associated with introgressions from a wild background (Collard *et al.* 2005) and for selection of more complex traits where problems can arise in phenotypic selection (Gupta *et al.* 2010). MAS could therefore be beneficial in selection for phenotypic traits linked to *RUE* in wide crossing. The application of MAS and other laboratory based breeding approaches should be used in parallel to field based selection, rather than replacing the traditional methods (Koebner & Summers 2003). Therefore, phenotypic field assessments are still required for accurate marker-trait identification, in order to facilitate the use of MAS in selection for improved *RUE*.

To utilise photosynthetic diversity available outside of the modern wheat genepool, phenotypic assessment is required to identify potential donors. The dramatic increases in wheat yields during the 'green revolution' coincided with an improvement in understanding of photosynthesis, although the two advancements were not linked (Richards 2000). Traditional measurements of photosynthetic components linked to *RUE*, were made using custom built gas-exchange chambers (e.g. Austin *et al.* 1982; Dunstone *et al.* 1973; Johnson *et al.* 1987b). These approaches typically used infra-red gas analysers (IRGA) to measure the absorbance of infra-red radiation at specific wavelengths and hence calculate fluxes of CO_2 and H_2O molecules (Hall & Rao 1994). Custom built chambers have been largely replaced by 'off-the-shelf' commercial systems (Figure VII), which still utilise IRGA technology but do not require prior expertise with the systems (Long *et al.* 1996). With this technology, parameters of gas-exchange are quantitated using mathematical models (von Caemmerer & Farquhar 1981). In addition to the commercialisation of IRGA technology, there has been an increase in the accessibility of instruments that measure chlorophyll fluorescence (Baker 2008; Murchie & Lawson

2013). These measurements can be used to rapidly derive traits underpinning plant photochemistry which can scale with CO_2 assimilation (Edwards & Baker 1993; Genty *et al.* 1989). The coupling of IRGA and chlorophyll fluorescence technology can be a powerful tool in non-invasive physiological assessment (Baker 2008).

Figure VII – An example of a portable commercial infra-red gas analyser system used in the field to measure gas-exchange parameters of crop species (LI-COR, LI-COR Inc., Lincoln, NE, USA).

The increased accessibility of technology has improved homology between physiological investigations and provided accessible equipment for the interrogation of photosynthetic performance in field conditions. In spite of these advancements and the increased awareness of the benefits of raising *RUE* to improve yield potential, there is still a bridge to gap between plant breeding and physiology. Regardless of the improved availability of photosynthetic phenotyping equipment, an understanding of physiology is still essential to acquire meaningful results (Long *et al.* 1996). Furthermore, as highlighted by Rebetzke *et al.* (2000):

> *"A common criticism of exploiting physiological characters in applied breeding programs is that some traits, such as leaf conductance, are slow and expensive to measure".*

These criticisms could account for why per unit area photosynthetic improvement has not been a major target of wheat breeding in recent history (Richards 2000). It may be unrealistic to expect members of the breeding industry to employ gas-exchange analysis in their large scale breeding populations. However, if physiological markers can be identified which correlate to the more complex integrative photosynthetic traits; indirect selection could be applied. The use of indirect selection could aid the breeder in applying

greater selection pressure for a primary unselected trait in large breeding populations (Babar *et al.* 2007). For effective use of indirect selection, the physiological marker may have higher heritability than the primary trait, or be easier and faster to measure, ultimately widening the breeding population available for trait discovery (Rebetzke *et al.* 2001). If traits are screened for marker-trait associations, large populations are required for increased accuracy in estimating marker effects and improving the power of detection (Collard *et al.* 2005; Hospital *et al.* 1997). This means that high throughput techniques are required for rapid phenotyping of large mapping populations. Therefore, if a platform of physiological markers amenable to high-throughput phenotyping and relating to more complex targeted primary traits can be identified, selection could be implemented in large scale breeding programs that incorporate diversity from extended gene pools.

Thesis aims.

In brief, the aims of this thesis are:

1. To identify potentially valuable traits in accessions from the primary genepool of wheat that could improve flag leaf CO_2 assimilation in modern varieties.
2. To consider the importance of awns to ear photosynthesis, flag leaf photosynthesis and grain yield.
3. To propose an ideotype of complex targeted primary traits and physiological markers that could be used for indirect selection.
4. To identify marker-trait associations linked to the physiological markers in a tetraploid background.

1 IDENTIFYING DESIRABLE FLAG LEAF PHOTOSYNTHETIC TRAITS IN PROGENITOR SPECIES

Abstract

High photosynthetic rates have previously been identified in progenitor wheat species, but ambiguity exists in pinpointing the components driving this productivity. The potential determinants and limitations of flag leaf CO_2 assimilation were broken down into photosynthetic supply and demand components. A diverse range of techniques were used to measure these components on field grown plants, including analyses of gas-exchange parameters, chlorophyll fluorescence and content, carbon isotope discrimination, leaf dry matter and flag leaf area. Two *Triticum dicoccoides* accessions (dic71 and dic72) were identified with higher flag leaf CO_2 assimilation, expressed on a standardised leaf area basis (A, μmol CO_2 m^{-2} s^{-1}), when compared to modern wheat cultivars. There was evidence that photosynthetic supply components were driving the higher A observed in *T. dicoccoides*, including CO_2 supply (stomatal and mesophyll conductance) and traits linked to photochemistry.

CO_2 assimilation expressed on a per leaf basis, A ($leaf^{-1}$), was higher in the cultivated wheats due to an increased photosynthetic capacity determined by organ surface area. Offspring progeny, formed through crossing the *T. dicoccoides* individuals with elite hexaploid wheat cultivars, showed increases in A per unit area, but mostly an overall lower A ($leaf^{-1}$), due to a reduction in flag leaf area. Yield analysis indicated that maintaining a large flag leaf area was more advantageous to grain yield than increasing A per unit area. Therefore, if photosynthetic diversity is to be exploited from a wild tetraploid background, introgressions need to be made without reductions to flag leaf area.

1.1 Introduction

1.1.1 Flag Leaf Photosynthesis and Grain Yield.

An ongoing physiological discussion exists in literature regarding whether grain yield is limited by source or sink components. The source determinant of yield is assimilate production over the growing season and the sink determinant is assimilate storage capacity via grains (Shearman *et al.* 2005). The source determinant is controlled by the rate of photosynthesis and the total area of photosynthetic tissue (Thorne 1974). CO_2 enrichment studies have demonstrated that increasing photosynthetic assimilation in wheat can have direct beneficial effects on grain yield (e.g. Ainsworth & Long 2005; Thilakarathne *et al.* 2013), supporting the idea that grain yield is to some degree source limited, regardless of additional sink limitation. When water availability is not a major limiting factor, the flag leaf is a substantial contributor of assimilates to the grain (Thorne 1974), as demonstrated by correlations between overall grain yield and flag leaf photosynthetic traits (Carmo-Silva *et al.* 2017; Fischer *et al.* 1981, 1998; Gaju *et al.* 2016; Reynolds *et al.* 2000). Conversely, a recent large-scale study by Driever *et al.* (2014) found no correlation between grain yield and flag leaf photosynthesis, when measured at different CO_2 concentrations in 64 modern elite wheat cultivars. Gas-exchange measurements of flag leaves at ambient field conditions, rather than under artificially high CO_2 concentrations, may be more informative on the relationship between photosynthesis and grain yield (Carmo-Silva *et al.* 2017; Lawson *et al.* 2012). If selection can be implemented to improve photosynthesis at a leaf level, overall canopy photosynthesis could be increased, leading to higher yields (Horton 2000).

1.1.2 Photosynthesis in the Progenitors of Wheat

There is evidence to suggest that CO_2 assimilation, expressed on a standardised leaf area basis (A, μmol CO_2 m^{-2} s^{-1}), has decreased through domestication and modern breeding practices. Progenitor tetraploid wheat flag leaves have shown higher rates of A than cultivated hexaploids (Austin *et al.* 1982; Dunstone *et al.* 1973; Evans & Dunstone 1970; Johnson *et al.* 1987a; Khan & Tsunoda 1970). Differences in photosynthetic performance between old and more modern wheat varieties suggest that breeders may have unintentionally selected against flag leaf photosynthetic capacity in order to improve other agronomically important traits (Driever *et al.* 2014). Wild relatives and landraces of wheat are generally recognised to be an untapped genetic reserve for crop improvement (Skovmand *et al.* 2001). A plethora of novel diversity exists directly in the primary

genepool of wheat, such as the tetraploid progenitor *T. dicoccoides* (Peng *et al.* 2012), a species which has shown high photosynthetic capacity in wild populations (Carver & Nevo 1990). Recent reports have highlighted that introgressions from *T. dicoccoides* into modern wheat can increase flag leaf photosynthetic capacity (Merchuk-Ovnat *et al.* 2016b).

Ambiguity exists in pinpointing which particular traits are responsible for a potential decline in *A* in the flag leaves of modern wheat in comparison to progenitor species. For instance, Austin *et al.* (1982) found higher stomatal and vein densities in tetraploid flag leaves compared to hexaploid cultivated varieties and Khazaei *et al.* (2009) found stomatal size varied across wheat ploidy. Alternatively, Prins *et al.* (2016) found superior photosynthetic enzyme catalytic properties across the Triticeae tribe and Johnson *et al.* (1987) concluded that a higher capacity for mesophyll photosynthesis may be linked to variation in CO_2 assimilation across ploidy, whilst Merchuk-Ovnat *et al.* (2016b) found that an introgression from *T. dicoccoides* into bread wheat was linked to improved photochemistry. However, it could simply be that the smaller leaf area typical of progenitor wheat (Evans & Dunstone 1970), may have more concentrated photosynthetic capacity (Long *et al.* 2006), and hence photosynthesis measurements expressed on a standardised leaf area basis ($\mu mol\ CO_2\ m^{-2}\ s^{-1}$) could account for variation across ploidy. To utilise the diversity in progenitor wheat as a source for photosynthetic improvement in modern varieties, further analysis is needed to identify the driving components of improved CO_2 assimilation found across contrasting wheat species.

1.1.3 The Driving Components of Leaf CO_2 Assimilation.

The determinants of flag leaf *A*, and thus potential opportunities for improvement, can be separated into two categories: photosynthetic supply and down-stream demand (Figure 1-1). ‘Supply’ consists of the quantity of products produced through the light-dependant reactions and the delivery of CO_2 to the sites of carboxylation (Mellers & Wright 2017). The demand component entails the down-stream enzyme-regulated mechanisms of CO_2 fixation and, additionally, the absolute area based leaf photosynthetic capacity governed by organ surface area and density.

The development of portable Infrared Gas Analyser systems (IRGA) has facilitated real-time field measurements of supply and demand components of leaf photosynthesis within a controlled cuvette (Long *et al.* 1996). Plotting measurements of *A* against different intercellular CO_2 concentrations (C_i) can provide information on biochemical features

and parameters of leaf photosynthesis (Bellasio *et al.* 2016; Sharkey *et al.* 2007; von Caemmerer & Farquhar 1981). Following models from Farquhar *et al.* (1980), these responses can be used to analyse limitations on photosynthesis, including carboxylation activity of photosynthetic enzymes and the regeneration rate of the acceptor molecule ribulose-1,5-bisphosphate (RuBP). Parameters which relate to the supply and demand components of flag leaf CO_2 fixation (Figure 1-1) can be extracted from measurements of field grown plants using an IRGA and leaf cuvette system and quantified in relation to comparable data following models from von Caemmerer & Farquhar (1981).

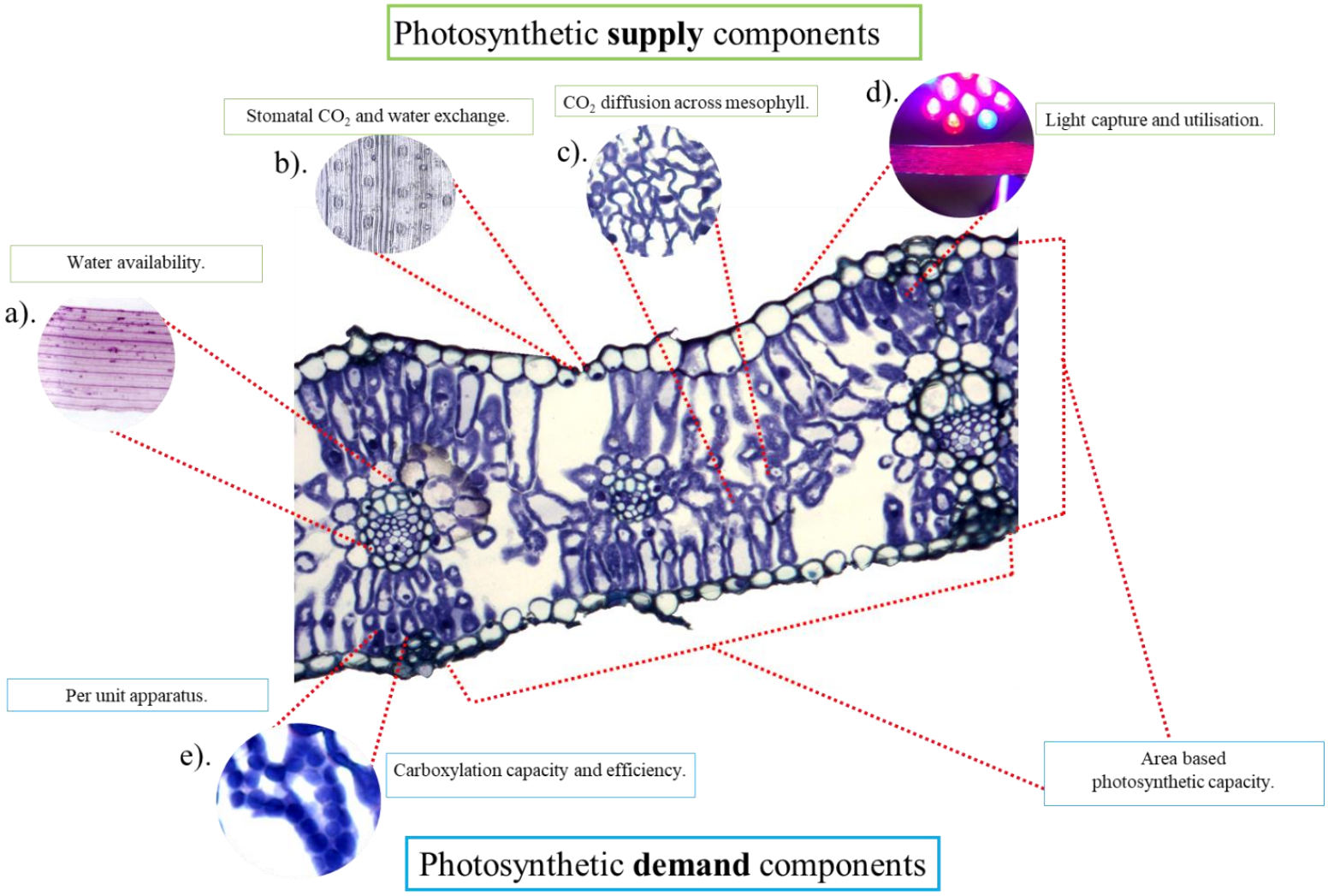

Figure 1-1 - A schematic of a flag leaf cross section, showing the photosynthetic supply (highlighted in green) and demand components (highlighted in blue) which ultimately determine CO_2 assimilation and represent potential targets for improvement: a). Leaf veins are visible in a cleared *T. dicoccum* flag leaf from the 2016 field trial (L. McAusland, personal communication, 2016); b). Stomata visible on an impression taken from the 2017 field trial (see: 1.2.2); c). Leaf mesophyll cells are shown in a zoomed image from the 2016 field trial taken at 60x (see: 1.2.2); d). A photo taken during the 2016 field trial showing a leaf illuminated by a LED light; e) Chloroplasts are visible in the zoomed image of a mesophyll cell from the 2016 field trial taken at 60x.

Photosynthetic Supply

The supply components that are determinants, and potential limitations, of CO_2 assimilation include the delivery of CO_2 to the sites of carboxylation and the availability of products from the light dependant reactions. CO_2 delivery is governed by a number of diffusive boundaries, primarily: stomatal conductance (g_s) and mesophyll conductance (g_m). When stomata are closed, water loss is minimal, but the shut pores act as the sole limitation to carbon fixation (Farquhar *et al.* 1982). Therefore, there is a fundamental trade-off between the flux of CO_2 entering the leaf and flux of H_2O exiting through the stomatal pores (Lawson & Blatt 2014). Selection to increase or decrease g_s largely depends on the targeted environment, as higher g_s in water-rich environments has resulted in higher yields in bread wheat (Fischer *et al.* 1981, 1998). Conversely, selection for decreases in g_s would merit improvements in drought tolerance (Hughes *et al.* 2017). Reductions in g_s are often to the detriment of carbohydrate status over the growing seasons leading to an overall yield penalty (Lawson & Blatt 2014). Disassociating this trade-off is key to breeding drought tolerant varieties that are productive under a range of environmental conditions. Water shortage leads to substantial reductions in leaf photosynthesis (Lawlor & Cornic 2002; Schapendonk *et al.* 1989) and is a major abiotic constraint on global wheat production (Shiferaw *et al.* 2013). The leaf-level proportion of CO_2 gained to H_2O transpired is termed Water Use Efficiency (*WUE*) (Farquhar & Richards 1984) and can be useful physiological tool for assessing drought tolerance (Condon *et al.* 2004). High *WUE* can be associated with reduced water loss and lower g_s, but also decreased *A* and slower growth (Lawson & Blatt 2014). Relative Water Content (*RWC*) is a useful tool for screening leaf water relations, as estimates of leaf relative turgidity can provide an insight into potential water deficits (Barrs & Weatherley 1962) and has been used for assessing drought tolerance (Ober *et al.* 2005; Tambussi *et al.* 2005).

Once CO_2 has diffused into the leaf through the stomata, the delivery of CO_2 to the sites of carboxylation is largely governed by mesophyll conductance to CO_2 (g_m). The diffusion of CO_2 across the mesophyll is restricted by a series of physical barriers, reflecting diffusion from the substomatal cavity into the mesophyll cells, then transport to the chloroplasts and the site of carboxylation (Flexas *et al.* 2012, 2013). Variation in g_m between genotypes occurs due to differences in mesophyll anatomy (Evans *et al.* 2009; Evans & Von Caemmerer 1996; Tomás *et al.* 2013) and biochemical features such as aquaporins or carbonic anhydrases (Flexas *et al.* 2012). Significant variation has been

observed in g_m within crop cultivars (Barbour *et al.* 2010; Jahan *et al.* 2014; Tomás *et al.* 2014), suggesting selection could be implemented in breeding programs with the aim of increasing leaf level CO_2 assimilation.

The fractionation of the heavier carbon isotope (^{13}C) during the diffusion of CO_2 through the stomata, and during the uptake by Rubisco, is a tool for determining limitations relating to leaf level photosynthetic supply and demand components (Farquhar *et al.* 1982). The degree of discrimination against ^{13}C is dependent on the ratio of C_i to the external CO_2 concentration (C_a) (Gillon *et al.* 1998). This ratio is determined by the relative magnitudes of the supply component (g_s) and the downstream demand component controlled by Rubisco (Dawson *et al.* 2002). If carbon isotope discrimination ($\Delta^{13}C$) and the ratio of C_i to C_a (C_i / C_a) is low, then the supply component (g_s) is limiting diffusion, or possibly CO_2 drawdown by Rubisco is high (Farquhar *et al.* 1989). Alternatively, a higher ratio of C_i / C_a, caused by either reduced diffusive restrictions or decreased CO_2 drawdown, may result in higher $\Delta^{13}C$. Low leaf $\Delta^{13}C$ is often associated with high carbon gain and low water loss (Farquhar & Richards 1984) and is usually used as a tool for screening drought tolerance (Rajabi *et al.* 2009). However, $\Delta^{13}C$ can be used as a surrogate for diffusive supply limitations, but could also represent photosynthetic (demand) limitations during the lifespan of a leaf.

The supply components of CO_2 assimilation also includes the availability of products from photochemistry (adenosine triphosphate and reductant generated by the light-dependant reactions). As described by Horton (2000), limitations to leaf level light harvesting capacity can arise from: poor absorption caused by inefficient leaf angles; the inability of the leaf to deal with high-light saturation; photoinhibition and ineffective photoprotection; and slow recovery times under heterogeneous light conditions. Chlorophyll fluorescence is a useful diagnostic tool for estimating the performance of photosystem II photochemistry, which can relate to photosynthetic performance in field conditions (Maxwell & Johnson 2000). The quantum yield of photosystem II (Φ_{PSII}), provides an estimate of the proportion of absorbed light energy used in photochemical pathways and is used to derive an estimate of the rate of electron transport (Genty *et al.* 1989; Murchie & Lawson 2013). The per unit chlorophyll content can also be used as a tool for screening leaf level investment into light harvesting and can be proportionate to photosynthesis under optimum conditions (Fleischer 1935).

Photosynthetic Demand

The determinants, and limitations, imposed by photosynthetic demand components relate to the down-stream enzyme regulated mechanisms of CO_2 fixation. Demand for CO_2 is restricted by the carboxylation (V_c) and oxygenation (V_o) activities of the enzyme Rubisco (Farquhar *et al.* 1980; Seibt *et al.* 2008). Rubisco initiates the first stage of CO_2 uptake in the Calvin Benson Cycle (CBC), by catalysing the carboxylation of RuBP (Raines 2003). Although Rubisco constitutes up to half of the soluble protein in a C3 plant (Nobel 2005), increasing the capacity and efficiency of the enzyme is a substantial bottleneck in raising wheat yields (Parry et al., 2011). Correlations between flag leaf nitrogen content and CO_2 assimilation (Evans, 1983, 1989) have highlighted the importance of per unit Rubisco content in carbon fixation. Furthermore, the catalytic properties of the enzyme, such as carboxylation velocity, Michaelis-Menten constants for CO_2 and O_2 and specificity factor, have been shown to vary in different Triticeae genotypes (Prins *et al.* 2016). Traits such as Rubisco specificity factor ($S_{C/O}$) are important tools for screening Rubisco efficiency, as in addition to V_c, Rubisco is also responsible for catalysing the oxygenation of RuBP (V_o). Photorespiration is the energetically expensive process of converting the by-products of the oxygentation reaction and is a significant constraint on wheat productivity (Long *et al.* 2006; Parry *et al.* 2011, 2007). Photorespiration can be responsible for loss of 30% of the potential carbohydrates formed through photosynthesis (Monteith & Moss 1977).

The demand components of leaf level CO_2 assimilation also include area based leaf photosynthetic capacity, which is ultimately determined by organ surface area or thickness. Theoretically, a larger leaf may have a higher demand for supply components to maintain CO_2 assimilation over an extended photosynthetic surface area. Canopy photosynthesis can be increased by targeting higher *A*, but also by selection for increased leaf area (Beadle & Long 1985). Increased leaf thickness is often associated with higher photosynthetic capacity (McClendon 1962; Oguchi *et al.* 2003), due to supporting more concentrated photosynthetic apparatus per unit area (Evans & Poorter 2001). Direct measurements of leaf thickness can be difficult, however, specific leaf area (*SLA*, the ratio of leaf area to dry mass) can be used as a suitable proxy (Vile *et al.* 2005). In terms of organ surface area, *A* has been negatively associated with larger leaf area (Austin *et al.* 1982; Bhagsari & Brown 1986; Evans & Dunstone 1970; Johnson *et al.* 1987a), which could be the result of a dilution of photosynthetic capacity per unit area (Long *et al.* 2006).

Ultimately, investigation is needed to address the potential costs or benefits of selection for increased absolute and specific leaf area on assimilation rate per unit leaf area.

1.1.4 Chapter Aims

Preliminary analyses were completed in the present study and by White and Leigh (unpublished) on a large collection of different wheats that existed at NIAB (Cambridge, UK). Based on these results, a subset of diverse wheat lines consisting of different species was selected for detailed experimental investigations.

1. This subset was grown in field trials in 2016. Flag leaf CO_2 assimilation was measured to confirm the observations made in preliminary analyses and to identify potential donors for modern wheat improvement.

2. Using a range of diagnostic phenotypic tools, the aim was to establish which photosynthetic supply and demand components were driving the diversity within the collection.

3. In a field trial grown the following year (2017), existing introgression populations formed from direct hexaploid x tetraploid crossing were included. The tetraploid parents were lines with high flag leaf CO_2 assimilation identified in the 2016 field trial. The aim was to analyse whether photosynthetic diversity can be incorporated into a modern wheat background from a tetraploid source.

1.2 Methodology

Each methodology section in the following three chapters consists of a description of plant genetic material and trial layout, phenotypic methodology and (where present) genotypic methodology. In all chapters and sections, the mentioned growth stages (GS) refers to the Zadoks *et al.* (1974) growth stages for cereals (see: Appendix 4).

1.2.1 Materials and Trials

Material

A diverse collection of diploid, tetraploid and synthetic hexaploid wheat exists at NIAB forming the working material for the synthetic pillar of the Wheat Strategic Improvement Program (WISP - www.wheatisp.org). A portion of this material was grown in a demonstration field plot in 2016 (Table 1-1), hereafter termed in this chapter the '2016 field trial'. Within this plot, a smaller subset of lines were selected for gas exchange analysis, with the selection aiming to encompass representatives from different species and sub-species. Two elite bread wheats were included, Paragon (spring-type) and Robigus (winter-type), these lines had significance in ongoing pre-breeding programs and were good examples of modern cultivars. Two *T. durum* lines were also included, Hoh501 is the tetraploid parent in NIAB Synthetic Hexaploid Wheat (SHW) breeding programs and 67-1 was a diverse Ethiopian landrace of interest. Tios and dic12b were the *T. dicoccum* mapping population parents that showed photosynthetic variation in the glasshouse, discussed further in Chapter 3. Another *T. dicoccum* landrace was also included (18209), which had significance in the WISP program. Two *T. dicoccoides* accessions, dic71 and dic72, showed diverse flag leaf photosynthetic responses in preliminary trials. Therefore, these lines were included to identify potential donors for modern wheat photosynthetic improvement. Additionally, dic007 was included as an example of einkorn wheat (*Triticum monococcum*). Two accessions of primary synthetic hexaploid wheat developed at NIAB were also included (SHW-008 and SHW-012). The contributors to the material selection and preliminary analyses are discussed in Appendix 6.

Table 1-1 - The subset of lines from the 2016 field trial on which gas-exchange measurements were completed.

Line	Species	Common Name	Reason for inclusion
Paragon	*T. aestivum*	Bread Wheat	Pre-breeding hexaploid parent
Robigus	*T. aestivum*	Bread Wheat	Pre-breeding hexaploid parent
Hoh501	*T. durum*	Durum Wheat	Tetraploid component of NIAB synthetics.
67-1	*T. durum*	Durum Wheat	Ethiopian landrace
Tios	*T. dicoccum*	Cultivated emmer	High CO_2 *A* in glasshouse[1]
18209	*T. dicoccum*	Cultivated emmer	Tetraploid landrace
dic12b	*T. dicoccum*	Cultivated emmer	Low CO_2 *A* in glasshouse[1]
dic72	*T. dicoccoides*	Wild emmer	High g_s in glasshouse[2]
dic71	*T. dicoccoides*	Wild emmer	High g_s in glasshouse[2]
SHW008	*T. aestivum*	Synthetic Wheat	NIAB primary synthetic
SHW012	*T. aestivum*	Synthetic Wheat	NIAB primary synthetic
dic007	*T. monococcum*	Einkorn Wheat	Diploid Landrace

[1] Measured in glasshouse trial by White and Leigh (unpublished). [2] Measured in a preliminary winter glasshouse field trial in 2015.

Based on the results from the 2016 field trial: Tios, Paragon, Robigus, dic12b, dic71, dic72 and tetraploid x hexaploid crossing (T x H) offspring lines were included in a trial during 2017 (Table 1-2). The offspring T x H lines consisted of 16 accessions formed through crossing dic72 with Paragon, backcrossing the F1 individuals with Paragon and then self-fertilising through to the F6 generation. The other 4 T x H offspring lines also consisted of backcrossed F6 lines, but were initially formed via crossing dic71 and Paragon. This trial is hereafter referred to in this chapter as the '2017 field trial'. The tetraploid mapping population parents used in Chapter 3 (Tios and dic12b) were also included. Robigus was included for additional comparisons between modern and progenitor wheat.

Table 1-2 - Tetraploid parental lines, hexaploid parental lines and the introgressed offspring lines grown in the 2017 field trial.

Line	Type	Species	Tetraploid Parent	Hexaploid Parent
dic12b	Mapping Parent	*T. dicoccum*	-	-
dic71	Tetraploid Parent	*T. dicoccoides*	-	-
dic72	Tetraploid Parent	*T. dicoccoides*	-	-
Paragon	Hexaploid Parent	*T. aestivum*	-	-
Robigus	Hexaploid Individual	*T. aestivum*	-	-
Tios	Mapping Parent	*T. dicoccum*	-	-
31_07K	BC1 F6	*T. aestivum*	dic71	Paragon
31_07L	BC1 F6	*T. aestivum*	dic71	Paragon
31_12K	BC1 F6	*T .aestivum*	dic71	Paragon
31_17A	BC1 F6	*T .aestivum*	dic71	Paragon
32_06L	BC1 F6	*T. aestivum*	dic72	Paragon
32_16J	BC1 F6	*T. aestivum*	dic72	Paragon
32_21C	BC1 F6	*T. aestivum*	dic72	Paragon
32_23D	BC1 F6	*T. aestivum*	dic72	Paragon
32_23E	BC1 F6	*T. aestivum*	dic72	Paragon
32_23G	BC1 F6	*T. aestivum*	dic72	Paragon
32_23I	BC1 F6	*T. aestivum*	dic72	Paragon
32_23J	BC1 F6	*T. aestivum*	dic72	Paragon
32_24K	BC1 F6	*T. aestivum*	dic72	Paragon
32_08G	BC1 F6	*T. aestivum*	dic72	Paragon
32_08L	BC1 F6	*T. aestivum*	dic72	Paragon
32_09F	BC1 F6	*T. aestivum*	dic72	Paragon
32_15G	BC1 F6	*T. aestivum*	dic72	Paragon
32_15I	BC1 F6	*T. aestivum*	dic72	Paragon
32_15J	BC1 F6	*T. aestivum*	dic72	Paragon
32_16E	BC1 F6	*T. aestivum*	dic72	Paragon

Trials

The trials used in this chapter are:

- The 2016 field trial used for A/C_i curve measurements.
- The 2017 field trial used for ambient gas-exchange and leaf area field measurements of the introgressed offspring lines and their parents.

2016 Field Trial

A selection of lines were sown into a 96 well tray filled with M3 compost on the 20th of January 2016 (Table 1-1). Seedlings were vernalised for two months; on removal they were hand transplanted into the Innovation Farm Demo Field (Park Farm, NIAB, Cambridge) on the 29th of March 2016. Transplants were made into a large plot (8 m x 2

m) consisting of 7 rows spaced 30 cm apart (Figure 1-2). For each line, a mini-plot was created by transplanting 10 individuals along 80 cm of one row, there were 7 mini-plots formed per row. A 20 cm gap separated each mini-plot. As this plot was also used for demonstration purposes, the order was not randomised. Species were planted together in non-replicated blocks (Figure 1-2), which had the advantage of reducing potential shading, as interspecific variation in height was greater than intraspecific variation. In an effort to reduce edge effects, Paragon seed was sown as a buffer at the beginning and end of each row and in the two outer rows. The Robigus individuals showed signs of Pythium disease following artificial vernalisation. One month after the initial transplanting date, all Robigus plants were replaced with heathy individuals which had been kept as spare plants in vernalisation. This resulted in a later transplanting date for Robigus and that these transplanted individuals missed the N application.

The field plot was treated and fertilised as a typical spring wheat trial. To achieve a universal N application of 150 kg/N; the plot was fertilised with ammonium nitrate (34.5% N) in two separate applications of 116 and 319 kg ha^{-1}. One pesticide and two fungicide applications were also applied. No herbicide was used, as the plot was routinely hand weeded. Due to the field space restrictions, plants which were being used for yield analysis were dug up during senescence on the 27th of July 2016 and moved to large bread crates (0.051 m^3) full of potting compost. Crates were transported to an outside growing area at Park Farm, Cambridge and left to senesce completely before harvest. Harvest was completed between the 15th and 25th of August 2016, when maturity had been reached.

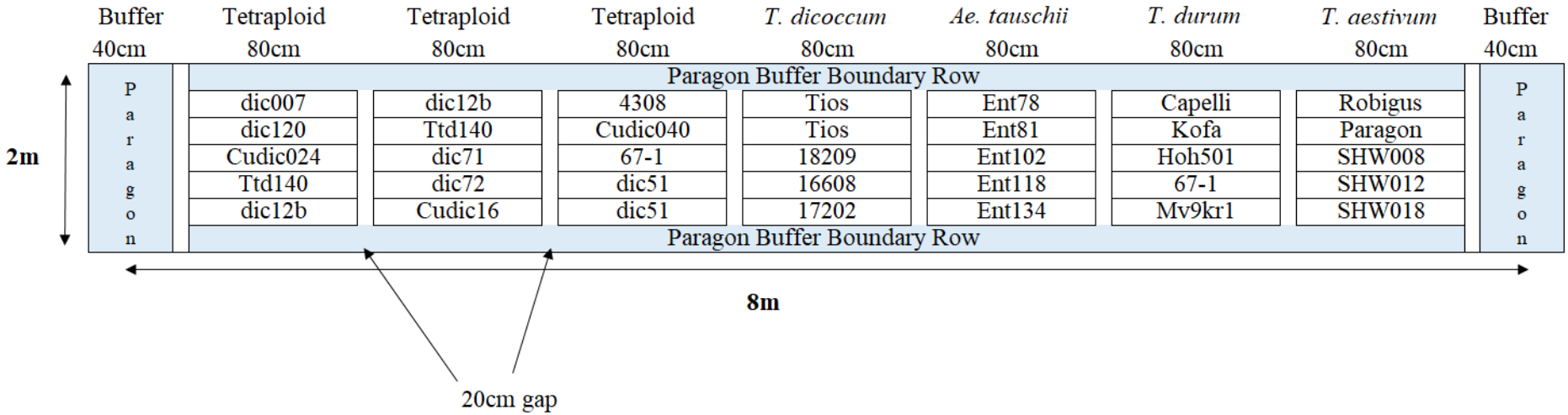

Figure 1-2 – The layout of the 16 m^2 2016 field trial used for the *A/C$_i$* curve measurements. For each line, 10 replicates were planted in an 80 cm row mini-plot, spaced 8 cm apart. Each line was separated by a 20 cm gap. The outer rows and the first 40 cm of each row was sown with Paragon to act as a buffer.

2017 Field Trial

The TxH parents (Paragon, dic71 and dic72), the T x H offspring lines and three additional lines (dic12b, Tios and Robigus) were sown into 96-well trays between the 13th and 16th of January 2017 (Table 1-2). To avoid the problems with Pythium transmitted through the vernalisation chamber in the 2016 field trial, the seedlings were vernalised naturally in an unheated glasshouse at Park Farm, Cambridge from the 18th of January 2017. On the 31st of March 2017, lines were hand transplanted into a 24 m^2 plot (8 m x 3 m) in the New Ornamentals Field Park Farm, NIAB Cambridge (Figure 1-3). The plot had nine rows spaced 30 cm apart, the 3rd, 4th, 6th and 7th row were each transplanted with 9 lines spaced out in 80 cm mini-plots. Within each mini-plot, there were 8 individuals transplanted and spaced 10 cm apart. The mini-plot order was randomised before transplanting. For uniformity and phenotyping accessibility, the 2nd, 5th and 8th row were not planted, so that each transplanted row was exposed to a gap row on one side. The 50 cm start and end of each row, and the 1st and 9th outer boundary rows were sown with a Paragon buffer.

From the date of transplanting to the start of senescence, the plot was well irrigated every 5 days in the absence of rainfall. On the 19th of April 2017, one application of ammonium nitrate fertiliser (34.5% N) was applied at a rate of 434 kg ha^{-1} to achieve a universal application of 150 kg/N. On the 18th of May 2017 the first application of fungicide was made. The second application of fungicide was made on the 25th of June 2017. Herbicide was not applied to the plot, as routine hand weeding was carried out. Once the plants had reached GS39 they were all individually staked to avoid lodging. On 3rd to 4th of August 2017 whole plants were taken from the field and stored for processing.

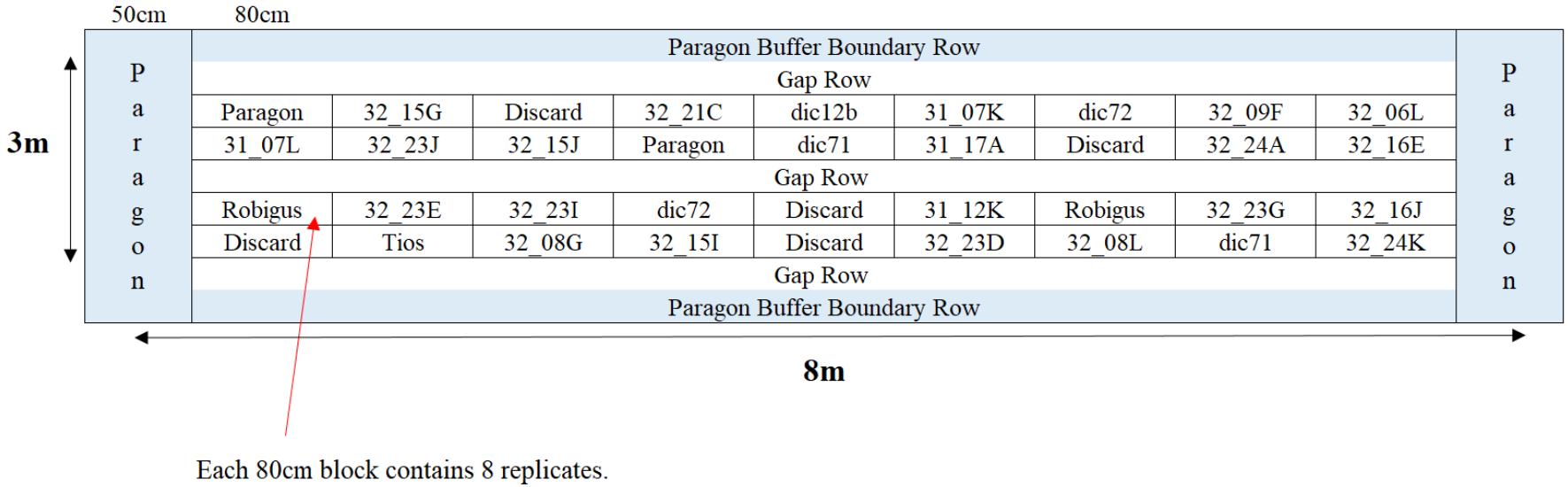

Figure 1-3 - The layout of the 24 m^2 plot which contained the collection of tetraploid and hexaploid parental lines and the introgressed offspring individuals grown in the 2017 field trial. The plants were randomly transplanted into mini-plots in 4 rows. Each 80 cm mini-plot consisted of 8 replicates. The outer rows and the first 50 cm of each row was sown with Paragon to act as a buffer.

1.2.2 Phenotypic Methodology

2016 field trial

Material Sampling

From the 5th of June to the 11th July 2016, healthy main tillers were selected from plants at inflorescence emergence (GS51 to GS59). Following Driever *et al.* 2014, the measurements were made before anthesis to reduce potential variation in sink size between the lines influencing the photosynthetic rates. As the equipment required to take measurements from these tillers included a large 2% O_2 gas cylinder, it was impractical to complete analysis in the field. Therefore, main tillers were cut off just above ground level and immediately re-cut under, and stored, in deionised water to prevent cavitation. Only one tiller was sampled at a time and immediately transported to the field lab (located in close proximity to the demo field). No significant variation was identified between measurements made in the field and the lab using this technique (see: Appendix 1). Five or six A/C_i curves (details below) were completed on different replicates of each line. Measurements were conducted between 9:30 to 18:00. The transplanted Paragon individuals showed signs of disease stress (mainly rust) on the flag leaves. Therefore, only 1 healthy individual was available from all those transplanted. However, the 40 cm start and end of each row had been sowed with Paragon to act as a buffer. Therefore, healthy main tillers from the central regions of the 40 cm boundary blocks at the beginning and end of each row of the plot were used instead. Once the A/C_i curves were complete, each leaf was imaged and leaf cores were taken for dry matter analysis. Leaves were then stored in moist tissue paper, sealed in a plastic bag and transported back to NIAB HQ, Cambridge, where undamaged sections of the flag leaves were sampled for the cross-section analysis.

Measurements

The methodology used in the 2016 field trial examined a range of physiological markers related to the supply and demand components of flag leaf CO_2 assimilation. The techniques used were diverse and are shown for clarity in Table 1-3.

Table 1-3 - Targeted traits used for analysis of the supply and demand components linked to CO_2 assimilation in the 2016 field trial. The acronym for each trait is shown in the table.

Trait	Acronym	Units	Methodology	Reference
Supply Component				
Per unit leaf net CO_2 assimilation	A	µmol CO_2 m^{-2} s^{-1}	A/C_i curve	von Caemmerer & Farquhar (1981)
Per unit leaf transpiration	E	mmol H_2O m^{-2} s^{-1}	A/C_i curve	von Caemmerer & Farquhar (1981)
Stomatal conductance to H_2O	g_s	mol H_2O m^{-2} s^{-1}	A/C_i curve	von Caemmerer & Farquhar (1981)
Mesophyll conductance to CO_2	g_m	mol CO_2 m^{-2} s^{-1}	A/C_i curve	Harley et al. 1992
Quantum yield of photosystem II	Φ_{PSII}	-	A/C_i curve	Genty et al. 1989
Calibrated electron transport rate	J_{CAL}	µmol e^- m^{-2} s^{-1}	A/C_i curve	Bellasio et al. 2016
Chlorophyll content	*Chl*	mg m^{-2}	Chlorophyll Content Meter	-
Carbon isotope discrimination	$\Delta^{13}C$	‰	Dry matter analysis	Farquhar et al. (1989)
Relative water content	*RWC*	%	Dry matter analysis	Barrs & Weatherley (1962)
Instantaneous water use efficiency	*WUE*	µmol CO_2 (mol H_2O)$^{-1}$	A/C_i curve	-
Percentage intercellular airspace	*% Airspace*	%	Cross Sectioning	-
Demand Component				
Per unit leaf net CO_2 assimilation	A	µmol CO_2 m^{-2} s^{-1}	A/C_i curve	von Caemmerer & Farquhar (1981)
Maximum photosynthetic rate	A_{MAX}	µmol CO_2 m^{-2} s^{-1}	A/C_i curve	von Caemmerer & Farquhar (1981)
Intercellular CO_2 concentration	C_i	µmol mol^{-1}	A/C_i curve	von Caemmerer & Farquhar (1981)
Carboxylation efficiency	CE_{amb}	mol m^{-2} s^{-1}	Curve fitting EBT	Bellasio et al. 2016
CO_2 assimilation per leaf	*A (flag leaf^{-1})*	µmol CO_2 leaf $^{-1}$ s^{-1}	A/C_i curve	-
Percentage nitrogen content	$N_{\%}$	%	A/C_i curve	-
Carbon isotope discrimination	$\Delta^{13}C$	‰	Dry matter analysis	Farquhar et al. (1989)
Flag leaf area	FL_A	cm^2	Image analysis	-
Specific leaf area	*SLA*	cm^2 g^{-1}	Dry matter analysis	Garnier et al. (2001)

Combined Fluorescence, A/C_i curves and R_{DARK} measurements.

A LI-COR-6400XT Portable Infrared Gas Analyser (LI-COR, LI-COR Inc., Lincoln, NE, USA) with a Leaf Chamber Fluorometer (LCF) was used to generate A/C_i curves coupled to PSII fluorescence under both ambient and low O_2 (2%) concentrations. Initial LI-COR chamber conditions were: leaf fan set to fast, gas flow rate set to 200 µmol s^{-1}, and a CO_2 reference concentration of 400 µmol mol^{-1}. A block temperature (25 ºC) slightly higher than ambient conditions was used (see: Appendix 5), in order to conform to studies where fixed values of physiological parameters were taken and used in the mesophyll conductance estimation. Physiological estimates of Rubisco specificity or CO_2 compensation are often estimated at 25 ºC (e.g Alonso *et al.* 2009; Galmés *et al.* 2005). Based on preliminary light curves completed with the LI-COR (see: Appendix 1), a near-saturating photosynthetic photon flux density (PPFD) of 1500 µmol m^{-2} s^{-1} was set (90% red and 10% blue light). Reference relative humidity was controlled at 60 ± 10% to match the ambient lab conditions. Following Loriaux *et al.* (2013) and Bellasio *et al*. (2016) the LCF conditions were set to: measuring light frequency = 10 KHz, intensity = 4, filter = 5 and gain = 10. A multiphase pulse flash was selected with a ramp depth of = 40%, target intensity = 10, high measuring frequency = 20 KHz and filter = 50 KHz.

Leaves were placed in the chamber, half way along the length of the leaf, with the adaxial side facing the internal LED light source. If the flag leaves did not completely cover the gasket area, leaf width was measured and gas-exchange results were recalculated using the correct leaf area (Carmo-Silva *et al.* 2017). The leaves were left to acclimatise for 10-60 minutes, until A and g_s had stabilised. At this point an automated fluorescence step-wise A/C_i curve was prompted on the LI-COR with: CO_2 reference steps of: 400, 300, 200, 100, 400, 600 and 1200 µmol mol^{-1}; matching at each step with a 30 s post match recovery; and a 120 s minimum and maximum wait time. At the 100 µmol mol^{-1} CO_2 step the automated program was paused and flow rate was changed to 100 µmol s^{-1}, A and g_s was left to stabilise before recording. Flow rate was decreased with the intention that more discrete CO_2 and H_2O differentials, expected at low reference CO_2 steps, were measured accurately (Li-Cor 2012). After the measurement was taken the program was resumed and flow rate returned to 200 µmol s^{-1}.

After the ambient O_2 A/C_i curve was completed, CO_2 reference was returned to 400 µmol mol^{-1} and a low oxygen supply of 2% O_2 / N_2 gas was fed through a humidifier and connected to the air inlet on the LI-COR. Using a flowmeter and regulator, the gas flow

was maintained between 1.7 and 1.8 L min^{-1}. The change in O_2 supply was entered into the LI-COR calibration system. Leaves were left for 10 minutes to acclimatise and then the automated A/C_i curves were replicated under the low O_2 supply. Once the second curve was complete, the protocol for measurement of respiration in the dark (R_{DARK}) was followed using the method described in Bellasio *et al.* (2014b). The actinic chamber light was switched off, the reference CO_2 was set at 550 µmol mol^{-1} and flow rate was changed to 50 µmol s^{-1}, the CO_2 concentration was increased to reflect the ambient laboratory environment and minimise diffusive leaks (Bellasio *et al.* 2014b; Boesgaard *et al.* 2013). Leaves were left 5 - 10 minutes before the measurement was recorded at a steady state. Using the above procedure the time needed for one complete replicate was roughly 90 - 120 minutes, largely depending on the acclimatisation time required for each leaf.

Chamber Leak Test

Running A/C_i curves requires working with chamber CO_2 concentrations that are very different from the external environment. Large gradients increase the risk of diffusive leaks of CO_2 through the gaskets of the chamber, leading to error prone measurements of A and C_i (Flexas *et al.* 2007; Long & Bernacchi 2003; Rodeghiero *et al.* 2007). To correct for erroneous measurements a method for CO_2 leak correction was followed from Flexas *et al.* (2007). Paragon flag leaves were collected from the boundary rows of the field plot and thermally denatured by boiling in water for 3 minutes. Leaves were checked for the absence of biologically meaningful chlorophyll fluorescence using the LI-COR. The denatured leaf was then run through the steps of the A/C_i curves (Figure 1-4). This protocol was completed weekly during the period of measurements, in total seven denatured leaves were measured and the mean apparent A values calculated for each step. All the A/C_i curves in the trial were corrected, by subtracting the mean apparent A values for the denatured leaves from the recorded CO_2 reference concentrations of each step.

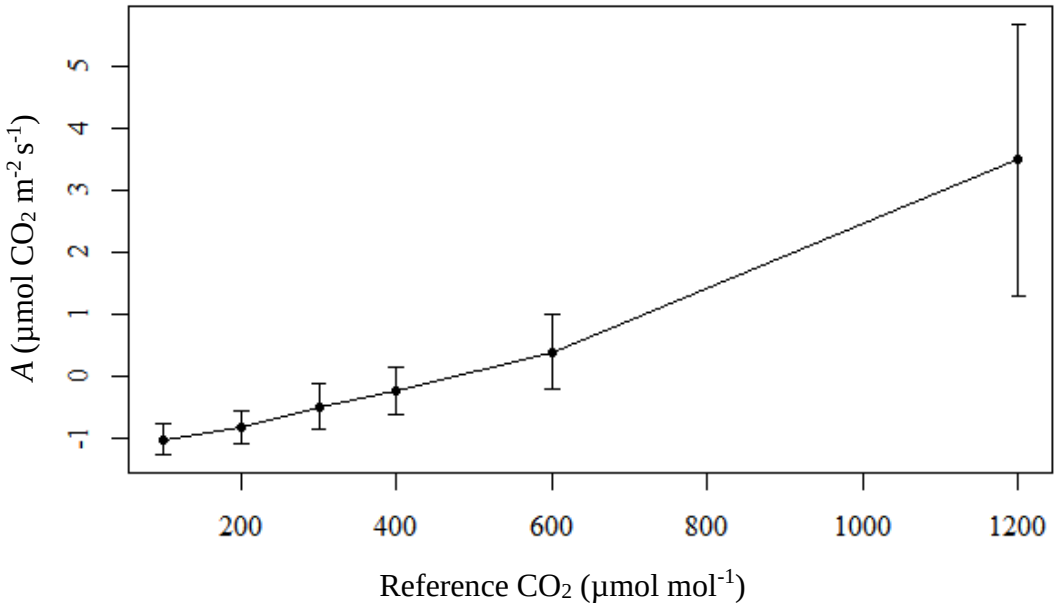

Figure 1-4 – Apparent CO_2 assimilation (*A*) mean values of denatured leaves against each CO_2 reference step used in the *A/Ci* curve protocol. These mean values were used for the CO_2 leak correction at each CO_2 reference step following Flexas *et al.* (2007) . Error bars represent standard deviation (n = 7).

Leaf Area Image Analysis

Leaves were cut off from each tiller at the leaf sheath. Each leaf was imaged against a plain background and weighed down with a sheet of clear cellophane, a ruler was included in each image for scale (Figure 1-5). The images were analysed using ImageJ (V - 1.51, Abràmoff *et al.* 2004) for flag leaf area (FL_A).

a).

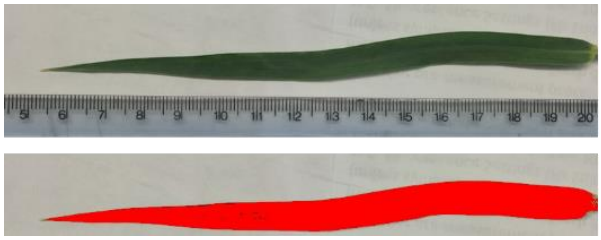

b).

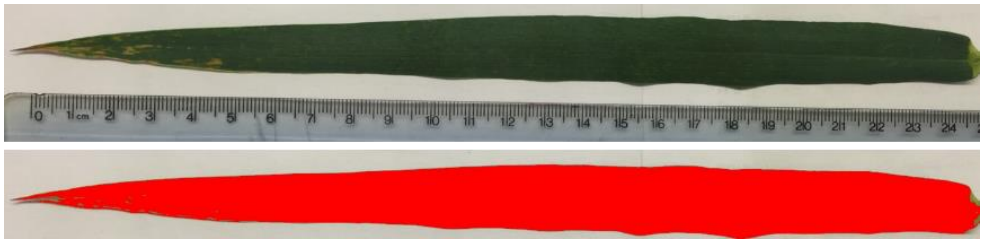

Figure 1-5 – Images of flag leaves of dic71 (a) and Paragon (b) from the 2016 field trial taken against a white background. Colour thresholds were altered for estimations of flag leaf area (FL_A), leaf area selection is shown highlighted in red. The scale shown is in cm.

Chlorophyll Content Measurement

Flag leaf chlorophyll content (*Chl*) was determined using a CCM-300 Chlorophyll Content Meter (Opti-Sciences, Inc. Hudson, USA). Three technical replicates of *Chl* readings were taken half way up each flag leaf; the three readings were then averaged.

Dry Matter Analysis

A 0.44 cm^2 borer was used to take two tissue cores, half way up each flag leaf. Cores were placed in previously labelled and weighed Eppendorf tubes and were immediately weighed to obtain fresh weight (*FW*). Losses in leaf dry matter can be observed during a saturation phase of 24 hours, which can be reduced by storage at low temperatures in the dark (Barrs & Weatherley 1962). Therefore, the leaf cores were hydrated in deionised water for 24 hours, then stored in the dark at 4 ºC. The cores were plotted on tissue paper and a fully saturated weight was then taken (*SW*) before placing in the oven for 48 hours at 60 ºC. Dry weight measurements were then taken (*DW*). Using these weight measurements, Relative Water Content (*RWC*) was derived following Barrs & Weatherley (1962):

$$RWC(\%) = \frac{(FW - DW)}{(SW - DW)} \times 100$$

Specific Leaf Area (*SLA*) was calculated following Garnier *et al.* (2001):

$$SLA\left(cm^{-2}\,g^{-1}\right) = \frac{LC_{area}}{DW}$$

Where LC_{area} is area of leaf core taken, which was 0.88 cm^2.

The leaf cores were ground to a fine powder and ~0.5 mg of the tissue was transferred into 8 mm x 5 mm tin capsules for each sampled leaf. Percentage N content ($N_{\%}$) and carbon isotope composition ($\delta^{13}C$) was analysed at the Godwin Laboratory (Department of Earth Sciences, University of Cambridge) using a Costech Elemental Analyser (Costech Analytical Technologies, Inc., Valencia, USA) and a DELTA V Isotope Ratio Mass Spectrometer (Thermo Scientific, Massachusetts, United States). The parameter $\delta^{13}C$ was calculated following Farquhar *et al.* (1982):

$$\delta^{13}C\ (‰) = \left(\frac{R_{sample}}{R_{standard}} - 1\right) \times 100$$

Where R_{sample} and $R_{standard}$ are the ratios of ^{13}C to ^{12}C, within the sample and a universal standard (Pee Dee Belemnite) respectively. Again following Farquhar *et al.* (1989), carbon isotope discrimination ($\Delta^{13}C$) was then calculated by:

$$\Delta^{13}C = \frac{\delta_{source} - \delta_{product}}{1 + \delta_{product}}$$

Where δ_{source} and $\delta_{product}$ are the $\delta^{13}C$ of atmospheric air and the leaf sample respectively. Atmospheric air δ^{13} for field grown plants was assumed to be -8 ‰ (Farquhar *et al.* 1989).

Leaf Cross Sectioning for Intercellular Airspace Analysis.

On an undamaged central section of each flag leaf, 3 x 1 mm thin strips were cut using a scalpel. Under a fume hood, the strips were transferred into a pre-prepared solution 4% paraformaldehyde + 2.5% glutaraldehyde in a 0.05 M phosphate buffer. Leaves were stored in this solution at 4 ºC for 1 - 2 months (depending on sampling date). On the 26th to the 27th of July the samples were washed in deionised water for 30 minutes in three repeated steps and stored in 50% ethanol at 4 ºC. On the 16th of August cross sections were trimmed to 2 mm in length and then taken through a series of 45 minute dehydration steps of 60, 70, 80 and 90% ethanol, then stored overnight in a solution of 95% ethanol and 0.1% eosin. The following day, samples were washed in three 45 minute steps with 100% ethanol. Samples were infiltrated and embedded using the Technovit7100 embedding medium (Kulzer GmbH, Wehrheim, Germany) and allowed to polymerise overnight. Resins were heated and trimmed, then mounted to a wooden block.

An electronic rotary microtome (HM 340E, Thermo Scientific) was used to trim 2 µm sections of the mounted samples, blades were hand-cut with a diamond cutter from microscope slides. Sections were mounted to clean microscope slides with a droplet of water. The mounted leaf sections were then stained with filtered 0.1% toluidine blue for three minutes, before the stain was washed off. Slides were saturated with DI water for 5 minutes to remove residue stain. The slides were then imaged using an Olympus BX41 light microscope (Shinjuku, Tokyo, Japan) and a Micropublisher 3.3 RTV camera (QImaging, Surrey, BC, Canada). An example of the images taken is shown in Figure 1-6.

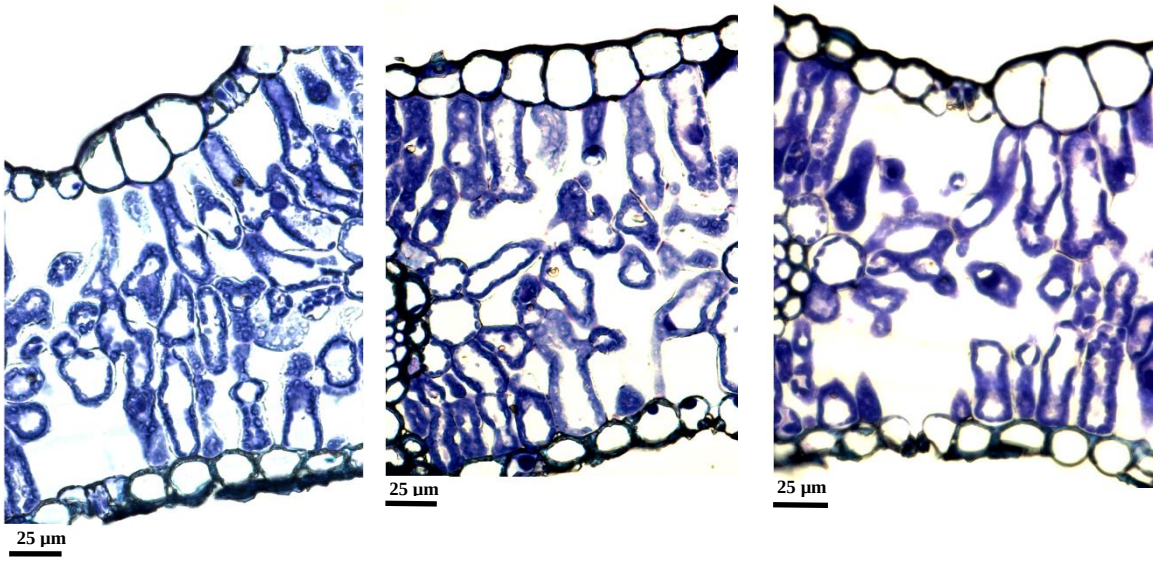

Figure 1-6 - Example flag leaf cross section images produced from the 2016 field trial. All images shown were taken at 60x magnification of mesophyll regions several veins down from the main vein. These images were used to estimate percentage mesophyll intercellular airspace. The scale bar shown is 25 µm.

ImageJ (V - 1.51) was used for the image analysis. On 60x images taken in mesophyll regions 1 to 4 veins down from the main vein, 4 x 5625 μm^2 squares were overlaid on the images. The mesophyll regions excluded the palisade cell layer (treated as the row of cells closest to the upper epidermis) and bundle sheath cells. Substomatal cavities were included if they fell within the square. Percentage airspace coverage was calculated within each square using the freehand selections tool to highlight individual airspace regions and calculate the area (Figure 1-7). A Wacom Intuos CTL-490 (Wacom Co., LTD, Saitama, Japan) pen tablet was used for precision in the freehand selections. Percentage airspace coverage of the four squares was then averaged to give a percentage mesophyll airspace value *(% airspace*) for each line.

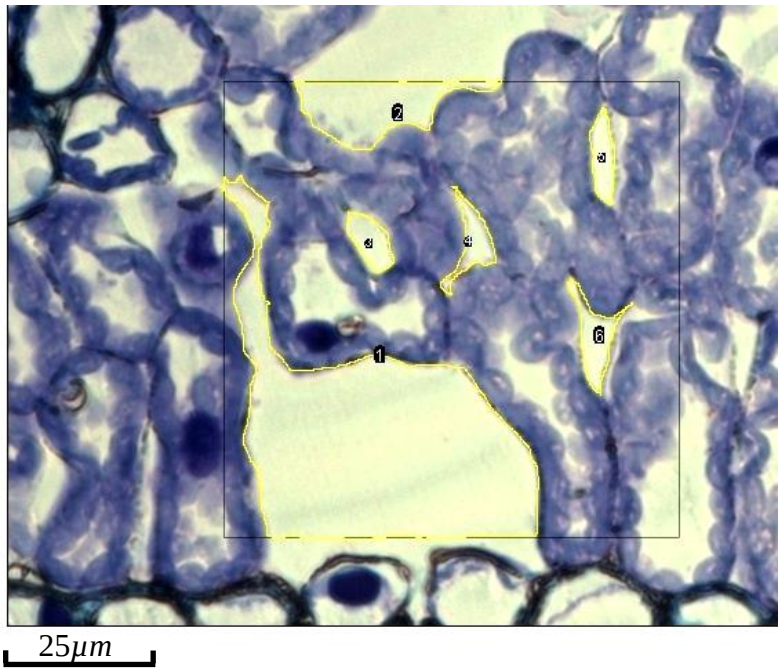

Figure 1-7 – An example of the analysis used to estimate the percentage of the mesophyll occupied by airspace. Freehand selections of airspaces are shown in yellow, these selections were drawn using a Wacom Intuos CTL-490 (Wacom Co., LTD, Saitama, Japan) pen tablet. Percentage airspace was determined in an overlaid 75 x 75 µm square (shown by the black square). The scale bar shown is 25 µm.

Yield Component Analysis

Once maturity had been reached, between the 15th to the 25th of August 2016, each individual plant was cut off at ground level. Prior to cutting, the plants were bagged within a perforated clear bag to prevent loss of seed through ear shattering. Plants were stored for several weeks under cover, before an above-ground biomass measurement was taken per plant at a field dried weight. Total tiller number and number of fertile tillers were counted and ears were removed. Five plants were processed for each of the 6 lines used in the cross sectioning analysis (dic71, Paragon, Robigus, Tios and dic12b). However, only four replicates were available for dic72. The plants used in the yield analysis were not necessarily the same replicates used in the gas-exchange analysis, as plants with the fewest missing tillers were selected. All the ears were hand threshed and the seed was cleaned manually. Seed weight was taken and grain yield data were expressed as g plant^{-1}. Harvest index (*HI*) was then calculated as the proportion of total grain mass to plant mass.

The number of missing tillers was recorded per plant, for instance where one had been cut off during the gas-exchange measurements or broken during the removal of plants

from the field. The missing tillers were corrected for by calculating seed weight per ear (total seed weight / fertile tiller number). Then adding the calculated seed weight per ear to the overall total seed weight for each missing tiller. The maximum recorded missing tillers for the plants used in the analysis was, however, 1.

2016 Field Trial - Analysis.

Calculation of g_m

The variable *J* method is a commonly used estimation to calculate mesophyll conductance to CO_2 (g_m) following the Harley *et al.* (1992) model:

$$g_m = \frac{A}{C_i - \frac{\Gamma^*(J+8(A+R_L))}{J-4(A+R_L)}}$$

Where Γ^* is the CO_2 compensation point in the absence of respiration in the light (R_L) and *J* is the non-calibrated rate of photosynthetic electron transport. Calculations of g_m are sensitive to errors in estimations of Γ^* (Harley *et al.* 1992; Martins *et al.* 2013). Alonso *et al.* (2009) calculated that flag leaves of spring wheat had an average $\Gamma^*$of 32.0 µmol mol^{-1} (standard error = 0.6) when measured at 25 ºC. An evaluation was completed in this study to test the effect of using the fixed value of 32.0 µmol mol^{-1} in comparison to estimating Γ^* through A/C_i curve fitting for each individual replicate. The Bellasio *et al.* (2016) Excel based fitting tool was used to determine Rubisco specificity factors ($S_{C/O}$) for all the replicates of six lines (Paragon, Robigus, dic71, dic72, Tios and dic12b). Then following Bellasio *et al.* (2016) and Martins *et al.* (2013) Γ^* was estimated using:

$$\Gamma^* = 0.5O/S_{C/O}$$

where O is the ambient O_2 concentration (210000 µmol mol^{-1}). There were no significant differences in Γ^* across the subset of lines, which was determined using a one-way ANOVA (F (5, 23) = 0.3, P = 0.91). Furthermore, there were no significant differences in estimates of mean g_m when using the Alonso *et al.* (2009) fixed value or the curve fitting estimate of Γ^*, as determined using a Welch Two Sample t-test (t (9.7) = -0.37, P = 0.72). However, when using the individual curve fitting estimate of Γ^*, standard deviation increased within each line (Table 1-4) and the amount of erroneous g_m estimations increased. For instance, one replicate of dic71, dic72 and of Tios was unusable due to unrealistically high or low g_m for every step of the curve. The curve fitted

values of Γ^* were averaged across the subset of lines: mean = 33.4 µmol mol^{-1} and *S.D* = 12.5. Although very varied, the calculated mean was close to the Alonso *et al.* (2009) value of 32.0 µmol mol^{-1}. Therefore, the Alonso *et al.* (2009) fixed value of 32.0 µmol mol^{-1} was used for each estimate of g_m. Fixed values of Γ^* have been used in other studies and in C3 plants Γ^* has been considered relatively invariable (Warren 2006).

Table 1-4 - A comparison determining how the use of a fixed value of Γ^* (taken from Alonso et al., 2009) influenced g_m calculations, compared with using estimations of Γ^* through the Bellasio *et al.* (2016) fitting tool. For each step of the A/C_i curves, g_m was calculated using the Harley *et al.* (1992) model with a calibrated electron transport value (J_{CAL}) following Bellasio *et al.* (2016). There were 4 - 5 replicate A/C_i curves used for each of the six lines in the comparison. Means values and standard deviation are shown.

	g_m (Γ^* = 32.0)			g_m (Γ^* = curve-fitting)		
Trait	*n*	*Mean*	*S.D*	*n*	*Mean*	*S.D*
dic12b	4	0.31	0.04	*4*	*0.45*	*0.25*
dic71	5	0.51	0.10	4	0.35	0.19
dic72	5	0.39	0.11	4	0.37	0.18
Paragon	5	0.32	0.05	5	0.43	0.16
Robigus	5	0.26	0.07	5	0.30	0.09
Tios	5	0.22	0.06	4	0.23	0.10

Trait units: g_m = mol CO_2 m^{-2} s^{-1} ; Γ^* = µmol mol^{-1}

The accuracy of g_m estimations can also be influenced by error in *J* calculations (Harley *et al.* 1992; Martins *et al.* 2013). Quantum yield of photosystem II (Φ_{PSII}) is determined by the LI-COR following Genty *et al.* (1989):

$$\Phi_{PSII} = (F_m' - F_s') / F_m'$$

Where, within a light adapted leaf, a saturating light pulse is used to diagnose a maximal fluorescence reading (F_m') and another reading is taken during steady-state fluorescence (F_s'). Then *J* is calculated by the LI-COR following:

$$J = \Phi_{PSII} \times PPFD \times \alpha \times \beta$$

Where PPFD is the photosynthetic photon flux density, α is the absorbance of the leaf and β is the partitioning of energy between the two photosystems (Tomás *et al.* 2014). However, there can be inaccuracies associated with assumptions linked to this model (Martins *et al.* 2013). The assumption that α and β remain constant can be discredited by electron demand to alternative sinks (Bellasio *et al.* 2016). The parameter *J* can be calibrated under non-photorespiratory conditions (Warren 2006), these techniques do not rely on the previously mentioned assumptions and provide a better estimate of actual

biochemical leaf adenosine triphosphate demand (Bellasio & Griffiths 2014). Therefore, a method for determining a calibrated rate of electron transport (J_{CAL}) to photorespiration activity was used for each step of the A/C_i curves following Bellasio *et al.* (2016):

$$J_{CAL} = 4GA \frac{\Phi_{PSII\,amb}}{\Phi_{PSII\,low}}$$

Where $\Phi_{PSII\,amb}$ and $\Phi_{PSII\,low}$ is Φ_{PSII} measured under ambient and low O_2 concentration respectively. Gross Assimilation (GA) was calculated following Bellasio *et al.* (2014):

$$GA = A_{low} + R_L$$

Where A_{low} is A at each step of the low O_2 concentration A/C_i curve. In order to predict R_L, respiration in the dark (R_{DARK}) was measured for each leaf as an adequate estimation (Bellasio *et al.* 2014b; Tomás *et al.* 2013).

Finally, using the J_{CAL} values, g_m was calculated with the Harley *et al.* (1992) model for each step of the ambient oxygen A/C_i curve. The g_m values were averaged across the steps to provide a g_m value per leaf. The A/C_i steps of 100 and 1200 ppm CO_2 were excluded from the average, as the risk of unrealistic values of g_m increase at high or low C_i (Martins *et al.* 2013). Furthermore, following Martins *et al.* (2013) only g_m values which were between 0 and 1 where included in the average.

A/C_i Curves

The parameters of A, g_s, C_i, E and Φ_{PSII} were taken from the first step (400 ppm CO_2) of the ambient O_2 A/C_i curve, as measurements of photosynthetic components at ambient CO_2 conditions. The J_{CAL} values shown in the results were calculated from the first step of both the ambient and low O_2 A/C_i curves, using the method described in the g_m calculation. The maximum photosynthetic rate (A_{max}) was taken from the 1200 ppm CO_2 step of the ambient O_2 curve. A and E were also expressed on a per leaf basis: A (leaf^{-1}) and E (leaf^{-1}), respectively, by multiplying A or E by the imaged area for each leaf.

Following Bellasio *et al.* (2016), A/C_i curves under different oxygen concentrations were fitted for a subset of lines in the 2016 field trials (Paragon, Robigus, Tios, dic12b, dic71 and dic72). The curve fitting was completed to extract the carboxylation efficiency for CO_2 fixation at ambient O_2 (CE_{amb}) and $S_{C/O}$.

Measurement Time

Gas-exchange measurements were taken from 0900 to 1800. Care was taken to prevent any measurement bias, ensuring replicates of each line were measured at sporadic times during different days. To test for potential bias caused by measurement timings and circadian clock effects, the *A* results were separated into different groups based on the time of day measurements were taken. The groups consisted of early morning (0900 - 1100), midday (1100 - 1300), early afternoon (1300 - 1500) and late afternoon (1500 - 1800). Due to the unbalanced design a type II ANOVA was completed in RStudio (V-3.4.3) with the 'car' package to test for potential variation in *A* between the measurement time groups (https://CRAN.R-project.org/package=car). There was no evidence of significant variation (F (3, 61) = 0.66, P = 0.58). However, chamber acclimatisation took longer during the late afternoon time period (visual observations).

Replicate Number

A small proportion of the measured A/C_i curves were unusable in the g_m calculations due to a technical error or g_s depletion. The technical error was caused by an IRGA match recovery issue, which sporadically influenced some of the A/C_i curve steps over 2 measurement days. Spread across 6 lines, there were 8 replicates out of the total 69 measured that were influenced by the error. The specific steps of each curve affected by the error were easily distinguishable. Therefore, although the affected curves were not used in the g_m calculations, where the error had not influenced the ambient O_2 A/C_i curve steps of 400 ppm and 1200 ppm CO_2, the data were still used to extract other gas-exchange traits of interest (Table 1-5). In some replicates there was g_s depletion after the ambient O_2 A/C_i curve had been completed, this meant the low O_2 A/C_i curve was not utilised. Although no g_m calculations were made from these replicates, the ambient A/C_i curve was still used to extract the other gas-exchange parameters of interest.

Table 1-5 - The number of useable A/C_i curves measured in the 2016 field trial for the parameters extracted from the 400 ppm CO_2 step, the 1200 ppm CO_2 step and for the g_m and J_{CAL} calculations, in comparison to the total taken. CE_{AMB} was estimated through A/C_i curve-fitting.

Line	Species	Total A/C_i curves	400 ppm CO_2	1200 ppm CO_2	g_m and J_{CAL}	*Curve fitting*
18209	*T. dicoccum*	5	5	5	5	-
67-1	*T. durum*	6	6	4	3	-
dic007	*T. monococcum*	5	5	5	5	-
dic12b	*T. dicoccum*	5	4	5	4	4
dic71	*T. dicoccoides*	6	6	6	5	5
dic72	*T. dicoccoides*	6	6	5	5	5
Hoh501	*T. durum*	6	4	4	4	-
Paragon	*T. aestivum*	6	6	6	5	5
Robigus	*T. aestivum*	6	6	6	5	5
SHW008	*T. aestivum*	6	5	6	4	-
SHW012	*T. aestivum*	6	6	5	3	-
Tios	*T. dicoccum*	6	6	6	5	5
Total	-	69	65	63	53	29

The majority of leaves used in the gas-exchange analysis were measured for the other physiological parameters (Table 1-6).

Table 1-6 - The number of replicates per line used for the other measured parameters in the 2016 field trial.

Line	Species	FL_A	$\Delta^{13}C$	$N_{\%}$	*RWC*	*SLA*	*Chl*	*A* (leaf^{-1})	*E* (leaf^{-1})
18209	*T. dicoccum*	5	5	5	5	5	5	5	5
67-1	*T. durum*	4	4	4	2	4	4	4	4
dic007	*T. monococcum*	5	5	5	5	5	5	5	5
dic12b	*T. dicoccum*	5	4	4	4	4	5	4	4
dic71	*T. dicoccoides*	6	6	6	6	6	6	6	6
dic72	*T. dicoccoides*	6	6	6	5	5	6	6	6
Hoh501	*T. durum*	6	6	6	6	6	6	4	4
Paragon	*T. aestivum*	6	6	6	6	6	6	6	6
Robigus	*T. aestivum*	6	6	6	5	6	6	6	6
SHW008	*T. aestivum*	6	6	6	6	6	6	5	5
SHW012	*T. aestivum*	6	6	6	6	6	6	6	6
Tios	*T. dicoccum*	6	6	6	6	6	6	6	6
Total	-	67	66	66	62	65	67	63	63

Statistical Analysis.

All analysis was completed in RStudio (V - 3.4.3). One-way analysis of variance models (ANOVA) were fitted to test for significant variation in each trait across the lines. In the cases of an unbalanced design, where the number of replicates per line varied, a type II ANOVA was used instead with the 'car' package. However, this had little influence on the overall results. Residuals were extracted from each model and assumptions of normality were checked using a Shapiro-Wilk test. Where assumptions were violated, the non-parametric Kruskal-Wallis Rank Sum test was used in the place of an ANOVA. Homogeneity of variance was tested using a Bartlett's test. Where a non-parametric test was used, homogeneity of variance was tested using a Levene's test, which is part of the 'car' package. As the assumptions of homogeneity of variance was violated in the grain yield data (Figure 1-19), a log transformation was used to stabilise sample variance before statistical analysis. In Figure 1-11 (b), Figure 1-14 (b) and Figure 1-16 (b) a Duncan's new multiple range post-hoc test was used to determine significance grouping to aid visual comparisons. The Duncan's test is part of the 'agricolae' package (https://CRAN.R-project.org/package=agricolae).

Trait correlation matrices were created using the mean values of each of the 12 lines and Pearson's correlation. The matrices were formed using the RStudio (V - 3.4.3) package 'corrplot' (https://CRAN.R-project.org/package=corrplot). Finally, where described, multiple linear regression models were fitted to identify trait relationships not shown in the matrices.

2017 field trial

Material Sampling

On the 25th and the 26th of May 2017, gas-exchange measurements were made on healthy leaves of main tillers. The plants were ranging in growth stage from GS37 - 47, the majority of measurements were made on flag leaves, except Tios and Robigus, where the youngest fully expanded leaf was measured, as the flag leaf was not fully expanded. Measurements were made between 11:00 to 15:00, on sunny clear days. Four replicates of different plants were measured per line. Measurements were completed on 9 offspring lines, both *T. dicoccoides* parents, the hexaploid parent Paragon, the tetraploid mapping parents described in Chapter 3 and Robigus. As technical replicates, all lines of dic71 and dic72 were measured on both days. Furthermore, 2 replicates of Paragon and 3 of Robigus were measured on both days. These repeats were averaged over both days for the analysis.

Gas-exchange Measurements.

A LI-COR-6400XT with a 2 x 3 cm standard LED head was used for the measurements made in the field. Chamber conditions were set to reflect the ambient environment. A CO_2 reference of 400 µmol mol^{-1} was set. Humidity control was fully bypassed and ambient conditions were used, which fluctuated between 40 to 55% relative humidity. The PPFD was set to 1500 µmol m^{-2} s^{-1} (90% red and 10% blue light), which was shown to be near-saturating for field grown flag leaves in the 2016 field trial. Gas flow rate was set to 500 µmol s^{-1}, block temperature was controlled at 23 ºC and the leaf chamber fan was set to fast. Leaves were measured half-way up, with the adaxial side facing the internal chamber light source. The leaves were left within the chamber to acclimatise for 2 - 3 minutes, until steady-state *A* and g_s was reached. The IRGAs were matched before each measurement. Where a leaf did not fully cover the 6 cm^2 gasket area, the width of the central leaf region measured in the chamber was taken and multiplied by the gasket length (3 cm). Results were then recalculated on the new area basis.

From this gas-exchange analysis, CO_2 assimilation expressed on a per unit basis was used (*A*). Assimilation data were also calculated on a total leaf basis, *A* ($leaf^{-1}$), by multiplying the mean *A* measurement by mean leaf area measurements for each line.

Leaf Area Measurements.

The main tiller flag leaf length and width was recorded on the first four plants to reach anthesis (GS61) of each line used in the gas-exchange analysis. Flag leaf area was then estimated using the Teare & Peterson (1971) equation which is discussed further in Chapter 3. Due to the difference between measurement timings, the area measurements were not necessarily completed on the same leaves or plants as the gas-exchange analysis.

Stomatal Density

On the 4 plants not used for area measurements in each mini-plot, flag leaf stomatal density was estimated for dic71, dic72, Paragon and Robigus at GS61 on main tillers. A droplet of Loctite Power Flex Ehyl-2-Cyanocrylate (Loctite, Düsseldorf, Germany) was dispensed onto a labelled frosted microscope slide. Halfway up the flag leaf, on an undamaged mesophyll section, the abaxial surface was firmly pressed to the glue on the slide for ~ 30 seconds. Slides were imaged using a Leica DM2500 Optical Microscope (Leica Biosystems, Nussloch, Germany) at 5x magnification. Using the Leica Application Suite software, one image was taken of a uniform mesophyll area for each leaf impression, avoiding damage and the main vein.

Using ImageJ (V - 1.51) a 0.3 mm^2 square grid was imposed on to each image. Stomata were counted from the 5x images in three different 0.3 mm^2 overlaid grid squares, the mean values were taken and stomatal density was calculated per mm^2 (S_D).

Yield Analysis.

The plants used for leaf area measurements were covered in a perforated plastic bag close to harvest (30th of July 2017) to prevent any potential ear loss or fragmentation. The *T. dicoccoides* lines were bagged at a slightly earlier date to prevent spikelet loss due to ear shattering. The plants were pulled out of the field on the 3rd – 4th of August and transported to a drying wall for 72 hours before storage.

Roots were subsequently removed and the remaining samples were weighed for biomass. Fertile and non-fertile tillers were counted; ears were then removed for threshing. The *T. dicoccoides* lines were all hand threshed. The offspring and bread wheat lines were threshed through a LD350 laboratory thresher (Wintersteiger, Ried im Innkreis, Austria), care was taken not to lose any seed in this processing. As described for the 2016 field trial, seed was weighed for grain yield and *HI* was calculated. There were four replicates per line, apart from dic72 where only three replicates were taken.

Statistical Analysis

The same methodology of statistical analysis was followed from the 2016 field trial. A large potential outlier was present in the *A* data for the line 31_12K (49.5 µmol m^{-2} s^{-1}, shown in Figure 1-20), this data point was removed in the ANOVA testing for significant variation in *A* across the different lines, as it caused violations of the assumptions of normality. This had little effect on the overall results of the ANOVA, the possible outlier was included in all other parts of the analysis and results. When testing for variation across line, the assumption of residual normality was violated in the 2017 grain yield results (Figure 1-22), therefore, a Kruskal-Wallis Rank Sum test was used instead of an ANOVA.

In both the 2016 and 2017 field trial results, the bar graphs are presented with ranked mean values, from minimum to maximum, to aid visual comparisons between the extremes of the data. In all Chapters in this study, box plots are used to present data across both trials. The lower and upper hinge of each boxplot represents the first and third quartile, respectively. The median is also shown and the whiskers expand to the extremes of the data, unless an individual data point is 1.5 times the box length outside the inner quartile range, where that data point is marked by a black dot, representing a possible

outlier (R Core Team 2017). Additionally, red dots are overlaid on the boxplots to show primary data points. A slight random jitter has been applied to the red dots, so individual points are distinguishable.

1.3 Results

1.3.1 The 2016 field trial

CO_2 Assimilation

Across the collection of wheat lines measured in the 2016 field trial, there was significant variation observed in both flag leaf *A* at ambient CO_2 (F (11, 53) = 5.1, P = < 0.001) and flag leaf A_{max} (F (11, 51) = 3.0, P = 0.004). The ranked mean values for the assimilation traits are shown in Figure 1-8, where the *T. dicoccoides* line dic71 had the highest mean flag leaf *A* and A_{max}, 33.8 µmol CO_2 m^{-2} s^{-1} ($S.D$ = 2.4) and 47.9 ($S.D$ = 6.4), respectively. The dic71 line had a 36.2% and 52.6% higher mean *A* than the bread wheat lines Paragon and Robigus. The other *T. dicoccoides* line studied, dic72, had the second highest *A* (27.9 µmol CO_2 m^{-2} s^{-1}), but also the largest variation of the mean with a standard deviation of 8.9. The *T. dicoccum* line dic12b had the second highest mean A_{max} (45.5 µmol CO_2 m^{-2} s^{-1}, $S.D$ = 5.9), whereas the *T. dicoccum* line 18209 had the lowest mean *A* and A_{max}. Across the collection of lines there was a larger range in mean values of *A* compared to A_{max}, 15.8 µmol CO_2 m^{-2} s^{-1} compared to 13.5 respectively.

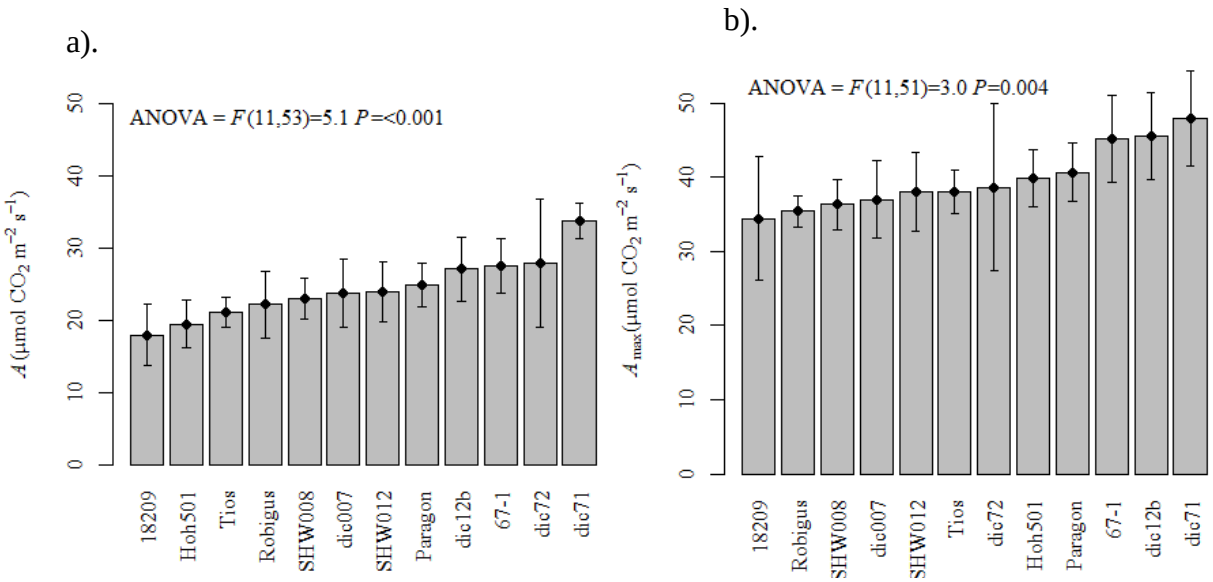

Figure 1-8 – Mean values of flag leaf CO_2 assimilation values extracted from the ambient O_2 A/C_i curves of the 2016 field trial, shown at 400 ppm CO_2 (a) and at 1200 ppm CO_2 (b). Error bars show standard deviation. The ANOVA results are overlaid on each graph, indicating significant variation across lines. Sample size for each line is shown in Table 1-5.

An example of the *A*/*C*$_i$ curves recorded during the 2016 field trial is shown in Figure 1-9, for the lines: dic71, Paragon and Tios.

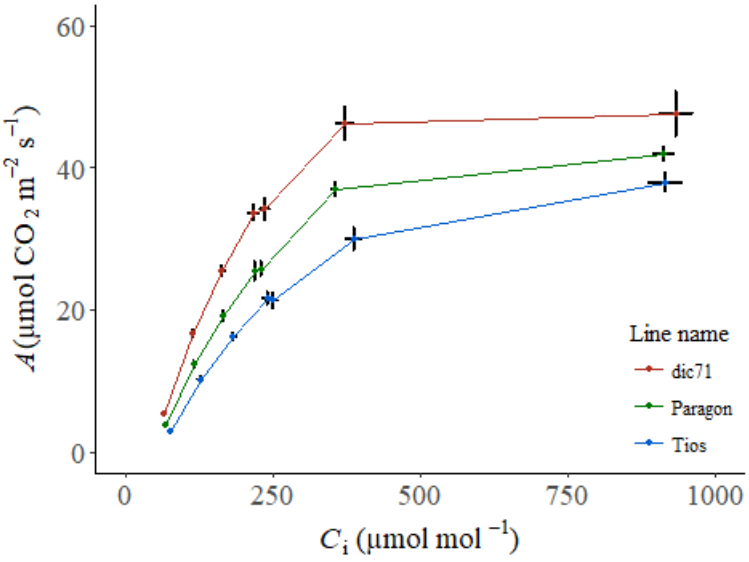

Figure 1-9 - Example *A*/*C*$_i$ curves taken at ambient O_2 for the lines dic71 (*T. dicoccoides*), Paragon (*T. aestivum*) and Tios (*T. dicoccum*) from the 2016 field trial. Each point reflects mean values of *A* and *C*$_i$ for each line. Standard error bars are shown (n = 5).

Supply Components.

The correlation matrix shown in Figure 1-10 provides an indication of which photosynthetic supply traits were linked to the variation in *A*. Significant correlations were observed between *A* and 6 supply component related traits, which were all positively correlated. Strong correlations with *A* were observed for J_{CAL} and Φ_{PSII} (Pearson's correlation (r) = 0.92 and 0.86, respectively). The lines with the highest J_{CAL} were the *T. dicoccoides* accessions dic71 and dic72 (Table 1-7). In comparison, Φ_{PSII} was highest in dic71, but dic72 had a 17.8% lower mean which was the median of the collection. Paragon had the highest mean *Chl* within the collection (515.3 mg m^{-2}, *S.D* = 37.2). There was some indication of a relationship between *Chl* and *A*, although the correlation test proved not to be statistically significant (r = 0.55 *P* = 0.06).

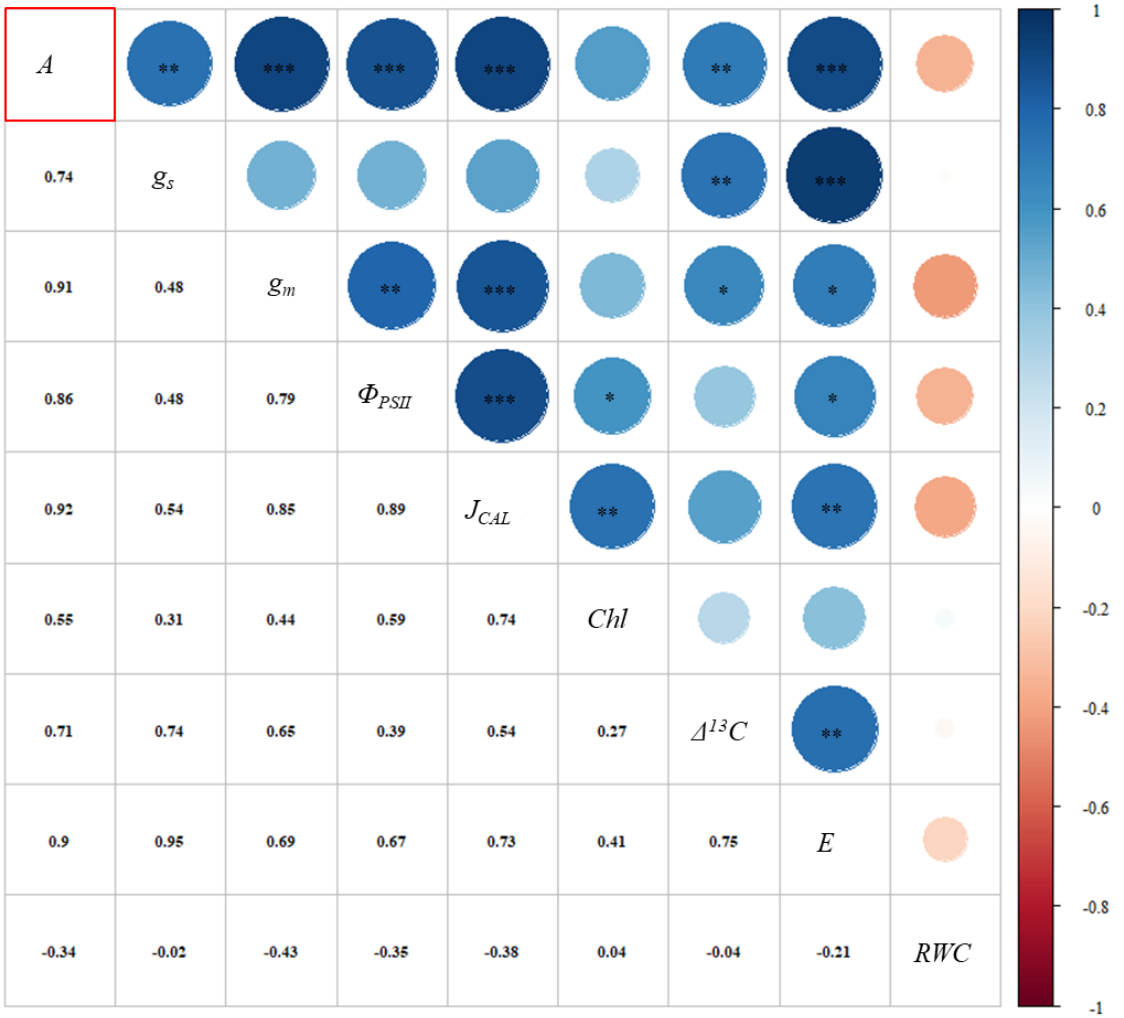

Figure 1-10 – Pearson's correlation matrix of photosynthetic supply traits measured in the 2016 field trial. Mean values were used for each of the 12 lines, values are shown in Table 1-7. The upper right-hand triangle shows a colour heat map of pairwise correlation coefficients and significance thresholds for each paired comparison (* $P < 0.001$; ** $P < 0.01$; * $P < 0.05$). The bottom left-hand triangle shows the actual values of Pearson's correlation coefficients for each paired comparison.**

The means and standard deviation values for the 8 photosynthetic supply traits from the 2016 field trial are shown in Table 1-7.

Table 1-7 - Mean values of the photosynthetic supply component traits for the wheat collection in the 2016 field trial. Standard deviation is shown (*S.D*). Gas-exchange derived measurements were taken from the *A*/*C*$_i$ curves, sample size for each line is shown in Table 1-5. The sample size of each line for the other traits is shown in Table 1-6.

	g_s		g_m		Φ_{PSII}		J_{CAL}		*Chl*		$\Delta^{13}C$		*E*		*RWC*	
Trait	*Mean*	*S.D*	*Mean*	*S.D*	*Mean*	*S.D*	*Mean*	*S.D*	*Mean*	*S.D*	*Mean*	*S.D*	*Mean*	*S.D*	*Mean*	*S.D*
18209	0.18	*0.07*	0.25	*0.05*	0.27	*0.06*	143.3	*37.5*	407.3	*61.9*	20.36	*1.04*	1.98	*0.61*	81.8	*4.9*
67-1	0. 31	*0.09*	0.38	*0.12*	0.35	*0.03*	212.5	*10.4*	469.0	*61.4*	20.93	*0.52*	3.00	*0.46*	74.9	*0.8*
dic007	0.41	*0.12*	0.23	*0.04*	0.30	*0.02*	170.0	*26.3*	445.7	*45.1*	22.18	*0.94*	3.26	*0.73*	87.9	*3.4*
dic12b	0.32	*0.06*	0.31	*0.04*	0.34	*0.03*	213.5	*32.4*	454.8	*63.1*	20.84	*0.61*	3.08	*0.43*	81.0	*7.6*
dic71	0.37	*0.06*	0.51	*0.10*	0.37	*0.02*	255.0	*25.4*	507.9	*23.2*	22.94	*0.66*	3.61	*0.56*	78.0	*4.9*
dic72	0.36	*0.14*	0.39	*0.11*	0.31	*0.08*	215.5	*57.2*	457.7	*77.8*	23.00	*0.73*	3.19	*0.86*	79.4	*5.4*
Hoh501	0.21	*0.09*	0.21	*0.02*	0.31	*0.03*	184.2	*14.1*	461.1	*27.2*	20.54	*1.12*	2.14	*0.63*	76.8	*4.9*
Paragon	0.28	*0.04*	0.32	*0.05*	0.31	*0.03*	214.2	*10.8*	515.3	*37.2*	21.25	*0.93*	2.73	*0.18*	86.0	*2.7*
Robigus	0.27	*0.07*	0.26	*0.07*	0.31	*0.05*	183.8	*20.4*	466.0	*30.9*	21.66	*0.91*	2.53	*0.46*	90.5	*3.3*
SHW008	0.29	*0.09*	0.23	*0.03*	0.30	*0.03*	180.1	*25.7*	473.6	*25.5*	21.28	*1.15*	2.70	*0.55*	83.2	*4.6*
SHW012	0.33	*0.11*	0.26	0.03	0.30	*0.02*	195.6	*29.5*	463.3	*44.1*	21.17	*0.71*	3.07	*0.93*	76.0	*14.0*
Tios	0.27	*0.08*	0.22	0.06	0.30	*0.02*	184.2	*6.4*	480.1	*44.5*	20.04	*0.52*	2.48	*0.42*	87.7	*3.4*

Trait units: g_s = mol H_2O m^{-2} s^{-1}; g_m = mol CO_2 m^{-2} s^{-1}; J_{CAL} = µmol e^- m^{-2} s^{-1}; *Chl* = mg m^{-2}; g_m = mol m^{-2} s^{-1}; $\Delta^{13}C$ = ‰; *E* = mol H_2O m^{-2} s^{-1}; *RWC* = %.

There was a significant positive correlation between *A* and g_s (r = 0.74 *P* = 0.006). As g_s and *E* are highly linked traits (r = 0.95 *P* = < 0.001), a strong correlation between *A* and *E* was also observed (r = 0.90 *P* = < 0.001). Significant variation was observed in g_s across the collection (*F* (11, 53) = 2.53, *P* = 0.012), although the highest mean was found in dic007 (0.41 mol H_2O m^{-2} s^{-1}, *S.D* = 0.12) which in comparison had a more medium ranked *A* (Figure 1-8). The *T. dicoccoides* also showed high g_s and *E*; mean g_s in dic71 was 32.2% and 36.5% higher than in Paragon and Robigus, respectively. Leaf impressions were taken in the 2017 field trial for the *T. dicoccoides* and bread wheat lines (Figure 1-11), dic71 and dic72 had significantly higher stomatal density compared to the bread wheat lines (*F* (3, 12) = 5.2, *P* = 0.02).

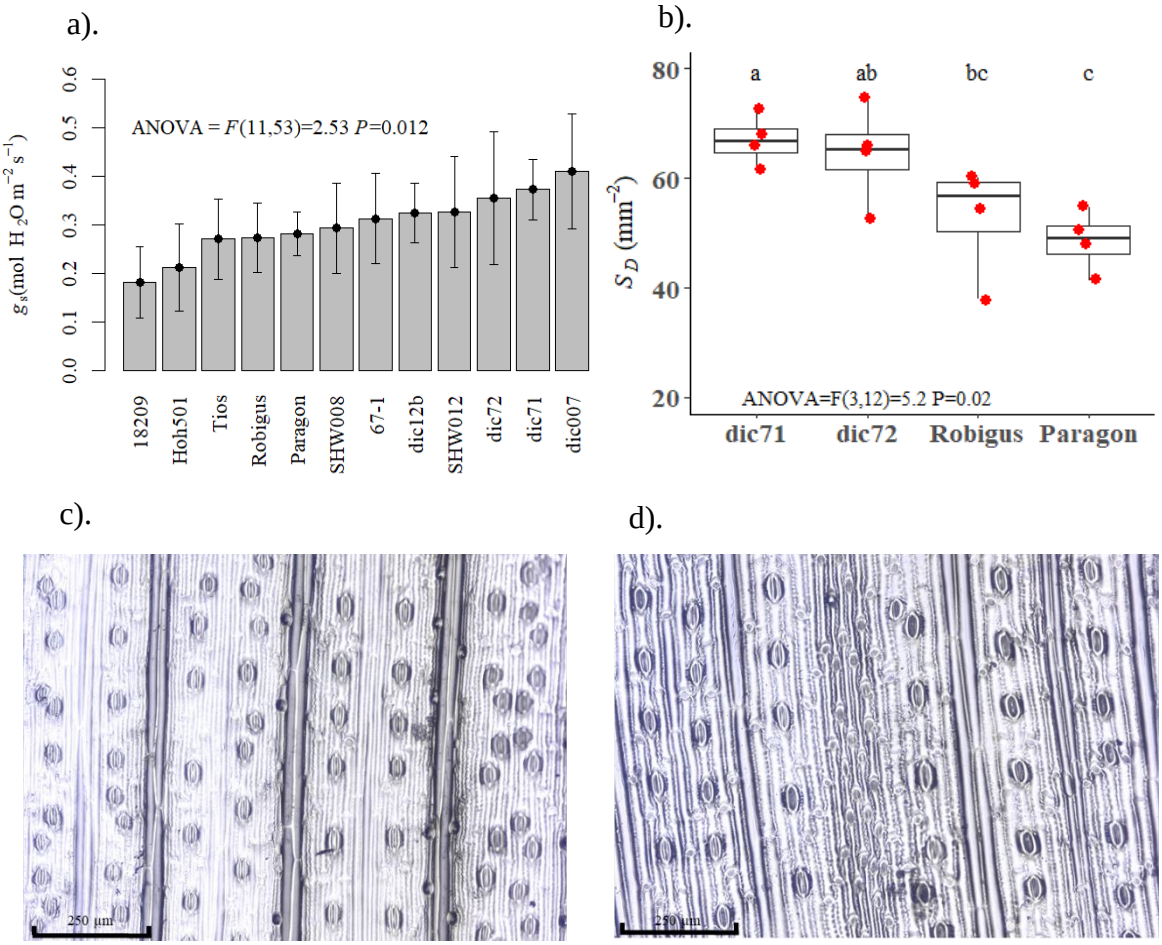

Figure 1-11 - a). A ranked mean comparison from the 2016 field trial for g_s measured at an ambient CO_2 concentration (400 ppm CO_2), standard deviation bars are shown and sample size for each line is shown in Table 1-5. ANOVA results are overlaid on the graph, indicating significant variation across lines. b). Abaxial surface flag leaf stomatal density counts taken on four replicates of four lines included in the 2017 field trial, ANOVA and Duncan's new multiple range test Post-hoc grouping is shown. Lastly, an example impression of the abaxial side of a flag leaf from dic71 (c) and Paragon (d) is shown, taken at 10x magnification.

As discussed, the *T. monococcum* line dic007 had the highest mean *E*, but had a mean *A* close to the median in the ranked comparison. Therefore, the high water loss and moderate *A* resulted in low *WUE* (Figure 1-12). *WUE* varied significantly across the collection (*F* (11, 53) = 2.1, *P* = 0.04). Despite having comparatively high *E*, dic71 had the highest mean *WUE* (9.49 µmol CO_2 (mmol H_2O)$^{-1}$, *S.D* = 1.13), which was driven by the high *A* (Figure 1-8).

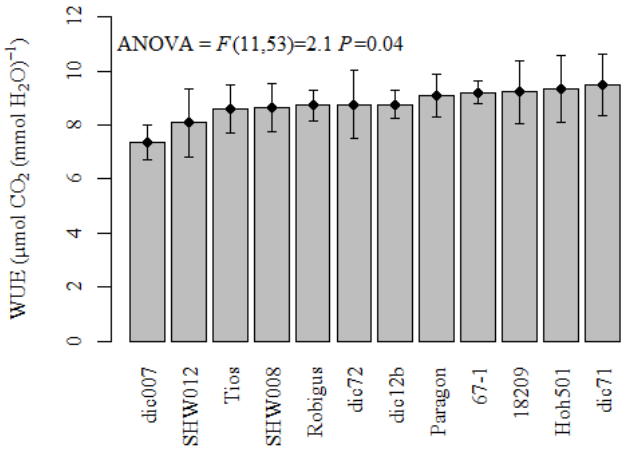

Figure 1-12 - Per unit instantaneous water use efficiency (*WUE*) taken from the first step of the *A*/*C*$_i$ curves from the 2016 field trial, mean values and standard deviation are shown. ANOVA results are overlaid on the graph, indicating significant variation between the lines. Sample size per line is shown in Table 1-5.

There was a strong correlation between *A* and g_m (r = 0.91 *P* = < 0.001), and significant variation was observed in g_m across the collection of lines (*F* (11, 41) = 8.0 *P* = < 0.001). The highest mean g_m were observed in the *T. dicoccoides* lines dic71 and dic72 (Figure 1-13). The line dic71 had 2.5 and 2.3 fold higher g_m than the *T. durum* line Hoh501 and the *T. dicoccum* line Tios, respectively. Both the *T. dicoccoides* lines had higher g_m mean values than the bread wheat lines Paragon and Robigus (Table 1-7).

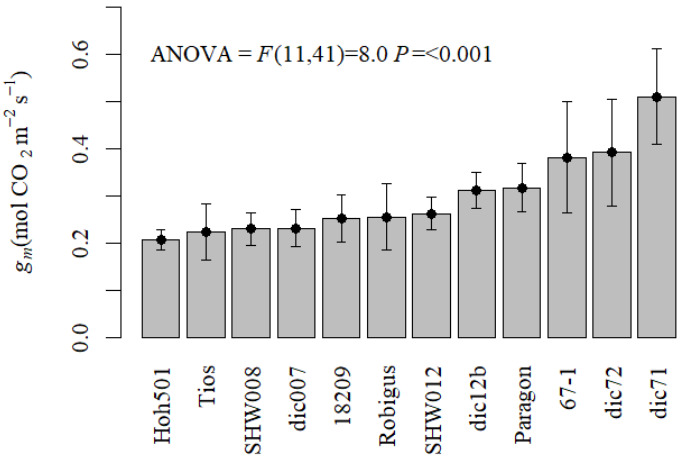

Figure 1-13 - Mean mesophyll conductance (g_m) in the 2016 field trial collection. For selected steps of each replicate A/C_i curve, g_m was calculated using the Harley *et al.* (1992) model with a calibrated electron transport value (J_{CAL}) following Bellasio *et al.* (2016). ANOVA results were overlaid on the graph, indicating significant variation across the lines. Standard deviation bars are shown. Sample size per line is shown in Table 1-5.

The mesophyll cross section analysis completed on a subset of lines from the trial identified a link between percentage intercellular airspace and g_m (Figure 1-14). A significant linear regression model was fitted (F (6, 22) = 9.27, P = < 0.001, R^2 = 0.64) to predict g_m based on line name and intercellular airspace. As shown in Figure 1-13, g_m was dependant on line (F = 10.1, P = < 0.001). Additionally, g_m showed a significant positive regression with percentage intercellular airspace (F = 5.0, P = 0.036). Significant variation in mesophyll percentage airspace was observed across the 6 lines (Figure 1-14, F (5, 24) = 5.1, P = 0.002). The *T. dicoccoides* line dic72 had significantly higher intercellular airspace than the other species studied; dic71 also had high intercellular airspace. The lowest intercellular airspace was observed in Robigus.

a).

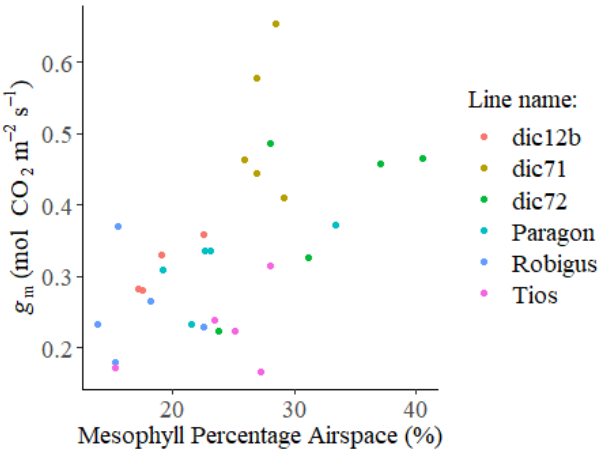

b).

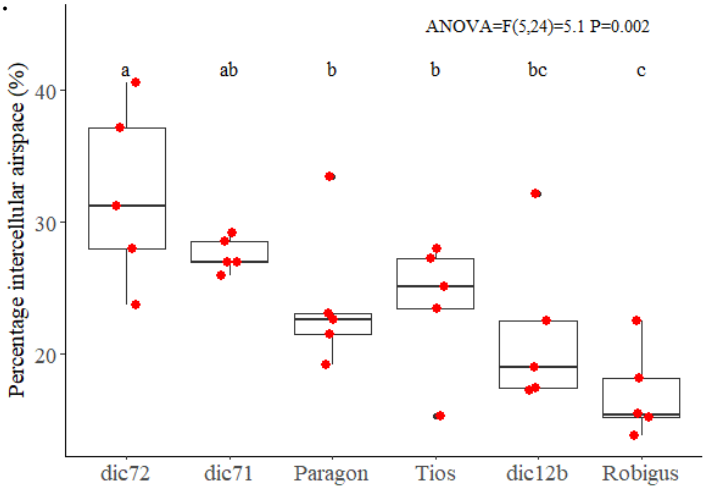

c). d).

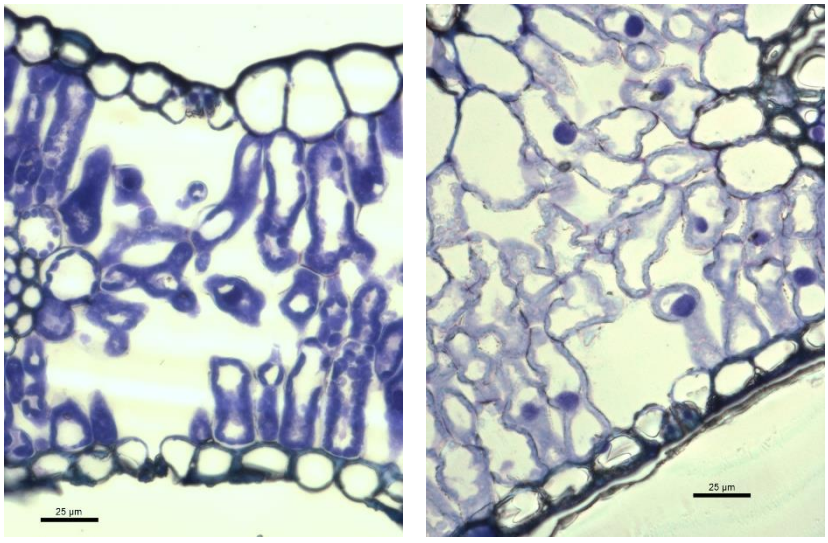

Figure 1-14 – Flag leaf cross section analysis was completed on a subset 6 lines from the 2016 field trial with 5 replicates for each line. (a) A scatter plot showing the relationship between mesophyll percentage airspace and g_m in the subset (one replicate was not available for dic12b, so n = 29). (b) Results from the flag leaf cross sectioning analysis, showing percentage mesophyll airspace across the subset of lines from the 2016 trial, ANOVA and Duncan's new multiple range post-hoc test grouping is shown (n = 5). Raw data points are overlaid on the boxplot in red. Images c). and d). show an example of variation in mesophyll airspace between dic72 (c) and Tios (d) individuals, images were taken of flag leaf cross sections at 60x magnification. The scale bar shown is 25 µm.

Across the collection of lines in the 2016 field trial significant variation in $\Delta^{13}C$ was identified (F (11, 54) = 7.0, P = < 0.001). There were significant positive correlations between $\Delta^{13}C$ and a number of photosynthetic supply-related traits: g_m (Figure 1-10, r = 0.65 P = 0.02), A (r = 0.71 P = 0.01) and g_s (r = 0.74 P = 0.006). The lines with both the lowest mean A and g_s values, 18209, Hoh501 and Tios, had the lowest mean $\Delta^{13}C$ (Table 1-7), and Hoh501 and 18209 had high *WUE* (Figure 1-12). The two lines with the highest A and high g_s, dic71 and dic72, also had the highest $\Delta^{13}C$ of 22.94 ‰ ($S.D$ = 0.66) and 23.00 ($S.D$ = 0.73), respectively. A significant linear regression model was found (F (12, 52) = 9.90, P = < 0.001, R^2 = 0.63) to predict C_i based on line and g_s. C_i *was* dependant on line (F = 6.4, P = < 0.001) and also showed a significant positive regression with g_s (F = 48.0, P = < 0.001).

Demand Components.

There were fewer traits linked to A in the photosynthetic demand correlation matrix shown in Figure 1-15 compared to the supply parameters (Figure 1-10). The means and standard deviation for the demand traits in the 2016 field trial are shown in Table 1-8. Only 3 traits of 7 showed correlation with A. The trait A_{max} had the highest positive correlation with A (r = 0.8 P = 0.002), where the line with the highest A, dic71, also had the highest mean A_{max} (Table 1-8). Similarly, the *T. dicoccum* line with the lowest A, 18209, also had the lowest mean A_{max} which was 39.2% lower than dic71. No correlation was found between A and a number of traits, including C_i, FL_A, $N_{\%}$, and *SLA*.

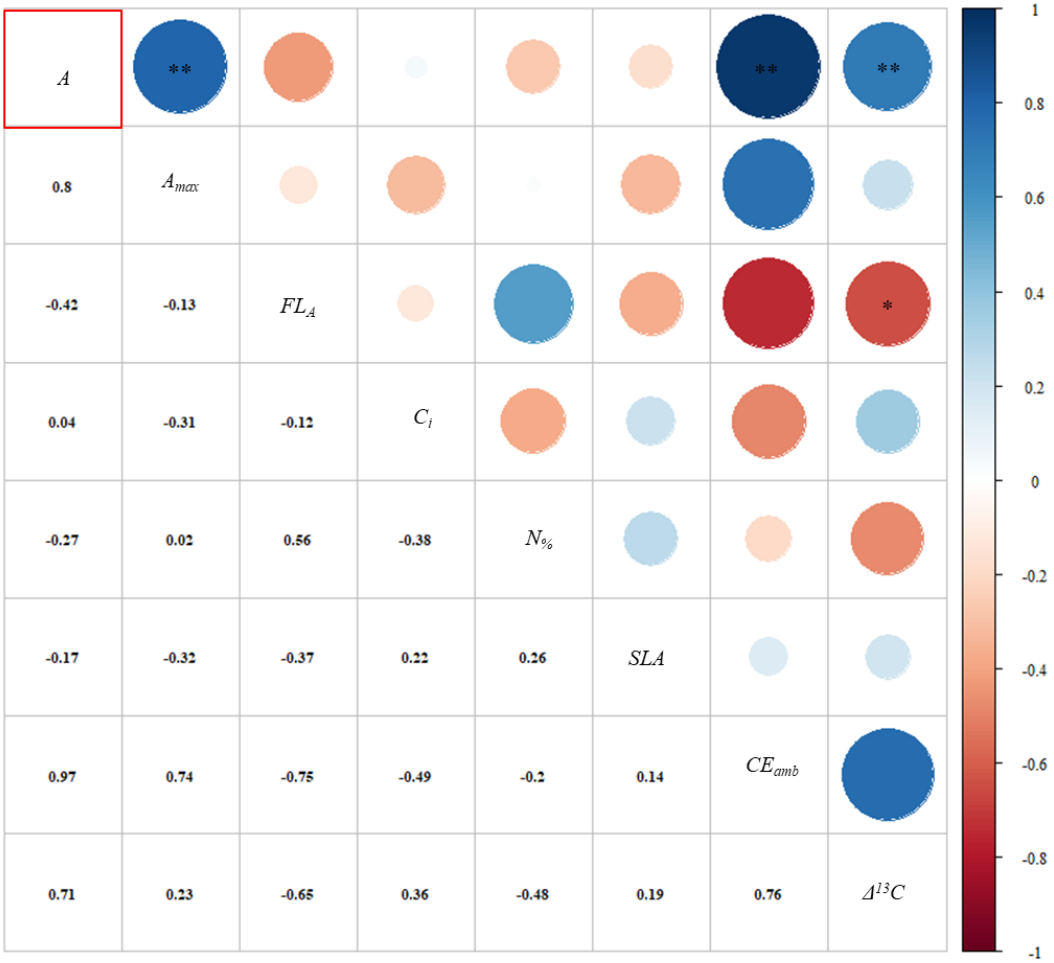

Figure 1-15 - Pearson correlation matrix of photosynthetic demand traits measured in the 2016 field trial. Mean values were used for each of the 12 lines, except for the trait CE_{amb} as means were only available for 6 lines. The mean values used are shown in Table 1-8. The upper right-hand triangle shows a colour heat map of pairwise correlation coefficients and significance thresholds (* $P < 0.001$; ** $P < 0.01$; * $P < 0.05$). The bottom left-hand triangle shows the values of Pearson correlation coefficients for each paired comparison.**

Table 1-8 - Means values of the photosynthetic demand traits for the wheat collection in the 2016 field trial. Standard deviation is shown (S.D). Gas-exchange derived measurements were taken from the A/C_i curves, sample size for each line is shown in Table 1-5. Sample size of each line for the other traits is shown in Table 1-6.

	A_{MAX}		FL_A		C_i		$N_{\%}$		SLA		CE_{AMB}	
Trait	*Mean*	*S.D*	*Mean*	*S.D*	*Mean*	*S.D*	*Mean*	*S.D*	*Mean*	*S.D*	*Mean*	*S.D*
18209	34.42	*8.31*	15.66	*6.37*	210.99	*27.53*	2.89	*0.62*	244.49	*20.89*	-	-
67-1	45.10	*5.87*	21.81	*2.17*	221.73	*14.47*	2.90	*0.32*	194.61	*23.35*	-	-
dic007	37.00	*5.20*	15.11	*4.67*	275.35	*20.24*	2.53	*0.58*	242.38	*29.88*	-	-
dic12b	45.54	*5.88*	24.76	*3.82*	230.85	*0.78*	2.77	*0.22*	222.95	*21.53*	0.16	*0.02*
dic71	47.89	*6.38*	10.47	*2.68*	221.54	*22.54*	2.37	*0.13*	193.19	*23.05*	0.23	*0.03*
dic72	38.62	*11.28*	11.85	*4.28*	241.43	*27.72*	2.44	*0.53*	215.79	*26.33*	0.19	*0.03*
Hoh501	39.84	*3.80*	32.93	*8.19*	215.41	*29.28*	2.93	*0.41*	203.00	*18.37*	-	-
Paragon	40.66	*3.86*	39.54	*5.80*	223.84	*13.63*	3.16	*0.76*	203.17	*28.75*	0.15	*0.02*
Robigus	35.37	*2.16*	22.27	*8.86*	237.69	*12.77*	2.28	*0.34*	207.63	*29.52*	0.14	*0.01*
SHW008	36.27	*3.46*	26.58	*9.80*	238.03	*22.03*	2.86	*0.90*	209.56	*31.71*	-	-
SHW012	37.99	*5.26*	34.88	*7.40*	242.71	*20.71*	3.02	*0.97*	228.14	*28.26*	-	-
Tios	38.04	*2.89*	35.33	*7.90*	240.09	*21.98*	2.42	*0.40*	157.40	*17.61*	0.14	0.02

Trait units: A_{MAX} = µmol CO_2 m^{-2} s^{-1}; FL_A = cm^2; C_i = µmol mol^{-1}; *N %* = %; *SLA* = cm^{-2} g^{-1} and CE_{AMB} = mol m^{-2} s^{-1}

The trait CE_{amb} was calculated on the subset of lines used in the mesophyll cross sectioning analysis (dic71, dic72, Robigus, Paragon, dic12b and Tios). Although the samples size of 6 mean values was small, there was strong positive correlation observed between *A* and CE_{amb} (Figure 1-15, r = 0.97 *P* = 0.001). Across the subset of lines significant variation was observed in CE_{amb} (*F* (5, 23) = 13.4, *P* = < 0.001). The two *T. dicoccoides* lines with the highest *A* and g_m, had significantly higher CE_{amb} than the domesticated lines Paragon, Tios and Robigus. No correlation was found between *A* and $N_{\%}$. Furthermore, $N_{\%}$ did not significantly vary across the collection in the 2016 field trial (Figure 1-16, *H* = 17, *d.f* = 11, *P* = 0.11). Although no statistically significant difference was found, Paragon did have 33.3% and 29.5% higher mean $N_{\%}$ content than the *T. dicoccoides* lines dic71 and dic72. Robigus had the lowest $N_{\%}$ (mean = 2.3%, *S.D* = 0.34).

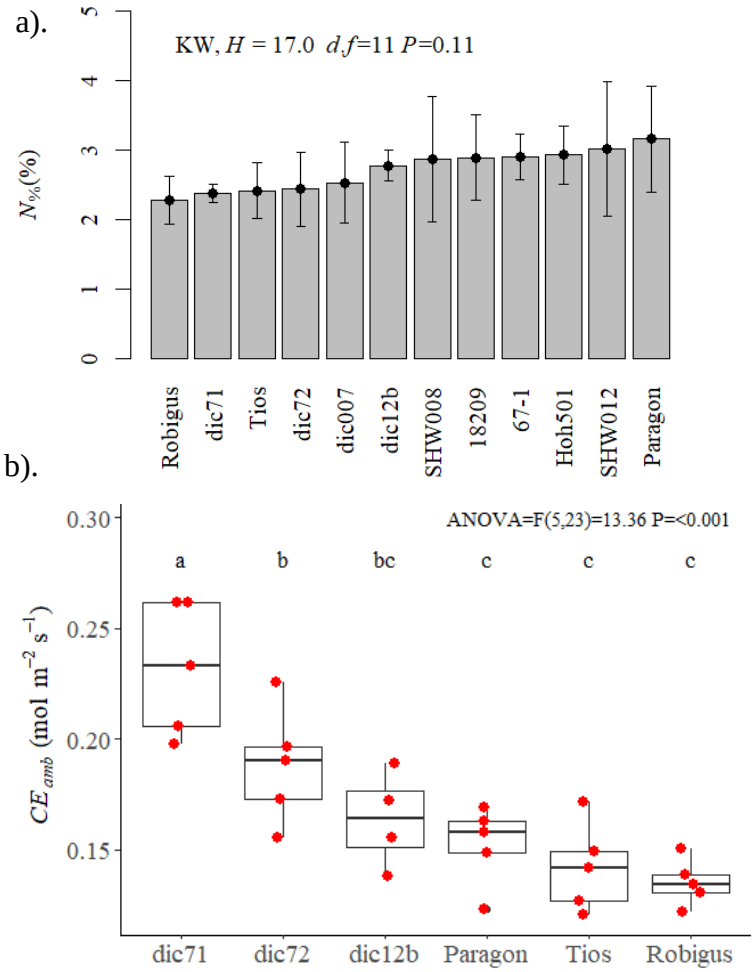

Figure 1-16 – a). Flag leaf percentage nitrogen content in the 2016 field trial, mean and standard deviation are shown. Kruskal-Wallis Rank Sum test results are overlaid on the graph. Sample size for each line is shown in Table 1-6. b). Carboxylation efficiency at ambient O_2 concentration (CE_{amb}) for a subset of lines in the 2016 field trial, extracted from A/C_i curve fitting (sample size is shown in Table 1-5). Raw data points are overlaid in red. ANOVA and Duncan's new multiple range post-hoc test grouping is shown.

To further explore the demand components driving the high *A* in the *T. dicoccoides* accessions, *A* was shown relative to leaf dry matter and N content (Table 1-9). For comparison, *A* was also expressed relative to the supply component *Chl* (Table 1-9). The two *T. dicoccoides* accessions had the highest means for all three methods of expressing the *A* results. The accession dic71 possessed the highest *A* relative to flag leaf dry matter content (estimated from the leaf core measurements), as this line had high *A* but a comparatively low *SLA* (Table 1-8), this variation was most likely driven by *A*. The *T. dicoccoides* individuals had considerably higher means of *A* relative to $N_{\%}$. Compared to the cultivated accessions (Table 1-9), the *T. dicoccoides* lines had both high *A* and a low mean $N_{\%}$ content (Figure 1-16), suggesting a high photosynthetic nitrogen use efficiency. For *A* relative to the supply component *Chl*, the two *T. dicoccoides* accessions also had the highest mean values in the collection, whilst lower means were observed in the cultivated types: Hoh501, Tios and 18209 (Table 1-9). The dic71 line had a comparatively high mean *Chl* content (Table 1-7), so as with the expression of *A* relative to leaf dry matter content, variation in *A* may have had the largest impact on these trends.

Table 1-9 – Mean values for each accession from the 2016 field trial showing flag leaf per unit CO_2 assimilation (*A*) in proportion to leaf dry mass, chlorophyll content (*Chl*) and nitrogen content (N). The number of replicates for each line used in the calculations are shown (n). *S.D* = standard deviation.

	A			*A / dry mass*			*A / Chl*			*A / N*		
Trait	*n*	*Mean*	*S.D*	*n*	*Mean*	*S.D*	*n*	*Mean*	*S.D*	*n*	*Mean*	*S.D*
18209	5	17.94	4.22	5	0.44	0.14	5	43.78	4.88	5	15.45	3.80
67-1	6	27.52	3.81	4	0.51	0.10	4	55.93	4.59	4	17.65	3.58
dic007	5	23.77	4.70	5	0.59	0.18	5	53.90	12.00	5	23.01	3.84
dic12b	4	27.10	4.49	3	0.56	0.06	4	62.13	7.25	3	20.77	1.86
dic71	6	33.79	2.40	6	0.66	0.11	6	66.64	5.66	6	27.58	4.05
dic72	6	27.94	8.94	5	0.61	0.19	6	60.71	14.09	5	26.39	7.08
Hoh501	4	19.43	3.29	4	0.39	0.10	4	41.43	7.91	4	14.00	5.15
Paragon	6	24.81	3.01	6	0.50	0.08	6	48.54	8.25	6	16.24	2.66
Robigus	6	22.14	4.63	6	0.47	0.14	6	47.33	8.18	6	20.37	5.06
SHW008	5	23.01	2.83	5	0.48	0.08	5	47.90	4.88	5	18.08	3.90
SHW012	6	23.94	4.14	6	0.54	0.09	6	51.67	7.26	6	18.83	4.38
Tios	6	21.11	2.16	6	0.33	0.07	6	44.37	6.57	6	14.24	4.05

Trait units: *A* = µmol CO_2 m^{-2} s^{-1}; *A / dry mass* = µmol CO_2 g dry mass s^{-1};
A / Chl = µmol CO_2 g^{-1} chlorophyll s^{-1}; *A / N* = µmol CO_2 g^{-1} N s^{-1}.

There was limited evidence that $\Delta^{13}C$ was influenced by components associated with photosynthetic demand, as fewer demand traits correlated significantly with $\Delta^{13}C$. For example, no significant correlation was found with either A_{max} or $N_{\%}$ (Figure 1-15).

Because g_s and C_i showed a significant regression, the supply function seems to have predominated over demand, as represented by A_{max} and $N_{\%}$ (Figure 1-15).

Although not statistically significant, there was an indication of a negative correlation between *A* and the photosynthetic demand component FL_A (r = -0.42 P = 0.17). Across the collection in the 2016 field trial, significant variation was observed in FL_A (Figure 1-17, F (11, 55) = 12.8, P = < 0.001). There was a range of 29.1 cm^2 across the mean values of FL_A in the collection of lines grown in the 2016 field. The line with the highest mean *A*, dic71, also had the smallest mean FL_A. Paragon had a 3.8 and 3.3 fold larger mean flag leaf than dic71 and dic72, respectively. Therefore, when *A* is considered on an absolute basis, Paragon had the highest *A* (flag $leaf^{-1}$) mean of 0.099 µmol CO_2 $leaf^{-1}$ s^{-1} (*S.D* = 0.025). The ranked means for *A* (flag $leaf^{-1}$) are shown in Figure 1-17, where significant variation was observed across the trial (F (11, 51) = 9.1, P = < 0.001). The two lines with the lowest g_m and comparatively low *A* (Figure 1-8), Hoh501 and Tios, had an 89.5% and 106.1% higher mean *A* (flag $leaf^{-1}$) respectively than dic71, which was the line with the highest per unit *A* and g_m.

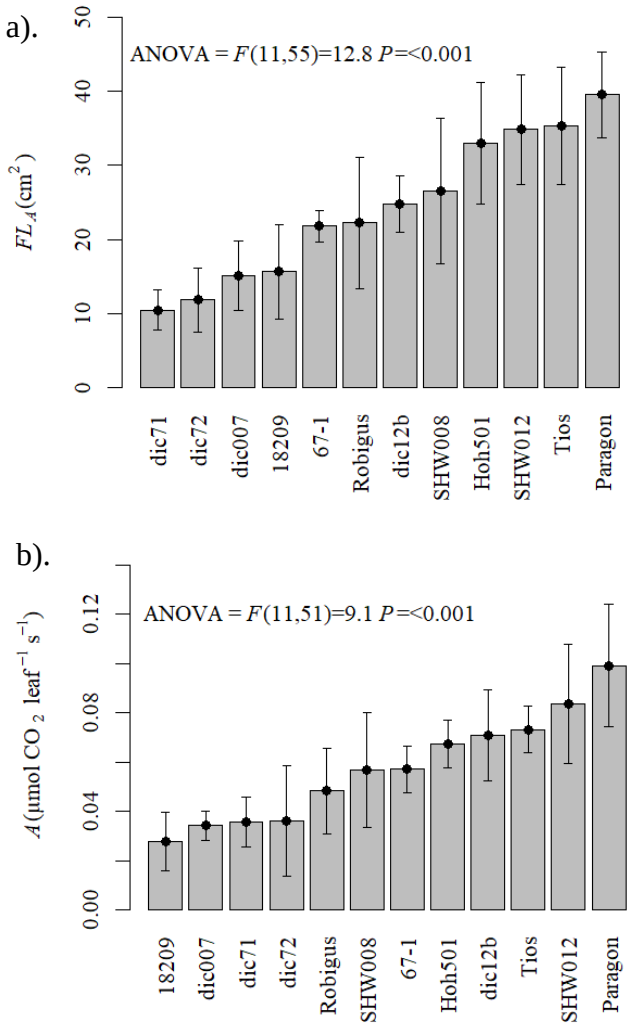

Figure 1-17 – a). Ranked mean flag leaf area (FL_A) in the 2016 field trial for each line, calculated from image analysis using ImageJ (V - 1.51). b). Ranked mean CO_2 assimilation shown on a per flag leaf basis for each line from the 2016 field trial, calculated through multiplying A by FL_A. Both plots show standard deviation bars. Sample size for each line is shown in Table 1-5 and Table 1-6. ANOVA results were overlaid on each graph, indicating significant variation across the lines.

In terms of absolute area based E (flag leaf^{-1}), significant variation was found across the collection (F (11, 51) = 7.9, P = < 0.001). Following the same trend as A (flag leaf^{-1}), the highest E (flag leaf^{-1}) was found in Paragon (Figure 1-18). Paragon had a 2.85 fold higher water expenditure than the *T. dicoccoides* line dic71. Overall 18209 had the lowest mean A and E (flag leaf^{-1}).

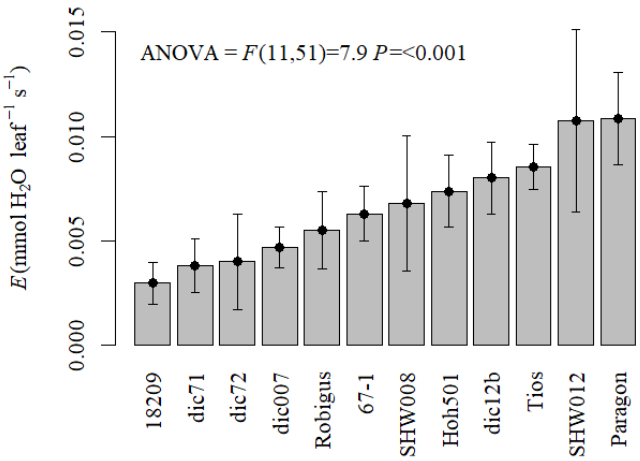

Figure 1-18 – Mean transpiration expressed on a per flag leaf basis for each line in the 2016 field trial, calculated through multiplying *E* by FL_A. Standard deviation bars are shown, sample size for each line is shown in Table 1-5 and Table 1-6. ANOVA results are overlaid on the graph, indicating significant variation across the lines.

Yield components.

Across the subset of lines taken from the 2016 field trial that were included in the cross section analysis, significant variation was observed for every yield component trait shown in Figure 1-19 (P = < 0.01). Mean grain yield was 6.4 and 6.2 fold higher in Tios and Paragon respectively, compared to dic71. Robigus yielded considerably lower (mean 3.0, $S.D$ = 1.2) than the expected for winter wheat; this was shown to be anomaly created in the experimental design when compared to the yields observed in the 2017 trial shown in the next section. *HI* was highest in both the hexaploid lines, Paragon and Robigus when compared to the tetraploids (Figure 1-19). Tiller number was highest in the *T. dicoccum* line dic12b (mean = 20.4, $S.D$ = 4.2) and lowest in the highest yielding lines Tios and Paragon. Biomass was comparatively high in Tios compared to the other lines, 3.0 and 2.2 fold higher than dic71 and Robigus, respectively. Robigus has the lowest biomass in the subset.

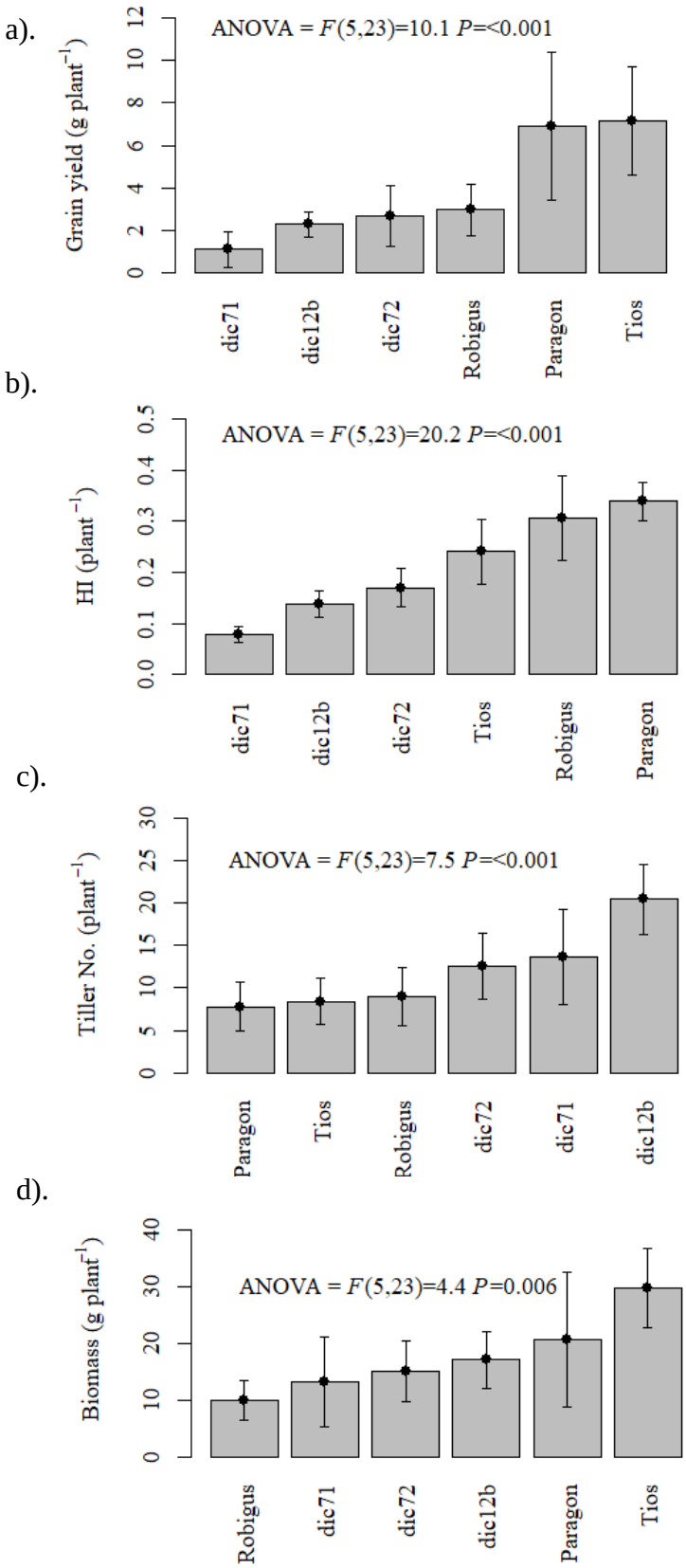

Figure 1-19 – The means and standard deviation of yield component data averaged from single plants of six lines from the 2016 field trial. Grain yield (a), harvest index (b), tiller number (c) and biomass (d) are shown. Five replicates were used for each line, except dic72 where there were four. ANOVA results are overlaid on the graphs, indicating significant variation between lines.

1.3.2 The 2017 field trial

The 2017 field trial supported trends observed in the 2016 trial, in particular that the *T. dicoccoides* lines dic71 and dic72 had high *A* (Figure 1-20). Significant variation was found across the collection (F (14, 44) = 6.7, P = < 0.001). The line dic71 had a mean 42.6% and 25.3% higher *A* than the bread wheat lines Paragon and Robigus, respectively. For the parental lines measured in both trials, the *A* mean values were considerably higher in the 2017 trial compared to 2016 (e.g. 18.1% and 12.7% higher in dic71 and Paragon, respectively). Mean *A* was 43% higher in Robigus in the 2017 trial compared to 2016, increases were also observed in leaf area and grain yield suggesting the later sowing date in the 2016 influenced the performance of the line. The majority of the offspring lines in the 2017 field trial had higher mean *A* than the hexaploid parent Paragon, excluding 32_23I and 31_07K. The offspring line 32_23D had a slightly higher mean than the *T. dicoccoides* parent dic72. However, the other offspring lines did not have as high mean *A* as the tetraploid parents (Figure 1-20). There was a 2.78 µmol CO_2 m^{-2} s^{-1} mean difference (*S.D* = 5.3) between the plants measured across both days. The individuals measured on the first day of measurements had a higher mean than on the second (35.7 compared to 32.9 µmol CO_2 m^{-2} s^{-1}). However, there was not strong evidence to suggest the variation was significant (determined using a two-tailed paired t-test: t = 1.905, df = 12, P = 0.081) and thus no correction for the date variation was applied.

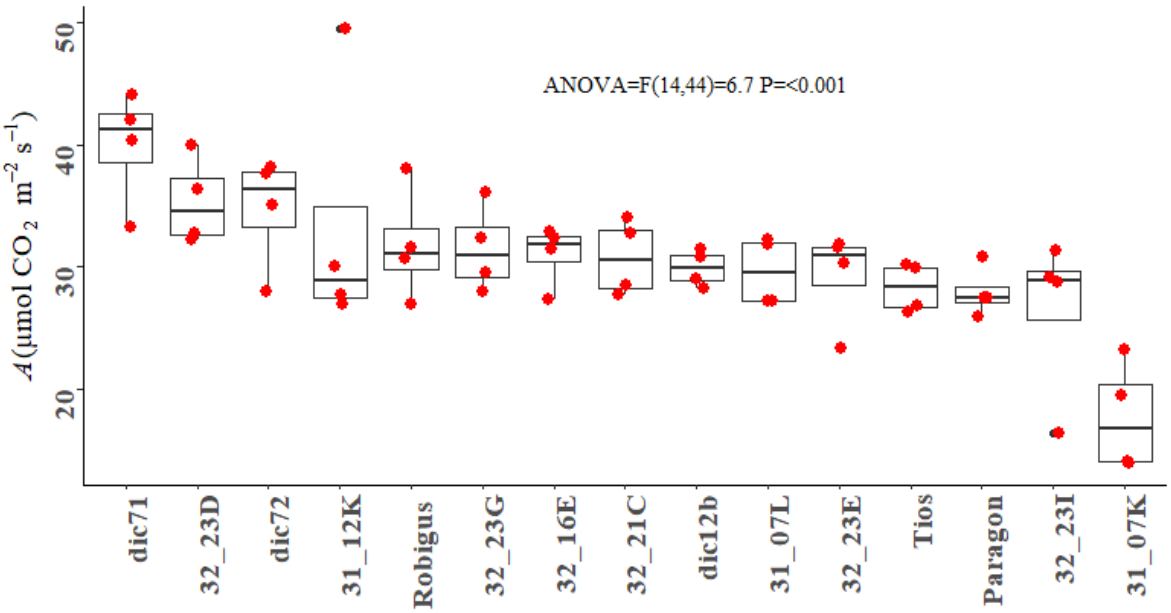

Figure 1-20 – Measurements of leaf CO_2 assimilation taken at ambient condition on single plants in the 2017 field trial. All measurements were taken on flag leaves excluding Robigus and Tios. The red dots indicate individual data points overlaid on the box plots. A selection of offspring lines, formed through crossing tetraploid and hexaploid individuals, were measured in the 2017 field trial with the parental lines. ANOVA results are overlaid on the boxplot, indicating significant variation between the lines.

Leaf area followed the same trend as the 2016 field trial, where Paragon had a mean 3.2 and 2.7 fold larger flag leaf than the *T. dicoccoides* lines dic71 and dic72 (Figure 1-21). Significant variation in leaf area was observed across the offspring and parental lines assessed in the trial (F (14, 45) = 16.6, $P < 0.001$). The 31_07K offspring accession had the largest mean flag leaf area (53.5 cm^2, $S.D$ = 2.8) and lowest mean A. The gas exchange results for this line may have been influenced by measurement timing, as it was the last accession to be analysed in the collection. There were 8 offspring individuals with higher flag leaf area than the *T. dicoccoides* parents and higher A than the Paragon hexaploid parent: 32_23D, 31_12K, 32_23G, 32_16E, 32_16E, 32_21C, 31_07L and 32_23E. Although the same leaves were not necessarily used in both measurements, simple linear regression was used to estimate A based on leaf area using mean values for each line; a significant negative relationship was observed (F (1, 13) = 8.1, P = 0.014) with an adjusted R^2 = 0.34. Using these estimates of mean A and leaf area for each line in the 2017 field trial, an estimate of A ($leaf^{-1}$) per line was calculated (Table 1-10). Only one offspring accession, 31_12K, had a higher A ($leaf^{-1}$) than the bread wheat lines Paragon and Robigus. The mean A for this accession may have been influenced by a possible outlier present in the data (Figure 1-20), where a reading was taken at 49.5 µmol m^{-2} s^{-1}. None of the other offspring lines had as high A ($leaf^{-1}$) as Robigus and Paragon (0.142 and 0.136 µmol $leaf^{-1}$ s^{-1}, respectively). However, the offspring lines, 31_07L and 32_23D, were close with 0.134 and 0.131 µmol $leaf^{-1}$ s^{-1}, respectively.

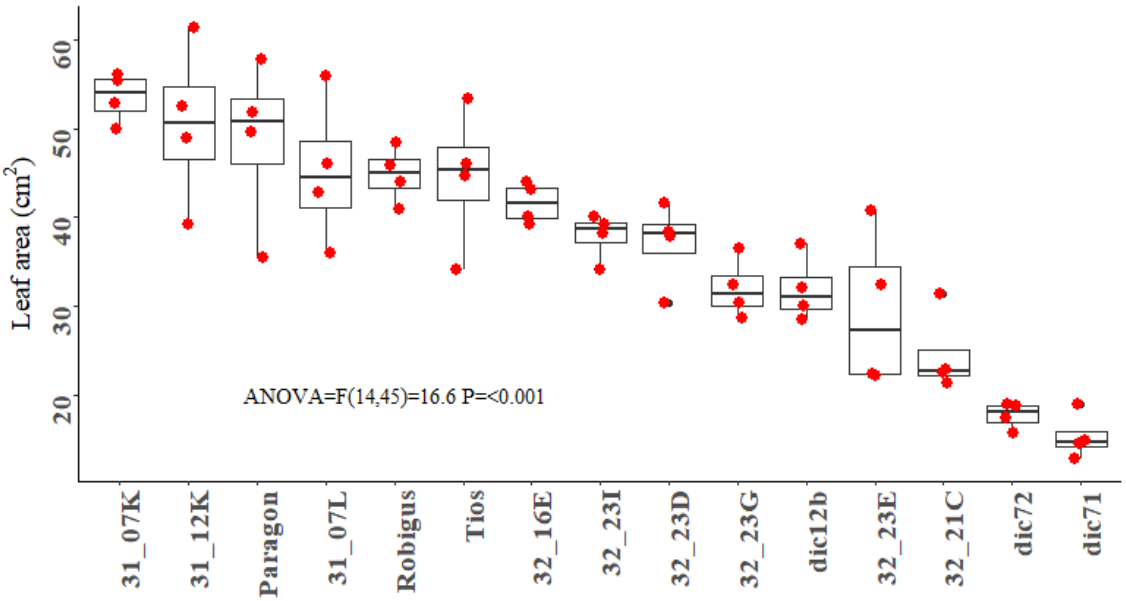

Figure 1-21 – Leaf areas calculated from leaf length and width measurements of single plants in the 2017 field trial. All measurements were completed on flag leaves, except Tios and Robigus. The red dots indicate raw data points overlaid on the box plots. The same selection of lines as measured in the leaf photosynthesis measurements are shown. ANOVA results are overlaid on the boxplot, indicating significant variation between the lines.

Table 1-10 - Mean values of *A* and leaf area for each line, determined from measurements made in the 2017 field trial. The values were used to calculate an estimate of *A* (leaf^{-1}) per line.

Trait	*A*	*Leaf area*	*A (leaf^{-1})*
dic71	*39.89*	*15.27*	*0.061*
dic72	*34.74*	*17.70*	*0.061*
Paragon	*27.97*	*48.64*	*0.136*
Robigus	*31.82*	*44.77*	*0.142*
31_07K	*17.73*	*53.51*	*0.095*
31_07L	*29.63*	*45.14*	*0.134*
31_12K	*33.57*	*50.46*	*0.169*
32_16E	*31.00*	*41.57*	*0.129*
32_21C	*30.76*	*24.55*	*0.076*
32_23D	*35.35*	*37.06*	*0.131*
32_23E	*29.30*	*29.39*	*0.086*
32_23G	*31.53*	*31.98*	*0.101*
32_23I	*26.44*	*37.88*	*0.100*
dic12b	*29.90*	*31.88*	*0.095*
Tios	*28.31*	*44.52*	*0.126*

Trait units:
A = µmol CO_2 m^{-2} s^{-1}; FL_A = cm^2; *A* (flag $leaf^{-1}$) = µmol CO_2 $leaf^{-1}$ s^{-1}.

Both grain yield (Kruskal-Wallis rank sum test: H = 29.7, $d.f$ =10, P= < 0.001) and biomass (F (10, 32) = 2.35, P = 0.03) varied significantly across the lines included in the gas-exchange analysis in the 2017 field trial (Figure 1-22). The lines 32_16E and 32_23I demonstrated pre-harvest ear shattering and were removed from the analysis. Following the same trend as observed in the 2016 field trial, the lowest grain yields were observed in the *T. dicoccoides* lines dic72 and dic71, where the highest yielding line Paragon had a 4.8 and 4.3 fold higher grain yield than dic72 and dic72, respectively. The grain yields were considerably higher in the 2017 field trial compared to 2016 trial, for all the lines included in both years. This was particularly evident in Robigus plants, where there was an 8.9 fold higher mean grain yield in 2017 compared to the 2016 trial. Out of the offspring individuals, none yielded higher than the hexaploid parent Paragon. Biomass followed a similar trend to grain yield, where the *T. dicoccoides* lines dic72 and dic71, had considerably lower biomass than the cultivated wheats Paragon and Robigus. The offspring line 32_023G also had comparatively low biomass.

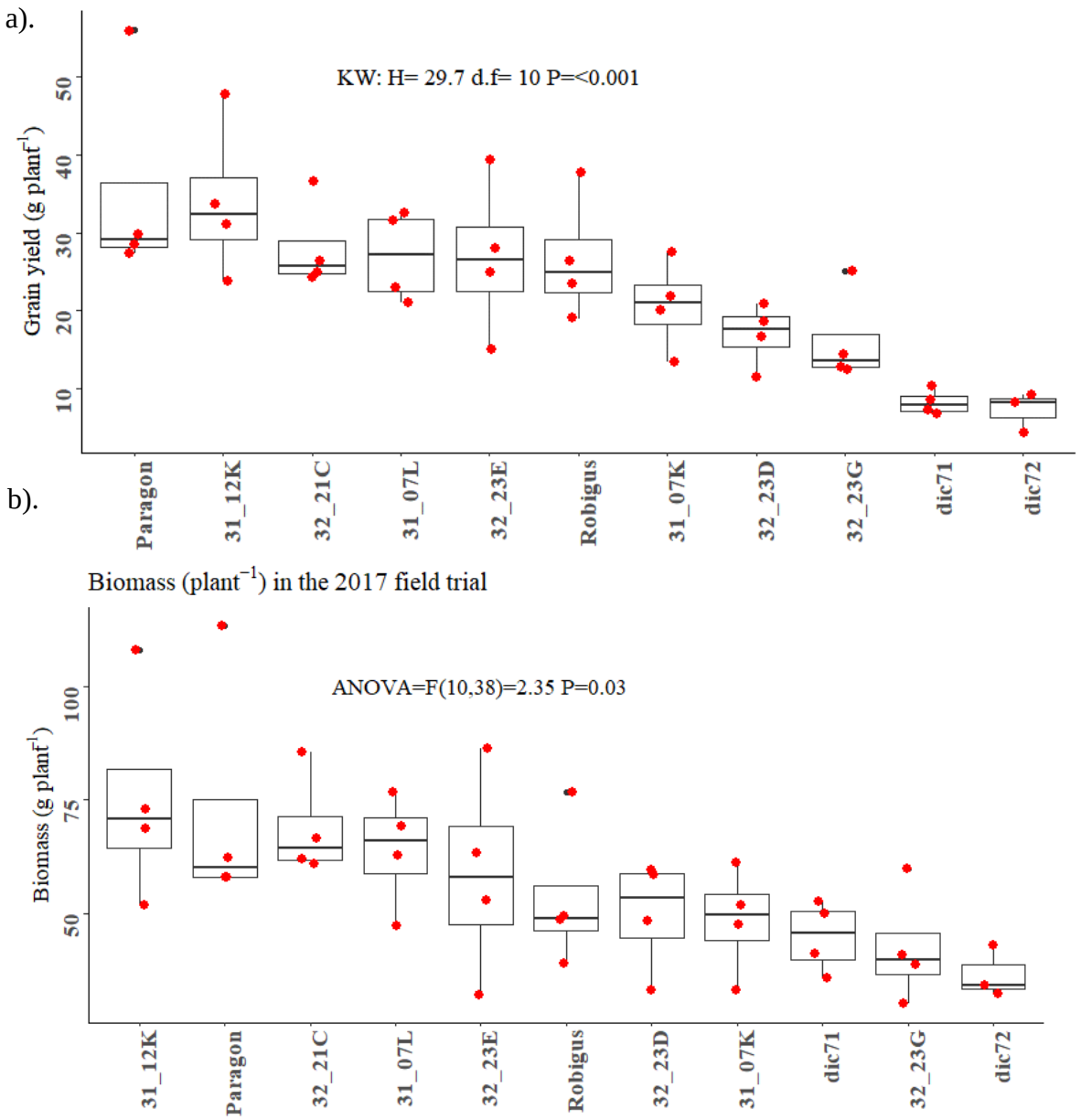

Figure 1-22 - Grain yield (a.) and biomass (b.) per plant from the 2017 field trial for a selection of the offspring wheat lines (formed through tetraploid and hexaploid crossing) and parental lines. The red dots indicate individual data points overlaid on the box plots. a). Kruskal-Wallis Rank Sum test (a.) and ANOVA (b) results are overlaid on the boxplots, indicating significant variation between the lines.

A simple linear regression model was used to test the effect of mean *A*, leaf area and *A* (leaf^{-1}) on mean grain yield and biomass. No significant regression model was found between *A* and grain yield (plant^{-1}) or for the effect of *A* and leaf area on biomass. A significant model, with a positive regression, was fitted for leaf area and grain yield (F (1, 9) = 8.25, P = 0.02, Figure 1-23) with an adjusted R^2 of 0.42. Furthermore, a significant model, with a positive regression, was also fitted for *A* (leaf^{-1}) and grain yield (F (1, 9) = 8.28, P = 0.02, Figure 1-23) with an adjusted R^2 of 0.42. Lastly, *A* (leaf^{-1}) had a significant

effect on biomass, where a positive linear relationship was identified (F (1, 9) = 4.95, P = 0.05, Figure 1-23), with an adjusted R^2 of 0.28.

a).

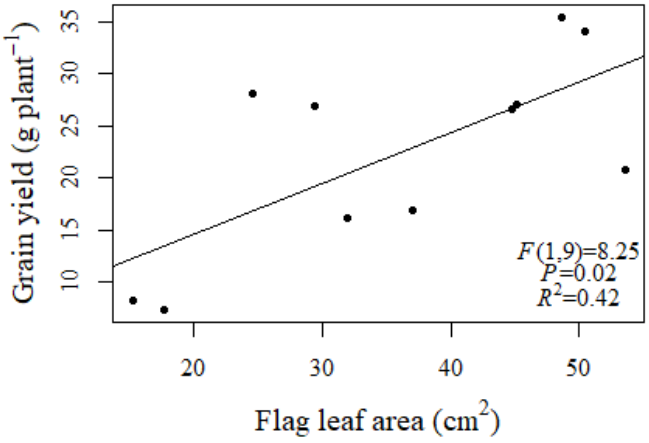

b).

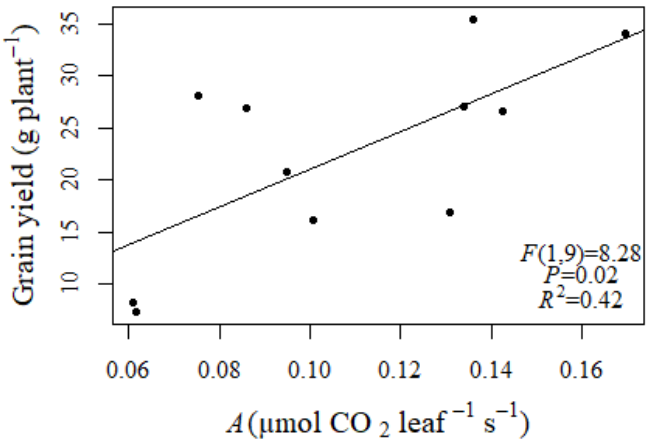

c).

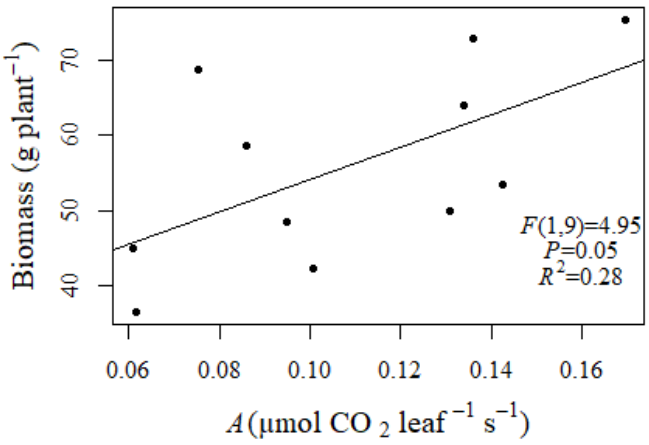

Figure 1-23 – Significant regression models from the 2017 field trial, showing a positive regression between: FL_A and grain yield (a); A (leaf^{-1}) and grain yield (b); A (leaf^{-1}) and biomass (c). Mean values from 4 replicate plants were used for each data point. Data were available for 7 tetraploid and hexaploid crossing offspring accessions, the hexaploid parent (Paragon), the two tetraploid parents (dic71 and dic72) and the elite bread wheat 'Robigus'. Therefore, sample size was 13 with 4 replicates for each line.

1.4 Discussion.

1.4.1 CO_2 Assimilation

Across the trials in both years, flag leaf *A* varied significantly in the studied material. Significant variation in rates of photosynthesis between different cultivar flag leaves of field grown wheat has been observed in a number of other studies (Carmo-Silva *et al.* 2017; Driever *et al.* 2014; Gaju *et al.* 2016). The two *T. dicoccoides* lines had the highest *A* per standardised unit leaf area measured at ambient conditions (400ppm CO_2, Figure 1-8), these results follow trends observed by Austin *et al.* (1982) where the wild *T. dicoccoides* had a higher per unit CO_2 assimilation rate (35 mg CO_2 dm^{-2} h^{-1}) than the *T. aestivum, T. durum, T. dicoccum* and *T. monococcum* lines included in the analysis. Flag leaf *A* is considered to have dropped through the domestication of modern wheat (Evans & Dunstone 1970) and high photosynthetic capacity is commonly found in *T. dicoccoides* individuals (Carver & Nevo 1990; Nevo *et al.* 1991). In the present study, high mean *A* was observed in the dic71 individuals, particularly within the 2017 field trial (mean = 39.9 µmol CO_2 m^{-2} s^{-1}). Carver & Nevo (1990) also found high *A* of *T. dicoccoides* grown in a growth chamber (32.4 µmol CO_2 m^{-2} s^{-1}). The high values of *A* found in the present study, particularly in the 2017 field trial, are a demonstration of the combined effect of genetics x environment (favourable field agronomic conditions and irrigation).

1.4.2 Photosynthetic Supply Components

Light Capture Capacity

A number of supply-side component traits were linked to the high *A* observed in the *T. dicoccoides* lines. The traits related to photochemistry, J_{CAL} and Φ_{PSII}, were strongly correlated with *A* (Figure 1-10). The regeneration rate of the acceptor molecule RuBP in the CBC cycle is a limitation to carbon fixation (Farquhar *et al.* 1980) and is influenced by the supply of products from the light dependant reactions. Photochemistry traits, such as electron transport and Φ_{PSII}, are proxies for estimating the capacity of supply from those reactions and therefore scale with *A* (Edwards & Baker 1993; Genty *et al.* 1989). As CO_2 assimilation is the primary sink for energy from photochemistry (Edwards & Baker 1993), the high J_{CAL} and Φ_{PSII} observed for the *T. dicoccoides* line dic71 (Table 1-7), was linked to the high electron sink and demand associated with high *A*. Measurements taken in the absence of photorespiration can increase the clarity of the relationship between *A* and electron transport (Murchie & Lawson 2013). The estimates of electron

transport in the present study were made following a calibration for photorespiration (Bellasio *et al.* 2016), which could have contributed to the high correlation coefficients observed (Figure 1-10). The trends observed help validate the use of J_{CAL} and Φ_{PSII} as high throughput proxies for CO_2 assimilation of field grown material. Although a positive correlation was observed, *Chl* was not as highly associated with CO_2 assimilation as the other photochemical parameters. J_{CAL} and Φ_{PSII} are instantaneous spot measurements which may be more likely to correlate with the measure of *A* taken at the same time. In comparison, *Chl* may reflect a more long term investment of the leaf into light capture capacity over the season. Light limitation can be detrimental to grain yields in the UK (Beed *et al.* 2007). Paragon had the highest mean *Chl*, which may be a reflection on past selection in domesticated cultivars for increased light capture in a shaded environment (Figure 1-24).

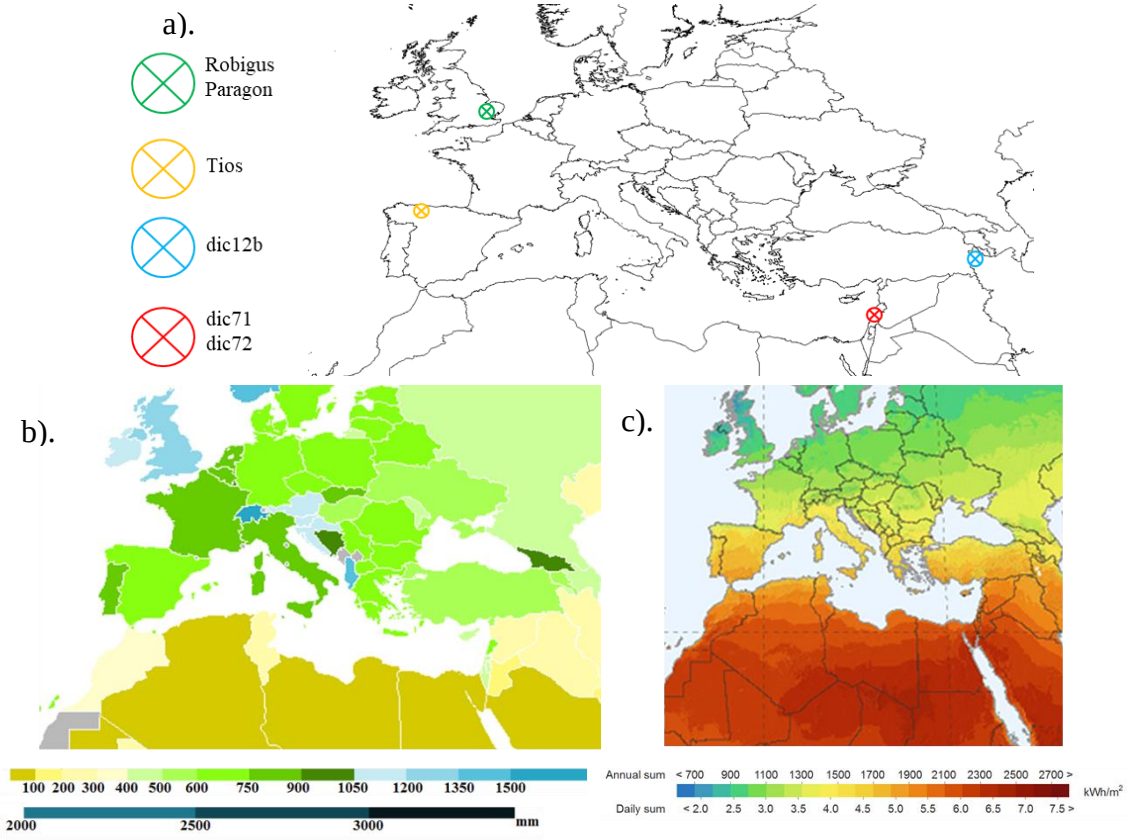

Figure 1-24 – a). A map showing the coordinates that a subset of accessions were previously collected from. The UK locations of breeding companies that released the cultivars 'Paragon' and 'Robigus' were used. The map was formed using the 'rworldmap' package in RStudio (V - 3.4.3, South 2011). b). A map showing average annual precipitation (mm) by country using data from: www.data.worldbank.org. The map was adapted from: www.commons.wikimedia.org/wiki/File:Countries_by_average_annual_precipitation.png. c). A heat map showing a long term average of horizontal global irradiation (kWh m^{-2}). Adapted from: www.solargis.info (SolarGIS © 2014 GeoModel Solar).

CO_2 supply

Stomatal Conductance

In the 2016 field trial, the main determinants of CO_2 supply to the sites of carboxylation (g_s and g_m) were both highly correlated with *A* (Figure 1-10). The parameter g_s often strongly correlates with CO_2 assimilation (Wong *et al.* 1979). The highest g_s was found in the *T. monococcum* line and the two *T. dicoccoides* lines. In *T. dicoccoides* high g_s has been previously observed in comparison to cultivated hexaploid varieties (Johnson *et al.* 1987a). Although the relationship can be complicated, anatomical features of the leaf such as stomatal density and size can influence g_s (Lawson & Blatt 2014). The two *T. dicoccoides* lines possessed a significantly higher stomatal density than the hexaploid varieties Paragon and Robigus (Figure 1-11), which is a trend previously observed in other comparisons between progenitor tetraploids and modern hexaploids (Austin *et al.* 1982; Dunstone *et al.* 1973). High g_s in the *T. dicoccoides* lines was also linked to the high *E* (Table 1-7). The increased per unit water expenditure does not correspond to the arid environment from where these accessions originate (Figure 1-24). The *T. dicoccoides* lines had an earlier heading date and flowering time than the cultivated varieties (see: Appendix 4), which is known to be linked to drought avoidance (Kenney *et al.* 2014; Shavrukov *et al.* 2017) and is a strategy previously observed in *T. dicoccoides* (Peleg *et al.* 2005). Species that originate from drought prone environments can develop strategies to maintain high g_s and water uptake under mild water deficits (Read & Farquhar 1991), the high *E* losses might reflect efficient utilisation of resources when available. However, in terms of dic71, the high carbon gain associated with the high water loss, resulted in the highest *WUE* in the collection. Similarly, Parmer (2005) found that *T. dicoccum* individuals possessed high *WUE* due to increased photosynthetic rates. If *E* is considered on an *E* (flag leaf^{-1}) basis, dic71, dic72 and dic007 had some of the smallest ranked mean water losses per flag leaf (Figure 1-18). Therefore, the high per unit water expenditure seems to be more advantageous to overall flag leaf water use when considered on a total area basis. To maintain a high per unit water expenditure and improve adaptation to a drought prone environment (Figure 1-24), the progenitor lines may possess effective stomatal sensitivity to fluctuating environmental conditions. Slow stomatal responses to varying light conditions are limiting to productivity within a crop canopy (Lawson *et al.* 2012). The progenitor lines might be a possible source of diversity for improved stomatal sensitivity in modern wheat and further work is needed to confirm this.

Conclusions about potential water deficits cannot be informed by the *RWC* measurements, as the detached tillers were stored in water before leaf cores were taken at the end of each measurement day (~18:00 h). This procedure was followed to minimise potential damage to the flag leaves until leaf cross section samples were taken for the airspace analysis.

The $\Delta^{13}C$ results can be informative of limitations on leaf carbon fixation, provided one recognises the interplay between supply and demand components of photosynthesis (Farquhar *et al.* 1982; Seibt *et al.* 2008). However, there was greater evidence that both the high or low $\Delta^{13}C$ signals were led by the stomatal and mesophyll supply components in the 2016 field trial. The results indicated that C_i was influenced by g_s, rather than proxies for photosynthetic demand, including A_{max} or $N_{\%}$. The *T. dicoccoides* lines showed both high $\Delta^{13}C$ and g_s. Increases in g_s can increase the ratio of C_i / C_a leading to higher $\Delta^{13}C$ (Farquhar *et al.* 1982, 1989), simply indicating that CO_2 can diffuse more easily in and out of the leaf due to increased g_s (Richards & Condon 1995). If the high $\Delta^{13}C$ and C_i / C_a were led by low CO_2 demand, then traits linked to photosynthetic capacity, including A_{max} and $N_{\%}$ would negatively correlate with $\Delta^{13}C$; which was not observed. The accessions with the highest photosynthetic capacity, dic71, had comparatively high $\Delta^{13}C$, reinforcing that supply components had the largest impact on the $\Delta^{13}C$ signals. In other studies, *T. dicoccoides* and *T. dicoccum* accessions have demonstrated significantly lower $\Delta^{13}C$ than cultivated wheat (Konvalina *et al.* 2011; Peleg *et al.* 2005). In this study, a number of the cultivated lines (18209, Hoh501 and Tios) had the lowest $\Delta^{13}C$ mean values. These accessions had the lowest ranked g_s (Figure 1-11) and low to moderate ranked means of A_{max} (Figure 1-8), reinforcing further that CO_2 supply led the $\Delta^{13}C$ signals, and ultimately, may have imposed the greatest limitation to flag leaf photosynthesis in these individuals.

Conversely, it could be argued that low CO_2 demand may have resulted in a reduction in g_s. There are augments both for and against stomatal response being linked photosynthetic activity in the mesophyll (Lawson *et al.* 2014). Johnson *et al.* (1987) also observed a correlation between *A* and g_s, although they concluded that as *A* did not correlate with C_i, CO_2 supply was not necessarily important in determining photosynthetic differences across wheat ploidy. The parameters of C_i and *A* did not correlate in the present study either. However, this interpretation may be overlooking factors such as internal leaf CO_2 supply. Following Fick's law, the diffusion of CO_2 assimilation into a leaf (*A*) can be simplified to: $A = g_s (C_a - C_i)$, where $C_a - C_i$ reflects the drawdown between C_a and C_i

caused by mesophyll photosynthesis (Gilbert *et al.* 2011). If g_s is high but A is comparatively low (such as dic007), this would indicate limitations in mesophyll photosynthesis rather than CO_2 supply. However, one issue with this simplification is the potential variation in the diffusive restrictions of $C_i - C_c$ (Warren & Adams 2006), where C_c is the chloroplast CO_2 concentration. Control of the CO_2 gradient within the leaf ($C_i - C_c$) is determined by g_m, which consequently has a significant impact on Rubisco capacity and efficiency over the growing season (Evans & Von Caemmerer 1996). Therefore, if g_s is non-limiting, $C_a - C_i$ or more appropriately $C_a - C_c$, is determined by the downstream photosynthetic demand component and g_m.

Mesophyll Conductance

The *T. dicoccoides* lines with the highest g_m also had the highest ranked means of A (Figure 1-13). In comparison, g_m was lower in the domesticated wheat and lowest in the lines with the smallest A means (Hoh-501 and Tios). These results indicate that g_m was an important determinant of the variation in A, which is an interpretation supported by similar correlations observed in other studies (Barbour *et al.* 2015; Evans & Von Caemmerer 1996; Tazoe *et al.* 2009; Tomás *et al.* 2014). There have been limited investigations into how g_m varies across wheat ploidy. The grasses group are considered to have comparatively high g_m (Flexas et al., 2012), which may have been decreased through the domestication of wheat, as negative correlations have been observed with g_m and potentially desirable flag leaf traits including leaf N content and Leaf Mass Area (LMA, Gu *et al.* 2012). Supporting this hypothesis is evidence in the present study where a significant correlation was observed between percentage mesophyll intercellular airspace and g_m (Figure 1-14). Increased mesophyll airspace proportion is an anatomical feature that promotes higher g_m (Evans *et al.* 2009; Loreto *et al.* 1992; Parker & Ford 1982). Increases in intercellular airspace volume can increase g_m, as CO_2 travels through air faster than in water, so an extension of the passage through air rather than water is advantageous (Evans & Von Caemmerer 1996). Secondly, higher mesophyll airspace increases mesophyll cell surface area exposed to those airspaces (Slaton & Smith 2002), leading to a higher chloroplast exposure to the airspaces, which is an important characteristic in promoting higher g_m (Evans *et al.* 2009; Tomás *et al.* 2013).

Visual observations during the image analysis of mesophyll airspace indicated that stomatal cavities appeared to have a large positive influence on the percentage mesophyll airspace. Stomatal density was highest in the *T. dicoccoides* accessions, which would have increased the frequency of stomatal cavities across the leaf and may have contributed

to the high percentage of airspaces and g_m observed. Furthermore, correlations between g_s and g_m were observed across the collection and have been observed in literature (Flexas *et al.* 2013; Loreto *et al.* 1992). A disassembly between the relationship of g_s and g_m has been shown (Barbour *et al.* 2015), which could be fundamental in ideotype design for in a drought prone environment, where g_s needs to be reduced to minimise water loss and g_m needs to be increased to promote CO_2 supply.

For the methods used in this chapter, measurements of both percentage intercellular airspace and g_m were time consuming and expensive. It would be inconceivable to use these techniques for selection in large breeding programs and a suitable proxy needs to be identified. Within the present study, no link was found between *SLA* and g_m. However, other studies have found negative associations between leaf mass per area and g_m (Flexas *et al.* 2008, 2013; Tomás *et al.* 2013). These observations, coupled with the positive association observed between percentage intercellular airspace and g_m in the present study, are indicative that measurements of per unit leaf mass and thickness could be used as a suitable proxy. Measurements of leaf mass can be easily obtained in a high throughput manner (Vile *et al.* 2005), but further analysis is required to validate the link to g_m or intercellular airspace for development as a proxy.

1.4.3 Demand Components

Carboxylation Capacity and Activity

The photosynthetic demand components were not as highly linked to *A* as the supply components. The trait A_{max} had a strong positive correlation with *A* and was highest in the three tetraploid lines (dic71, dic12b and 67-1), followed by the hexaploid variety Paragon. Measurements of photosynthetic capacity (A_{max}) can be less informative compared to operational CO_2 assimilation (*A*), as limitations imposed by CO_2 supply are removed (Driever *et al.* 2014). Also A_{max} can be impacted mostly by triose phosphate use (TPU) limitation, which is a state not observed under field conditions (Sharkey *et al.* 2007). However, A_{max} is a useful parameter in determining maximum operating capacity of the demand components, in the absence of limitations imposed by CO_2 supply. For instance, in 64 wheat cultivars, Carmo-Silva *et al.* (2017) found A_{max} to scale with leaf Rubisco content and carboxylation capacity. Although no link was found between $N_{\%}$ and A_{max} in the present study, a correlation was identified with CE_{amb}. Cultivated wheat has been bred for increased N uptake leading to a higher $N_{\%}$, which could translate to an increased photosynthetic capacity (Makino 2011). However, the *T. dicoccoides* accession dic71 had

the highest A_{max} out of the collection (Figure 1-8) which would refute this link. Selection for traits related to agronomic performance, aside from photosynthesis, may have decreased photosynthetic capacity in modern varieties (Driever *et al.* 2014). Variation in *A* across the collection was greater than variation in A_{max}, indicating that limitations in operational CO_2 assimilation (*A*) impose more variation in flag leaf photosynthesis than variation associated with photosynthetic capacity.

The carboxylation activity of Rubisco is a limitation to carbon fixation (Farquhar *et al.* 1980) and a restriction that reflects the boundaries imposed by photosynthetic downstream demand. Rubisco is a major target for crop improvement due to a slow catalytic turnover and inefficiency (Carmo-Silva *et al.* 2015; Orr *et al.* 2016; Parry *et al.* 2011). The initial linear relationship between *A* and C_i is termed CE_{amb} and was positively correlated with both *A* and A_{max} (Figure 1-15). At low C_i the major limitation of *A* is imposed by Rubisco, so principally CE_{amb} can be informative of Rubisco activity (von Caemmerer 2000). The highest CE_{amb} was found in the *T. dicoccoides* lines dic71 and dic72, which was significantly higher than the cultivated hexaploids. Merchuk-Ovnat *et al.* (2016b) observed increases in carboxylation efficiency in hexaploid wheat linked to an introgression from *T. dicoccoides* on chromosome 7A. As correlations have been observed between Rubisco activity and content (Carmo-Silva *et al.* 2017), the interpretation could be made that the *T. dicoccoides* had a higher per unit Rubisco content. However, no correlation in the present study was found between CE_{amb} and $N_{\%}$ and no significant variation was found in $N_{\%}$ across the collection in the 2016 trial, although the *T. dicoccoides* lines had some of the lowest ranked means. Additionally, when *A* was expressed relative to $N_{\%}$ the *T. dicoccoides* individuals had the highest mean values. If the smaller flag leaves observed in the *T. dicoccoides* lines led to an increased concentration of photosynthetic demand apparatus (e.g. Rubisco), there would be a lower proportion of *A* to $N_{\%}$. Furthermore, there was little evidence of a dilution effect on $N_{\%}$ caused by flag leaf size, as accessions with large FL_A had some of the highest $N_{\%}$ (e.g. Paragon and SHW12). The fact that the individuals with the highest *A* had the lowest $N_{\%}$, suggests that supply components may have imposed a greater limitation than demand to variation in *A* across the collection and that there may have been an overinvestment in some accessions intondemand components. A high proportion of *A* to $N_{\%}$ could also indicate high photosynthetic nitrogen-use efficiency and higher Rubisco activity (Poorter & Evans 1998). Leaf N allocation to photosynthetic pathways can be separated into two categories: enzymes involved in the CBC cycle (e.g. Rubisco) and thylakoid N (e.g. light

harvesting components) (Evans 1989; Mu *et al.* 2016). As the *T. dicoccoides* lines originate from a high irradiance environment (Figure 1-24), over investment of N to light harvest components may be unnecessary or even potentially damaging. Higher light absorption than energy utilisation through photosynthesis can lead to detrimental effects and the production of reactive oxygen species (Lawson *et al.* 2012). Reduction of investment into light harvest components may have resulted in a larger pool of N available for photosynthetic demand components in the progenitor lines. Alternatively, cultivated varieties may have been unintentionally bred for increased allocation to thylakoid N, at the expense of investment into the CBC cycle. Supporting this hypothesis is the high *Chl* and low CE_{amb} observed in Paragon (Table 1-8). Validation of this hypothesis could be achieved through comparisons of actual flag leaf Rubisco content and parallel gas-exchange measurements. However, Driever *et al.* (2014) found a weak correlation between Rubisco content and CE_{amb}, suggesting the variables are not dependant.

Area Based Leaf Photosynthetic Capacity

In the 2017 field trial, a negative trade-off was apparent between *A* and FL_A. This is a common observation in studies of flag leaf photosynthesis across the wheat ploidy continuum (Austin *et al.* 1982; del Blanco *et al.* 2000; Evans & Dunstone 1970) and supports the hypothesis that there has been a loss of *A* through domestication. Increased leaf area can result in a dilution of per unit area photosynthetic apparatus (Long *et al.* 2006). Khan & Tsunoda (1970) found that due to an extended flag leaf area, domesticated varieties possessed a lower $N_{\%}$, leading to lower photosynthetic rate per unit area at the expense of increased light capture. Contradictorily to this observation, no significant relationship was found between FL_A and $N_{\%}$ in the present study. Furthermore, no association between FL_A and *SLA* was identified, indicating there was not increased thickness in smaller leaves. The higher percentage of intercellular airspace in the smaller flag leaves of *T. dicoccoides* may have contributed to these trends. If increases in FL_A did not influence photosynthetic demand components, area based changes to CO_2 supply components may have been linked to the observed variation in *A*. Austin *et al.* (1982) found strong links between flag leaf anatomical features and FL_A, where stomatal density decreased with increases in FL_A and increases in ploidy. Following this trend, in the present study the *T. dicoccoides* lines with smaller FL_A had a higher stomatal density than the cultivated hexaploid varieties. Dunstone & Evans (1974) observed that the decreases in *A* in modern wheat compared to progenitor species were associated with an increase in

mesophyll cell size linked to larger FL_A. Whether this was also linked to changes in intercellular airspace was not determined in the present study.

1.4.4 Capturing Diversity from Tetraploid Wheat

Donors for Improvement in Modern Varieties

In the 2017 field trial, mean *A* was higher in the flag leaves of the majority of offspring lines in comparison to their bread wheat parent Paragon (Figure 1-20), suggesting that the *T. dicoccoides* parental lines could be suitable donors for increasing *A* per unit in modern varieties. Introgressions from progenitor species of wheat have been shown to increase flag leaf *A* in hexaploid wheat in other studies (del Blanco *et al.* 2000; Merchuk-Ovnat *et al.* 2016b). However, based on the estimates of *A* (leaf^{-1}) in only 1 offspring line (31_12K) was there an improvement in overall total leaf CO_2 assimilation, which was caused by the negative association between FL_A and *A*, and the majority of the offspring lines had a reduced leaf area compared to Paragon. It is most likely that the *T. dicoccoides* parents were the donors for the decreases in FL_A. This observation highlights one of the issues with introgression of diversity available from wild backgrounds, which is the linkage drag of undesirable characteristics (Haggard *et al.* 2013; Reynolds *et al.* 2009).

The conclusion could be drawn that FL_A is more advantageous to *A* (leaf^{-1}) than *A* per unit area. There are limitations in estimating *A* (leaf^{-1}) based on measurements of the central region of each flag leaf, as the assumption is made that photosynthesis is constant over the entire leaf surface, which has been proven to be incorrect (Allwood *et al.* 2015). However, the estimate of *A* (leaf^{-1}) can provide an adequate approximation of carbon fixation per leaf. Strong positive correlations between *A* (leaf^{-1}) and leaf area are typically observed, although FL_A is an element of both variables (Righetti *et al.* 2007). Increases in canopy photosynthesis have been associated with high leaf area index (Joggi *et al.* 1983; Watson 1958). To utilise the diversity identified within the tetraploid progenitor lines, increased *A* will need to be introgressed into modern wheat without reduction to FL_A.

No prior selections were completed on the offspring lines before phenotyping. In an effort to minimise the deleterious effects of linkage drag, selection could have been implemented at an earlier generation to select offspring individuals with high FL_A. Alternatively, if the precise leaf components linked to the trade-off between area and *A* can be identified, selection to promote or demote those characteristics could be used in breeding programs. On the results of the 2016 trial and the parental diversity, the

hypothesis could be made that CO_2 supply components are controlling the association between area and *A*.

1.4.5 Flag Leaf Photosynthesis and Yield

Comparison in Yield Components between Progenitor and Modern Wheat.

Across both years and trials, the high *A* found in *T. dicoccoides* was not linked to any grain yield benefits, as the *T. dicoccoides* had the lowest ranked mean values of grain yield in both trials (excluding dic12b in 2016). Comparisons of yield between cultivated and wild varieties are often biased, as domesticated wheat has had years of selection for increased remobilisation of photoassimilates to the developing grain. Preece *et al.* (2017) found that mean grain yield was 187% higher in a domesticated diploid wheat compared to the wild diploid progenitor and 52% higher in *T. dicoccum* compared to *T. dicoccoides*. Progenitor species have not evolved to be generally high yielding, as natural selection would not necessarily favour agronomic yield (Leister 2012). While grain yield reflects a plant's economic yield, total biomass is often referred to as 'biological yield' (Acquaah 2012). Yield increases in cultivated wheat have been associated with optimisation of *HI*, without major changes to biological yield (Austin *et al.* 1980). This was evident in the 2016 trial (Figure 1-19), where *HI* was highest in the two bread wheats and biomass varied less between the *T. aestivum* and *T. dicoccoides* lines. Biomass was still highest in Tios and Paragon in the 2016 field trial and Paragon in the 2017 field trial (Figure 1-22). 'Biological yield' is primarily determined by the amount of carbohydrates produced through photosynthesis across the growth period of a cereal crop (Thorne 1974). The domesticated lines had the highest *A* ($leaf^{-1}$) and comparatively later flowering time (see: Appendix 4), therefore contributing to a higher 'biological yield' than the shorter lived wild tetraploids. The *T. dicoccoides* lines and the *T. dicoccum* accession dic12b had the highest mean tiller number per plant. Tiller number may be a trait which favours natural selection through reproductive success rather than agronomic yield, as it has been selected against in the domestication of cereals (Remigereau *et al.* 2011).

Grain Yield in the Introgressed Offspring Lines.

In the 2017 field trial, both leaf area and *A* ($leaf^{-1}$) correlated with grain yield. However, as *A* per unit area did not, it is likely the correlation was driven by area variation rather than photosynthesis per unit area. Correlations between flag leaf area and grain yield in other studies have been observed (Dhiman *et al.* 1980; Voldeng & Simpson 1967). As the rate of photosynthesis and the area of photosynthetic tissue determines the source

component of grain yield (Thorne 1974), higher *A* (leaf^{-1}) driven by increases in leaf area is of more benefit to the plant than high *A* per unit area.

There was evidence of a grain yield penalty associated with introgressions from the *T. dicoccoides* parents in the 2017 field trial, where all the offspring individuals had lower mean grain yield than their hexaploid parent Paragon (Figure 1-22). This trend was also evident for biomass (excluding 31_12K). As discussed above for the trait FL_A, linkage drag and yield penalties can occur when introgressions are made from wild grasses (Summers & Brown 2013). Ultimately there were no advantageous effects of increasing *A* in relation to grain yield in the present study. It is important to note that the 2017 field trial was irrigated. As smaller FL_A was associated with decreased *E* (leaf^{-1}) in the 2016 field trial (Figure 1-18), the offspring lines may theoretically have improved yield stability in a water-limited environment, which could be investigated through further work.

Variation Across Trials

Considerably higher grain yields were observed in the 2017 trial in comparison to 2016. In 2016, the yield data may have been influenced by mechanical damage to the plants when transferring to crates during senescence, which was evident from the lower yield and high standard deviation observed within each line (Figure 1-19). Furthermore, the 2017 trial was well irrigated and the plants were grown with increased spacing, which also may have been beneficial to yield. In the 2016 trial, Robigus had to be re-transplanted due to disease. Later sowing dates can have detrimental effects to grain yield (Dhiman *et al.* 1980). Additionally, Robigus missed the applications of N in the trial due to the later transplant date, these factors will have contributed to the low $N_{\%}$ and grain yield observed in the 2016 trial.

1.5 Chapter Outlook.

While improved photosynthetic capacity and efficiency has previously been identified in *T. dicoccoides*, the diversity available from the progenitor tetraploids is relatively untapped (Peng *et al.* 2012). High per unit CO_2 assimilation was found in the progenitor *T. dicoccoides* lines (dic71 and dic72) that could be introgressed into modern wheat to increase productivity. However, the introgressed offspring individuals highlighted that incorporating higher *A* in to a modern background cannot be made at the expense of flag leaf area.

Conversely, the potential benefits of increased flag leaf area are environment specific. Based on the reduced water loss shown to be associated with a smaller flag leaf, decreased leaf area with a higher per unit *A* would still be beneficial in ideotype design for a water-limited environment. Finally, the smaller leaf areas observed in the progenitor species may reflect a greater investment, and larger reliance, on other photosynthetic organs such as the ear and awns.

Chapter Findings Summary.

1. Using a diverse collection of field grown plants, two *T. dicoccoides* accessions were identified with high CO_2 assimilation on a standardised leaf area basis (*A*). These lines could be used as donors for modern wheat improvement.
2. There was stronger evidence that photosynthetic supply components (e.g. CO_2 supply and photochemistry) were linked to the variation in *A* observed across the collection. There was weaker evidence that the variation was a result of photosynthetic demand components (e.g. flag leaf nitrogen content and specific leaf area).
3. Due to a smaller flag leaf area (FL_A) in the *T. dicoccoides* individuals, when CO_2 assimilation was expressed on a per leaf basis, *A* (leaf^{-1}), modern wheat outperformed the progenitor individuals.
4. A collection of tetraploid and hexaploid crossing progeny and parental lines were screened in a field trial in 2017. Within this collection, FL_A was of greater importance to grain yield than *A.* Furthermore, there was a dilution effect on *A* associated with increased FL_A. These trends highlighted that an introgression of higher *A* from a wild background should be achieved without a reduction to FL_A.

2 THE PHOTOSYNTHETIC CONTRIBUTION OF AWNS.

Abstract

Unlike the majority of UK modern bread wheat varieties, the tetraploid progenitor (*T. dicoccoides*) is typically awned, which in the present study was shown to be linked to higher CO_2 assimilation (*A*) per ear. To test the importance of awn photosynthesis in a more adapted material than *T. dicoccoides*, gas-exchange analysis was used to measure ear and flag leaf photosynthesis in 3 field grown pairs of synthetic hexaploid wheat near isogenic lines (SHW NILs), varying only for awn presence. Measurements were taken during flowering and grain-filling, and organ area was calculated to express data on both a per unit and per organ basis. Multiple linear regression models were fitted to analyse the influence of awn presence, NIL pair number and growth stage, on 10 response variables linked to ear and flag leaf photosynthesis. Yield component data were collected for 5 NIL pairs included in the trial. Additionally, a genome-wide association (GWAS) study was carried out to identify marker-trait associations linked to awn presence, using 323 individuals of a SHW breeding program.

Awn presence was associated with an increase in ear area, leading to higher *A* per ear, but no change in per unit area ear *A*. However, there was a negative association between awn presence and *A* per flag leaf, caused by a reduction in per unit *A* rather than reduced leaf area. Mean water use efficiency (*WUE*) was higher in the ears than flag leaves at both growth stages. In 4 out of 5 NIL pairs included in the field trial, mean grain yield was lower in the awned line; but this effect was not consistent over multiple years and locations. The GWAS identified 22 significant marker-trait associations, all located between 43 and 72 cM on chromosome 5A. The single nucleotide polymorphism (SNP) with the highest association with a $-\log_{10}$ (*P*) value of 39.3 was located at 58 cM on chromosome 5A. There is a known awn inhibiter on chromosome 5A, which was most likely responsible for the observed variation. This study suggested awn presence may not be an important trait to consider in ideotype design for a 'well-watered' environment. However, with the current concerns relating to changing climates, traits linked to the preservation of photosynthesis under unfavourable environmental conditions may be fundamental to future crop production.

2.1 Introduction

2.1.1 Organ Photosynthesis in Wheat.

Photo-assimilates are remobilised to the developing kernel during grain-filling, from three main stores: the senescing leaves (Bell & Incoll 1990), stem and peduncle carbohydrate reserves (Raven & Griffiths 2015) and the ear (Zhou *et al.* 2016). However, there has been historic and an ongoing debate over which source is most relevant to overall grain yield. The flag leaf has been traditionally considered the most important photosynthetic organ (see: 1.1.1). However, there has been a shift in physiological discussion, focusing on how the contribution of reproductive structures may have previously been underestimated. Photosynthetic apparatus is well distributed across the wheat ear (Teare *et al* 1972a; Teare & Peterson 1971). An awn is a barbed needle-like projection of the lemma, which evolved in wild wheat to provide selection advantages of grazing deterrents, seed dispersal and seed burial (Evangelista *et al.* 2011; Guo & Schnurbusch 2016). When present, awns can form up to 40% of spikelet biomass (Rebetzke *et al.* 2016), hence awns can be the main contributor for total ear photosynthesis (Tambussi *et al.* 2007). Awns have been bred out of the majority of domesticated crops, due to historic logistical problems in harvesting and processing (Mach 2015). Advancements in agricultural machinery and technology have largely removed these limitations. The second highest yielding group 1 bread wheat is currently the awned variety 'Skyfall' (nabim 2018), which has held considerable market share since release, and the possible advantages of awns to wheat production is a topical question in the agricultural industry. Awn presence could be a useful trait for promoting ear photosynthesis by extending the photosynthetic surface area of the organ.

The Wheat Yield Consortium identified phenotypic selection for higher ear photosynthesis as an important strategy for addressing plateauing yields (Parry *et al.* 2011). There are several advantages of increasing ear and awn photosynthesis in wheat. Evans *et al.* (1972) proposed that in comparison to the flag leaf, the awns were favoured with a better canopy position for light interception, a shorter pathway for assimilate remobilisation and potentially delayed senescence. Furthermore, the ear has a larger surface area than the flag leaf, particularly with the presence of awns (Blum 1985). There is also evidence of re-assimilation of respired CO_2 in the ear, particularly in the green pericarp, which reduces respiratory losses (Tambussi *et al.* 2007). However, arguably the greatest reason for exploiting ear photosynthesis is linked to drought tolerance.

Compared to the flag leaf, ear photosynthesis is maintained to a greater degree under drought stress (Ding *et al.* 2017; Li *et al.* 2017), due to a number of factors. Firstly, the bracts and awns of the ear have the potential for high osmotic adjustment, coupled with a high overall relative water content (Tambussi *et al.* 2005). Secondly, parts of the ear have distinctive xeromorphic characteristics, such as a thick epidermis (Araus *et al.* 1993). Lastly, fundamental to drought tolerance is the ratio of CO_2 gained to water lost. Awns in particular have been reported to have high *WUE*, driven by high CO_2 assimilation and low transpiration (Blum 1985). Awns and glumes possess a lower $\Delta^{13}C$ than the flag leaf (Araus *et al.* 1993; Gebbing & Schnyder 2001), also indicating a higher *WUE* (Farquhar *et al.* 1982). This evidence indicates ear photosynthesis is a valuable source of assimilates to the developing grain under drought stress.

In contrast, there has been less focus in recent literature on the benefits of promoting flag leaf photosynthesis and the potential detrimental effects of investment into ear photosynthesis. In organ comparisons, some studies have found higher photosynthetic rate per unit area in the leaf under well-watered conditions (Li *et al* 2017; Teare *et al*. 1972), which is also supported by a higher per unit Rubisco content (Zhou *et al.* 2016). Awns have been shown to contribute up to 46% of ear biomass (Teare & Peterson 1971), and as the ear and leaf compete for nitrogen allocation (Parry *et al.* 2011) there may be a detrimental downstream effect of awn development. The assimilates used in awn formation are the cost of awn development (Guo & Schnurbusch 2016). Though there are conflicting reports about the benefits and drawbacks of different investment into ear and leaf photosynthesis; the ultimate determinant is the effect on grain yield.

2.1.2 Quantifying the Contribution of Ear Photosynthesis to Yield.

Invasive experiments, such as organ detachment and shading methods, have previously been used to quantify the importance of source supplies to grain sink (e.g. Khaliq *et al.* 2008; Lupton & Ali 1966). These techniques can artificially change conditions surrounding the organs (Tambussi *et al.* 2007) and detachment methods can induce stress whilst enhancing compensatory activity in the remaining source supplies (Chanishvili *et al.* 2005). With these limitations in mind, Sanchez-Bragado *et al.* (2014) used natural abundance carbon isotope ratios to quantify the contribution of awned ears and flag leaves to grain-filling in elite bread wheat varieties, finding that even under irrigated treatment the ear contributed considerably more than the leaf. However, Raven & Griffiths (2015) proposed that this method may hold inaccuracies as not all sources of organic carbon and

possible fractionations during grain-filling are considered, although they did verify the potential application of natural stable isotope labelling in organ comparisons. In a recent study, Zhou *et al.* (2016) used a ^{15}N labelling technique to identify higher remobilisation of N from the ear than the flag leaf. The significant disadvantage of isotope labelling studies is the requirement of controlled conditions, limiting field scale application. Furthermore, the majority of studies have not used genetically comparable material.

Awn presence reflects investment into ear photosynthesis. A technique for assessing the potential yield effects of this investment is the use of Near Isogenic Lines (NILs), which are sibling-lines that differ only for one phenotype. This reduces the off-target genetic or phenotypic variation that can mask the impact of the trait of interest. Experiments designed using NILs can be completed within field environments, without invasive measurements. For example, Rebetzke *et al.* (2016) used 45 awned and awnletted (ears with very short awns) NILs to assess grain yield and characteristics across several environments and watering regimes. NILs have also been used to test the importance of awn photosynthesis within controlled environments (e.g. Olugbemi *et al*. 1976a; Teare *et al*. 1972; Weyhrich *et al*. 1995). Field measurements of gas-exchange and yield in awned/unawned NILs would be a powerful tool in quantifying the importance of awn presence to organ photosynthesis and ultimately grain yield.

2.1.3 Genetic Control of the Awns.

Using genetically comparable material would also help in identifying genetic control behind the awn trait. Three dominant inhibitor genes are known to suppress the presence of awns in hexaploid wheat. The *Hooded* (4A, *Hd*) gene results in awn bending and shortening (Rao 1981). The *Tipped 1* (5A, *B1*) mutant is linked to short awn tips increasing in length towards the top of the ear, whereas the *Tipped 2* (6B, *B2*) mutants possess very short awn tips which are mostly evenly distributed in length along the ear (Sourdille *et al.* 2002; Watkins & Ellerton 1940). A fully awned wheat has the recessive form of all three inhibitor genes (Yoshioka *et al.* 2017). Genotypes with dominant alleles at two of the three loci (for instance: *Hd B2*, *B1 B2* or *Hd B1*) are unawned (Mcintosh *et al.* 2013). In a large collection of material varying in awn presence, a genome-wide association study (GWAS) could be used to pinpoint genetic polymorphisms relating to the trait. Using GWAS for genetic investigation can provide detailed information on genetic variability and architecture of targeted traits within crop species (Huang & Han

2014). A GWAS could inform which inhibitor gene (or genes) is responsible for the awn variation, or whether novel genetic diversity is linked to the trait.

2.1.4 Chapter Aims

The focus of this chapter was to establish the importance of awn presence in contributing to grain yield within a UK field environment, using the presence of awns as an example of investment into ear photosynthesis. Five different pairs of synthetic hexaploid wheat near isogenic lines (SHW NILs) were used for this investigation, all of which were presumed to be effectively isogenic except for awn presence. The aims of the chapter were:

1. In replicated yield plots, analyse potential variation in grain yield, yield components and seed characteristics between the 5 SHW NIL pairs. Compare existing yield trial data of the same material, collected previously over different years and locations.
2. In 3 pairs of the SHW NILs, use gas-exchange analysis to determine how awn presence influences ear photosynthesis and respiration at two development stages: anthesis and grain-filling. Make parallel measurements of flag leaf photosynthesis and respiration to determine possible effects of awn presence to the leaf.
3. Determine organ size in the same 3 pairs of SHW NILs to examine the relationship between awn presence, ear area and flag leaf area.
4. Using a larger collection of SHW individuals, including the selected NILs, evaluate the genetic control behind awn presence and establish which of the known awn inhibitor genes are linked to the phenotypic variation.

2.2 Methodology

2.2.1 Material and Trials.

2.2.1.1 Material

Previous to the current study (see: Appendix 6), the five SHW NIL pairs were created as part of the Biotechnology and Biological Sciences Research Council (BBSRC) funded Wheat Improvement from Synthetic Hexaploids (WISH) project. Primary SHW were formed at CIMMYT (El Batán, Mexico) through crossing different tetraploid and diploid parents (Table 2-1). Through the WISH program, different CIMMYT primary SHW lines were backcrossed to the UK elite bread wheat Xi19.

Table 2-1 - Pedigree information about the 5 pairs of Synthetic Hexaploid Wheat Near Isogenic Lines included in the 2017 NIL SHW yield plots field trial grown at KWS. The lines were formed through backcrossing primary synthetic wheat (created at CIMMYT) with the UK elite bread wheat Xi19. In WISH Code: A = awned lines and NA= unawned line.

Pair Number	WISH Individuals	CIMMYT Synthetic	Tetraploid Parent	Diploid Parent	Hexaploid Parent
1	WISH 18 (A) + 19 (NA)	SHW052	Altar-84	Tauschii 221	Xi19
2	WISH 75 (A) + 76 (NA)	SHW109	Chen_7	Tauschii 429	Xi19
3	WISH 121 (A) + 122 (NA)	SHW170	68.111/RGB-U//WARD/3/FGO/4/RABI	Tauschii 900	Xi19
4	WISH 242 (A) + 243 (NA)	SHW330	Decoy-1	Tauschii 370	Xi19
5	WISH 297 (A) + 299 (NA)	SHW441	Decoy-1	Tauschii 1024	Xi19

The backcrossed offspring were taken through a single seed decent (SSD) program to the BC_1F_5 generation, where contrasting awned and non-awned individuals were separated within families still segregating for awn presence. The lines were stabilised thereafter through maintaining as single plant progenies. In each of the resulting five pairs of SHW NILs, the two individual lines were assumed to have similar genetic makeup, varying only in awn presence (Figure 2-1). The 5 pairs of SHW NILs are hereafter referred to by pair number (1 to 5) and awn presence (A = awned, NA = unawned).

Figure 2-1 - Field grown mature ears of pairs 1-5 (top to bottom) of synthetic hexaploid wheat near isogenic lines (SHW NILs), showing differences in awn presence within each pair. Ears were collected from the 2017 NIL SHW yield plots field trial grown at KWS. Scale bar = 10 cm.

2.2.1.2 Trials

Trials used in this chapter included:

- The 2017 NIL SHW yield plots field trial grown at KWS. Hereafter referred to as the NILs field trial.

- The 2017 Park Farm New Ornamentals Field Trial used for ear photosynthesis measurements at ambient conditions of different wheat ploidy, here after referred to as the ploidy field trial.

NILs Field Trial

A replicated block design was used in the NILs field trial, with 1 yield plot per block for each SHW NIL (Figure 2-2). Within each block, NIL pairs were kept together, but both the sequence of NIL pairs and the A/NA orientation within each pair was randomised. Yield plots were 7 m^2 and consisted of roughly 2250 seeds. The plots were drilled on the 10th of October 2016 in a field at Fowlmere, Cambridgeshire by KWS Ltd. The elite bread wheat KWS Santiago was included as a control, with two replicated yield plots per block. To achieve a universal N application of 204 kg / N; the plot was fertilised with ammonium nitrate (34.5% N) in three applications of 145, 175 and 115 kg ha^{-1} and a further application of an ammonium sulphate and nitrate mix (27% N) at a rate of 200 kg ha^{-1}. The fertiliser was applied at GS25, GS30, GS31 and GS32 (Zadoks *et al.* 1974). At GS32, an application of fungicide and plant growth regulators was applied. Between GS30 to 34 the plots were treated with herbicide. At GS39, the plots were treated with a second dose of fungicide and at ear emergence the plots were treated with fungicide and insecticide. The trial was harvested on the 4th of August 2017.

Block1	4-NA	4-A	KWS Santaigo	2-A	2-NA	5-A
Block2	1-NA	1-A	3-A	3-NA	KWS Santaigo	5-NA
	2-NA	2-A	3-A	3-NA	KWS Santaigo	1-NA
	KWS Santaigo	4-A	4-NA	5-NA	5-A	1-A

Figure 2-2 – The layout for the NILs field trial, consisting of a randomised block design. Two blocks were included in the trial. In each block, the order of the NIL pairs and the A/NA positioning within each pair was randomised, but the individual NIL pairs were kept together.

Ploidy Field Trial

The design and establishment of the ploidy field trial was previously described in the 2017 field trial of Chapter 1 (see: 1.2.1).

2.2.2 Phenotypic Methodology

2.2.2.1 Material Sampling.

NILs Field Trial

Gas exchange and anatomical measurements were restricted to Pairs 1, 2 and 3, in an effort to ensure a suitable number of replicates were collected for each line, whilst additionally taking into consideration the time required for each measurement and equipment limitations. Measurements were completed at two growth stages: flowering and grain-filling. Flowering was defined as being when 50% of main tillers in each plot had reached GS61 (Zadoks *et al.* 1974). Following Araus *et al.* (1993) and Zhou *et al.* (2016), two weeks after flowering was specified as the grain-filling stage, where the measurements were repeated on different plants from the same three pairs. Measurements during 'flowering' were completed from the 27th of May to the 3rd of June 2017 and those during 'grain-filling' were completed from the 11th to the 20th of June 2017. At each growth stage, 6 plants were sampled per line (3 per plot in each block). At both growth stages, the pairs were measured in the order 1 to 3: pair 1 reached anthesis at the earliest date (27th of May), whilst pairs 2 and 3 reached anthesis on the 30th of May (although pair 2 had an earlier heading date). The delayed measurements of pair 3 at the grain-filling stage was a result of equipment failure (Table 2-2).

Table 2-2 – The dates and growth stages (Zadoks *et al.* 1974) that measurements were completed at for each of the 3 pairs included during the NILs field trial conducted in 2017 at Fowlmere, Cambridgeshire (KWS Ltd.).

Pair Number	Measurement Period	Growth-stage (GS)
Flowering		
1	27/05/17 - 31/05/17	GS61 - 67
2	31/05/17 - 01/06/17	GS63 - 65
3	01/06/17 - 03/06/17	GS67 - 69
Grain-filling		
1	11/06/17 - 13/06/17	GS71 - 73
2	13/06/17 - 15/06/17	GS73 - 77
3	19/06/17 - 20/06/17	Late milk stage (~ GS77)

Main tillers of healthy plants were randomly selected from the centre of each plot; no measurements were made on plants in the outer three rows to reduce the bias introduced by edge effects. Gas-exchange measurements were made between 1000 and 1500 hours. After 15:00, each measured main tiller was cut and immediately re-cut under water, and stored in, deionised water to prevent cavitation. The detached tillers were then transferred back to Park Farm (NIAB, Cambridge) for immediate processing and imaging. At maturity, the harvest index (*HI*) sample and 30 ears were taken on the 30th of July 2017

from every plot. All of the SHW NILs and control plots were combined on the 4th of August 2017.

Ploidy field trial

Ear gas-exchange measurements were completed on main tillers of separate plants at anthesis (GS61 - 67) in the ploidy field trial on two different days. On the 4th of June 2017, 4 ears of dic71 and dic72 were measured. Then on the 10th of June 2017, 4 ears of Paragon and Robigus were sampled.

2.2.2.2 Measurements.

NILs field trial

Gas-exchange Measurements

A LI-COR 6400XT combined with a 6400 - 22 Opaque Conifer Chamber and a 6400 - 18A RGB Light Source (LI-COR, Lincoln, USA) was used for the gas-exchange measurements and is hereafter referred to as the LI-COR CC. The IRGA conditions were set to reflect the ambient field environment, with the aim of reducing time needed for acclimatisation of the sample to the chamber. Relative humidity was maintained at 50 ± 10%. Leaf fan was set to fast and block temperature was controlled at 23 ºC. Reference CO_2 was set at 400 µmol mol^{-1}. Due to the size of the chamber a high gas flow rate of 600 µmol s^{-1} was used. Based on preliminary light curves completed with the LI-COR CC (Figure 2-3), a near-saturating PPFD of 1500 µmol m^{-2} s^{-1} was set (90% red and 10% blue light).

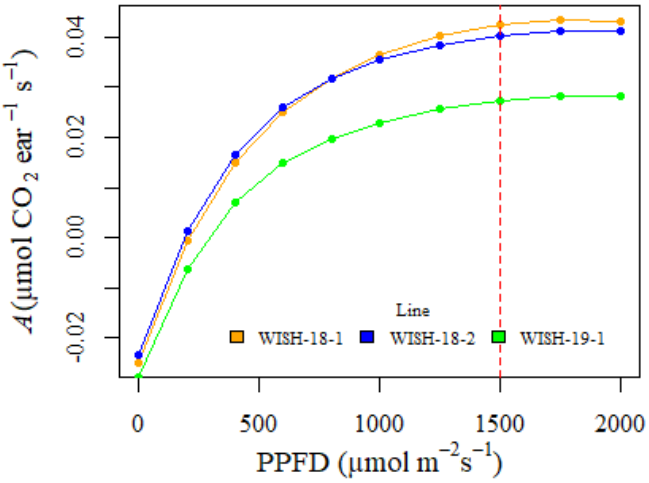

Figure 2-3 - Light response curves measured in the NILs field trial for 3 separate ears from main tillers of SHW ears at GS57 (Zadoks *et al.* 1974). The curve shows *A* (ear $^{-1}$) plotted against a range of light intensities, in order to determine a near-saturating light intensity to conduct measurements at. The chosen near-saturation point of 1500 µmol m^{-2} s^{-1} is shown by a dashed red line.

For the non-invasive gas-exchange measurements, entire ears were measured within the chamber. Awns and ears were bent around the inner chamber cavity to stop protrusion. Where leaves were measured, the central region of a single flag leaf was placed in the chamber, with the adaxial side facing the internal LED light source. The area of the leaf enclosed in the gasket was imaged later and results were recalculated on the basis of the actual leaf area. Ears and leaves were left to acclimatise until *A* and g_s had stabilised, which took around ~ 3 minutes per measurement (see: Appendix 2). Ears and leaves were then dark adapted under foil for a period of 15 minutes before steady state R_{DARK} was recorded for each organ with the actinic chamber light turned off (Kromdijk *et al.* 2010).

Chamber Leak Tests.

Diffusive leaks can significantly influence the reliability of data when chamber CO_2 levels differ from ambient conditions (Li-Cor 2012). In this chapter all measurements were made at ambient CO_2 concentrations in the field (400 ppm CO_2). Unlike the measurements taken in the laboratory (e.g. Chapter 1), the potential changes to the ambient CO_2 concentration by respiratory build up were not a concern. However, to identify possible leaks through-out the period of measurements, an oven dried awned ear was used, in which no gas exchange was occurring. This dried ear was used to test for potential leaks in the field environment with the chamber set-up. The same protocol was followed as for measuring ear gas-exchange. Across the 15 days that the dried ear was measured, the mean apparent *A* was -0.010 µmol CO_2 m^{-2} s^{-1} (S.D = 0.41 µmol CO_2 m^{-2}

s^{-1}). Therefore, as potential leak effects were inconsequential, no leak correction was applied to the data.

Ear Area Estimation.

Considerable error can be introduced by inaccurate estimates of ear surface area due to the complex and irregular ear shape (Tambussi *et al.* 2007). The LI-COR CC chamber can fully enclose a wheat ear, meaning that data can accurately be expressed on an ear^{-1} basis. Measurements on a per unit basis (cm^{-2}) were calculated by estimating ear area and recalculating the gas-exchange results based on the estimated organ area. An Olympus Stylus Tough TG - 4 (Shinjuku, Tokyo, Japan) attached to a fixed tripod was used to image 3 central spikelets from each side of every measured ear (Figure 2-4). The 6 individual spikelet areas were calculated by converting the image to binary in ImageJ (V-1.51); mean spikelet area was then determined. For each ear, mean spikelet area was multiplied by spikelet number to estimate ear area.

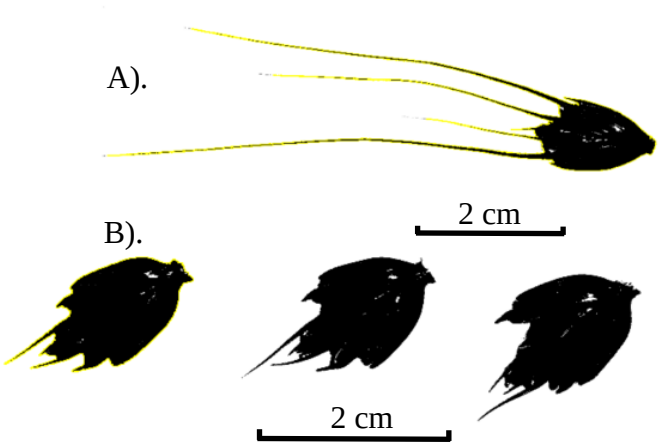

Figure 2-4 – Imaged spikelets from pair 1 collected during the flowering growth stage measurements. Images were converted to binary in ImageJ (V - 1.51), the yellow outline shows the selection used for the area calculations. The area of spikelets were determined to estimate an area for each measured ear. A). An awned spikelet from 1-A. B). Unawned spikelets from 1-NA. Scale bars shown were 2 cm.

Flag Leaf Area Estimation

To show leaf gas-exchange results on a total leaf surface area basis ($leaf^{-1}$), flag leaf length and width was recorded and flag leaf area estimated using the Teare & Peterson (1971) equation discussed in Chapter 3. To show data on a per unit basis (cm^{-2}) a LI-COR CC foam gasket was placed over the same central region measured in the field of each flag leaf and a photo was taken, the gas-exchange data were corrected based on the estimated area enclosed in the gasket. Analysis on ImageJ (V - 1.51) was used to calculate the leaf

area coverage of the gasket and the gas-exchange parameters were re-calculated with the new area.

Yield Measurements

Harvest Index

At maturity, a 50 cm ruler was horizontally placed against the base of the plants in two different central rows in each plot; the tillers that fell within the ruler were cut off at ground level. The samples from both rows were bunched together in each plot. Samples were dried for 72 hours at 25 °C before dry weights were taken (Biomass); after threshing a seed weight was taken. Harvest Index was expressed as the proportion of seed weight to biomass.

Collected Ears

At maturity, 30 ears from each plot were collected and dried at 30 °C for 24 hours. Of those ears, 15 were randomly selected per plot and the number of total and unfertile spikelets were counted per ear. All ears were then threshed; seed weight and dimensions were determined using the MARVIN seed analyser (GTA Sensorik GmbH, Neubrandenburg, Germany). A complete list of traits measured on the SHW NILs in the NILs field trial is shown in Table 2-3.

Grain Yield

For the NILs field trial, combine harvester data provided grain yield (t ha^{-1}) which was adjusted to 15% moisture. Prior to this study, the SHW NILs had been included in a number of other yield trials across different years and locations. In total, yield data were available for 3 different years (2014, 2015 and 2017) and across 6 different locations. In 2014, the SHW NILs were grown in 2 replicates at 2 locations (Cambridge and Callow, Herefordshire), these replicates were averaged. In 2015, the SHW NILs were grown in single replicates at 5 different locations: RAGT Seeds (Ickleton), KWS Ltd (Thriplow), Morley (Wymondham), NIAB (Cambridge) and at Limagrain (Rothwell). However, due to the augmented trial design used, pairs 2 and 5 were absent at KWS, and pairs 2 and 4 were absent at Limagrain. Yield data were also provided by the combine harvester for these other trials and adjusted to 15% moisture content. In 2017, yield data were only generated in the NILs field trial at KWS.

Table 2-3 – The traits measured in the NILs field trial on the SHW NILs. The acronyms used for each trait throughout the Chapter are also included. The measuring technique for each trait and, where applicable, the references to where methods have been replicated from are shown.

Trait Measured	Acronym / Name	Units	Measurement technique	Reference
Per ear net CO_2 assimilation.	*A* (ear $^{-1}$)	µmol CO_2 ear^{-1} s^{-1}	LI-COR CC *.	-
Ear per unit area net CO_2 assimilation.	Ear *A* (cm $^{-2}$)	µmol CO_2 cm^{-2} s^{-1}	LI-COR CC.	-
Per flag leaf net CO_2 assimilation.	*A* (flag leaf $^{-1}$)	µmol CO_2 leaf^{-1} s^{-1}	LI-COR CC.	-
Flag leaf per unit area net CO_2 assimilation.	Flag leaf *A* (cm^{-2})	µmol CO_2 cm^{-2} s^{-1}	LI-COR CC.	-
Per ear respiration in the dark.	R_{DARK} (ear^{-1})	µmol CO_2 ear^{-1} s^{-1}	LI-COR CC.	-
Per flag leaf respiration in the dark.	R_{DARK} (flag leaf^{-1})	µmol CO_2 leaf^{-1} s^{-1}	LI-COR CC.	-
Per ear transpiration.	*E* (ear^{-1})	mmol H_2O ear^{-1} s^{-1}	LI-COR CC.	-
Per flag leaf transpiration.	*E* (flag leaf^{-1})	mmol H_2O leaf^{-1} s^{-1}	LI-COR CC.	-
Estimated ear area.	Ear Area	cm^2	Spikelets imaged using ImageJ (V - 1.51).	-
Estimated leaf area.	Leaf Area	cm^2	Estimated from leaf width and length.	Tear & Peterson (1971)
Gross assimilation rate.	*GAR*	µmol CO_2 organ^{-1} s^{-1}	$A + R_{DARK}$	Araus et al. (1993) and Zhou et al. (2016)
Instantaneous water use efficiency.	*WUE*	µmol (CO_2) mmol (H_2O)$^{-1}$	*GAR* / *E*	-
Grain yield.	*Grain Yield*	t ha^{-1}	Combine Harvester data.	-
Harvest index.	*HI*	-	Seed weight / biomass	-
Per ear seed number.	*Seed No. (ear $^{-1}$)*	-	Measured on a MARVIN seed analyser.	-
Thousand grain weight.	*TGW*	g	Measured on a MARVIN seed analyser.	-
Seed area.	*Seed area*	mm^2	Measured on a MARVIN seed analyser.	-
Per ear average total spikelet number.	*Spikelets*	-	Counted for 15 ears per line.	-
Per ear average infertile spikelet number.	*Infertile Spikelets*	-	Counted for 15 ears per line.	-

* LI-COR CC - A LI-COR 6400XT combined with a 6400 - 22 Opaque Conifer Chamber and a 6400 - 18A RGB Light Source (LI-COR, Lincoln, USA).

Ploidy field trial

The same protocol was followed for the ploidy field trial as in the NILs field trial using the LI-COR CC. In this trial the ears were left to acclimatise for 30 minutes before only an ambient reading of ear photosynthesis was taken on an ear^{-1} basis. Ear area was estimated by treating the ear as a parallelepiped, by measuring length and width of each face to calculate the area (Fortineau & Bancal 2018; Zhou et al. 2016). This method did not take into account awn presence.

2.2.2.3 Analysis.

NILs Field Trial

Using the package 'lme4' (Bates *et al.* 2014) in RStudio (V - 3.4.3) mixed linear regression models were fitted to test the responses of 10 dependant variables relating to ear and flag leaf photosynthesis. The fixed effects included in the models were awn presence, NIL pair number (1 - 3), measurement growth stage (flowering or grain-filling) and the interactions between these variables. The random effect included in the model was block number. In the case where the random effect had negligible influence on the dependent variable, it was dropped and multiple linear regression models were fitted instead using the 'lm' function in RStudio (V - 3.4.3). Backward selection was used to fit the most appropriate regression model for each trait, eliminating non-significant variables ($P > 0.05$) using ANOVA table comparisons of different models. Once the most appropriate model had been identified, ANOVA tables were computed for the fitted model.

For each model, normality quantile-quantile plots and residual diagnostic plots were created to inspect that the assumptions of linear regression were met. Assumptions of constant error variance were violated for the dependent variables of ear area and R_{DARK} (ear^{-1}). For ear area, an outlier was removed for the model fitting analysis (a 1-A ear measured at flowering = 57.1 cm^2), the results changed inconsequentially with the inclusion and exclusion of the outlier. The outlier was included in all other parts of the description of results. Furthermore, a log transformation was used to stabilise error variance for these variables and thereafter model assumptions were met. Finally, a Pearson correlation coefficient test was used to assess potential correlation between the dependent variables: A (ear^{-1}) and R_{DARK} (ear^{-1}).

Ploidy Field Trial

Analysis was conducted using RStudio (V - 3.4.3), ANOVA comparisons were made between the different lines and residuals were checked for violations. Post-hoc tests were completed using Duncan's New Multiple Range test.

Grain Yield

For each of the NILs, separate pairwise comparisons were completed with the compiled yield data set, using a paired sample t-test in RStudio (V - 3.4.3) with awn presence as the treatment. *P*-values were extracted from the results and adjusted for multiple comparisons using the False Discovery Rate method (Benjamini & Hochberg 1995). Furthermore, RStudio (V-3.4.3) functions 'shapiro.test' and 'Bartlett test' were used to analyse data normality and the homogeneity of variance within each pair to ensure t-test assumptions were met.

2.2.3 Genotypic Methodology

2.2.3.1 SNP Genotyping

The complete WISH panel, was genotyped as part of the WISH project. This panel consisted of 323 individuals, including: 313 offspring lines, 9 SHW parents and Xi19. This collection contained all of the SHW NILs (apart from 5-A) and the primary SHW parents for pairs 1, 3 and 4. Genotyping was completed by Bristol University using the Axiom Wheat Breeder's Genotyping Array, which consisted of 35,000 SNPs (Allen et al. 2017). This array was also used for genotyping in Chapter 3, where it is discussed in more detail. The SNP calling was completed prior to the current project, from this data 11,415 high resolution polymorphic markers were extracted. Markers with matching genotypes were removed using the function 'findDupMarkers' in the Rstudio package 'R/QTL' (Broman 2010). The mapped positions were obtained from the consensus map available on CerealsDB (Allen *et al.* 2017; Wilkinson *et al.* 2012). The consensus map was formed through the merging of 5 separate genetic linkage maps, which came from different mapping populations genotyped using the Wheat Breeder's Array (Allen *et al.* 2017). Further markers were removed which did not have mapped positions. Of the remaining markers and individuals the average heterozygosity was 5.9%. Missing genotype data were present at 0.06% in the markers and 0.6% in the individuals. Markers with over 10% heterozygosity were removed and the remaining heterozygous genotypes were set to NA. This left 6247 markers and increased missing genotype data to 1.29% of the total marker and individual data. Finally, markers were removed with too low minor allele frequency (< 5%), which left 5330 markers that were used in the GWAS. A SNP density plot was

formed in RStudio (V - 3.4.3) using the package 'LinkageMapView' (Ouellette *et al.* 2018).

2.2.3.2 Genome Wide Association Analysis (GWAS)

A genome wide association study (GWAS) was completed in RStudio (V - 3.4.3) using the package 'GWASpoly' (Rosyara *et al.* 2016). Issues in association studies can arise from varied levels of relatedness between individuals leading to erroneous results, accounting for relatedness by estimating population structure and kinship reduces these errors (Yu *et al.* 2006). The 'GWASpoly' package used Q + K mixed linear models for single-marker analysis, where Q represents subpopulation covariates and K represents the kinship matrix treated as a random effect (Rosyara *et al.* 2016). The marker-estimated kinship matrix was calculated on a thinned marker set using the package function 'set.K'. Markers were thinned by removing one marker in each pairwise comparison with over 0.80 correlation coefficient, using a Pearson's coefficient test in Rstudio (V - 3.4.3); leaving 1528 markers. This was carried out in an effort to reduce linkage disequilibrium between SNP markers influencing the kinship estimate. The complete marker set (n = 5330) was used for the GWAS and missing genotypes were imputed using population means. Population structure can be inferred using principle components analysis (Price *et al.* 2006; Stich *et al.* 2008). Using the marker data, principle component analysis was completed within the 'GWASpoly' package, eigenvalue size was inspected and 10 principle components were used as covariates to correct for population structure (Ferrão *et al.* 2018).

The GWAS analysis was completed using the function 'GWASpoly' with an additive marker-effect model. The genetic control of awn presence is not additive, but as heterozygote genotypes were removed from the data the marker-effect model selection was inconsequential. For each marker, the software returned a –log10 (*P*) value and a marker effect, where the marker effect reflects the dosage of 0.5 of the genotype that was classed as the BB allele in the SNP array formation. Following Bock (2017), a Bonferroni correction to 5% was used to determine a significance threshold for the –log10 (*P*) values and quantile-quantile (Q-Q) plots were formed to inspect and validate the model. After the initial analysis, the markers with the highest –log10 (*P*) were treated as co-variates and the analysis was repeated to test for additional loci. Finally, using the GWAS results, a circular-Manhattan plot was created in RStudio (V - 3.4.3) using the 'CMplot' package (available from: www.github.com/YinLiLin/R-CMplot).

2.3 Results

2.3.1 Gas-exchange Results in the Ploidy Field Trial.

Significant variation was observed in *A* (ear $^{-1}$) across the four individual lines (Figure 2-5 (a.), ANOVA: *F* (3, 12) = 28.4, *P* = < 0.001). The *T. dicoccoides* lines dic72 and dic71 had significantly higher mean *A* (ear $^{-1}$) than Paragon and Robigus (dic72 = 0.038 µmol CO_2 ear^{-1} s^{-1}, dic71 = 0.033, Paragon = 0.029 and Robigus = 0.028). The standard deviations of the means for dic72, dic71, Paragon and Robigus were 0.0028 µmol CO_2 ear^{-1} s^{-1}, 0.0013, 0.0014 and 0.0004 respectively. Estimated ear area also varied significantly across the group (Figure 2-5 (b.), *F* (3, 12) = 107.2, *P* = < 0.001). Despite the *T. dicoccoides* lines having significantly smaller ears, dic71 and dic72 maintained higher *A* per ear. Awn presence was not included in the ear area calculations. When awn length was measured as the distance from the top of the ear to the top of the longest awn (Pask *et al.* 2012); dic71 and dic72 had mean awn lengths of 15.1 and 14.1 cm respectively, whereas Paragon and Robigus were unawned.

a).

b).

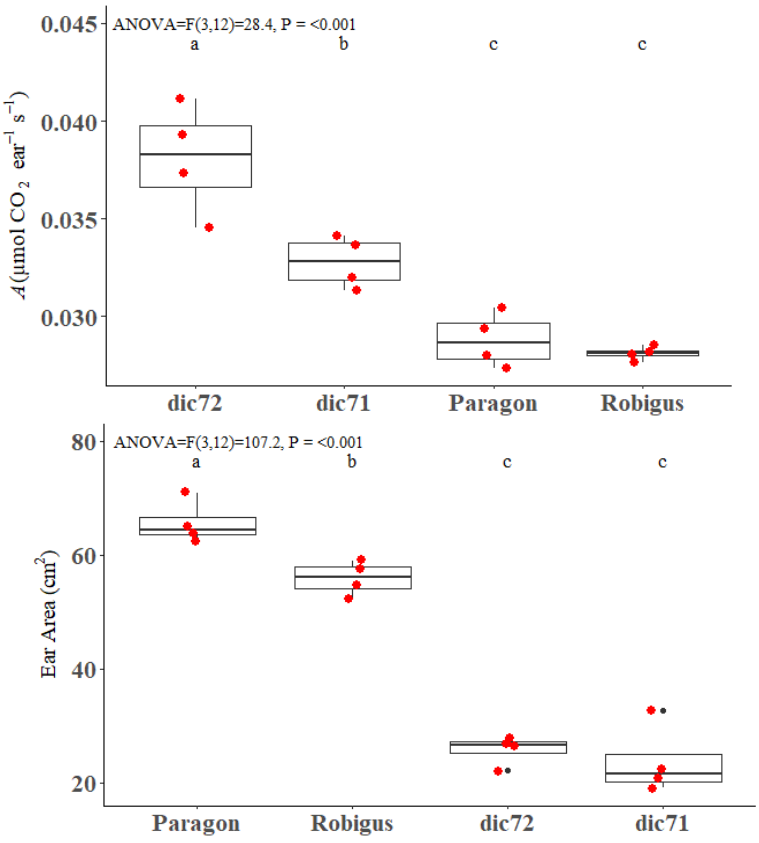

Figure 2-5 – a). *A* (ear^{-1}) of the *T. dicoccoides* lines (dic72 and dic71) and the bread wheat varieties Paragon and Robigus from the ploidy field trial, measured using a LI-COR CC. b). Estimated ear areas of the same group, determined by measuring the length and width of each face to calculate an estimate of ear area (see: Fortineau & Bancal 2018; Zhou et al. 2016). Significance groups, determined by an ANOVA and Duncan test, are shown by letter grouping above each box.

2.3.2 Gas-exchange Results of the NILs Field Trial.

For every dependent variable tested in the linear mixed model analysis, block number was found to have a negligible effect on each dependent variable (except for leaf area). For example, for *A* (ear $^{-1}$) variance caused by the block random effect was 4.2 x 10^7. Therefore, multiple linear regression models were used hereafter with the random variable dropped.

2.3.2.1 Ear Gas-exchange.

A significant model was identified for *A* (ear $^{-1}$) (F (8, 63) = 21.35, $P < 0.001$), which had an adjusted R^2 of 0.70. *A* (ear $^{-1}$) was influenced by awn presence (F = 15.5, $P < 0.001$), pair number (F = 51.7, $P < 0.001$) and growth stage (F = 23.6, $P < 0.001$). Significant interactions were observed between the independent variables of awn presence and pair number (F = 4.8, P = 0.01) and also pair number and growth stage (F = 9.4, $P < 0.001$). Within the 3 NILs, mean *A* (ear $^{-1}$) was higher in every awned line than the unawned lines at both growth stages (Table 2-4); pairwise comparisons are shown in Figure 2-6. The greatest variation was observed in pair 1, where, in comparison to the unawned line, the awned NIL had a 48% and 30% higher mean *A* (ear $^{-1}$) at flowering and grain-filling respectively. There were more subtle mean differences between the other pairs, explaining the significant interaction between awn presence and pair number. In terms of variation across pairs, at flowering the awned lines of pair 1 had comparatively higher *A* (ear $^{-1}$) than the other awned and unawned ears (Table 2-4).

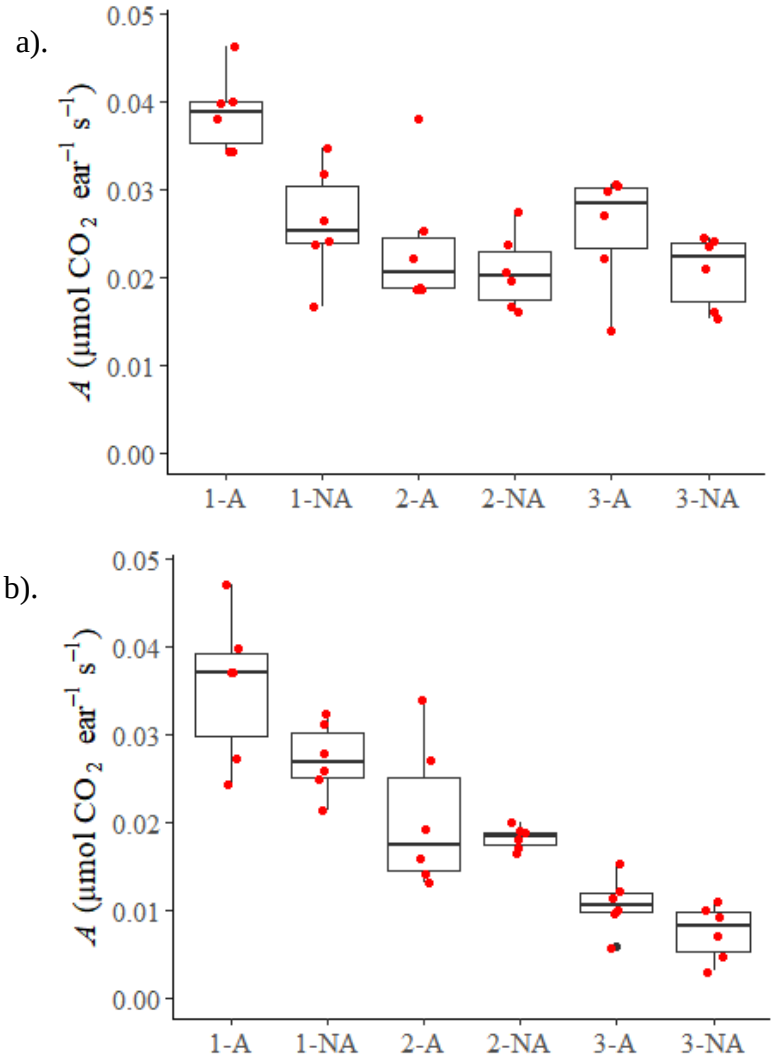

Figure 2-6 – CO_2 assimilation per ear (*A* ear^{-1}) of the of NIL pairs 1 to 3 in the NIL field trial at the growth stages of flowering (a) and grain-filling (b). Measurements were completed in the field using a LI-COR CC. Primary data are shown by the red points overlaid on each boxplot, representing single ears measured on different plants.

Across growth stage, *A* (ear $^{-1}$) moderately decreased in pairs 1 and 2 (excluding 1-NA where there was a slight increase). However, in pair 3 there was a substantial drop between growth stage, *A* (ear $^{-1}$) was 2.3 and 2.6 fold higher at flowering than grain-filling in 3-A and 3-NA respectively (Figure 2-6). The model interaction between growth stage and pair number was caused by both lines in pair 3 having a substantially lower *A* (ear $^{-1}$) than pairs 1 and 2 at grain-filling, variation that was not present at flowering. By the time pair 3 was measured during grain-filling, which was the last set of measurements (Table 2-2), there was visual evidence that awn senescence had started.

The decreases in *A* (ear $^{-1}$) in pair 3 during grain-filling were also observed for ear *A* (cm $^{-2}$), although similar means were found across all three pairs at the flowering stage (Table

2-4). In comparison, ear *A* (cm^{-2}) was relatively unchanged in pair 1 across growth stage and there was only a slight drop from flowering to grain-filling in the means of pair 2 (Figure 2-7, 2-A = 17% and 2-NA = 18%). This variation explained the influence of growth stage and pair number in the significant model identified for ear *A* (cm^{-2}) (F (5, 66) = 18.84, $P < 0.001$) with an adjusted R^2 of 0.56. Where the variable ear *A* (cm^{-2}) was significantly influenced by pair number (F = 22.4, $P < 0.001$), growth stage (F = 25.8, $P < 0.001$) and an interaction between these variables (F = 11.8, $P < 0.001$). Awn presence had no significant influence on ear *A* (cm^{-2}) and was excluded from the model.

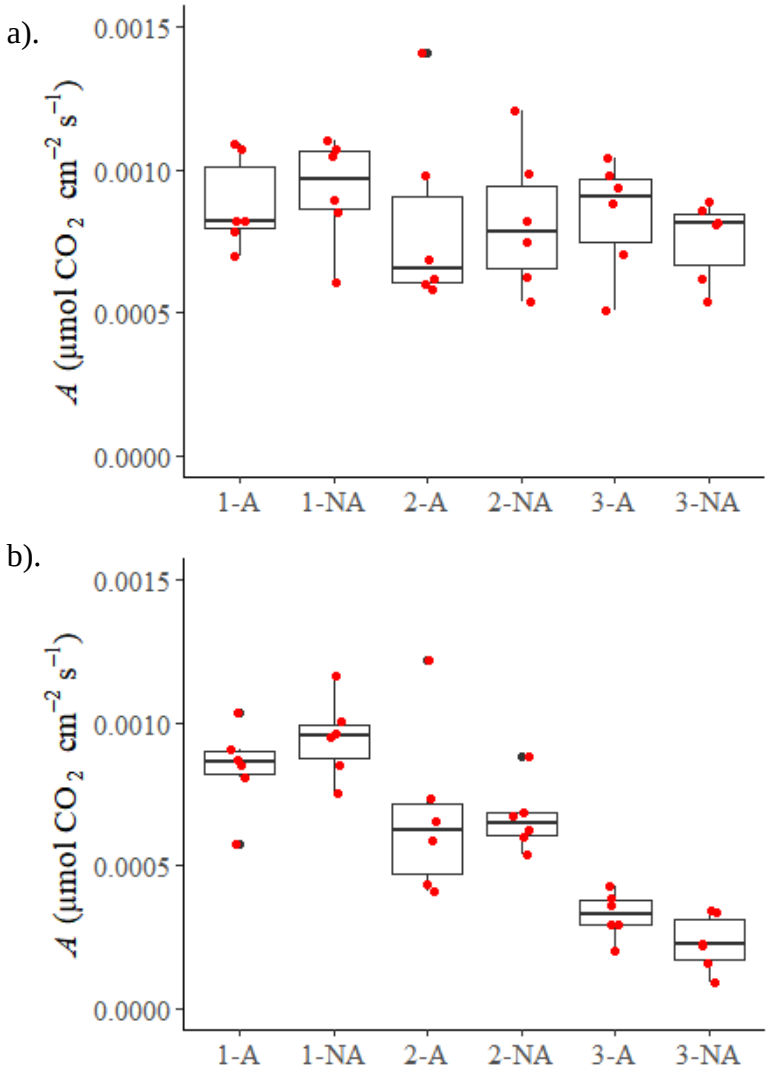

Figure 2-7 - CO_2 assimilation per unit ear area *A* (cm^{-2}) of NIL pairs 1 to 3 in the NIL field trial at the growth stages of flowering (a) and grain-filling (b). measured using a LI-COR CC. Primary data are shown by the red points overlaid on the boxplots, representing single ears measured on different plants.

A Pearson's correlation coefficient test was used to show a positive correlation between *A* (ear^{-1}) and R_{DARK} (ear^{-1}) at both growth stages (Figure 2-8). A significant model was identified for R_{DARK} (ear^{-1}, F (8, 63) = 35.4, $P < 0.001$) with an adjusted R^2 of 0.80, which

was dependent on awn presence (F = 16.4, P < 0.001), pair number (F = 6.6, P = 0.002) and growth stage (F = 223.3, P = < 0.001). Significant interactions were found between awn presence and pair number (F = 10.1, P < 0.001), also between pair number and growth stage (F = 5.1, P = 0.009). Similarly to the A (ear $^{-1}$) results, in pairs 1 and 3 the awned lines had higher R_{DARK} (ear^{-1}) than the unawned counterparts at both growth stages (Table 2-4). However, in pair 2 the mean R_{DARK} (ear^{-1}) for the unawned lines was slightly higher at both growth stages, which explains the significant model interaction observed between awn presence and pair number. In terms of the variation observed across pairs, the awned line in pair 1 had considerably higher mean R_{DARK} (ear^{-1}) than all other lines at both growth stages. In every line, mean R_{DARK} (ear^{-1}) increased from flowering to grain-filling. However, the degree of increase was pair specific, which explains the interaction observed between pair number and growth stage. For example, in pair 2 there was a mean increase of 93% in the awned line and 96% in the unawned line, whereas in pair 3 there was a mean increase of 38% in the awned lines and 59% in the unawned line.

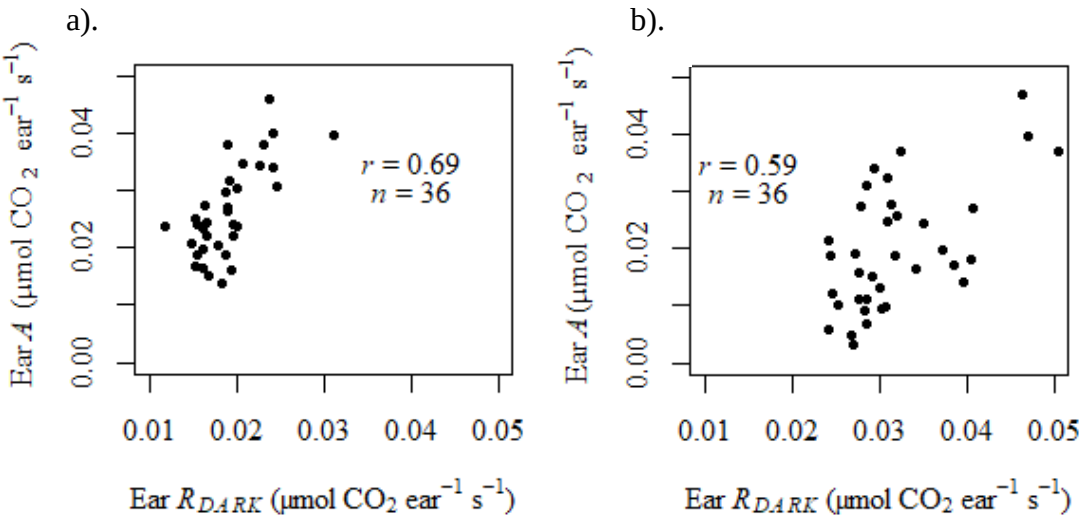

Figure 2-8 – Positive correlations between A (ear^{-1}) and R_{DARK} (ear^{-1}) at the growth stages of flowering (a) and grain-fill (b) for all the individual ears measured in the NIL field trial using the LI-COR CC. Sample size was 36 ears at each growth stage and the Pearson's correlation coefficient is overlaid for each comparison (r).

A significant model was found for ear area (F (6, 64) =17.06, P < 0.001) with an adjusted R^2 of 0.58 (Figure 2-9). Where ear area was significantly influenced by awn presence (F = 44.2, P < 0.001), pair number (F = 16.0, P < 0.001) and growth stage (F = 4.1, P = 0.048). Interactions were observed between awn presence and pair number (F = 11.0, P < 0.001). At both growth stages, the presence of awns increased ear area in every pair (Table 2-4), except Pair 3 at grain-filling. However, the degree of increase was pair

dependent, explaining the interaction between awn presence and pair number in the model. Visual observations of the ears also indicated that there was variation in awn area between the different NILs (see: Figure 2-1). The greatest difference was observed in pair 1, where the awns increased ear area by an average of 59% at flowering and 45% at grain-filling. However, more subtle increases were found in pair 2, increases of 15% at flowering and 12% at grain-filling. In pair 3 awn presence increased area by an average of 10% at flowering, but reduced area by 2% at grain-filling. There was limited variation in ear area between the unawned lines across different pairs. However, mean values in the awned line of pair 1 at both growth stages were higher than the awned lines in pair 2 and 3. Pair 3 showed the greatest increase in area across growth stage (mean difference: 3-A = 2 cm, 3-NA= 5.6 cm). Only the line 2-NA increased to a similar degree of 1.9 cm.

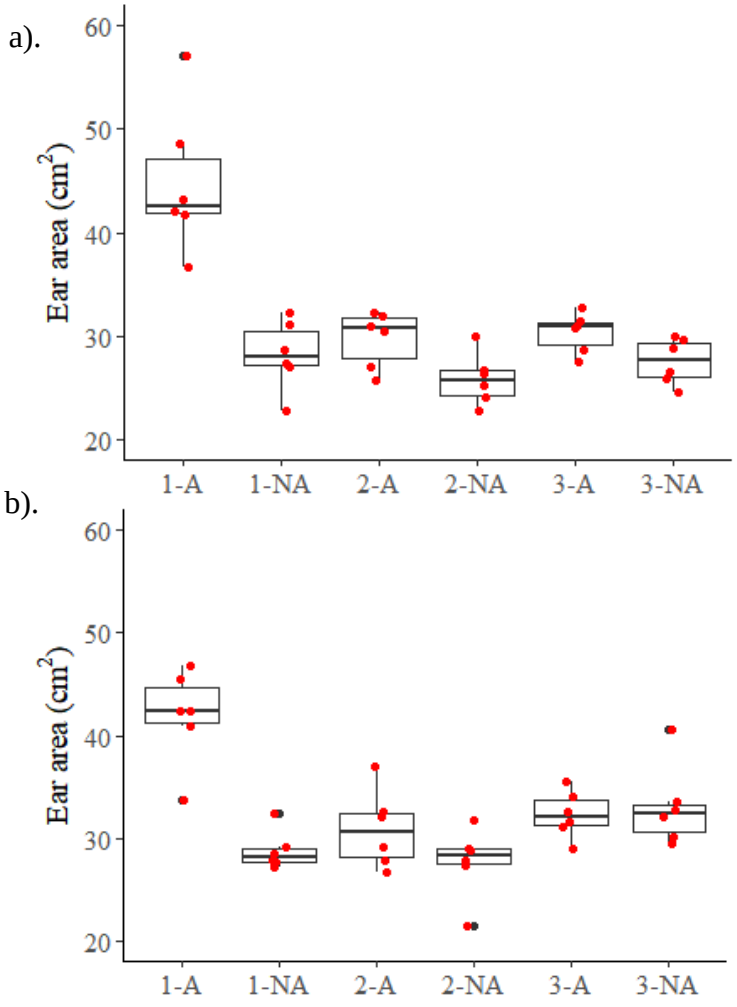

Figure 2-9 - Ear area (cm^2) of NIL pairs 1 to 3 in the NIL field trial at the growth stages of flowering (a) and grain-filling (b). For each measured ear, area was estimated by imaging 6 central spikelets, then multiplying average spikelet area by spikelet number. Primary data are shown by the red points overlaid on the boxplots, representing single ears measured on different plants.

A significant model was found for *E* (ear^{-1}, *F* (3, 68) = 14.5, *P* < 0.001) with an adjusted R^2 of 0.36. Where *E* (ear^{-1}) was influenced by the variable of awn presence (*F* = 29.5, *P* < 0.001), as *E* (ear^{-1}) was higher in every awned line in comparison to the unawned counterparts in each NIL pair (Table 2-4). Pair number also significantly influenced *E* (ear^{-1}) (*F* = 7.0, *P* = 0.002), the greatest variation was observed between pair 1 and pair 2 at flowering, with a mean difference of 0.0014 mmol ear^{-1} s^{-1} between the awned lines (1-A and 2-A).

2.3.2.2 Flag Leaf Gas-exchange

For *A* (flag leaf $^{-1}$) a significant model was identified (*F* (6, 64) = 20.1, *P* < 0.001) with an adjusted R^2 of 0.63, where variation was influenced by awn presence (*F* = 8.9, *P* = 0.004), pair number (*F* =16.7, *P* < 0.001) and growth stage (*F* = 57.2, *P* < 0.001). An interaction was found between pair number and growth stage (*F* = 12.2, *P* < 0.001). The trends in the data are shown in Figure 2-10. Excluding pair 3 at grain-filling, in every NIL pair and at every growth stage, mean *A* (flag leaf^{-1}) was higher in the unawned line. The largest variation within pairs was found in pair 2 at flowering, where there was a mean increase of 41% in the unawned lines and in pair 1 at grain-filling where there was a mean increase of 43%. For variation across pairs, *A* (flag leaf^{-1}) was consistently highest in pair 1 at both growth stages (Table 2-4). Following the same trend as *A* (ear^{-1}), *A* (flag leaf^{-1}) was lowest in pair 3 during grain-filling. In all lines, mean *A* (flag leaf^{-1}) dropped from flowering to grain-filling. The degree of decrease was pair dependent, explaining the interaction between growth stage and pair number. In 3-NA mean *A* (flag leaf^{-1}) decreased by 87% whereas in 1-NA there was a lower drop of 21%. A model slightly above the significance threshold (*P* = < 0.05) was observed for R_{DARK} (flag leaf^{-1}) (*F* (5, 65) = 2.35, *P* = 0.051), with an adjusted R^2 of 0.09. Although there was no significant influence of awn presence (*F* = 3.0, *P* = 0.09) or pair number (*F* = 0.96, *P* = 0.39) on R_{DARK} (flag leaf^{-1}), there was evidence for an effect of the interaction between the two factors (*F* = 3.4, *P* = 0.04).

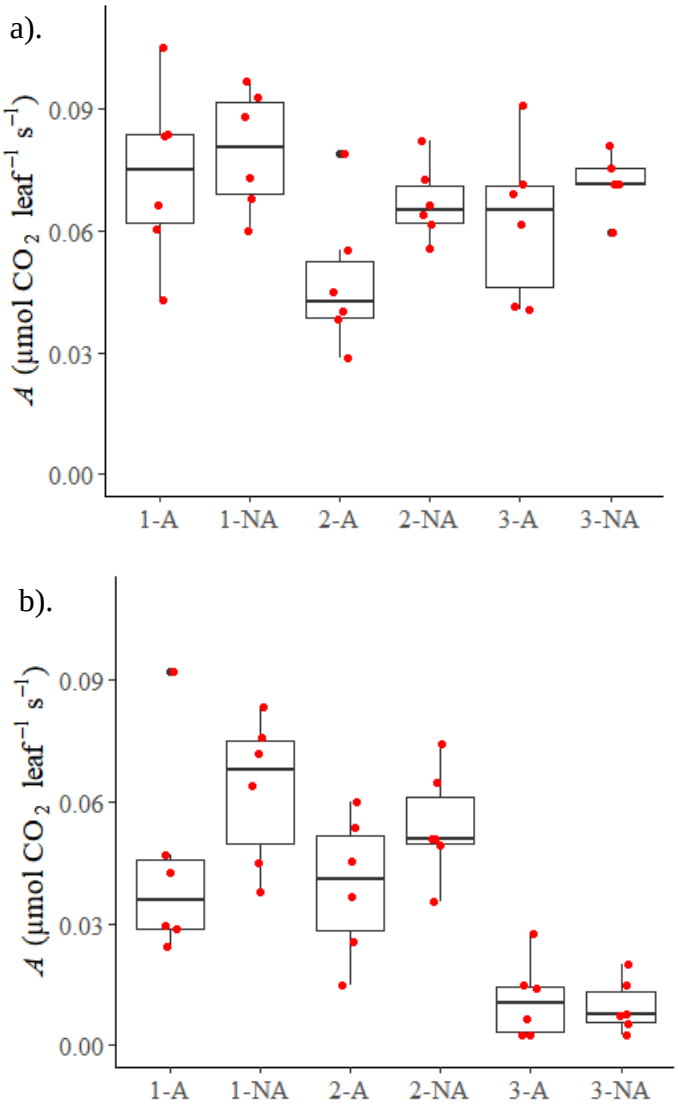

Figure 2-10 – CO_2 assimilation per flag leaf (*A* flag leaf^{-1}) of NIL pairs 1 to 3 in the NIL field trial at the growth stages of flowering (a) and grain-filling (b). Field measurements were taken using a LI-COR CC. Primary data are shown by the red points overlaid on each boxplot, representing single flag leaves measured on different plants.

Leaf area was the only dependent variable where variance associated with the random effect (block number) in the mixed linear model was not either arbitrarily small or zero (variance = 0.11). However, there was no difference in the independent variables that significantly influenced leaf area in both the mixed or multiple linear regression models, and the multiple linear regression is reported. A significant model was identified (F (2, 68) = 3.2, P = 0.05), although with an adjusted R^2 of 0.06 and significantly influenced by only pair number (F = 3.2, P = 0.05), where pair 2 had slightly smaller leaf areas at both growth stages than the other pairs (Table 2-4). A significant model was found for flag leaf A (cm^{-2}, F (6, 65) = 30.6, P < 0.001) with a high adjusted R^2 value of 0.71. Where

awn presence (F = 10.3, P = 0.002), pair number (F = 18.5, P < 0.001) and growth stage (F = 102.6, P < 0.001) influenced the variable of flag leaf A (cm^{-2}, Figure 2-11). An interaction was found between the influence of pair number and growth stage (F = 16.8, P < 0.001). As with A (flag $leaf^{-1}$), flag leaf A (cm^{-2}) was higher in all the unawned lines of each NIL compared to the awned counterparts, excluding pair 3 at grain-filling. The greatest variation was observed within pair 1 and 2 during grain-filling, where compared to the awned lines there was a mean percentage increase of 36% and 38% flag leaf A (cm^{-2}) in the unawned lines respectively. There was a large outlier in 1-A during grain-filling (0.0045 µmol CO_2 cm^{-2} s^{-1}) which was left in the analysis, as high A (ear^{-1}) was also observed in this individual suggesting it was not an erroneous measurement. Pair number influenced flag leaf A (cm^{-2}); at grain-filling pair 3 had a considerably lower mean values than the other pairs (Figure 2-11). The variation was only present at grain-filling explaining the interaction between growth stage and pair number. Flag leaf A (cm^{-2}) was lower in every line at grain-filling compared to flowering, which matched the A (flag $leaf^{-1}$) results.

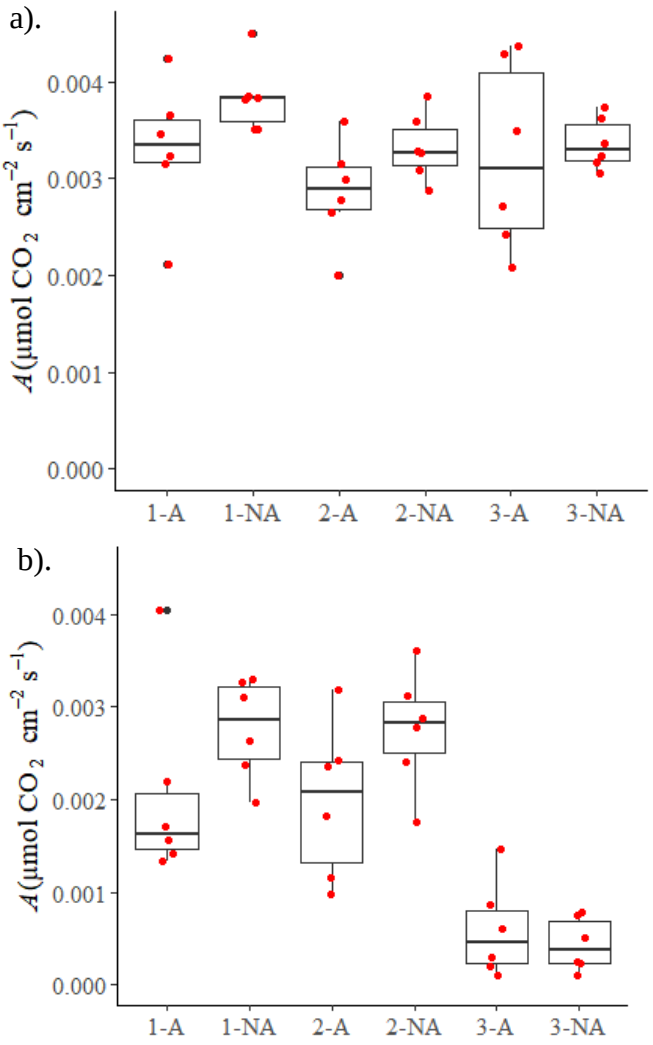

Figure 2-11 - Flag leaf per unit CO_2 assimilation (A cm^{-2}) of NIL pairs 1 to 3 in the NIL field trial at the growth stages of flowering (a) and grain-filling (b). Measurements were made using a LI-COR CC. Primary data are shown by the red points overlaid on each boxplot, representing single flag leaves measured on different plants.

A significant model was found for E (flag $leaf^{-1}$, F (6, 64) = 16.0, $P < 0.001$) with an adjusted R^2 of 0.56, where the variable was influenced by awn presence (F = 4.1, P = 0.05), pair number (F = 12.4, $P < 0.001$) and growth stage (F = 53.8, $P < 0.001$). An interaction was observed between pair number and growth stage (F = 6.6, P = 0.002). Across both growth stages, the unawned lines had higher mean values of E (flag $leaf^{-1}$) than the awned lines in the majority of the pairs, excluding pair 1 at flowering and pair 3 at grain-filling. Following the same trend as the A measurements, variation across pair increased at the grain-filling stage, when in pair 3 mean values of E (flag $leaf^{-1}$) were considerably lower than pairs 1 and 2 (Table 2-4). E (flag $leaf^{-1}$) dropped in every line from flowering to grain-filling. The decrease was most severe in pair 3 where the awned and unawned lines decreased by 61% and 68% respectively.

Table 2-4 - Mean values and standard deviation of 10 dependant variables from the NILs field trial.

Flowering	Pair No. 1				Pair No. 2				Pair No. 3			
	Awned		Unawned		Awned		Unawned		Awned		Unawned	
Trait	*Mean*	*S.D*	*Mean*	*S.D*	*Mean*	*S.D*	*Mean*	*S.D*	*Mean*	*S.D*	*Mean*	*S.D*
A (ear $^{-1}$)	0.039	0.004	0.026	0.006	0.024	0.008	0.021	0.004	0.026	0.007	0.021	0.004
Ear *A* (cm $^{-2}$)	0.0009	0.0002	0.0009	0.0002	0.0008	0.0003	0.0008	0.0002	0.0008	0.0002	0.0008	0.0001
A (flag leaf $^{-1}$)	0.074	0.022	0.080	0.015	0.048	0.018	0.067	0.009	0.062	0.019	0.072	0.008
Flag leaf *A* (cm^{-2})	0.0033	0.0007	0.0038	0.0004	0.0029	0.0005	0.0033	0.0003	0.0032	0.0010	0.0034	0.0003
R_{DARK} (ear^{-1})	0.025	0.0032	0.017	0.0032	0.017	0.0017	0.018	0.0019	0.020	0.0024	0.017	0.0019
R_{DARK} (flag leaf^{-1})	0.006	0.0014	0.004	0.0007	0.004	0.0013	0.005	0.0013	0.005	0.0010	0.005	0.0008
E (ear^{-1})	0.0058	0.0006	0.0044	0.0008	0.0042	0.0006	0.004	0.0008	0.0047	0.0010	0.0038	0.0006
E (flag leaf^{-1})	0.0089	0.0026	0.0088	0.0017	0.0062	0.0020	0.008	0.0009	0.0072	0.0019	0.0079	0.0012
Ear Area	44.9	7.1	28.2	3.4	29.7	2.7	25.8	2.5	30.3	1.9	27.5	2.2
Leaf Area	22.0	2.3	20.8	3.2	16.5	4.0	20.2	2.3	19.5	3.4	21.4	3.5
Grain-filling	*Mean*	*S.D*	*Mean*	*S.D*	*Mean*	*S.D*	*Mean*	*S.D*	*Mean*	*S.D*	*Mean*	*S.D*
A (ear $^{-1}$)	0.035	0.008	0.027	0.004	0.021	0.008	0.018	0.001	0.011	0.003	0.008	0.003
Ear *A* (cm $^{-2}$)	0.0008	0.0002	0.0009	0.0001	0.0007	0.0003	0.0007	0.0001	0.0003	0.0001	0.0002	0.0001
A (flag leaf $^{-1}$)	0.044	0.025	0.063	0.018	0.039	0.017	0.054	0.014	0.011	0.010	0.010	0.007
Flag leaf *A* (cm^{-2})	0.0020	0.0010	0.0028	0.0005	0.0020	0.0008	0.0028	0.0006	0.0006	0.0005	0.0004	0.0003
R_{DARK} (ear^{-1})	0.040	0.0092	0.030	0.0029	0.032	0.0061	0.034	0.0058	0.028	0.0028	0.027	0.0013
R_{DARK} (flag leaf^{-1})	0.004	0.0014	0.005	0.0011	0.004	0.0007	0.005	0.0006	0.004	0.0015	0.006	0.0015
E (ear^{-1})	0.0058	0.0008	0.0042	0.0003	0.0050	0.0006	0.004	0.0004	0.0052	0.0008	0.0044	0.0003
E (flag leaf^{-1})	0.0055	0.0012	0.0065	0.0007	0.0055	0.0023	0.0064	0.0019	0.0028	0.0012	0.0025	0.0008
Ear Area	42.0	4.6	28.8	1.9	30.9	3.7	27.7	3.4	32.3	2.3	33.1	4.0
Leaf Area	21.3	4.8	22.5	3.8	19.7	3.7	19.7	2.2	20.1	4.1	22.3	5.7

Units: *A* (ear $^{-1}$), R_{DARK} (ear^{-1}) = µmol CO_2 ear^{-1} s^{-1}; Ear *A* (cm $^{-2}$), Flag leaf *A* (cm^{-2}) = µmol CO_2 cm^{-2} s^{-1}; *A* (flag leaf $^{-1}$), R_{DARK} (flag leaf^{-1}) = µmol CO_2 ear^{-1} s^{-1}; *E* (ear^{-1}) and FL *E* = mmol ear^{-1} s^{-1}; Ear and Leaf Area = cm^{2}.

2.3.2.3 Ear and Leaf Comparison.

The measured ears across all lines had substantially higher R_{DARK} than the flag leaves (Table 2-4), which on average was 3.9 and 7.0 fold higher across all the NILs at flowering and grain-filling respectively. Following Araus *et al.* (1993) and Zhou *et al.* (2016), Gross Assimilation Rate ($GAR = A + R_{DARK}$) was used for visualising CO_2 assimilation corrected for respiration (Figure 2-12). At flowering, mean values of *GAR* were higher in the flag leaf than in the ear for every pair. However, during grain-filling the awned individuals in pairs 1 and 2 had higher mean *GAR* in the ear than flag leaf (on average 56% and 22% higher respectively). The shift in *GAR* in the organs was partially driven by increases in R_{DARK} (ear^{-1}). In pair 1 R_{DARK} contributed 39% to ear *GAR* at flowering, which increased to 53% at grain-filling. This trend in *GAR* was also contributed to by *A* (flag leaf^{-1}) dropping from flowering to grain-filling. In comparison, *A* (ear^{-1}) was maintained to a higher degree in pairs 1 and 2, which is visible in Figure 2-6. *GAR* dropped considerably in the flag leaves of pair 3 from flowering to grain-filling (Figure 2-12), which may have been an artefact of the delayed sampling time (Table 2-2).

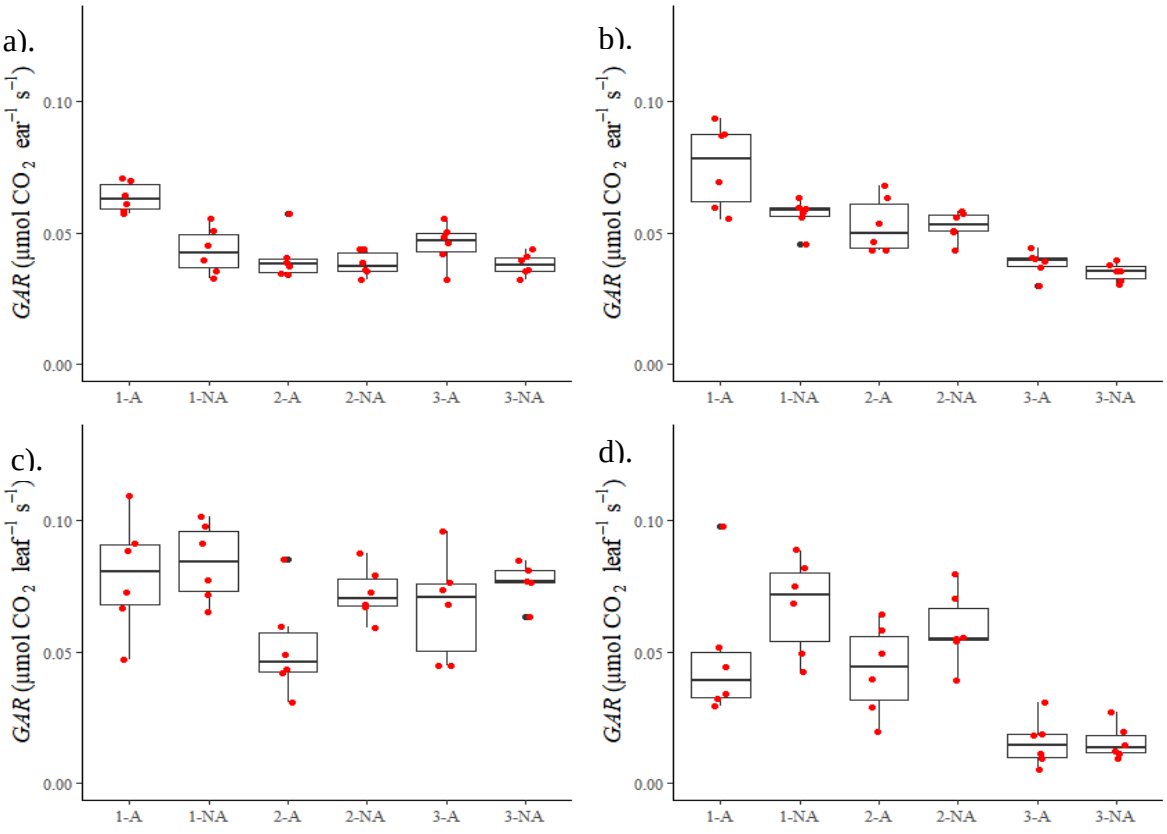

Figure 2-12 - Gross assimilation rate ($A + R_{DARK} = GAR$) per ear measured at flowering (a) and grain-fill (b). *GAR* per flag leaf is also shown at flowering (c) and at grain-filling (d). Measurements were conducted during the NILs field trial using a LI-COR CC on the three NILs. R_{DARK} was measured on dark adapted organs. Primary data points are overlaid in red on boxplots.

At both growth stages and in every line, mean ear *WUE* was higher than flag leaf *WUE* (Figure 2-13), 1.1 and 1.4 fold higher at flowering and grain-filling respectively. Ear *WUE* varied little between the awned and unawned lines within each pair (Figure 2-13), excluding a slightly higher mean of 1-A at flowering and 2-NA at grain-filling. However, mean flag leaf WUE was consistently higher in the unawned individuals in each pair at both growth stages, on average 6.3% and 17.5% higher in the unawned lines at flowering and grain-filling respectively. The higher WUE was driven by the significantly higher *A* (leaf^{-1}) found in the unawned lines of each NIL pair at both growth stages, except pair 3 at grain-filling.

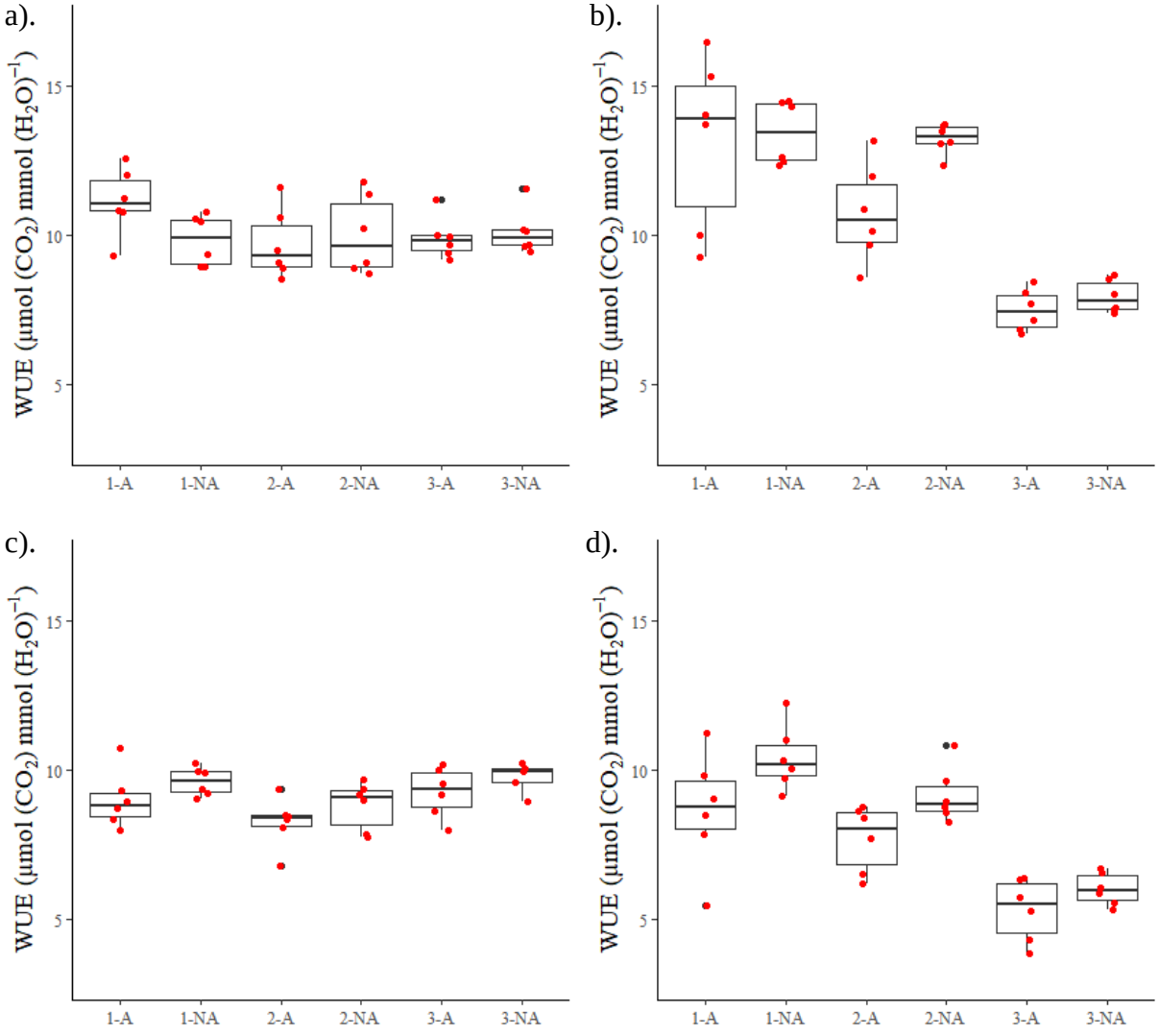

Figure 2-13 - Instantaneous water use efficiency (*WUE*) in the NIL field trial for ears (a and b) and flag leaves (c and d). Calculated from *GAR* and *E* measurements at the growth stages of flowering (a and c) and grain-filling (b and d), for the ears and flag leaves studied. Measurements were made using a LI-COR CC on three NILs. Primary data points are overlaid in red on boxplots.

2.3.3 Grain Yield and Characteristics of the SHW NILs.

In the NILs field trial (Table 2-5), in 4 pairs the unawned line had higher mean grain yield and *HI* than the awned counterparts. Only in pair 5 did the awned line have a higher mean grain yield (5-A = 8.11 t ha^{-1} *S.D* = 0.3 compared to 5-NA = 7.04 *S.D* = 0.5) and an identical *HI* of 0.42 (*S.D* = 0.02). There was some lodging observed in the plots of 2-A and 5-NA, which may have influenced the yield results for these lines. All the pairs yielded lower than the control variety Santiago which had a mean grain yield of 9.68 t ha^{-1}. The *S.D* of the controls was 0.76 t ha^{-1} across the four control replicate plots, which is larger than the variation in grain yield observed in pairs 2, 3 and 4. In pairs 2, 3 and 4 there was a higher mean spikelet and seed number in the unawned lines compared to the awned lines. In comparison, in pairs 1 and 5 the awned lines had a higher mean seed and spikelet number. Mean seed area was larger in every awned line, except in pair 1 and 4. Thousand grain weight (*TGW*) was higher in all the awned lines of pairs 2 and 3, but lower in pairs 1, 4 and 5. Of the pairs used for the gas-exchange analysis, in pairs 2 and 3 spikelet number was higher in the unawned lines. In comparison, in pair 1, spikelet number was higher in the awned line. These trends reflect the variation observed in ear area. Infertile spikelet number was higher in every awned line, except pair 5.

Table 2-5 – Mean grain yield and yield component data from the NILs field trial for all the material included in the trial. Grain yield was measured by the combine harvester and adjusted to 15% moisture, the rest of the traits were either measured manually or by using a MARVIN seed analyser (GTA Sensorik GmbH, Neubrandenburg, Germany). There were 2 replicate yield plots for all lines, except Santiago where a total of 4 were included. In pair, A = awned and NA = unawned. Standard deviation is shown (*S.D*).

Pair	*Grain Yield* (t ha^{-1})	*HI*	*Seed No.* ear^{-1}	*TGW* (g)	*Seed area* mm^2	*Total Spikelets* ear^{-1}	*Infertile Spikelets.* ear^{-1}
Santiago	9.68	0.46	63.88	32.98	15.24	22.45	1.93
S.D	*0.76*	*0.01*	*0.65*	*2.08*	*0.54*	*0.19*	*0.36*
1-A	7.66	0.43	69.22	28.47	13.90	26.80	2.00
S.D	*0.04*	*0.01*	*13.03*	*2.11*	*0.58*	*0.09*	*0.19*
1-NA	8.46	0.44	64.20	30.59	15.03	25.63	1.93
S.D	*0.08*	*0.01*	*2.55*	*0.66*	*0.17*	*0.24*	*0.28*
2-A	7.33	0.46	45.75	47.51	19.15	23.87	3.13
S.D	*0.43*	*0.01*	*2.47*	*2.79*	*0.50*	*0.47*	*0.19*
2-NA	7.69	0.48	56.18	42.55	17.72	24.73	2.53
S.D	*0.26*	*0.00*	*5.40*	*1.05*	*0.02*	*0.28*	*0.75*
3-A	7.31	0.44	56.04	38.44	16.54	23.73	2.80
S.D	*0.44*	*0.01*	*0.38*	*1.86*	*0.34*	*0.19*	*0.00*
3-NA	7.43	0.45	59.43	34.88	15.83	25.13	2.17
S.D	*0.83*	*0.03*	*2.69*	*2.43*	*0.52*	*0.09*	*0.14*
4-A	7.32	0.43	50.70	38.33	16.29	25.07	3.30
S.D	*0.75*	*0.02*	*2.21*	*2.53*	*0.50*	*0.57*	*0.42*
4-NA	7.71	0.44	58.15	38.59	16.68	25.10	2.23
S.D	*0.30*	*0.01*	*8.46*	*0.52*	*0.10*	*0.14*	*0.61*
5-A	8.11	0.42	67.70	32.59	16.05	25.97	2.47
S.D	*0.24*	*0.02*	*1.04*	*1.52*	*0.59*	*0.24*	*0.00*
5-NA	7.04	0.42	51.10	37.36	16.03	25.03	2.73
S.D	*0.51*	*0.02*	*4.24*	*2.00*	*0.28*	*0.61*	*0.47*

The pairwise comparison of the NILs across different years and locations highlighted that yield differences were only significant in 2 of the 5 pairs (Figure 2-14). In Table 2-5 the largest variation in yield was observed in pair 1 and 5, it was only these pairs which maintained the observed variation in the pairwise comparison. Significant difference in grain yield were found between 1-A (mean = 10.6 t ha^{-1}, *S.D* = 1.5) and 1-NA (mean = 11.5 t ha^{-1}, *S.D* = 1.8); adjusted *P*-value = < 0.05. Also between 5-A (mean = 11.0 t ha^{-1}, *S.D* = 1.8) and 5-NA (mean = 9.6 t ha^{-1}, *S.D* = 1.5); adjusted *P*-value = < 0.05.

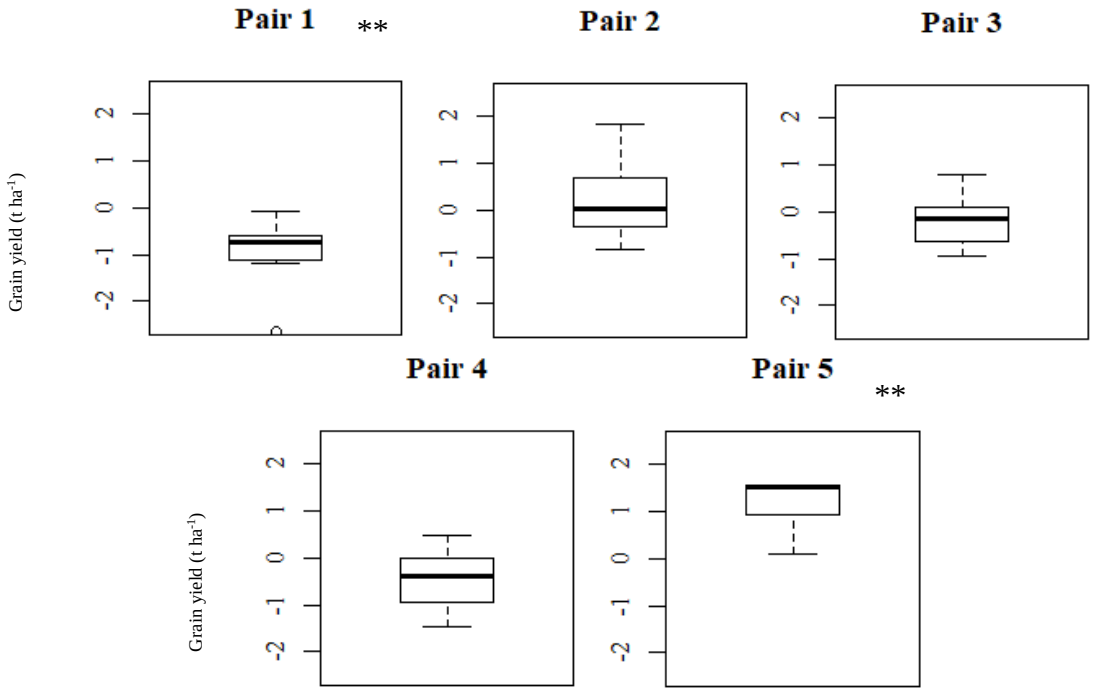

Figure 2-14 – The mean differences between each pair of SHW NILs across multiple yield trials, showing the effect of awns on yield. The trials ranged across three different years and included 6 locations. Grain yield adjusted to 15% moisture is shown. ** = *P* < 0.05 determined through paired t-tests with an adjustment for multiple testing using the False Discovery Rate method (Benjamini & Hochberg 1995). n = 8 (pairs 1 and 3), n = 6 (pair 2) and n = 7 (pairs 4 and 5).

2.3.4 Marker analysis.

2.3.4.1 SNP Markers and Genetic Map.

For the 5330 SNP markers used in the GWAS, map positions were taken from the consensus map on CerealsDB (Allen *et al.* 2017; Wilkinson *et al.* 2012). The selected markers have previously been mapped into 21 linkage groups, reflecting the expected 21 chromosomes pairs found in hexaploid wheat. For the selected markers, the total map was 4277.5 cM in length, with an average spacing of 0.8 cM respectively (Figure 2-15). Chromosome 1B had the highest number of mapped markers (n = 462), with an average and maximum spacing of 0.3 and 11.1 cM, respectively. The chromosome with the fewest markers (n = 42) was 4D, which had an average spacing of 4.0 cM and a large gap of 42 cM. This trend was also observed in the complete set of mapped markers from the consensus map (21,709 markers), where chromosome 4D had the lowest mapped SNP density (Allen *et al.* 2017). The largest gap of 62.2 cM was present on chromosome 6D. The D genome had the lowest percentage of mapped markers, followed by the A genome and then the B genome (11.8%, 39.7%, 48.5% respectively). The shortest chromosome

was 1A which was 38.32 cM in length, the longest chromosome was 7B which was 333.3 cM in length. There was a limited spread of markers across chromosome 1A, evident from the short length (Figure 2-15). Out of the 5330 SNPs used in the GWAS, all of the markers mapped to chromosome 1A were within the range of 52.46 to 90.78 cM. This limitation appears to be a constraint of the consensus map from Allen *et al.* (2017), where in the complete set of markers mapped to 1A, only 17 were mapped outside of this range. In the present study, these markers were either not called as poly high resolution in the WISH panel or dropped through the quality control, leading to a reduction in the mapped length of chromosome 1A (Figure 2-15).

The SHW NILs had been created through only phenotypic observations, where they were separated based on the awn trait. A comparison was completed to test isogeny of the NILs using the 5330 SNP marker data, with NA genotypes excluded and heterozygote genotypes included. The SNPs within the 28.8 cM region where significant marker-trait associations were found were excluded from the analysis. The NILs were all validated to be highly isogenic, apart from pair 5 where genotype data were unavailable for the awned line. Pair 4 had the highest percentage of matching SNP genotypes of 98.6%, followed by pair 1 (97.5%), pair 3 (96.3%) and pair 2 (94.5%).

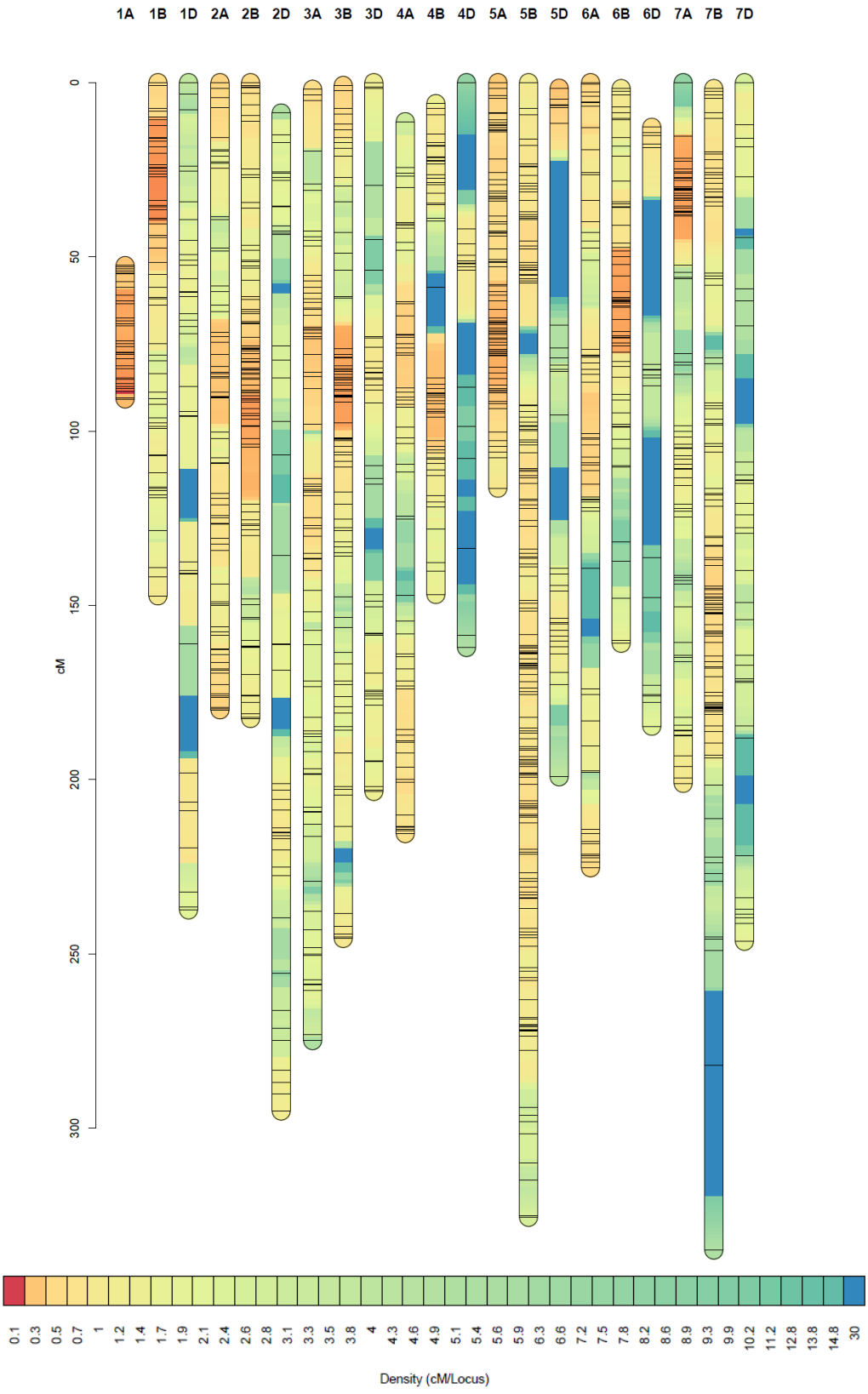

Figure 2-15 – The SNP density on each chromosome of the markers used in the WISH panel association analysis. The plot shows a density heat map (red = high, blue = low) with the black lines indicating the position of each SNP. Mapped positions (cM) were taken from the consensus map available from CerealsDB (Wilkinson et al. 2012). The figure was created using the 'LinkageMapView' package in RStudio (Ouellette *et al.* 2018).

2.3.4.2 Genome-Wide Association for Awned Character.

A significance threshold of -log10 (*P*) = 5.03 was determined using Bonferroni correction. Of the 5330 markers included in the study, 22 SNPs had -log10 (*P*) values over the threshold and all were found on chromosome 5A (Table 2-6). The marker with the highest -log10 (*P*) of 39.32 was AX-94729059, located at 58.38 cM. The marker also had the largest effect of 0.37. The markers AX-94796970 (-log10 (*P*) = 35.17, effect = 0.35), AX-94394580 (-log10 (*P*) = 22.12, effect = 0.31) and AX-94622557 (-log10 (*P*) = 19.78, effect = 0.30) were the following next most significant and located at 59.99, 70.36 and 70.36 on 5A respectively.

Table 2-6 – The significant marker associations with awn presence in the WISH Panel determined through genome-wide association. The -log10 (*P*-values) and marker effects are shown, highest -log10 (*P*) scores are shown in bold. Marker effects represent the dosage of 0.5 of the minor allele genotype (BB), unawned was scored as 0 and awned was scored at 1. The allele and minor allele frequency data (MAF[1]) were taken from EnsemblPlant (release 40 - July 2018, www.plants.ensembl.org). MAF[2] is the minor allele frequency in the complete WISH panel, calculated from the homozygous genotypes. The majority of the WISH panel were backcrossed into the unawned bread wheat 'Xi19'; the genotype of 'Xi19' at each SNP is shown.

Marker Name	Chromosome	cM	-log10 (*P*)	Effect	Allele	MAF[1]	MAF[2]	Xi19
AX-95628984	5A	43	5.37	0.17	NA	NA	0.29	AA
AX-95129770	5A	47.82	7.44	0.21	G/A	0.08	0.50	AA
AX-95230303	5A	51.53	8.47	-0.21	A/G	0.28	0.57	BB
AX-94405899	5A	58.38	12.01	-0.24	A/C	0.32	0.64	BB
AX-94729059	**5A**	**58.38**	**39.32**	**0.37**	**C/T**	**0.4**	**0.49**	**AA**
AX-94386526	5A	59.99	6.48	0.23	G/A	0.47	0.20	AA
AX-94453668	5A	59.99	7.61	-0.23	T/C	0.47	0.80	BB
AX-94472591	5A	59.99	9.7	-0.29	A/G	0.5	0.79	BB
AX-94519471	5A	59.99	16.36	-0.23	T/C	0.42	0.50	BB
AX-94560538	5A	59.99	6.38	-0.21	A/C	0.31	0.81	BB
AX-94742567	5A	59.99	7.53	0.27	C/A	0.5	0.21	AA
AX-94796970	**5A**	**59.99**	**35.17**	**0.35**	**C/T**	**0.35**	**0.48**	**AA**
AX-95097524	5A	65.24	7.36	-0.29	G/A	0.31	0.85	BB
AX-95111244	5A	67.59	9.78	0.28	C/A	0.26	0.19	AA
AX-94560945	5A	68.77	6.05	0.24	C/T	0.08	0.13	AA
AX-94394580	**5A**	**70.36**	**22.12**	**0.31**	**C/T**	**0.2**	**0.37**	**AA**
AX-94622557	**5A**	**70.36**	**19.78**	**0.3**	**G/A**	**0.17**	**0.36**	**AA**
AX-94753558	5A	70.36	7.93	0.28	C/T	0.46	0.12	AA
AX-94958942	5A	70.36	5.68	0.21	T/G	0.19	0.13	AA
AX-95002679	5A	70.36	5.05	0.15	C/G	0.45	0.32	AA
AX-94422894	5A	71.85	8.41	-0.21	A/G	0.3	0.77	BB
AX-94881303	5A	71.85	6.78	-0.2	C/A	0.18	0.84	BB

The scores and marker effects of the complete SNP collection are shown in a Manhattan plot in Figure 2-16 (a). Excluding the results in (Table 2-6), there were no other -log10 (*P*) scores found above the significance threshold on any chromosome. The four markers with the highest -log10 (*P*) (shown in bold in Table 2-6) were treated as covariates and the GWAS analysis was repeated; no additional significant marker-trait associations were found outside of chromosome 5A. The Quantile-quantile plot showed that the majority of -log10 (*P*) fitted the null hypothesis assumptions, excluding the significant results (Figure 2-16 (b)).

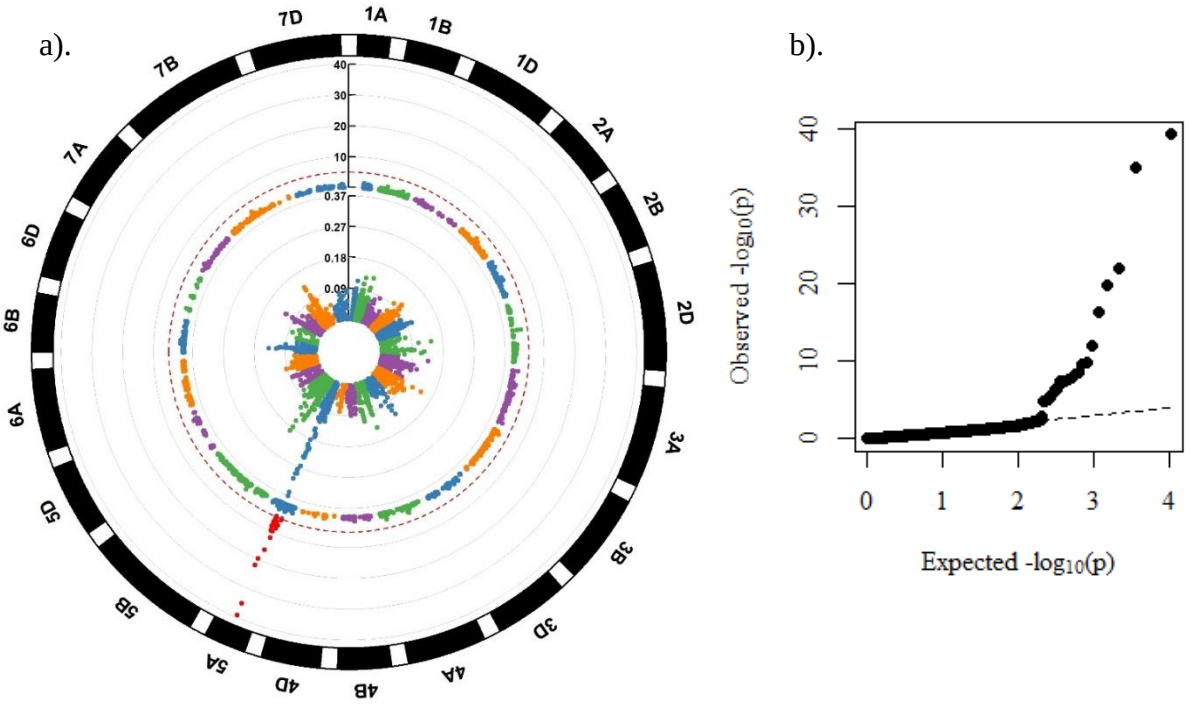

Figure 2-16 – a). A circular Manhattan plot showing genome-wide association results for awn presence in the WISH panel across 21 chromosomes for each mapped SNP. The SNP -log10 (*P*) scores are shown in the outer circle, scores above the red line threshold (determined using a Bonferroni correction to 5%) are coloured in red. SNP effects are shown in the inner circle (absolute values are shown, see Table 2-6 to determine if the effect was positive or negative). The plot was created using the CMplot package in RStudio (available at: https://github.com/YinLiLin/R-CMplot). b). A quantile-quantile plot showing the observed against expected -log10 (*P*) scores, used to inspect and validate the final model.

2.4 Discussion.

2.4.1 Progenitor vs. Modern Wheat Comparison.

A higher *A* (ear $^{-1}$) was found in the *T. dicoccoides* lines in comparison to the elite modern varieties, despite considerably smaller ears in the tetraploids. However, the progenitor wheats were awned, which suggested the awns contributed to the higher *A* (ear^{-1}). Comparing cultivated and wild tetraploid and hexaploid wheat types, Blum (1985) found that the awns contributed 49% of the total ear photosynthetic rate, whilst also identifying higher rates in the tetraploids than in hexaploids. Li *et al.* (2017) found that ears of *T. dicoccoides* maintained higher per unit *A* during grain-filling than *T. aestivum* and higher *WUE* under drought stress. The results of the ploidy field trial in the present study indicated the advantages of awn presence in promoting higher ear CO_2 assimilation, be it due to increases in overall *A* (ear $^{-1}$) by extension of photosynthetic surface area or higher ear *A* (cm^{-2}); this warranted the investigation of this investment into ear photosynthesis in an adapted material.

2.4.2 Gas-Exchange Results in the SHW NILs

2.4.2.1 Ear Gas-Exchange

In each of the 3 awned NILs studied here, *A* (ear $^{-1}$) was higher at both growth stages than in the unawned NILs, although substantial differences were only observed in pair 1. As ear *A* (cm^{-2}) did not significantly differ within the NILs, the variation in *A* (ear^{-1}) was driven by the differences in ear area. Awn presence increased *A* (ear^{-1}) by extending the photosynthetic surface area. This observation was made by Blum (1985) where total ear photosynthesis rates did not correlate with per unit photosynthesis rates, but did correlate with ear surface area. Furthermore, Teare *et al.* (1972b) also found that net per unit photosynthesis was not changed by awn presence, but that net per ear photosynthesis was higher in awned ears. Alternatively, Olugbemi *et al.* (1976a) found that awn presence was related to a decrease in photosynthesis in other ear components, although this could have been an effect of shading. Maydup *et al.* (2014) also found differences in photosynthetic activity in the ear body compared to the awns, with a higher electron transport rate in the body. In the present study, no increases in ear *A* (cm^{-2}) were observed in the unawned ears, suggesting there was no compensatory effect to awn presence or absence in the other ear components (glumes, lemma and palea).

The variation in ear area supports the conclusion that differences in *A* (ear^{-1}) were driven by photosynthetic surface area, as the largest variation in ear area and *A* (ear^{-1}) was observed in pair 1, which had the largest awns, at both growth stages (Table 2-4). There was an apparent compensation between spikelet number and awn presence in pairs 2 and 3 (Table 2-5), which was linked to reduced variation in ear area observed within these NILs. Spikelet number can be decreased due to allocation of assimilates to the developing awns (Guo & Schnurbusch 2016; Rebetzke *et al.* 2016). However, this was not apparent in pair 1, where the awned line had a higher mean spikelet number. Variation in ear area within NILs decreased at grain-filling, which could be linked to visual signs of senescence in the awns during this stage. Senesced area would not have been counted in the imaging of ear area, which could have reduced the variation. Awn tip senescence was particularly evident in pair 3 during grain-filling. Evans *et al.* (1972), suggested that awns had a tendency to senesce later than flag leaves during grain-filling. However, Olugbemi *et al.* (1976a) also observed earlier senescence in awns compared to the rest of the ear, which was only slightly later than the flag leaf.

In 5 of the 6 lines measured, *A* (ear^{-1}) decreased from flowering to grain-filling. Similarly, Zhou *et al.* (2016) measuring gas exchange at grain-filling using a LI-COR conifer chamber and the same development stages as the present study, also found that mean *A* (ear^{-1}) was reduced and also observed a decrease in R_{DARK} (ear^{-1}). In contrast, in the SHW NILs R_{DARK} increased substantially in every line through the development stages. High R_{DARK} at grain-filling can be attributed to maintenance respiration in the ear components, in addition to starch synthesis in the developing kernels (Knoppik *et al.* 1986). Araus *et al.* (1993) also observed high R_{DARK} during the same grain-filling, which was 1.74 fold higher than *A* (ear^{-1}). In the SHW NILs, the increases in R_{DARK} indicated that if respiration is considered, as shown by the parameter *GAR* (Figure 2-12), then in pairs 1 and 2 *A* (ear^{-1}) may have increased or at least maintained across the development stages.

The correlation observed between R_{DARK} (ear^{-1}) and *A*, indicated that the awned lines have higher respiration rates. Furthermore, this was proven by the variation within the NILs where 2 of the 3 pairs had higher R_{DARK} (ear^{-1}) at both stages in the awned lines (pair 1 and 3). These trends indicated that maintenance respiration of the awns may have increased R_{DARK} (ear^{-1}). The increase in R_{DARK} during grain-filling did not substantially change the variation between the NILs (Table 2-4), suggesting that the escalation across growth stage was caused by developing kernel respiration, which is independent of awn presence.

2.4.2.2 Leaf Gas-exchange

Within NIL pairs, mean *A* (flag leaf^{-1}) was higher in every unawned line (except pair 3 at grain-filling), with substantial variation observed in two pairs at different growth stages. As no relationship was found between awn presence and leaf area, the lower *A* (flag leaf^{-1}) in the awned lines was driven by flag leaf *A* (cm^{-2}) variation. Flag leaf *A* (cm^{-2}) was lower in every awned line at flowering and in 2 of the 3 at grain-filling. Olugbemi *et al.* (1976a) found similar results, where awn presence in awned-unawned NILs reduced photosynthesis in the flag leaf, leaf lamina and peduncle. In this study they hypothesised that shading from the awns could have reduced photosynthetic activity in the lower canopy levels. However, organ detachment studies have shown the leaf and ear compete for N allocation (Guitman *et al.* 1991; Liu *et al.* 2017). The developing ear (and presumably awns) competes for assimilates with several sinks, these include the uppermost leaves, stem and roots (Evans *et al.* 1981). Rawson (1970) observed that increases in ear area can lead to a reduction in flag leaf area, but speculated that the leaf photosynthetic apparatus was not diminished. In the present study, leaf area was unchanged between NILs but *A* (cm^{-2}) was decreased. As awn development can reduce assimilate partitioning to the spikelets and florets (Guo & Schnurbusch 2016; Rebetzke *et al.* 2016), there could also be a reduction of assimilate partitioned to the flag leaf. Allocation of assimilates to developing awns may have reduced investment into leaf photosynthetic apparatus. The lower flag leaf *A* (cm^{-2}) observed in the awned lines could have been driven by compensatory effects to photosynthetic downstream-demand linked to awn development. Comparisons of flag leaf N content between the NILs would be needed to support this hypothesis.

Alternatively, the variation could be linked to difference in photosynthetic supply. Mean *E* (flag leaf^{-1}) was mostly higher in the unawned NIL flag leaves (except pair 1 at flowering and pair 3 at grain-filling), which could indicate a higher g_s as the two parameters are closely linked (Lawson & Blatt 2014). However for reasons discussed later, g_s was not presented in this chapter. Maydup *et al.* (2014) found that the presence of awns increased hydraulic conductance to the ear, which is supported by evidence in the present study, where every awned NIL had higher *E* (ear^{-1}) at both growth stages. Empirically, visual observation of leaf rolling seemed more frequent in the awned lines during grain-filling (Figure 2-17). The higher ear water expenditure linked to awn presence, may have led to a reduction of water availability to the leaf, leading to decreased

g_s and *A*. Further work is needed to test this hypothesis, potentially by analysing the impact of awn presence on *RWC* and the hydraulic conductance of the different organs.

a).
b).

Figure 2-17 - Visible signs of leaf rolling in the canopies of pairs 3 (a) and 2 (b) during the growth stage period of grain-filling in the NILs field trial. Photographs on the left show the unawned canopy from each NIL, whilst photographs on the right show the awned counterparts.

2.4.2.3 Organ Comparison

Across all the lines and at both growth stages the ear maintained substantially higher R_{DARK} than the leaf, this trend has been observed in a number of studies (e.g. Araus *et al.* 1993; Knoppik *et al.* 1986; Teare *et al.* 1972b). At flowering mean *GAR* was higher in the flag leaves compared to the ears in every pair of NILs. During grain-filling this trend was reversed in the awned NIL of pairs 1 and 2 and both NILs in pair 3. This shift was driven by two factors, firstly, the increases in R_{DARK} (ear^{-1}) across growth stages. Secondly, the decreases in flag leaf *A* (cm^{-2}) during grain-filling, which was most severe in the awned lines and both NILs of pair 3. A possible explanation may be that during later stages of development chloroplast degradation takes place at a faster pace in the flag leaf compared to the awn (Li *et al.* 2006; Maydup *et al.* 2014).

Mean ear *WUE* was consistently higher than flag leaf *WUE*, which is a trend observed in a number of other studies (Abbad *et al.* 2004; Araus *et al.* 1993). Araus *et al.* (1993) found that *WUE* was 33% higher in the ear bracts compared to the leaf blade using carbon isotope analysis, linking the higher efficiency to a lower g_s and the xeromorphic features of the ear bracts. Measuring at the same grain-filling stage as the present study, they also

found through gas-exchange analysis that instantaneous *WUE* was higher in the ear than the leaf blade, as long as R_{DARK} was accounted for. We found the highest *WUE* in the most awned line (1-A). Blum (1985) found that awns contributed a low proportion of total ear transpiration (10 - 20%) but a high proportion of total ear photosynthetic rate (40 to 80%), hence high ear WUE. The present study confirms the general assumption that the ear has a higher *WUE* than the leaf, if *A* is adjusted for R_{DARK}.

2.4.3 Yield Results in the SHW NILs

Evidence supporting the yield advantages of awn presence is conflicting, ranging from positive effects (Scharen *et al.* 1983), to negative effects (McKenzie 1972) or no apparent variation (Rebetzke *et al.* 2016). The assumption could be made that the advantage of awn presence on yield is environment specific and dependent on water availability (Evans *et al.* 1972). However, across 25 environments Rebetzke *et al.* (2016) found that there were not significant differences in grain yield between 45 awned-unawned NILs. Out of the 5 NIL pairs in the present study, only two maintained consistent variation across different locations and years, with the awned line consistently yielding higher in one pair but lower in the other. Therefore, no conclusions could be drawn about the overall effect of awn presence on yield based on these five pairs of NILs across the multiple years and locations. However, every environment was 'rain-fed', so more variation might become apparent under different watering regimes.

For the pairs included in the gas-exchange measurements, a higher mean grain yield and *HI* was observed in each unawned NIL. In 2 of the 3 pairs seed number was also higher. Rebetzke *et al.* (2016) suggested that allocation to awn development reduced grain number and floret fertility. Another factor reducing the possible benefits of an increased *A* (ear^{-1}) as a consequence on awn presence, is the higher respiratory CO_2 losses resulting from the awn tissue (Scharen *et al.* 1983). This hypothesis is supported by the increased R_{DARK} linked to awn presence observed in 2 of the 3 pairs. Awn presence may increase the proportion of photo-assimilate remobilised to the developing grain from the ear. Resulting in less reliance on other source supplies (such as the flag leaf), this idea is supported by the lower *A* in the flag leaves of awned lines observed in this study. While this shift in source supply may have advantageous effects in drought conditions (Maydup *et al.* 2014), the presence of awns has been shown to have detrimental effects to grain yield under irrigation (Evans *et al.* 1972). If the supply of assimilate remobilised from

other sources is greater, there could be yield penalties related to awn presence, when water is not limiting.

2.4.4 Genetic Analysis of Awn Presence in the SHW Collection.

Results for the GWAS analysis identified significant markers relating to the awn trait, which were all located on chromosome 5A, ranging from 43.0 to 71.9 cM. The SNP with the highest –log10 (*P*) value (39.3) was AX-94729059 located at 58.4 cM, this marker has been developed into a kompetitive allele specific PCR assay (BS00106118, Wilkinson *et al.* 2012). Over separate years, the same SNP was the closest marker to QTL linked to awn presence in 10 bi-parental Paragon and Watkins mapping populations, with percentage phenotypic variation being explained from 14.7 to 74.6% by the QTL (JIC, WISP, DFW 2018). As discussed in section 2.1.3, there is the known *B1* awn inhibitor on 5A (Sourdille *et al.* 2002; Watkins & Ellerton 1940); although the inhibitors are identified the underlying genes are yet to be cloned (Mackay *et al.* 2014; Yoshioka *et al.* 2017). Olugbemi *et al.* (1976a) hypothesised that most unawned European wheat has the dominant form of the *B1* inhibitor gene, located near the centromere. Therefore, it could be assumed the *B1* inhibitor gene was linked to the variation observed in the WISH panel. The primary SHW used in the WISH project were awned, so backcrossing with the unawned UK variety 'Xi19' will have introduced the dominant form of the *B1* allele, this hypothesis is supported by the evidence in Table 2-6 where for every genotype similar to 'Xi19' there was a negative marker effect on awn presence.

The identified SNP and phenotypic associations could be used in Marker Assisted Selection (MAS) to promote or suppress awn development for breeding wheat in targeted environments. For the most significant marker association (AX-94729059), out of the total individuals in the complete collection, 89.3% of awned individuals were BB in genotype. In comparison, 90.1% of unawned individuals were AA in genotype. Within the NILs collection, including the parents used in the formation of the SHW families, the marker was associated with all of the phenotypic variation (Figure 2-18). This SNP could be used as an accurate marker linked to the genetic control of the awn trait on 5A. There was clear variation in awn formation between the 5 NIL pairs used in this study (Figure 2-1), suggesting differences in the genetic regulation of the trait. Other major genes have been linked to the development of awns, located on 4A and 6B (Rao 1981; Sourdille *et al.* 2002; Watkins & Ellerton 1940). However, the GWAS picked up no other significant genetic polymorphisms related to the trait other than on 5A.

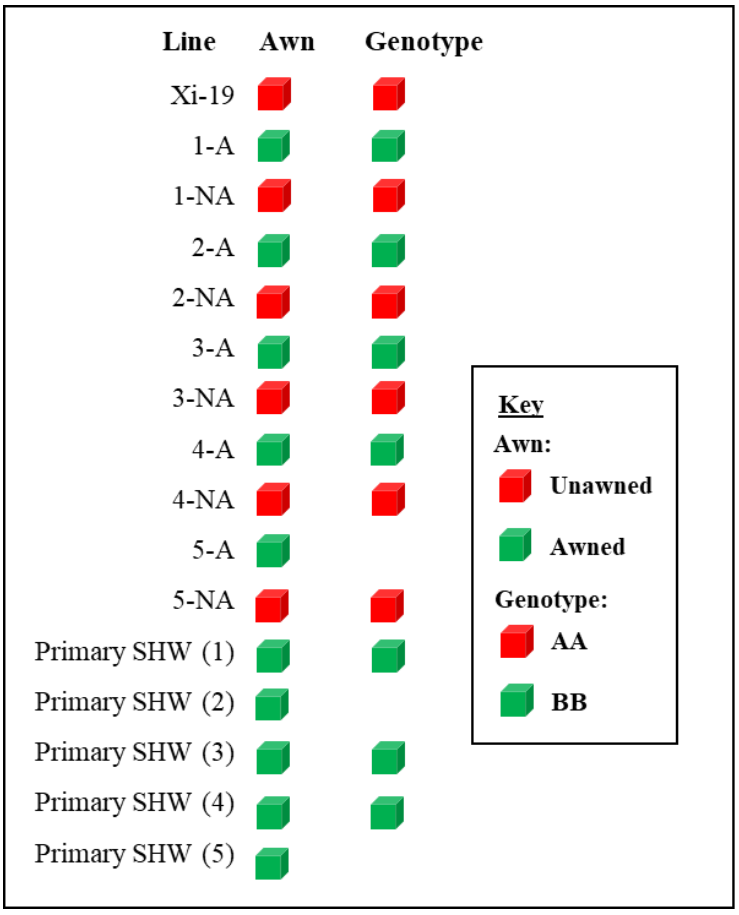

Figure 2-18 – Schematic showing the awn trait and genotype variation for the marker AX-94729059 in the NILs collection. The parents used in the SHW families formation are shown, including the primary SHW for each pair (pair number is shown in brackets) and the hexaploid parent used for backcrossing; Xi19. Missing data are shown by a blank space.

The SNP genotype data, before removal of the heterozygotes, showed that the individuals of each NIL pair were highly isogenic with their counterparts. This comparison was not possible for pair 5 as NIL 5-NA was not genotyped. Departures from the random association of alleles at different loci is termed linkage disequilibrium (LD), and selection for a particular allele can lead to increased LD for closely linked loci (Mackay & Powell 2007). Phenotypic selection for the awn trait in the formation of the SHW NILs could have resulted in increased allele frequency of a particular gene associated with either the presence or absence of awns, which may have influenced the gas-exchange or yield data. Other than the markers within the 28.8 cM region on 5A, none of the SNPs that varied within NIL pairs were the same across more than two pairs. This suggests that any background genetic effects (other than the presence/absence of awns) were random across all five pairs.

However, it is difficult to identify if any markers which varied across multiple pairs within the range of significant associations on 5A were linked to other phenotypes, such as grain yield. If a GWAS was completed using the WISH panel for the trait of grain yield, and marker associations were found on chromosome 5A, it could help identify the potential LD of other alleles influencing the yield data separate than effects associated with awn presence.

For a number of markers mapped to the same position in the Wilkinson *et al.* (2012) and Allen *et al.* (2017) consensus map, there was genotype variation in the WISP collection (e.g. the significant markers AX-94394580 and AX-94622557). This disparity suggests diversity was present in the WISH collection in genetic regions that were in LD in the populations used to create the consensus map.

2.4.5 Possible Study Limitations and Future work.

Due to differences in heading and flowering date between the NILs, the pairs were sampled numerically (pair 1 to 3). This was suitable for comparisons between awned and unawned individuals within each pair as alternate measurements were made. However, pair 3 was measured towards the end of each development phase, which influenced the data during the grain-filling stage when there were signs of senescence. The problem was exacerbated by equipment failure which delayed the measurement of pair 3 by several days during grain-filling. Therefore, some of the variation observed between pair number at grain-filling was related to sampling date. However, pair 1 was generally more productive in terms of *A* (ear^{-1}) and *A* (flag leaf^{-1}) than pair 3 (Table 2-4), resulting in difficulty gauging the severity of the effect. A single LI-COR CC was used in the NILs field trial; if multiple machines were available then measurements could be taken simultaneously which would reduce differences in development stage between the NILs.

The LI-COR CC has been used to measure wheat ear photosynthesis in other published studies (e.g. Tambussi *et al.* 2005; Zhou *et al.* 2016). However, a recent publication by Fortineau & Bancal (2018) has highlighted key limitations to the chamber in comparison to their custom built design. These limitations, to some degree, reflect observations made during the NILs field trial. Firstly, the LI-COR CC had a unidirectional light source. Although, Fortineau & Bancal (2018) found that at saturating light there was no variation in results between the custom built chamber (with homogeneous lighting) and the LI-COR CC. The LI-COR CC does have an internal chamber reflective white gloss coating, meaning the whole ear was still illuminated with sufficient light intensity. If

measurements are conducted at a near-saturating light (Figure 2-3), then the potential issues associated with unidirectional lighting are diminished. Another limitation was that the cuvette was too short in length to contain ears without bending. The effect of bending would have opened previously shaded regions to light, whilst possibly shading regions which were lit before. In the present study, care was taken to bend the ear in the same fashion, although it was a difficult parameter to control. The custom built chamber by Fortineau & Bancal (2018) is longer than the LI-COR CC and could accommodate most ears without bending. However, the awned ears in the present study mostly exceeded the length of their chamber (15 cm) and awn bending would still be needed. Furthermore, taking measurements in the centre of field plots required a portable chamber, at the current stage of development the Fortineau & Bancal (2018) chamber is restricted to the laboratory use only.

Measurements of leaf temperature were another limitation of the LI-COR CC. Leaf temperature is used in g_s calculations (Li-Cor 2012) but was measured without contact to the ear or leaf. Therefore, g_s estimations may have been inaccurate and for these reasons were not reported. Finally, large chambers can be susceptible to leaks, but significant leaks were not detected in the present study.

One of the difficulties in measurements of ear photosynthesis, is accuracy in ear area estimations (Tambussi *et al.* 2007). Other studies have measured the ear as a parallelepiped, by calculating the area of the different faces (e.g. Fortineau & Bancal 2018; Zhou *et al.* 2016). This method is unsuitable when working with awned lines. The technique in the present study was suitable for estimating how awn presence changed spikelet area. However, it was assumed all spikelets were of equal size to the six central ones measured. Visual observations of wheat ears will always show this assumption to be incorrect, indicating there was an over estimation in ear size. Furthermore, the spikelets were imaged in a planar fashion, which would have missed variation in spikelet width and depth. A similar assumption was made for the leaves, although both sides of the leaf were illuminated within the chamber, the organ was treated as a one sided by the imaging. It is also possible that A (flag leaf^{-1}) was overestimated as it was assumed the entire leaf would have the same A as the central region measured, which is not to the case (Allwood *et al.* 2015). These assumptions may have influenced the results of ear A (cm^{-2}) and A (flag leaf^{-1}). For ear A (cm^{-2}) no variation was found. Variation in leaf A was linked to differences in flag leaf A (cm^{-2}), as no variation was found in leaf area across the lines. Flag leaf A (cm^{-2}) would have been unaffected by potential error caused from these

assumptions, as the areas used in calculations were taken from direct imaging of the leaves. The area estimations in the present study were adequate for measuring differences between the awned and unawned lines, in a relatively high-throughput fashion. To improve accuracy, a more sophisticated method is required for measuring ear area and *A* of entire flag leaves, but this is beyond the scope of this study.

2.5 Outlook: Awns a Trait for Selection?

Judging from the gas-exchange and harvest results there was no overall benefit of awn presence to grain yield in the 3 pairs of NILs studied under typical UK field conditions. The accession with the largest abundance of awns also had the highest *A* and R_{DARK} (ear^{-1}), and consequently showed the greatest penalty in yield compared to the corresponding unawned counterpart, in a trend maintained over multiple years and locations. Therefore, as awn presence was also linked to a decrease in photosynthetic activity in the flag leaf, it would be a trait selected against in breeding for a well-watered environment. The SNP and phenotypic associations identified through the GWAS could be used to facilitate MAS to suppress this trait.

Across all five pairs of NILs studied in the yield analysis, in one pair awns did provide a yield advantage. However, no gas-exchange analysis was completed on these NILs, meaning the physiology driving this trend was unstudied. Further analysis should include a detailed comparison of the pairs where yield differences were observed across multiple trials (Pair 1 and 5). Natural stable isotope labelling could be implemented in parallel to further field gas-exchange analysis, to determine each organs contribution to grain-filling and the direct influence awn presence is having on the yield variation.

Chapter Findings Summary.

1. The two awned *T. dicoccoides* accessions from Chapter 1 possessed higher per ear net CO_2 assimilation, *A* (ear $^{-1}$), than the two unawned modern elite wheats: Paragon and Robigus.
2. In 3 pairs of field grown Synthetic Hexaploid Wheat Near Isogenic lines (SHW NILs), the presence of awns was associated with increased *A* (ear $^{-1}$), but no change to ear per unit CO_2 assimilation (ear *A* cm^{-2}). Therefore, this variation was driven by the increases in ear surface area associated with awn presence.
3. There was a reduction in flag leaf per unit CO_2 assimilation associated with awn presence, but no variation in leaf area between the NILs of each pair.

4. In 4 out of the 5 NILs, mean grain yield was higher in the unawned line. This trend was only significantly maintained in 2 of the NILs across multiple locations and years: in one pair the awned line yielded lower and in the other the awned line yielded higher.
5. A genome-wide association study was used to identify 22 significant marker associations with awn presence. All associations were found on chromosome 5A, where there is a known locus controlling awn presence.

3 IDEOTYPE FORMATION AND QTL MAPPING.

Abstract

The previous chapters have outlined flag leaf and ear photosynthetic characteristics which could be captured from a progenitor background to improve modern wheat. Genetic markers linked to these traits need to be identified in order to employ Marker Assisted Selection (MAS), to aid the introgression of this diversity. Based on data from previous chapters, and examples in literature, theoretical ideotypes were outlined to aid the secondary selection of physiological markers amenable to high-throughput screening that correspond with complex traits relating to photosynthesis and yield potential.

A novel bi-parental *Triticum dicoccum* mapping population was created and genotyped with the 35K Wheat Breeders' single nucleotide polymorphism (SNP) array. A new genetic linkage map was formed consisting of 1779 SNPs. Composite interval mapping (CIM) was used to identify quantitative trait loci (QTL) for 8 physiological markers in a glasshouse and field trial, which included 89 and 107 recombinant inbred individuals, respectively. These candidate marker-trait associations could be put forward for validation in subsequent field trials. The 8 physiological markers are proposed proxies for complex ideotype traits and were: awn length, flag leaf length and width, stomatal density, flowering time, leaf dry matter content, harvest index and ear number. However, no QTL was consistent over both trials. Physiological markers that correlated with yield components in the field trial were used to support the hypotheses made in the formation of the ideotype for a well-watered environment. The work in this chapter could aid the introgression of tetraploid landrace diversity into a modern hexaploid background, whilst also providing a framework of high throughput phenotype measurements that could aid selection for photosynthetic improvement in large breeding populations.

3.1 Introduction and Ideotype Formation.

There is a gap to bridge between plant physiology and wheat breeding, particularly in terms of genetic selection for improving photosynthesis. This is partially accounted for by the complexity of crop photosynthesis, which is a labyrinth of dynamic processes from molecular to canopy levels. Ambiguity also exists when pinpointing which characteristics would be most beneficial for trait-based selection. This is exacerbated by crop gas-exchange measurements being time consuming, expensive and reliant on complicated equipment, resulting in few opportunities for making selections in large breeding programs or mapping populations. If a platform of proxies could be identified that are both amenable to high-throughput phenotyping and secondary characteristics to more complex targeted traits, it would provide breeders with a physiological basis for making selections.

3.1.1 Crop Ideotypes and Trait-Based Breeding.

Recent progress in the physiological and genetic dissection of traits relating to crop performance have advanced opportunities in ideotype formation and trait-based breeding. The term 'crop ideotype' was originally defined as:

> *"...a biological model which is expected to perform or behave in a predictable manner within a defined environment. More specifically, a crop ideotype is a plant model which is expected to yield a greater quantity or quality of grain, oil or other useful product when developed as a cultivar" (Donald 1968).*

This approach suggests breeders should focus on trait-based selection towards an ideotype, instead of empirical selection for grain yield (Martre *et al.* 2015). Selection solely for yield increases the risk of missing untapped genetic diversity from unimproved collections, which may be essential for future progress (Rasmusson 1991). Trait-based selection overcomes this risk and may be particularly advantageous in capturing diversity from progenitor wheat linages. However, the degree to which trait-based selection has been implemented in modern plant breeding is questionable. The general opinion within the industry is that the contribution of physiology to plant breeding has been underutilised (Jackson *et al.* 1996) and selection for grain yield still predominates. There has been some application of physiological ideotype breeding within the breeding community, although the success of this application is trait specific (Rasmusson 1991). Application is limited in the difficulty and cost of measuring complex traits that physiologists identify as

important (Rebetzke *et al.* 2000). Plant breeders work with large populations and require both instantaneous and inexpensive phenotyping techniques. Brennan *et al.* (2007) suggested that physiological assessment before large scale field trials, can not only be beneficial for screening for yield potential but also economic by creating an earlier stage of selection. As highlighted by Jackson *et al.* (1996), if physiological reseach is to be utilised in breeding, a selection criteria of targeted traits needs to be outlined for specific environments and high throughput proxies for these traits needs to be identified. The opportunity to achieve these goals may exist through physiological ideotypes designed for targeted environments.

The use of crop ideotype frameworks over recent decades has focused mainly on major morphological traits, such as the introduction of dwarfing genes to improve harvest index (*HI)* (Reynolds *et al.* 2009), lodging resistance (Berry *et al.* 2007), optimisation of light capture and canopy formation (Peng *et al.* 2008; Sarlikioti *et al.* 2011). There has been considerably less focus on developing ideotypes for improvements directly related to photosynthesis or based on traits amenable to high-throughput phenotyping for genetic-marker association. Photosynthetic ideotypes that have been outlined either focus on complex gas-exchange measurements (e.g. Gu *et al.* 2012) or do not provide a source of diversity for trait manipulation (e.g. Tholen *et al.* 2012). If physiological markers could be developed for indirect selection of more complex traits, this would facilitate the development of a 'physiological ideotype', allowing diversity from progenitor wheat linages and across mapping populations to be incorporated.

In the Donald (1968) ideotype definition, it was argued that the model plant will yield a greater quantity of a useful product. Grain yield and yield stability are generally the overall goal of crops improvement. Effective combination of trait-based improvements should lead to a higher yielding plant within a target environment. However, the contribution of individual traits is difficult to estimate. Yield comparisons between progenitor and modern wheat can lead to biased estimations, due to evolutionary differences in selection pressure. In theory, trait and yield interactions can be split into three categories.

i. Traits which directly contribute to grain yield, including assimilate remobilisation and the source-sink balance.
ii. Traits that indirectly contribute to grain yield, but more accurately contribute to the amount of photo-assimilates pooled for remobilisation.

These traits include: CO_2 demand and supply, radiation capture and photosynthesis duration.

iii. Traits that contribute to yield stability in a targeted environment; including water expenditure and, potentially, investment into ear photosynthesis.

3.1.2 Forming a Photosynthetic Ideotype.

To enable effective trait-based ideotype breeding, a framework of targeted integrative traits needs to be outlined. From this framework, physiological markers can then be derived for indirect selection of the more complex traits. Using traits discussed in Chapter 1 and 2, typical ideotypes for two targeted environments, water-limited and well-watered environments, have been generated (Figure 3-1). The schematic highlights where selection could be implemented, to either promote or supress characteristics ranging from organ level to the entire plant. In principal, the traits reflect identified characteristics which have been shown to be important for photosynthetic productivity, and in theory grain yield, within a given environment. These concepts are based on direct observations made in the present project, whilst also incorporating more generally accepted targeted traits outlined for photosynthetic improvement. Furthermore, based on evidence from the present study, the ideotypes indicate where diversity within progenitor tetraploid wheat might be advantageous for modern wheat improvement, or where traits have already been fixed through domestication.

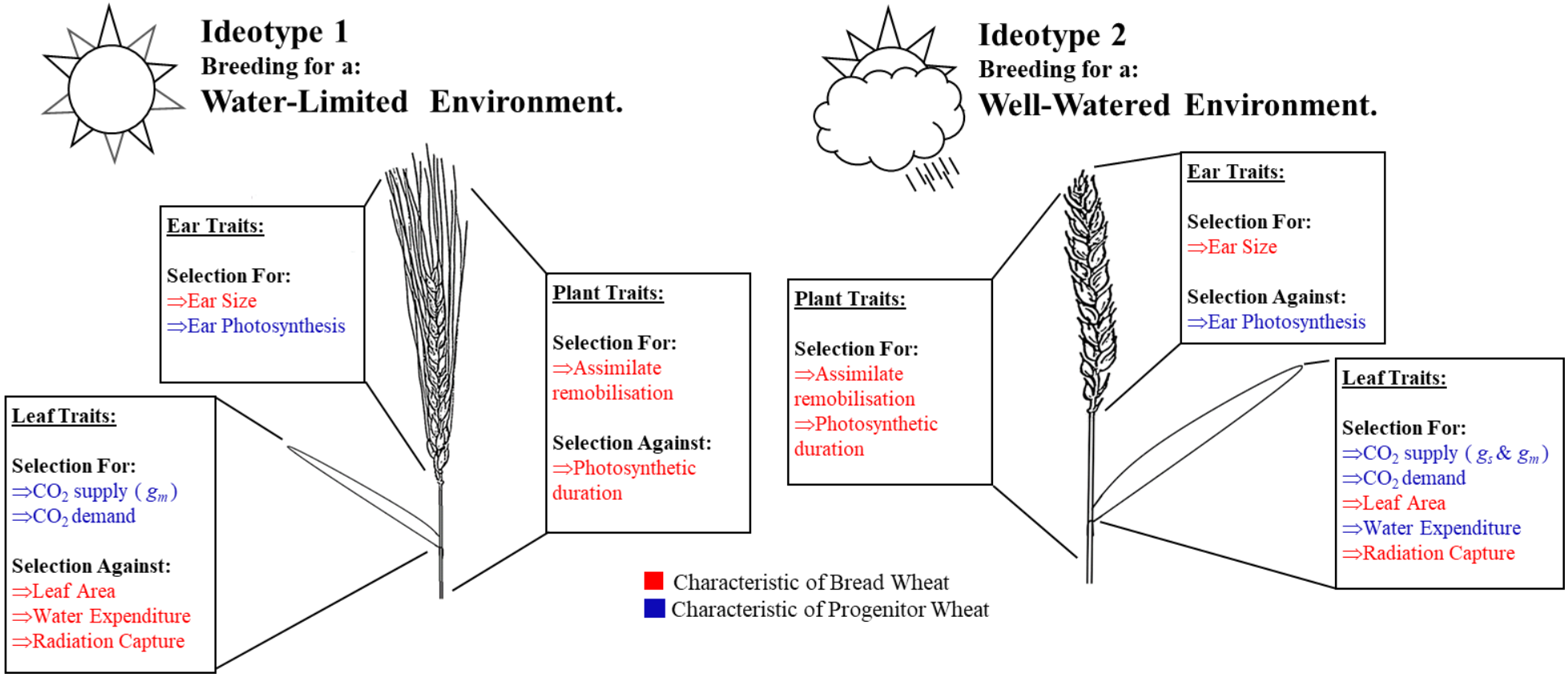

Figure 3-1 – Two theoretical ideotypes for different target environments (Water-Limited and Well-Watered) combining selection strategies for important complex traits identified in the previous chapters. The traits were either present in the progenitor background (blue) or in cultivated modern wheat (red), therefore, diversity from these backgrounds could be captured for trait selection. For each ideotype, traits are separated into three categories: ear traits, leaf traits and whole plant traits. The term 'Selection For' indicates complex traits breeders should try to promote in a particular environment. In comparison, 'Selection Against' indicates traits breeders should not aim to promote in the targeted environment. g_m = mesophyll conductance and g_s = stomatal conductance.

Leaf Traits

In the present study, increased mesophyll conductance (g_m) and stomatal conductance (g_s) were linked to higher CO_2 assimilation (*A)* (Chapter 1: 1.3.1). The *T. dicoccoides* accessions showed both high g_m and g_s, so are a promising source of diversity for either ideotype by improving CO_2 supply (Figure 3-1). Selection for high g_m is warranted to optimise CO_2 supply, regardless of the targeted ideotype environment. Increased g_m has potential for improving *WUE* (Tomás *et al.* 2014) and is already a major constraint of photosynthesis (Flexas *et al.* 2012). In comparison, g_s is a more environment-specific trait, as ideotype selection for increased g_s will have negative effects on water expenditure (Gu *et al.* 2012). However, promoting g_s in water rich environments can directly benefit grain yield (Barbour *et al.* 2000; Condon *et al.* 1987), by increasing CO_2 supply regardless of water-loss.

Down-stream photosynthetic demand mediated by Rubisco activity is a non-environment specific ideotype trait fundamental to CO_2 fixation. Observed correlations between flag leaf nitrogen content and photosynthesis (Evans 1983, 1989), have highlighted the importance of Rubisco content to *A*. Furthermore, down-stream demand could be increased by optimised catalytic properties of the enzyme, where there is still potential for selection based improvement (Figure 3-1; Prins *et al*. 2016). Mean leaf nitrogen was higher in modern wheat than progenitor lines (Chapter 1: 1.3.1), however, the *T. dicoccoides* line 'dic71' had a higher per unit area photosynthetic capacity (A_{max}); an indicator of higher photosynthetic nitrogen use efficiency (Poorter & Evans 1998). Furthermore, the progenitor lines also showed significantly higher carboxylation efficiency (CE_{amb}), suggesting the possibility of superior enzyme catalytic qualities.

Associations between grain yield and FL_A were measured (Chapter 1: 1.3.2) and selection for increased flag leaf area (FL_A) has been linked with increased spikelet number and ultimately grain yield in bread wheat (Rao 1992; Yue *et al.* 2006). Furthermore, within limits, increasing leaf area improves radiation interception (Parry *et al.* 2011). Domesticated wheat lines had considerably larger FL_A than progenitor individuals, which was linked to higher *A* ($leaf^{-1}$) (Chapter 1: 1.3). However, increases in leaf area can be associated with greater canopy shading and increased respiratory cost (Drewry *et al.* 2010; Srinivasan *et al.* 2017). In a high light environment where radiation capture is not limiting, investment into leaf thickness rather than size is typically observed (James & Bell 2000; Terashima *et al.* 2001). In Chapter 1, *T. dicoccoides* individuals had smaller

FL_A but higher *A* per unit area, possibly relating to a natural selection response to the arid environment typical of the geographic regions from which the accessions were originally collected. Therefore, selection for a smaller flag leaf with increased thickness could be beneficial in promoting photosynthetic capacity per unit area, provided light is not limited.

Ear Traits

Higher *A* (ear^{-1}) was shown to be of limited benefit to grain yield in a water rich environment (Chapter 2). In these conditions, investment into ear photosynthesis, via the presence of awns, has been associated with a trade-off leading to reduced flag leaf photosynthesis (Chapter 2; Olugbemi *et al.* 1976). However, in a drought prone environment the presence of awns is known to be beneficial to grain yield (Evans *et al.* 1972). Therefore, the higher *A* (ear^{-1}) observed in *T. dicoccoides* individuals in comparison to elite varieties (Chapter 2: 2.3.1), indicates a promising source of diversity for the 'Water-Limited' ideotype.

Sink strength can be a significant limiting factor to grain yield (Miralles & Slafer 2007; Slafer & Savin 1994; Zhang *et al.* 2010). Therefore, improvements to source aspects (assimilate availability) need to be complemented with increased sink strength across both ideotype environments. This could be achieved by selection for increased ear size, which is an important trait when forming ideotypes for improved yield (Donald 1968; Foulkes *et al.* 2011). Selection for increased ear length could lead to a higher spikelet number, and ultimately, more grains per ear (Denćić 1994). Genetic variation in ear size has been described in a number of publications (Sharma *et al.* 2003; Zhai *et al.* 2016). Furthermore, observed variations in overall ear surface area between species and accessions (see: 2.3.1 and 2.3.2), suggests selection could be implemented to improve sink strength.

Plant Traits

Photosynthetic duration is an ideotype trait dependent on the target environment. In the 'Water-Limited' environment early flowering is advantageous to limit drought exposure (Kenney *et al.* 2014; Shavrukov *et al.* 2017). Crops typically rely on photoperiod response to determine flowering time based on environmental cues such as day length. For example, the *Photoperiod-H1* (*Ppd-H1*) locus in barley (Turner *et al.* 2005), which has been shown to be an important gene in geographical adaptability (Jones *et al.* 2011). Early flowering was a characteristic present in *T. dicoccoides* lines (Chapter 1, Appendix 4),

which could be linked to drought avoidance in their environment of origin. Alternatively, prolonged leaf longevity, and therefore increased photosynthetic duration, has been shown to be advantageous to yield (Carmo-Silva *et al.* 2017), as long as water is not limiting during the grain-filling period (Richards *et al.* 2010). Extended photosynthetic duration was found in domesticated wheat lines rather than the progenitor species (Chapter 1, Appendix 4).

Maximising partitioning of assimilates to grain yield is a complex trait which theoretically should be selected for in both ideotype environments. Major improvements to grain yield were accomplished by increasing the partitioning of assimilates to the grain at the expense of stem biomass (Austin *et al.* 1980). Years of selection for grain yield in bread wheat has led to increased photo-assimilate remobilisation to the grain (Evans & Dunstone 1970). As natural selection does not inevitably favour agronomic grain yield (Leister 2012) and wild relatives do not undergo anthropogenic selection, it is not surprising that the progenitor tetraploid lines in this study were lower yielding (Chapter 1, see: 1.3.1 and 1.3.2). Therefore, this ideotype trait is mostly likely a characteristic already present in the bread wheat background.

3.1.3 Physiological Markers

Physiological markers are proxies for complex traits which are amenable to high-throughput phenotyping, and would facilitate screening of large populations or diverse wheat collections, in order to identify genetic markers to aid the introgression of desirable traits into the modern wheat genepool via MAS. Physiological markers linked to each complex trait are listed in Table 3-1. These markers are based on observations in previous chapters, examples in literature and available diversity between the mapping population parents. The relevance of each of the physiological markers to the complex traits are discussed in the following sections.

Table 3-1 - Proposed physiological markers relating to targeted ideotype complex traits shown in Figure 3-1. The link between each physiological marker and targeted trait was established either in analysis in Chapters 1 and 2, or through using evidence in literature.

Targeted Traits	Physiological Markers
Leaf Traits	
CO_2 Supply	*g_s: Stomatal density and size; carbon isotope discrimination ($\Delta^{13}C$).*
	g_m: Leaf dry matter content; specific leaf area.
CO_2 Demand	*Leaf N content; chlorophyll content; leaf area and thickness.*
Water Expenditure	*Stomatal density and size; carbon isotope discrimination ($\Delta^{13}C$); relative water content (RWC).*
Radiation Capture and Utilisation	*Leaf area; leaf angle; chlorophyll fluorescence.*
Ear Traits	
Ear Size	*Ear height, width and area; spikelet number.*
Ear Photosynthesis	*Awn presence; awn length.*
Plant Traits	
Assimilate remobilisation	*Grain yield; Harvest Index.*
Photosynthetic duration	*Flowering time; leaf longevity.*

CO_2 Supply and Water Expenditure.

The *T. dicoccoides* lines had higher g_s than modern wheat, which was linked to a higher stomatal density per unit area (Chapter1: 1.3.1). Stomatal size may also be linked to g_s, as trade-offs between stomatal density and size are often observed (Franks *et al.* 2009; Hetherington & Woodward 2003). Furthermore, the *T. dicoccoides* lines had higher $\Delta^{13}C$, which can be used as an indicator of stomatal relations and photosynthetic capacity over the lifespan of a leaf (Farquhar *et al.* 1982, 1989). The parameter *RWC* is also a useful tool for screening drought tolerance (Silva *et al.* 2007).

In section 1.3.1, there was a link between mesophyll intercellular airspace and g_m. Other studies have also reported negative correlations between g_m and leaf mass per area (see: Flexas *et al.* 2008, 2013; Tomás *et al.* 2013), suggesting leaf dry matter analysis could be used as a proxy for g_m.

CO_2 Demand

The downstream activity of photosynthetic enzymes is an important determinant of photosynthetic demand; chlorophyll and leaf nitrogen contents have been shown to be proportionate to Rubisco activity (Evans 1983), highlighting their potential use as proxies. Flag leaf area was an important determinant of A (leaf^{-1}, Chapter 1) and is an obvious indicator of the area based photosynthetic capacity of the organ. Furthermore,

flag leaf thickness could also be measured as physiological marker for photosynthetic capacity, as positive correlations have been observed in other studies (McClendon 1962; Oguchi *et al.* 2003).

Radiation Capture and Utilisation

When other factors are not limiting, chlorophyll content is proportional to the rate of photosynthesis (Fleischer 1935). Furthermore, chlorophyll fluorescence is used as a tool in measuring photosynthetic performance of crops (Maxwell & Johnson 2000) and is informative of the proportion of captured light energy invested into photochemical pathways (Baker 2008; Murchie & Lawson 2013). As canopy dry matter content can be positively correlated with radiation capture (Shibles & Weber 1966); selection for increased leaf area is an avenue for increasing canopy photosynthesis (Beadle & Long 1985). Conversely, it has also been argued that smaller flag leaves would increase light utilisation through the canopy (Donald, 1968).

Ear Size and Photosynthesis

Ear size and awn length are determinants of gross ear photosynthesis (Evans & Dunstone 1970), but accurate ear area estimations are difficult to obtain due to the complex shape of the organ (Chapter 2). However, Fortineau & Bancal (2018) and Zhou *et al.* (2016) made estimations of ear size (excluding awns) by treating the organ as a parallelepiped and calculating the area of each face. This method can be completed in a relatively high throughput fashion and was used in the ploidy field trial (Chapter 2). Variation in awn length in modern wheat has been observed in a number of studies (e.g Maydup *et al.* 2014; Rebetzke *et al.* 2016). As awn presence was linked to increased ear CO_2 assimilation (Chapter 2), it could be hypothesised that increasing awn length will have a similar effect and could be used as a proxy for selection to increase ear photosynthesis.

Assimilate Remobilisation

Assimilate remobilisation has been measured in other studies using a range of different techniques (e.g. Bell & Incoll 1990; Zhou *et al.* 2016). However, these techniques are not amenable to high throughput phenotyping. High yields are associated with the increased remobilisation of a crop's biomass to the harvestable product (Richards 2000). Therefore, measurements of grain yield and *HI* are, not only the overall goal of crop improvement, but suitable proxies for estimating assimilate remobilisation and partitioning to grain.

Photosynthetic Duration.

Flowering time is a trait that can be scored directly in the field (Pask *et al.* 2012). The duration of green area after flowering is dependent on the dynamics of senescence (Slafer & Savin 1994). To select for delayed senescence, and a thus extended photosynthetic duration, post-flowering flag leaf longevity can be used as a physiological marker.

3.1.4 Marker Assisted Selection and QTL mapping.

The selection of a phenotype based on an associated DNA marker is called marker assisted selection (MAS). The use of MAS can facilitate the introgression of quantitative trait loci (QTL) from a donor background (Hospital & Charcosset 1997) and introgressions from a wild background into domesticated wheat (Merchuk-Ovnat *et al.* 2016b; Nevo & Chen 2010). To use MAS effectively, accurate marker-trait associations need to be established via QTL mapping.

A QTL is the individual loci within a genome that is linked to the region controlling a quantitative trait (Tanksley 1993). The process of 'QTL mapping' involves connecting a genetic marker, assumed to be closely linked to the QTL, with the phenotypic variation present in a mapping population. A mapping population is typically formed via the hybridisation of two parental lines which contrast in the targeted phenotype. After the population has been created, genetic polymorphisms (DNA markers) need to be identified between the parental lines, which are then screened across the entire population (Collard *et al.* 2005). Using the genotype data in the population, linkage analysis is completed based on the recombination between markers, which forms a linear arrangement of the DNA markers into different linkage groups (or chromosomes) to provide a new genetic map (Doerge 2002). There are three stages to a genetic map formation: markers are first clustered in linkage groups, then markers are ordered within a linkage group; and finally the genetic distance between neighbouring markers is predicted (Wu *et al.* 2008) The genetic map is a guide to the location and distance of a marker or QTL along each chromosome. The mapping population is then phenotyped for the targeted trait, and a range of techniques can be used for identifying associations between the mapped DNA markers and the quantitative trait variation. These techniques range from single marker analysis to the more complex multiple QTL model fitting (Broman & Sen 2009). One of the most commonly used methods in bi-parental mapping studies is composite interval mapping (CIM, Li *et al.* 2007), which includes additional markers as cofactors within the analysis, reducing the variation associated with linked QTL (Doerge 2002) and offers increased accuracy in mapping QTL than single marker analysis (Collard *et al.* 2005).

Mapped QTL have provided a large abundance of marker-trait associations for adoption in MAS (Collard & Mackill 2008).

The increased availability of high density genotyping arrays has aided the application of QTL mapping and accessibility to genetic diversity in progenitors and related species (Winfield *et al.* 2016). Single Nucleotide Polymorphisms (SNPs) are powerful markers in high-throughput genotyping technology due to their abundance across the wheat genome (Rimbert *et al.* 2018). The 35K Wheat Breeders' array is an example of a SNP genotyping array which aids the formation of high density genetic maps of novel populations (Allen *et al.* 2017). The Wheat Breeders' array has been used in a number of studies for identifying QTL and population structures in tetraploid wheat (Kabbaj *et al.* 2017; Lucas *et al.* 2017).

The heritability of physiological traits relating to photosynthesis has been identified in a number of studies (e.g. Carver *et al.* 1989; Nevo *et al.* 1991; Rajabi *et al.* 2009; Rebetzke *et al.* 2001). Progenitor and tetraploid species have already shown merit as viable genetic resources for modern wheat in terms of diseases resistance (e.g. Peng *et al.* 2000, 2012) and abiotic stress tolerance (e.g. Simmonds *et al.* 2008). QTL have been identified in progenitor tetraploid wheat that relate to a large range of traits (e.g. Faris *et al.* 2014; Peleg *et al.* 2009; Peng *et al.* 2003). There has been limited investigation into QTL directly linked to photosynthetic traits. However, Merchuk-Ovnat *et al.* (2016a) used MAS to introgress a *T. dicoccoides* QTL to improve drought tolerance in cultivated wheat. Although not directly targeted, Merchuk-Ovnat *et al.* (2016b) showed that the QTL increased photosynthetic capacity, flag leaf area, sink capacity and grain yield. The drought tolerance QTL was identified in an earlier study by Peleg *et al.* (2009), where they found 110 QTL for 11 traits, including photosynthetic duration, carbon isotope ratio, dry matter content and chlorophyll content. These studies highlight the potential of using MAS to transfer beneficial diversity to modern wheat from a tetraploid background.

3.1.5 Chapter Aims

Alongside beneficial traits, introgressions from a wild source can lead to undesirable traits; a phenomenon termed 'linkage drag'. Undomesticated traits such as shattering and sterility can be introduced from wide crosses (Tanksley & Nelson 1996), leading to a reduction in yield. Yield penalties were associated with introgressions from *T. dicoccoides* in Chapter 1. To avoid these issues, but still aiming to access the genetic

reserve of the AB genome, QTL mapping of the physiological markers was conducted in a novel *T. dicoccum* population. Cultivated emmer was directly domesticated from *T. dicoccoides* (Civáň *et al.* 2013; Özkan *et al.* 2002; Peng *et al.* 2011). Furthermore, after domestication, gene flow still occurred between the cultivated and wild populations of emmer (Luo *et al.* 2007). Therefore, untapped diversity may still be present within the *T. dicoccum* background, reflecting the wild progenitor.

The aims of this chapter were:

1). Form a novel mapping population between two *T. dicoccum* landraces, which showed variation in ideotype related traits in preliminary observations.

2). Within different environments, phenotype the physiological markers outlined in the ideotype to identify variation in the mapping population and parental lines.

3). Genotype the mapping population after several generations of self-fertilisation using a high density SNP array.

4). Create a new genetic map with SNP genotype data.

5). Use QTL mapping to identify marker-trait associations for potential use in MAS to capture tetraploid diversity.

3.2 Methodology

3.2.1 Material and Trials.

Material

Mapping Population Formation and development

A tetraploid mapping population (*PS1*) was formed by crossing two *T. dicoccum* landraces. The maternal parent 'Tios' and the paternal parent 'dic12b', were *T. dicoccum* landraces originating from Spain and Iran, respectively. These landraces have ongoing pre-breeding significance in the Wheat Improvement Strategic Program (WISP). In preliminary gas-exchange glasshouse analysis, White and Leigh (unpublished) identified that Tios had higher leaf *A* per unit area than dic12b. When these lines were tested in the field during the present study (Chapter 1), this variation was not apparent. However, the mapping parents did show a range of variation for the physiological markers of interest in this Chapter and thus the population was continued. The contributors to the preliminary analysis, population formation and advancement, are listed in Appendix 6.

As the cytoplasm, and organelles within, show strict maternal inheritance (Griffiths *et al.* 1999; Leigh *et al.* 2013), the direction of the cross was fixed. Although, the targeted phenotypic traits (discussed later on) are not known to be linked to chloroplast genes. The parental lines were taken from single founder plants to reduce landrace genetic heterogeneity. The parental hybridisation took place in October 2014, where the maternal parent Tios was emasculated when plants had reached GS55 - 59 (Zadoks *et al.* 1974) and pollinated two days later with pollen from dic12b ears undergoing anthesis. From this cross the *PS1* population was formed; the stages of development are shown in Figure 3-2. Seed was hand threshed from crossed ears and 6 F1 plants (Table 3-2) were sown in into 1 L pots in a glasshouse at Park Farm, NIAB with supplementary lighting. Larger mapping populations provide higher resolution for QTL mapping (Collard *et al.* 2005). Therefore, to form a mapping population with 200 individuals, F2 seed was sown from each F1 plant (Table 3-2) into 96 well trays and placed in a glasshouse at Park Farm, Cambridge.

Table 3-2 – The formation of 200 individuals for the *PS1* mapping population, sown from F1 plants of crosses made between Tios and dic12b in October 2015.

F1 Plant	*Seeds sown*	*Individual codes*
PS1_A	*34*	PS1_A_1 to PS1_A_34
PS1_B	43	PS1_B_1 to PS1_B_43
PS1_C	34	PS1_C_1 to PS1_C_34
PS1_D	34	PS1_D_1 to PS1_D_34
PS1_F	22	PS1_F_1 to PS1_F_22
PS1_G	33	PS1_G_1 to PS1_G_33
Total	200	-

Single seed decent (SSD) is a technique used for fast advancement through generations, with the aim of increasing homogeneity (van Oeveren 1991), individuals are left to self-fertilise and one seed is then sown to advance to the next generation. This method was used in the development of the *PS1* population (Figure 3-2). During each generation, once the main tiller of each plant had reached GS57 - GS59, the ears were covered in a cellophane clear bag to prevent outcrossing and promote self-fertilisation. The F2 and F3 generations were sown in 96 well trays to promote single tillering. As discussed in the trial descriptions below, at the F4 generation all individuals were planted in 5 L pots. In total 100 individuals produced F5 seed which was sown into a field trial at the New Ornamentals Field, Park Farm, NIAB. By the F5 generation, the population size had been reduced due to germination failures and sterility, which may have been related to the poor adaption of the landraces to the glasshouse environment. To increase population size, F4 seed was also sown into the trial from 39 F3 lines which failed to produce ears in the F4 to F5 glasshouse grow out. Of the 100 F5 individuals sown 87 germinated; 33 of the F4 individuals germinated. In total phenotypic data were obtained from 120 *PS1* individuals in the 2017 field trial.

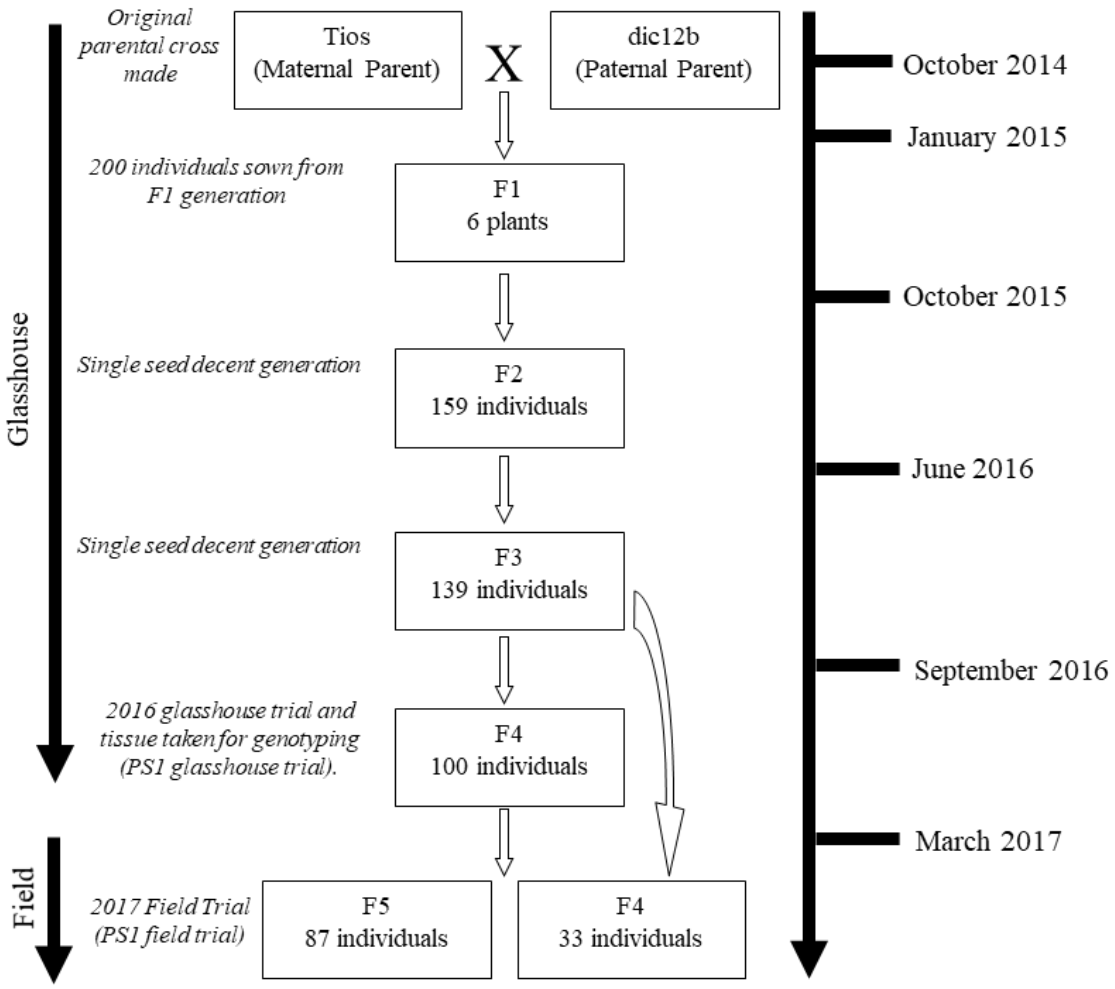

Figure 3-2 - A diagram showing the stages of development of the *PS1* mapping population including: the original parental cross, genotyping, the single seed decent program and the field trials used for phenotype analysis. Excluding the original cross, the dates reflect the month each generation was advanced to the next generation. From 6 F1 plants, 200 individuals were sown and taken through single seed decent to the F4 generation, then 33 F4 individuals were re-sown from the last generation into the 2017 field trial with 87 F5 individuals. Genotyping and the 2016 glasshouse trial was completed on F4 individuals in the glasshouse.

Trials.

Trials used in this chapter include:

- The 2016 winter preliminary glasshouse screen at Park Farm, Cambridge, NIAB. Hereafter called the '*PS1* glasshouse trial'.
- The 2017 summer field trial at Park Farm, Cambridge, NIAB. Hereafter called the '*PS1* field trial'.

PS1 Glasshouse Trial.

During the F4 stage of the SSD program (Figure 3-2), the mapping population and replicated parents (individuals of the landraces) were grown in 5 L pots in a randomised order and contained on the same bench in a heated research glasshouse at Park Farm, Cambridge. Two different *PS1* individuals were transplanted per 5 L pot using regular potting compost. Plants were supplied with regular manual irrigation, sodium 10000 lux supplementary lighting, day lengths of 16 hours, daytime temperatures of 22 °C and night-time temperatures of 15 °C. On the 10th of November 2016 plants were treated with an ammonium nitrate application at a rate of 352 kg ha^{-1}, to achieve a universal N application of 122 kg / N. During stem booting, plants were individually staked. On the 29th of September, 2016 a round of seed was sown for the 17 lines which failed to germinate, and these seedlings were transplanted to the 5 L pots on the 7th of October 2016 to be included in the trial. Plants were harvested on the 9th of February 2017.

PS1 Field Trial.

Seeds were hand sown into two replicated 25.5 m^2 plots (8.5 m x 3 m) on the 24th of March 2017 at the New Ornamentals Field, Park Farm, NIAB, Cambridge. Each plot had nine 8.5 m rows spaced every 30 cm. The 1st row, 9th row and the 25 cm at the start and end of each row was sown with Paragon seed to act as a buffer and to reduce edge effects. The 2nd, 5th and 8th rows were not sown with any seed to aid accessibility for phenotyping. The 3rd, 4th, 6th and 7th rows were organised into a randomised incomplete block design (Figure 3-3). The block design was incomplete as although the mapping parents were replicated over each block, the individuals were not. There were five blocks in total, each block took up 1.6 m of the four rows and contained the mapping population parents. The block design was used to ensure even distribution of parent replicates across the trial. Within each block, there were 32 mini-plots (30 mapping individuals and the 2 parents). Each mini-plot was a 20 cm row segment, consisting of a label and 3 seeds placed 5 cm apart. Three seeds were sown for each *PS1* individual due to the planned sampling strategy: 2 different plants were needed for invasive and non-invasive measurements and an extra plant was included as a spare. Therefore, there were 2 replicate 8.5 x 3 m plots, both containing 3 plants of each *PS1* individual.

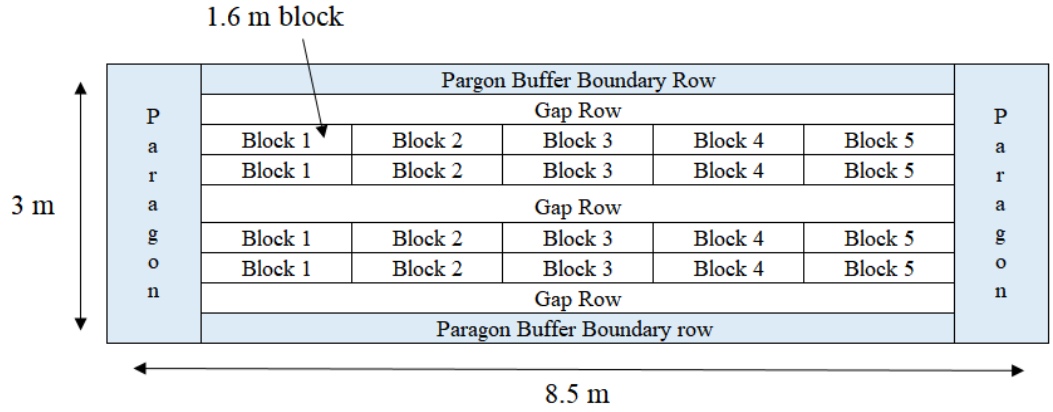

Figure 3-3 - The trial layout of one of two 25.5 m^2 plots in the *PS1* field trial. The plot consisted of 5 blocks, each block containing 32 lines. Each line occupied 20 cm of a particular row, with a label and 3 seeds placed 5 cm apart. Each of the parents were included in each block and the order of lines was randomised.

On the 28th of April 2017, gaps where seed had failed to germinate were filled with Paragon seed. On the 19th of April 2017, the plots were fertilised with on application of ammonium nitrate (34.5% N) at a rate 434 kg ha^{-1}, in order to achieve a universal N application of 150 kg / N. The plots were treated with fungicide on the 18th of May 2017. On the 25th of June 2017, the trial was sprayed with further fungicide and insecticide. Herbicide was not applied to the plot, as routine hand weeding was carried out. Once the plants had reached GS39 they were all individually staked with a bamboo support to avoid lodging. Until senescence, in the absence of rainfall for 4 - 5 days the plots were irrigated. During the period of the 14th to the 23rd of August 2017, when fully senesced, whole plants were individually pulled out of the ground and stored in a perforated bag. The samples were transported to a drying wall, where they were dried for 72 hours and then stored for processing.

3.2.2 Phenotypic Methodology

PS1 Glasshouse Trial

Material Sampling.

Measurements of flag leaf length (FL_L), width (FL_W), area (FL_A) and flowering time (F_T) were made on main tillers of individual plants at GS61, at the same time dry matter analysis was then completed on secondary main tillers (which were typically at GS55). During plant senescence, flag leaf longevity (FL_{LONG}) was recoded.

Measurements

Flowering time: F_T was scored when the first main tiller reached anthesis (GS61). The flowering time was then calculated from the number of days to flowering from the date of sowing (s-f).

Flag leaf area: On the tagged tiller, FL_L and FL_W were recorded. The length from the leaf base to tip was FL_L and FL_W was measured at the widest part of the flag leaf. Then FL_A was estimated using an equation from Teare & Peterson (1971):

$$FL_A = -0.64 + 0.813(FL_L \times FL_W)$$

This is a high-throughput proxy for estimating FL_A and less time consuming than using image analysis. A comparison between the methods is included in the appendices (see: Appendix 3).

Leaf Longevity: On the same main tiller, FL_{LONG} was scored by recording when each flag leaf reached 80% senescence. Then FL_{LONG} was calculated by subtracting this date with F_T, representing the number of days from flowering to 80% senescence (f-s).

Leaf dry matter analysis: The parameters of *SLA*, *LDMC* and *RWC* were recorded using the same protocol used in Chapter 1 (except leaf cores were dried at 65 ºC instead of 60 ºC).

PS1 field trial

Material Sampling

As discussed in section 3.2.1, there were two replications of the *PS1* population grown in the 2017 field trial, the two plots were numbered plot 1 and plot 2. The plots were located 5 meters apart from each other in the same field at NIAB, Cambridge. Plot 1 had the highest germination success and was the focus of the field phenotyping. If a line failed to germinate in plot 1 but did in plot 2, then the plant from plot 2 was used for analysis. The parents in plot 2 were also included in the analysis to identify potential variation between the plots.

From the three plants sown for each *PS1* individual, or parent replicate, two were assessed. The first plant of the three to reach GS61, was screened using non-invasive measurements and tagged with a red label. The second plant to reach GS61 was used in invasive measurements and tagged with a blue label. If only one plant germinated for an individual in plot 1, then that plant was used for non-invasive measurements and the invasive measurements were completed on plants grown in plot 2 if the line was present.

Every plant was measured at GS61, and as the population was segregating for flowering time the field screening was conducted from the 11th of June to the 1st of August 2017.

Non-Invasive Measurements.

Non-invasive measurements were completed in the field. Measurements for flowering time, flag leaf area, ear area and awn length were completed on main tillers at GS61 (Zadoks *et al.* 1974). Measurements of leaf longevity and leaf thickness were completed post-anthesis.

Flowering time: F_T was scored using the same protocol as the *PS1* glasshouse trial. The main tiller of each plant was then labelled with a red tag.

Flag Leaf Area: FL_L, FL_W and FL_A were recorded also using the same method as the *PS1* glasshouse trial.

Awn Length: On the same tagged tiller, awn length (A_L) was determined measuring the length from the tip of the ear to the tip of the longest awn (Pask *et al.* 2012).

Ear Length: On the tagged tiller, ear length (E_L) was measured from the base of the ear to the tip of the apical spikelet.

Ear Width: On the tagged tiller, ear width (E_W) was recorded in two measurements: the widest spikelet of the ear (E_{W1}) and the widest point of the ear in a side-on orientation (E_{W2}).

Ear Area: Following Zhou *et al.* (2014), calculated ear area (E_{CA}) was estimated by calculating the area of the four faces of each ear:

$$E_{CA} = (E_H E_{W1}) + (E_H E_{W1}) + (E_H E_{W2}) + (E_H E_{W2})$$

Leaf Longevity: On the tagged tiller, FL_{LONG} was scored using the same method as the *PS1* glasshouse trial.

Leaf thickness: Flag leaf thickness (FL_{THICK}) was measured on the tagged tillers using a Sylva S229 digital thickness gauge (Sylvac, Crissier). FL_{THICK} was determined halfway up each flag leaf to the right-hand side of the main vein, measurements were repeated on the same leaves over three separate days (21st, 23rd and 26th of June 2017). These three measurements were used for determination of mean FL_{THICK}.

Grain yield and harvest index: Roots were cut off at the stem base and the remaining sample was weighed to determine total biomass per plant. As the *T. dicoccum* landraces were not free-threshing, the population required hand-threshing. For each plant, ears were

removed and counted to determine ear number per plant (*EN*). Excluding the smaller ears, which most likely came from back tillers, 3 ears were randomly selected for each plant and hand-threshed. Seed weight was then determined using the MARVIN seed analyser (GTA Sensorik GmbH, Neubrandenburg, Germany). The sample of 3 ears was used to estimate grain weight (yield) per ear (*YE*), which was multiplied by ear number to estimate grain yield per plant (*YP*). To calculate harvest index (*HI*), *YP* was divided by biomass ($plant^{-1}$). A validation test for using 3 ears to estimate overall *YP* is shown in the appendices (see: Appendix 4).

Invasive Measurements.

Invasive measurements were completed on the second replicate plant to reach anthesis GS61. Flag leaves were collected in the field and wrapped in wet tissue, sealed in a plastic bag and transported in a cool box to the field lab where measurements were taken.

Leaf dry matter analysis: The traits *SLA*, *LDMC* and *RWC* were determined using the same method in Chapter 1, although a larger leaf corer was used and total of 1.28 cm^2 leaf tissue was sampled per individual and leaf cores were dried at 65 ºC.

Leaf surface impression and stomatal density: The same protocol was followed in Chapter 1 to estimate stomatal density per mm^2 (S_D) on the abaxial epidermis surface. Across a diverse collection of diploid, tetraploid and hexaploid wheat, Austin *et al.* (1982) demonstrated that S_D was consistently higher on the abaxial flag leaf surface compared to the adaxial. Furthermore, Wang *et al.* (2016) successfully mapped QTL linked to abaxial stomatal density in wheat, for these reasons only the abaxial flag leaf surface was measured in the present study. Non-invasive measurements were not taken for individuals where only 1 seed germinated across the two plots, however, leaf surface impressions were taken on secondary main tillers of these plants on the 3rd of July 2017.

A complete list of the physiological markers measured in the *PS1* field trial is shown in (Table 3-3).

Table 3-3 – The physiological markers (with acronyms included) measured in the *PS1* population. Each marker was hypothesised to be linked to the ideotype traits shown.

Physiological Marker	Acronym	Unit	Ideotype Trait
Flowering time	F_T	Sowing to Flowering	Photosynthetic duration
Flag leaf length	FL_L	cm	CO_2 demand / radiation capture
Flag leaf width	FL_W	cm	CO_2 demand / radiation capture
Flag leaf area	FL_A	cm^2	CO_2 demand / radiation capture
Awn length	A_L	cm	Ear photosynthesis
Ear length	E_L	cm	Ear size / photosynthesis
Ear area	E_{CA}	cm^2	Ear size / photosynthesis
Flag leaf longevity	FL_{LONG}	Flowering to Senescence	Photosynthetic duration
Flag leaf thickness	FL_{THICK}	mm	CO_2 demand
Specific leaf area	*SLA*	$cm^{-2}\ g^{-1}$	CO_2 supply / CO_2 demand
Leaf dry matter content	*LDMC*	$mg\ g^{-1}$	CO_2 supply / CO_2 demand
Relative water content	*RWC*	%	Water expenditure
Stomatal Density	S_D	mm^{-2}	CO_2 supply / water expenditure
Ear Number	*EN*	Ear no. $plant^{-1}$	Yield component
Grain yield per ear	*YE*	g ear^{-1}	Assimilate remobilisation/ yield component
Grain yield per plant	*YP*	g $plant^{-1}$	Assimilate remobilisation/ yield component
Harvest Index	*HI*	-	Assimilate remobilisation/ yield component

Analysis

Parent Variation

Parent physiological marker variation was analysed using a two-sample student t-tests in RStudio (V - 3.4.3). The data were checked for normality and variance using the 'shapiro.test' and the 'bartlett.test' functions in RStudio, respectively. If the data were non-normal in distribution the non-parametric 'Mann-Whitney U' test was used in place of the two-sample student t-tests and variance was checked using the 'leveneTest' function. If data were normal in distribution but the parents had unequal variance, a Welch's t-test was used.

Correlation Matrix

The correlation matrix was formed using Pearson's correlation and the package 'corrplot' (https://CRAN.R-project.org/package=corrplot) in RStudio (V - 3.4.3). Genotype and phenotype data was available for 107 individuals from the *PS1* field trial. The matrix included these lines and the averaged values for each parent (n = 8).

Heritability

Observed phenotypic variance (V_p) can be expressed as the sum of the unobserved genetic variance (V_g) and unobserved environmental variance (V_e, Visscher *et al.* 2008):

$$V_p = V_g + V_e$$

Calculations of heritability are valuable tools in crop breeding for determining the breeding value of a trait by analysing the proportion of V_p influenced by V_g (Acquaah 2012). Broad sense heritability (H^2) was calculated for each trait following Falconer (1960):

$$H^2 = V_g / V_p$$

Where V_p was the phenotypic variance of each trait across the unreplicated *PS1* individuals and V_g was calculated by subtracting V_p by V_e. The V_e was estimated from the error mean squared values from an ANOVA test for each trait using the parent replicates.

Germination Heterogeneity

Three seeds were sown for each line. However, only 53% of the seeds sown in plot 1 germinated. In both plots, these gaps were filled by sowing Paragon seed, 4 weeks after the original sowing date. For each line in plot 1, the number of seedlings that emerged after the initial sowing was recorded (1 to 3) and an ANOVA was completed in RStudio (V - 3.4.3) for each trait to test if remaining plants were influenced by the potential germination heterogeneity. The assumptions of the ANOVA tests were checked using the same methods listed in Chapter 1 and the non-parametric Kruskal-Wallis rank sum test was used where required.

3.2.3 Genotypic Methodology

DNA Extraction and Genotyping

DNA was extracted from 7 day old seedlings of F4 *PS1* individuals and parental lines following a modified Tanksley 96-well-microprep extraction method from Fulton *et al.* (1995). DNA samples were sent to Bristol University for genotyping using the Axiom Wheat Breeders' Genotyping Array, which consists of 35,000 SNPs (see: Allen *et al.* 2017).

The data returned from the genotyping needed to be clustered into the different allele classes for each of the 35,000 SNPs. Following Allen *et al.* (2017), the SNP allele calls

were made using the Affymetrix Axiom Analysis Suite software, following the 'Best Practices Genotyping Workflow' (see: Affymetrix 2011). An altered dish quality control (DQC) threshold of 0.8 was used, which was lowered by 0.02 due to the tetraploid ploidy of the material. All lines passed the DQC threshold and the average call rate was 98.6%. The software transformed the array intensities into X and Y coordinates and a clustering algorithm automatically organised the different allele classes at each SNP into either homozygote (AA or BB), heterozygote (AB) or 'no call' (if outside of the confidence threshold, see: Affymetrix 2011). 4193 'polyhigh resolution' markers were extracted for further analysis, this group were selected as they were high resolution and polymorphic at 2 minor allele classes.

Genotype Quality Control and Genetic Map Formation

To avoid false positives or errors in the genetic linkage map formation, a quality control of the SNP markers was necessary before the further analysis, which typically involves removing markers that differ from the expected segregation ratio and where too many missed calls were observed (Li *et al.* 2012). Initial quality checks were completed in Microsoft Excel, where markers that were monomorphic between the parents were removed. DNA was extracted from F4 generation leaf tissue. Therefore, the genotype heterozygosity should be roughly at a frequency of 12.5% (Xu 2010). The average heterozygosity for all the markers was 12.67%. A ChiSquare test was used in Microsoft Excel to identify markers and individuals which had heterozygosity significantly different from the expected amount ($P = < 0.05$). *P*-Values were adjusted within RStudio (V - 3.4.3) using a False Discovery Rate (FDR) adjustment. There were 322 markers that violated the expected ratios and were removed from the analysis. One individual with too many heterozygote genotypes, suggesting a contaminated or out-crossed sample, was also removed from the analysis.

Further quality control was completed using RStudio (V - 3.4.3) with the package R/QTL (V - 1.41-6) following protocol and script from Broman (2010). No individuals were identified with too many missing genotypes calls (Figure 3-4).

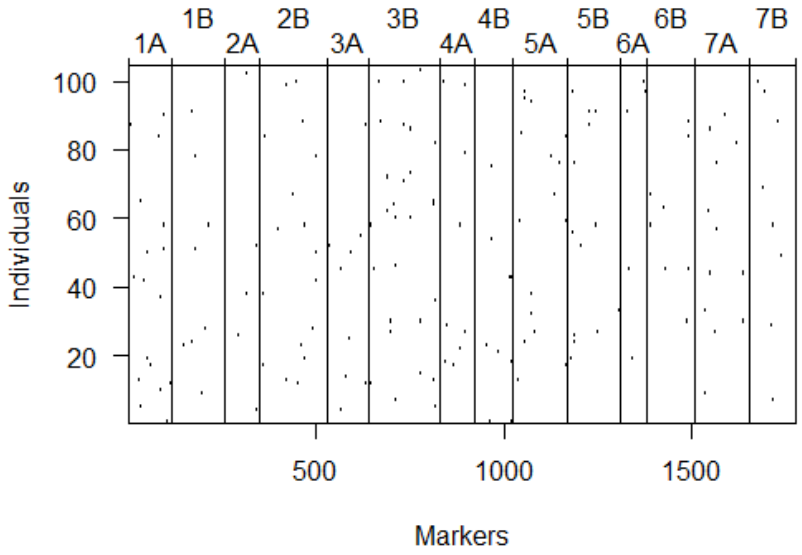

Figure 3-4 – The distribution of missing genotypes in the *PS1* population, indicated by black marks. No distinctive pattern indicated no offending markers or individuals (Broman, 2010). The horizontal straight lines separate the markers into each chromosome, which were determined after map formation.

Two pairs of individuals had over 80% matching genotype data, suggesting possible out-crossing or mixed samples at some stage of the SSD, an individual from each pair was removed from the analysis. A suitable distribution of matching genotypes was observed for the remaining individuals, on average sharing ~ 40% of markers (Figure 3-5).

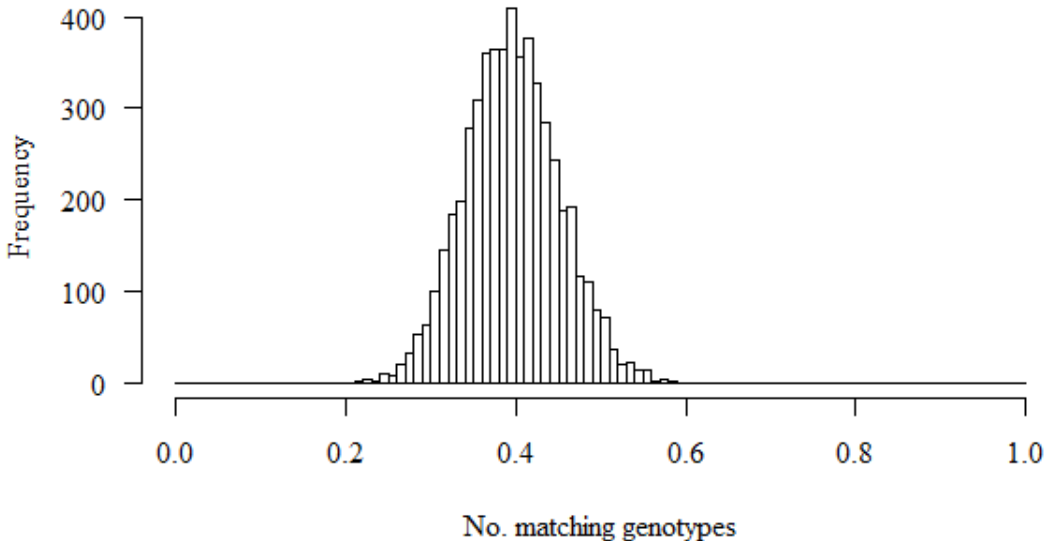

Figure 3-5 – A diagnostic plot created in R/QTL following Broman (2010) showing frequency of matching genotypes for the individuals in the *PS1* population, determined through pairwise comparisons. Two pairs of individuals were identified with higher than expected (>0.8) matching genotypes, data shown is after an individual from each pair was removed.

The R package ASMap (V - 1.0-2.0) was used for the remaining quality checks and map formation. Based on the marker data, this package implements a high-throughput algorithm for clustering linkage groups, determining marker order and genetic distances (see: Wu *et al.* 2008). After the initial steps of quality control, 3784 markers and 108 individuals remained.

Non-random segregation of alleles is termed 'segregation distortion' and can also be indicative of genotyping error (Doerge 2002). Following Taylor & Butler (2017), markers distorted from the expected Mendelian segregation ratio, were identified using the 'pullCross' function and 68 markers which showed significant segregation distortion ($P = < 0.02$) were removed. The function also removed 1908 co-located markers (markers with the same genotype). The genotype frequencies for each *PS1* individual, after the quality control was completed, is shown in Figure 3-6.

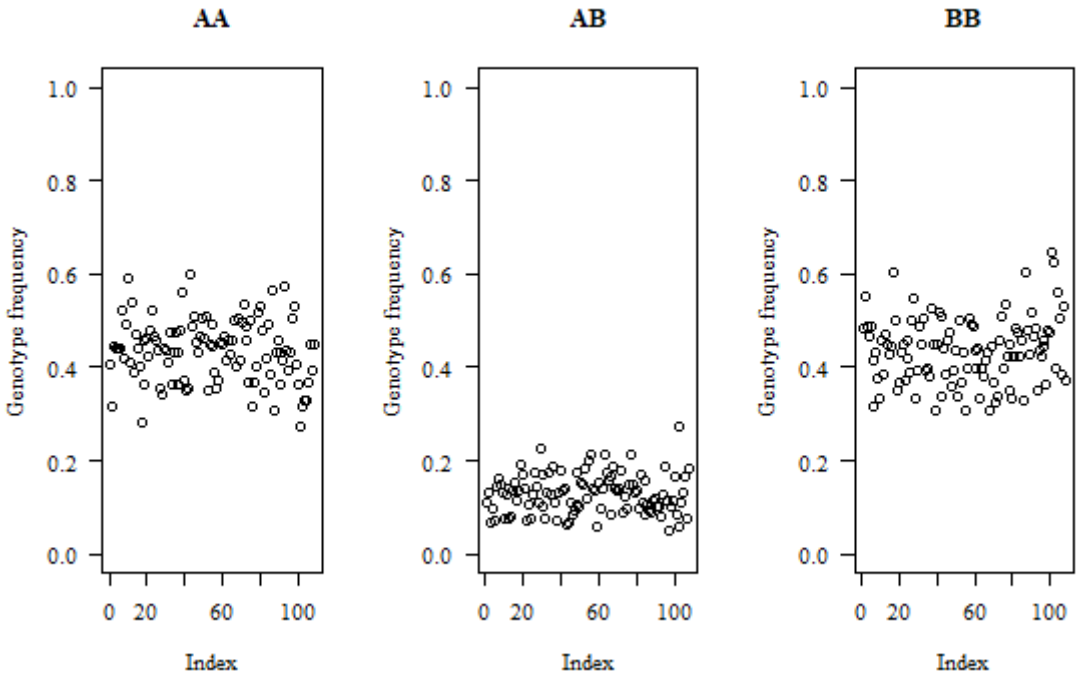

Figure 3-6 - The frequency of genotypes per mapping individual for each SNP allele class (AA, AB and BB) after applying quality control checks. 'AA' represented the homozygous allele class from Tios and 'BB' represented the homozygous allele class from dic12b. The heterozygous allele class was 'AB'. The plot was created following Broman (2010).

Meiosis crossovers are a fundamental component of genetic recombination, however, false crossovers are strong indicators of laboratory error and can increase apparent genetic distance intervals (Lincoln & Lander 1992). Individual crossover number was checked using the 'profileGen()' function. Using a one-tailed test of a Poisson mean, 4 individuals were removed with a significantly different ($P < 0.05$) crossover number than the

population mean. Using the 'mstmap' function, a numerical threshold value of P = 0.00000001 was set for linkage group clustering, which separated the markers into 18 different linkage groups. Following Broman (2010), genotype error rate was then estimated using the 'est.map()' function to obtain a maximum likelihood estimate of genotype error rate, which was identified at 2.5 / 1000 (Figure 3-7). Using the estimated genotype error rate, genotypes with the highest error logarithm-of-odds (LOD) scores (LOD > 6) were identified, where there was an apparent double crossover in intervals flanking an individual marker (Broman 2010). These errors were identified using the 'calc.errorlod()' function and marked as NA.

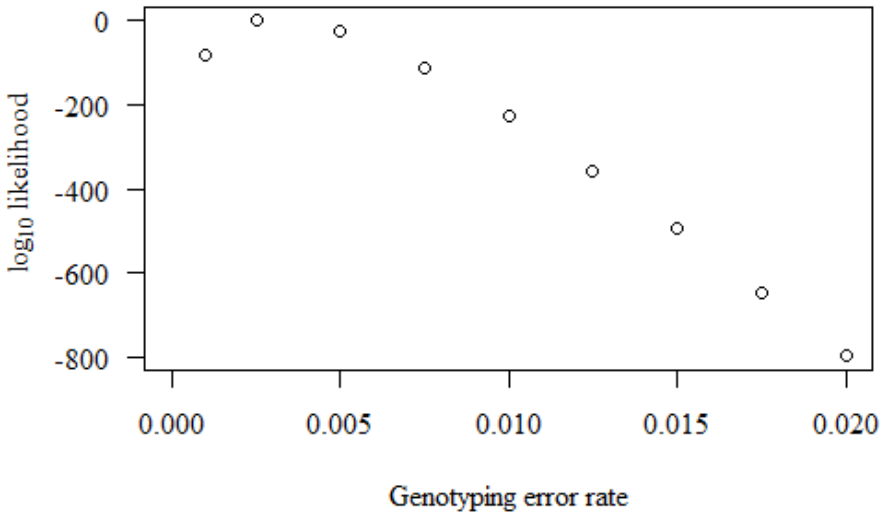

Figure 3-7 – An estimate of genotype error rate was determined following Broman (2010), maximum likelihood was used to determine the highest log_{10} likelihood for a genotyping error rate. The log_{10} likelihood for a number of genotype error rates were plotted, the highest was determined to be 0.0025.

The initially formed linkage groups were compared to the published hexaploid wheat genetic maps of Allen *et al.* (2017) and Winfield *et al.* (2016) and markers were dropped which appeared incorrectly clustered. The comparison with existing genetic maps, highlighted which linkage group corresponded to each chromosome and which smaller groups to merge. Merging was completed using the 'mergeCross' function, resulting in 14 linkage groups. Finally, heat maps were generated to ensure correct marker order (Figure 3-8) and the final maker number was 1779.

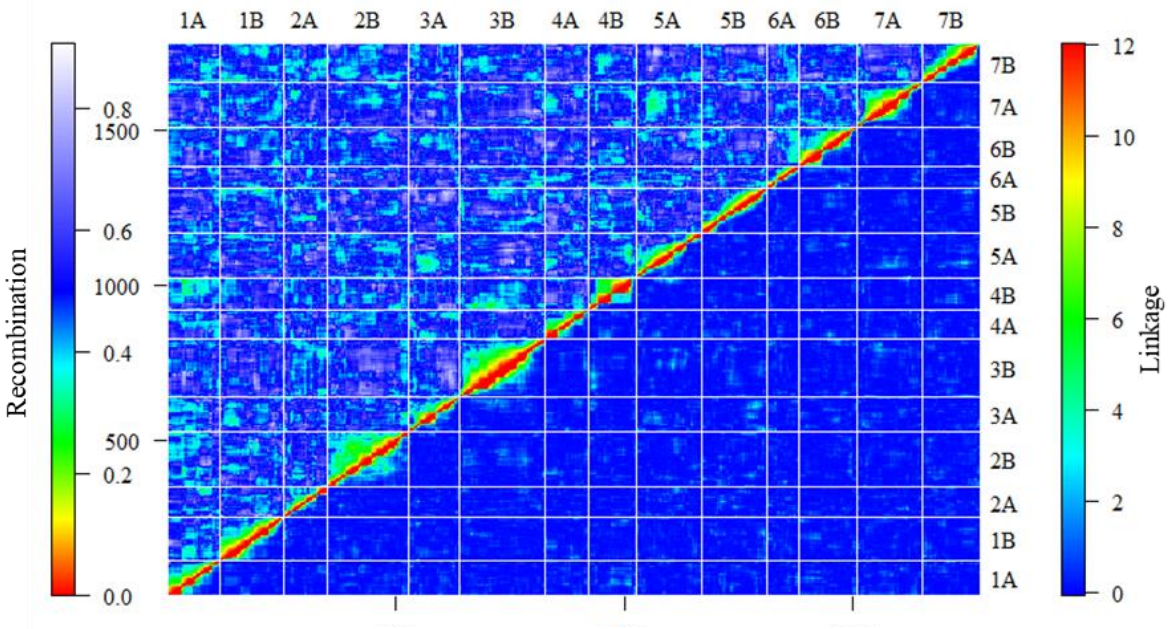

Figure 3-8 – A heat map showing the assembled *PS1* linkage map. The LOD linkage between ordered markers is plotted in the bottom corner and pairwise recombination fractions between ordered markers is shown in the upper triangle, the heat map was created following protocol from Taylor (2017). Red indicates low recombination and high linkage between markers, therefore, a red line running diagonally across the centre of the plot indicates well-ordered markers.

QTL mapping of the *PS1* Population.

QTL Detection

The *PS1* QTL mapping was completed on 107 individuals with complete genotype and phenotype data in the *PS1* field trial and 89 individuals in the *PS1* glasshouse trial, using the newly formed map consisting of 1779 markers. Following Broman and Sen (2009), QTL mapping was completed for each trait using Multiple Imputation Composite Interval Mapping in the R/QTL package (V - 1.42-8), using the 'cim' function with a window size of 10 cM and 3 markers used as covariates. The multiple imputation method simulates genotype data and missing values based on the marker data, and is a robust analysis tool (Broman & Sen 2009; Sen & Churchill 2001). Imputations were made using the 'sim.geno' function with 200 simulation replicates and maximum distance of 1 cM between where simulated genotypes were drawn.

The LOD thresholds at significance levels of 5% (0.05 Alpha) and 10% (0.1 Alpha) were determined through running multiple imputation permutations within the 'CIM' function for each trait with 5000 repeats. Permutation tests are the random assortment of phenotypic data relative to the genotype data, to determine a genome-wide maximum LOD score and significant thresholds (Broman & Sen 2009). The -1 LOD support

intervals were determined using the function ‘lodint’, with the interval expanded to the flanking markers.

QTL Validation

In an effort to reduce false positives in the QTL results, phenotypic data were separated into the three different genotype groups (AA, AB and BB) for each peak SNP marker. An ANOVA and Tukey’s HSD test were then completed to test the influence of genotype on phenotypic trait data. QTL were only accepted if a significant difference ($P < 0.05$) existed between the two homologous genotypes based on the trait data. On this basis several minor QTL hits were rejected due to significant variation only existing between one homologous genotype group and the heterozygous genotype group. Due to low heterozygosity in the population at the stage of genotyping (12.5%), the assumption was made that this variation was a product of phenotypic noise in the small sample population.

QTL Model Building

Following Broman & Sen (2009), the function ‘makeqtl’ was used to create a QTL object consisting of the QTL identified in the CIM mapping above the 10% significance threshold derived from the CIM permutations tests. The function ‘fitqtl’ was used to fit a multiple QTL model. The function ‘addint’ was used to test for potential pairwise interactions between existing QTL in the model. This model building approach was used to estimate QTL effects.

3.3 Results

3.3.1 Phenotypic Analysis Results of *PS1* Population

3.3.1.1 Parent variation, trait heritability and population distribution.

In total 10 mini-plots of each parent were sown, although only 8 for each parent germinated (4 from each plot). A comparison between the *PS1* mapping parental lines in the *PS1* field trial is shown in Table 3-4 and Table 3-5, which highlighted that there were significant statistical differences between the parent means for 11 out of the 17 physiological markers ($P = < 0.05$). The parent Tios had significantly higher mean values for the physiological markers: F_T, FL_{LONG}, FL_W, E_L, *YE*, and E_{CA}. In comparison, dic12b had significantly higher A_L, FL_{THICK}, S_D, *EN* and *HI* than the Tios parent. Two additional physiological markers were significant at a less stringent confidence level ($P = < 0.1$), where the parent Tios showed higher *RWC* and lower *SLA*. There was no significant variation ($P = > 0.1$) found between the parents for *LDMC*, FL_L, FL_A and *YP*.

Table 3-4 - Physiological marker data for the parents of the *PS1* population (Tios and dic12b), collected during the *PS1* field trial. The table shows mean values, standard deviation and two sample t-test results

	Tios		dic12b		Two Sample t-test		
Trait	*Mean*	*S.D*	*Mean*	*S.D*	*d.f*	*t*	*P*
FL_L	24.1	4	25.6	3.8	14	0.77	0.45
FL_A	36.6	10.4	29.7	7.8	14	-1.49	0.16
A_L	5.3	0.4	8.7	0.5	14	14.07	<0.01***
E_L	13.1	0.7	8.5	0.6	14	-14.38	<0.01***
E_{CA}	50.8	7.8	26.3	3	7.5^{+}	-7.84^{+}	$<0.01^{***+}$
SLA	188.3	15.6	200.8	10	14	1.91	0.08*
LDMC	259.6	19.6	252.9	22.9	14	-0.62	0.54
RWC	89.7	3.2	85.5	5.8	14	-1.82	0.09*
S_D	65.5	6.5	74.2	3.9	14	3.26	<0.01***
EN	10.3	5.4	24	2.31	14	6.65	<0.01***
YE	2.87	0.18	1.44	0.36	14	-10.05	<0.01***
YP	29.3	6.5	34.4	11	14	1.1	0.28
HI	0.4	0.05	0.64	0.1	14	6	<0.01***

Significance codes: *** P <0.01; ** P < 0.05; * P < 0.1.

Trait units: F_L, A_L, E_L = cm; FL_A = cm^2; *SLA* = cm^{-2} g^{-1}; *LDMC* = mg g^{-1}; *RWC* = %; *SD* = mm^{-2}; *EN* = number of ears per plant; *YE* = *g* ear^{-1}; *YP* = *g* $plant^{-1}$.

$^{+}$ = Welch's two-sample t-test was used due to unequal variance.

Table 3-5 - Physiological marker data for the parents of the *PS1* population (Tios and dic12b) from the *PS1* field trial where non-parametric tests were used to test for significance differences. The table shows mean values, median values, standard deviation and the Mann-Whitney U test results.

	Tios		dic12b		Tios	dic12b	Mann-Whitney U	
Trait	*Mean*	*S.D*	*Mean*	*S.D*	*Median*	*Median*	*w*	*P*
F_T	87.5	1.2	81.4	1.8	87	82	0	<0.01***
FL_W	1.9	0.2	1.4	0.2	1.885	1.36	3.5	<0.01***
FL_{LONG}	28.3	5	20.8	1.9	28.5	21.5	1.5	<0.01***
FL_{THICK}	0.26	0.02	0.29	0.02	0.255	0.292	57	<0.01***

Significance codes: *** P <0.01;

Trait units: F_T = s-f; F_W = cm; FL_{LONG} = f-s; FL_{THICK} = mm.

In comparison to the field trial, the *PS1* glasshouse trial also showed significant variation (P = < 0.05) between the parents for the trait means of F_T and FL_W and additional variation in the traits FL_A and *RWC* (Table 3-6). FL_{LONG} had inconsistent variation across the two environments: dic12b had a significantly higher score in the glasshouse (w = 250, P = 0.02), but lower in the field (Table 3-5).

Table 3-6 - Physiological marker data for the parents of the *PS1* population (Tios and dic12b) from the *PS1* glasshouse trial. a). Mean values and two-sample t-test results, where parent trait data were normally distributed. b). A table showing Mann-Whitney U test results, median and mean values, where parent trait data were non-normally distributed.

a).	Tios		dic12b		Two Sample t-test		
Trait	*Mean*	*S.D*	*Mean*	*S.D*	*d.f*	*t*	*P*
F_T	92.67	8.69	60.38	2.09	18.68^+	-15.39^+	$<0.01^{***+}$
FL_L	28.61	3.16	26.71	3.55	37	-1.745	0.09
FL_W	1.8	0.26	1.29	0.1	21.85^+	-7.91^+	$<0.01^{***+}$
FL_A	41.31	8.04	27.76	5.72	36	-6.03	<0.01***
LDMC	203.83	26.13	194.93	23.1	35	-1.1	0.28
RWC	86.81	4.15	81.63	4.89	35	-3.40	<0.01***
b).	Tios		dic12b		Tios	dic12b	Mann-Whitney U	
Trait	*Mean*	*S.D*	*Mean*	*S.D*	*Median*	*Median*	*w*	*P*
FL_{LONG}	27.83	6.24	33.68	5.72	32	34	250	0.02
SLA	249.92	46.42	267.57	42.9	247.94	251.4	203	0.29

Significance codes: *** P <0.01; ** P < 0.05; * P <0.1.

Trait units: F_T = s-f; FL_L, FL_W = cm; FL_A = cm^2; *SLA* = cm^{-2} g^{-1}; *LDMC* = mg g^{-1}; *RWC* = %; FL_{LONG} = f-s.

$^+$ = Welch's two-sample test was used due to unequal variance.

At a less stringent significance threshold (P = < 0.1) variation in FL_L was present in the glasshouse that was not observed in the field, as Tios had 7% higher mean FL_L than dic12b. As observed in the *PS1* field trial no significant variation between the parents was

found for *LDMC* (t = -1.10, P = 0.28) and unlike the field trial no significant variation was found for *SLA* (w = 203, P = 0.29).

The results of broad sense heritability (H^2) in the both trials are shown in Table 3-7. Some values are negative for the physiological markers *LDMC*, *RWC*, E_{CA} and FL_A, due to a larger V_e than V_p. In the *PS1* field trial, A_L had the highest H^2 (0.96) and the lowest was observed for *LDMC* (-0.32). Heritability was also high for *SLA*, *YE*, S_D and E_L (H^2 = 0.82, 0.74, 0.72 and 0.71, respectively). The traits FL_L and FL_W had moderately low heritability (H^2 = 0.35 and 0.19 respectively). In the *PS1* glasshouse trial, H^2 was higher for majority of traits. Only the traits FL_{LONG} (H^2 = 0.61) and SLA (H^2 = 0.30) had lower H^2 in the glasshouse.

Table 3-7 – The phenotypic variance (V_p), environmental variance (V_e) and genetic variance (V_g) used to calculate the broad sense heritability (H^2) from the phenotypic data for both the *PS1* field and glasshouse trial for each physiological marker. A '-' indicates where a physiological marker was not measured in the *PS1* glasshouse trial.

	PS1 Field Trial Heritability				*PS1* Glasshouse Trial Heritability			
Trait	V_p	V_e	V_g	H^2	V_p	V_e	V_g	H^2
F_T	7.13	2.28	4.86	0.68	180.48	37.05	143.42	0.79
FL_L	23.88	15.41	8.47	0.35	30.15	11.39	18.76	0.62
FL_W	0.05	0.04	0.01	0.19	0.06	0.04	0.03	0.43
FL_A	73.02	84.5	-11.48	-0.16	93.22	47.75	45.47	0.49
A_L	5.72	0.24	5.48	0.96	-	-	-	-
E_L	1.37	0.4	0.97	0.71	-	-	-	-
E_{CA}	25.63	32.79	-7.15	-0.28	-	-	-	-
FL_{LONG}	45.62	14.21	31.41	0.69	124.48	48.42	76.06	0.61
FL_{THICK}	0.0009	0.0004	0.0005	0.56	-	-	-	-
SLA	949.7	171.5	778.2	0.82	2824.42	1974.87	849.55	0.30
LDMC	344.65	455.56	-110.92	-0.32	553.94	597.67	-43.74	-0.08
RWC	20.16	21.94	-1.78	-0.09	32.77	21.05	11.72	0.36
S_D	103.75	28.77	74.98	0.72	-	-	-	-
EN	25.1	17.1	8	0.32	-	-	-	-
YE	0.31	0.08	0.23	0.74	-	-	-	-
YP	143.4	81.6	61.8	0.43	-	-	-	-
HI	0.016	0.006	0.010	0.60	-	-	-	-

Heritability: V_e = Environmental Variance; V_p= Phenotypic Variance; V_g = Genetic Variance.

For each physiological marker, the population means for the *PS1* individuals used in the QTL mapping from both trials are shown in Table 3-8. The population means for FL_A and FL_W were only slightly higher in the *PS1* field trial than the glasshouse trial (mean difference = 0.7 cm^2 and 0.2 cm respectively). However, FL_L was distinctly higher in the glasshouse than the field (mean difference = 2.3 cm). F_T was higher in the field (mean difference = 9 s-f), whereas FL_{LONG} was higher in the glasshouse (mean difference = 7.4 f-s). *RWC* was higher in the field (mean difference = 3.2%), in comparison, *SLA* was considerably lower in the field (mean difference = 56 cm^2 g^{-1}) corresponding to a higher *LDMC* in the field (mean difference = 63.3 mg g^{-1}). As shown by the Pearson correlation coefficients in Table 3-8, for individuals included in both trials (n = 89) there were no evidence of significant correlations between measurements of *SLA*, FL_{LONG}, *LDMC* and *RWC* across the two environments. These trends support the low H^2 observed for the majority of these traits across both trials (Table 3-7).

Table 3-8 - Means values, standard deviation and the number of individuals measured is shown for each physiological marker measured in the *PS1* glasshouse and field trial, for individuals used in the QTL mapping. Pearson correlation coefficients for trait data of individuals included in both trials are shown for each trait measured in the different environments.

Trait	*PS1* Glasshouse Trial			*PS1* Field Trial			Mean difference	Pearson correlation coefficient
	n	*Mean*	*S.D*	*n*	*Mean*	*S.D*		
F_T	87	76.6	11.7	107	*85.6*	2.7	-9	0.43^{***}
FL_L	88	25.9	5.7	107	23.6	4.9	2.3	0.27^{*}
FL_W	88	1.4	0.3	107	1.6	0.2	-0.2	0.46^{***}
FL_A	88	29.8	10.0	107	30.5	8.6	-0.7	0.22^{*}
SLA	89	262.9	49.3	89	206.9	30.8	-56	-0.08
LDMC	89	196.0	23.2	84	259.3	18.6	-63.3	-0.11
RWC	88	84.8	5.0	79	88	4.5	-3.2	0.17
A_L	-	-	-	107	6.6	2.4	-	-
E_L	-	-	-	107	10.1	2.4	-	-
E_{CA}	-	-	-	106	35.2	5.1	-	-
FL_{THICK}	-	-	-	107	0.26	0.03	-	-
FL_{LONG}	85	31.1	10.9	107	23.7	6.8	7.4	-0.08
S_D	-	-	-	105	67.9	10.2	-	-
EN	-	-	-	107	13.8	5.0	-	-
HI	-	-	-	100	0.47	0.13	-	-
YE	-	-	-	103	1.7	0.6	-	-
YP	-	-	-	103	23.4	12	-	-

Trait units: F_T = s-f; FL_L, FL_W, A_L, E_L = cm; FL_A, E_{CA} = cm^2; FL_{LONG} = f-s; FL_{THICK} = mm; *SLA* = cm^{-2} g^{-1}; *LDMC* = mg g^{-1}; *RWC* = %; S_D = mm^{-2}; *EN* = ears per plant; *YE* = g ear^{-1}; *YP* = g $plant^{-1}$.
Pearson correlation coefficient significance thresholds: * = $P < 0.05$; ** = $P < 0.01$; *** = $P < 0.05$.

For the *PS1* field trial, the population phenotypic frequencies for each physiological marker are plotted in Figure 3-9, also shown are graphical representations of the parent variation. Statistical analysis of the parent variation is shown in Table 3-4 and Table 3-5. The physiological markers F_T, FL_L, FL_W, A_L, E_L, E_{CA}, *RWC* and S_D were normal in distribution (Shapiro-Wilk normality test: $P = > 0.05$), which is evident in the frequency distributions (Figure 3-9). Excluding FL_L, these were physiological markers with significant variation between the parents (Figure 3-9). The traits FL_A, FL_{THICK}, *SLA* and *LDMC* showed right-skewed distributions (normality test: $P = < 0.05$). In these cases, there were outliers present with values considerably higher than the population mean. Excluding FL_{THICK}, these were traits where there was little evidence of variation between the parents. Out of the yield component traits, *EN* and *YP* showed a non-normal right skewed distribution (normality test: $P = < 0.01$), in comparison *HI* and *YE* were normal in distribution (normality test: $P = > 0.05$). The phenotypic distribution of FL_{LONG} in the population appeared bimodal (normality test: $P = < 0.01$), where a subgroup of individuals senesced early compared to the rest of the population. There was an outlier also present in each of the parents (Figure 3-9).

For the physiological markers F_T, FL_W, A_L, FL_{LONG}, FL_{THICK}, S_D, *RWC*, *HI*, *EN* and *YE*, there were *PS1* individuals outside of the range of the parental means (Figure 3-9), thus indicating transgressive segregation. Some physiological markers showed wide transgressive segregation in the progeny, but little variation between the parents (FL_L, FL_A, *LDMC* and *YP*). As there was weak evidence for significant parental variation for these traits (Table 3-4 and Table 3-5), the measurements that fell outside of the parental mean range may have been influenced by variance associated with the environment or error. Furthermore, the H^2 for these traits was low (Table 3-7). For the physiological markers E_L and E_{CA}, there was only transgressive segregation outside of the range of dic12b; no individual had a higher E_L and E_{CA} than the mean for Tios (Figure 3-9).

For the *PS1* glasshouse trial, the distribution for the physiological markers FL_L *and* FL_W were normal in distribution ($P = > 0.05$). As in the field trial, the traits FL_A and *SLA* showed right-skewed distributions and the trait *RWC* had a left-skewed distribution (normality test: $P = < 0.05$). In these cases, there were outliers present considerably higher or lower than the population means, which influenced the distribution. The phenotype frequencies of *LDMC* and FL_{LONG} were not normal in distribution (normality test: $P = <$ 0.05) and were influenced by outliers either side of the population mean.

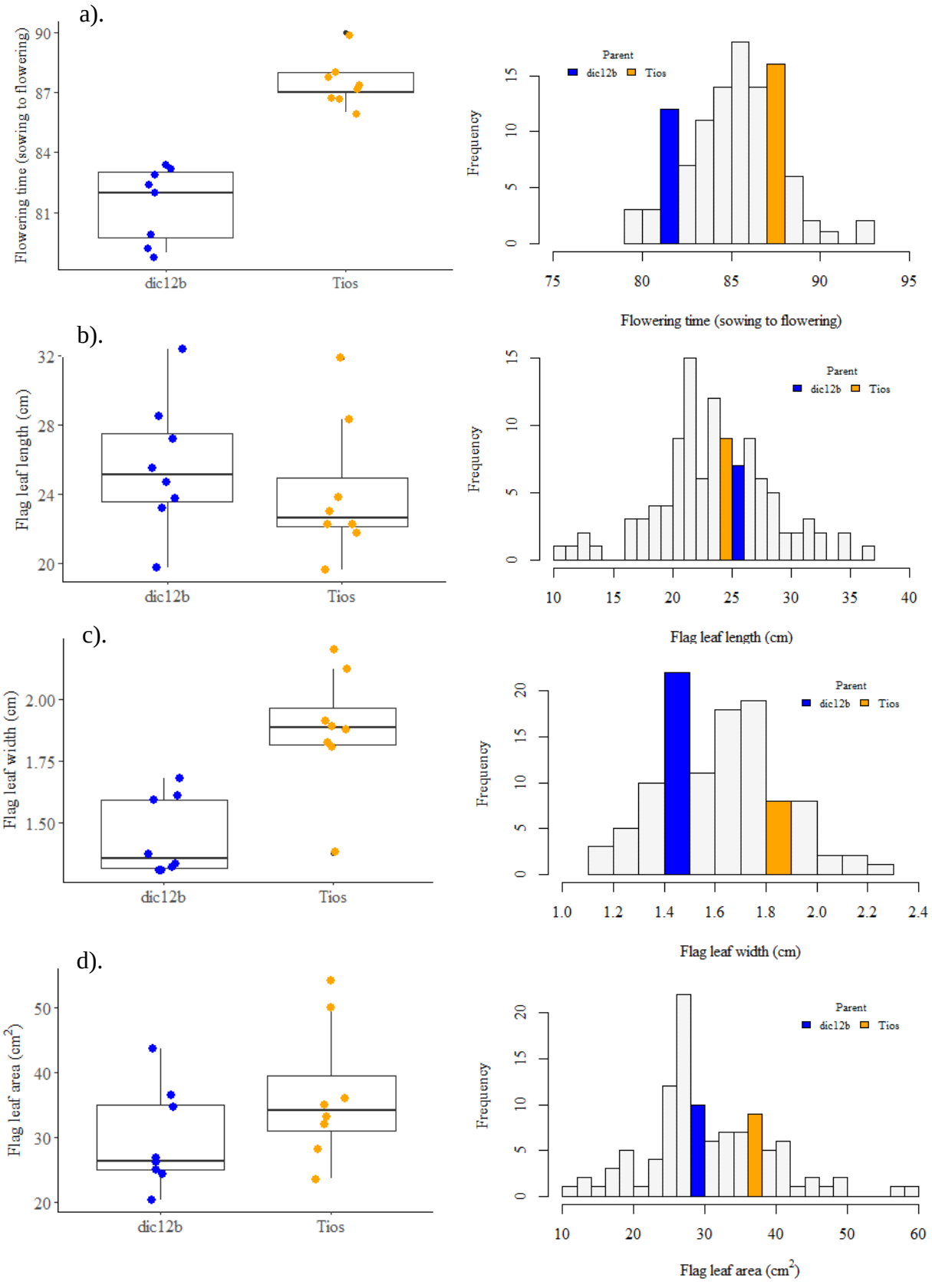

Figure continued on next page.

e).

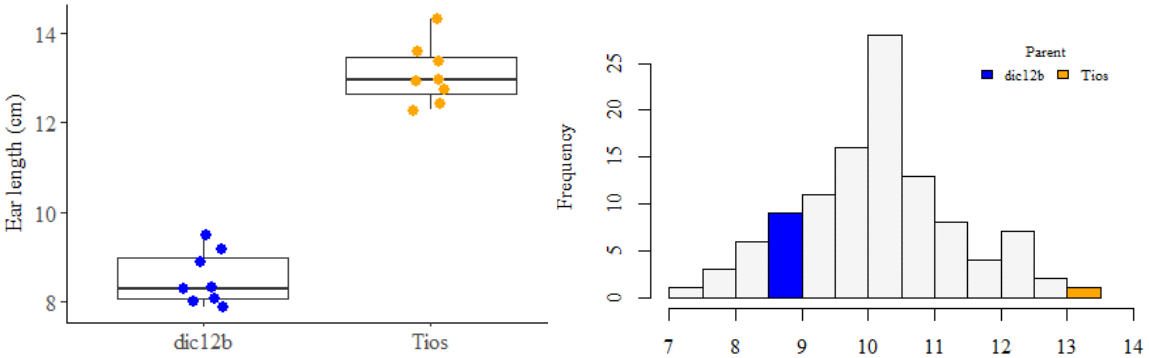

f).

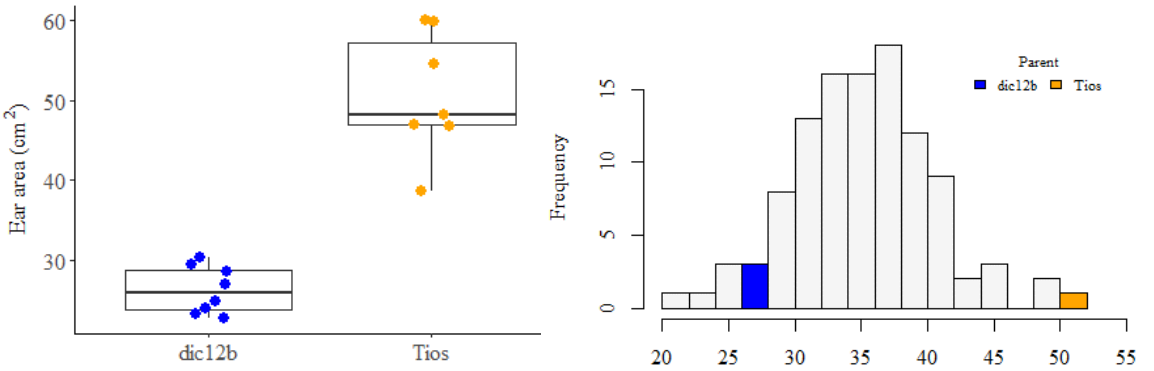

g).

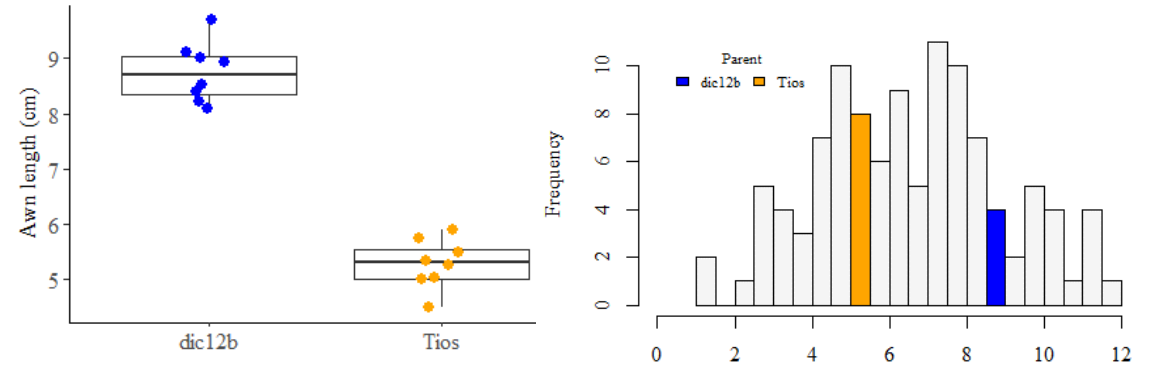

h).

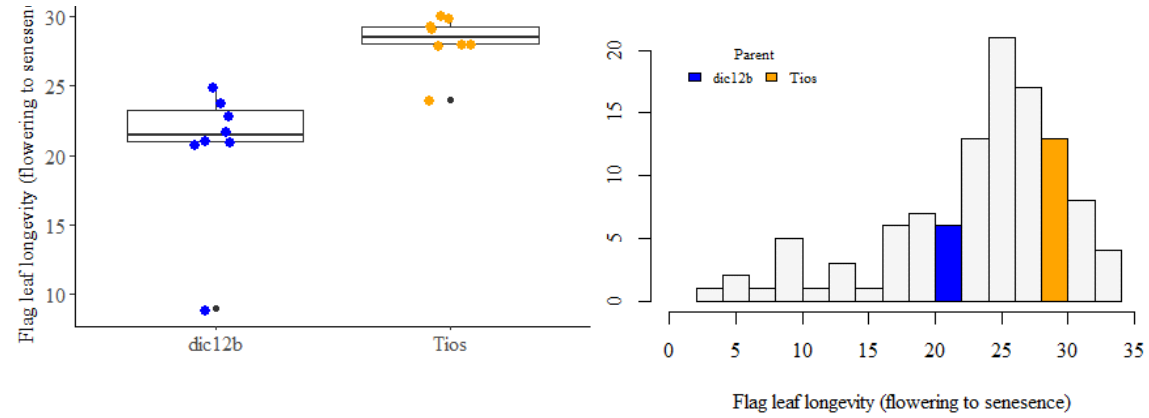

Figure continued on next page.

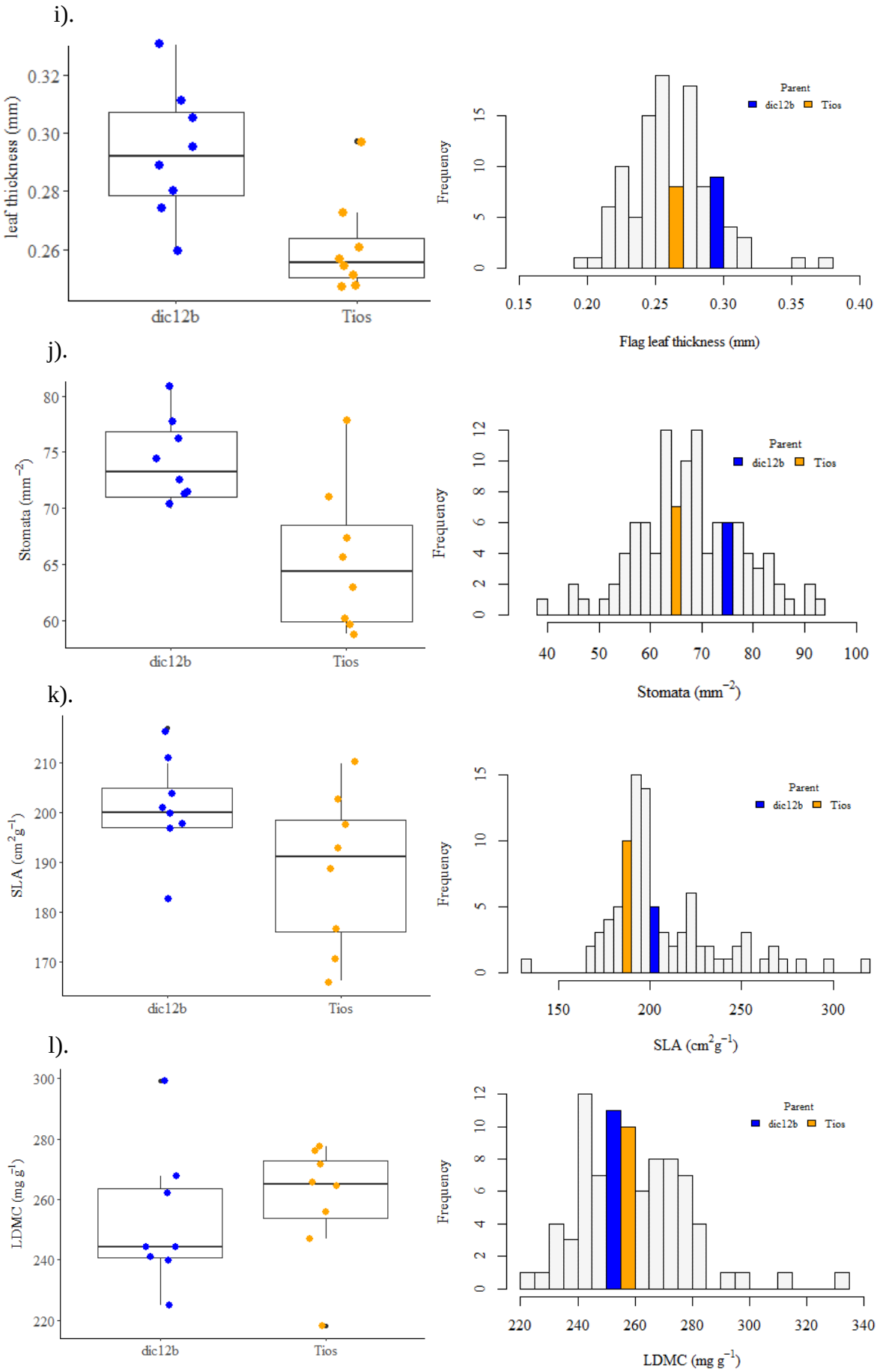

Figure continued on next page.

m).

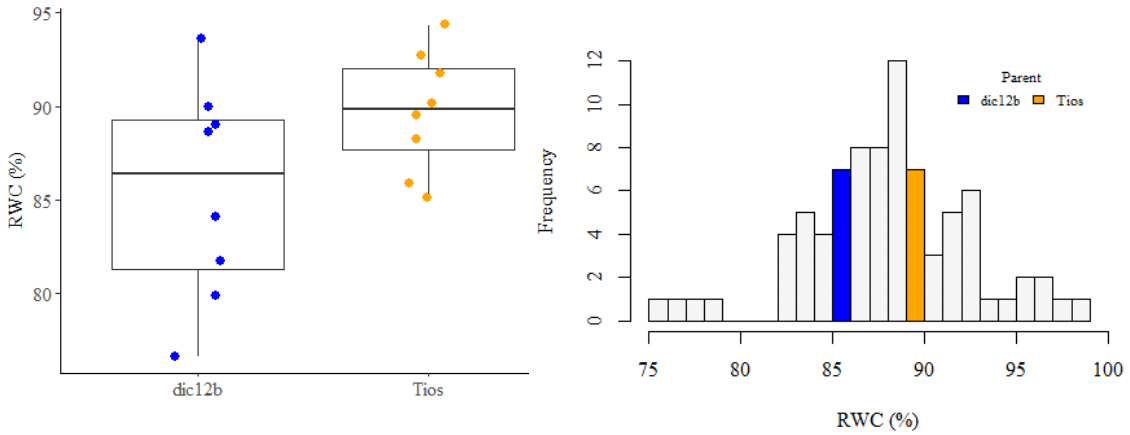

n).

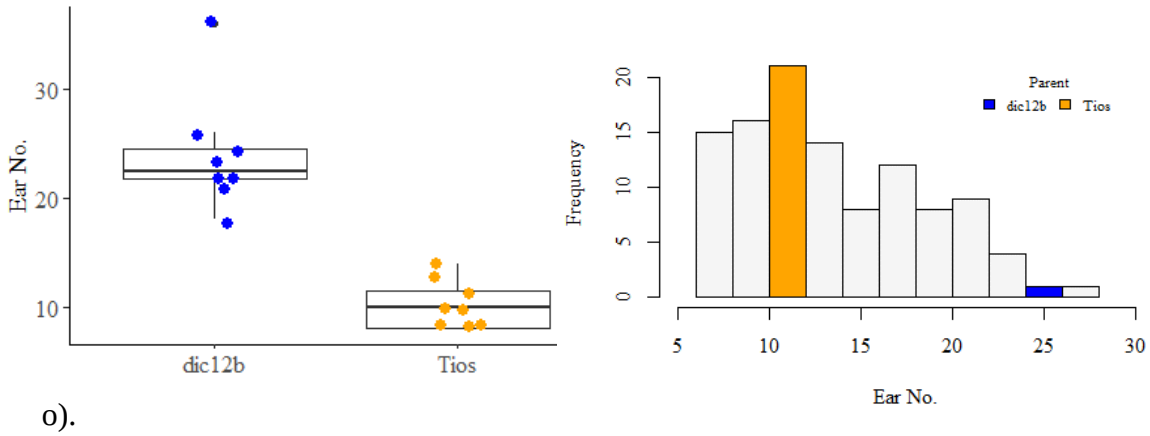

o).

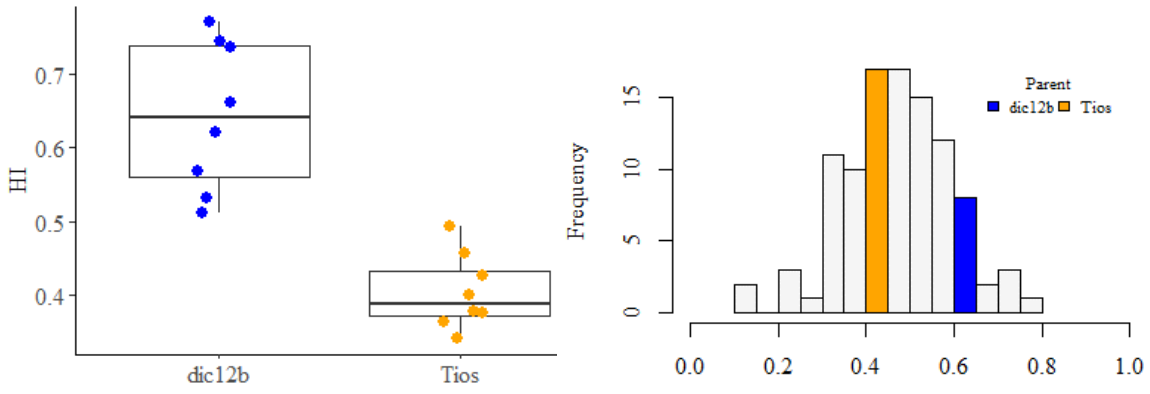

p).

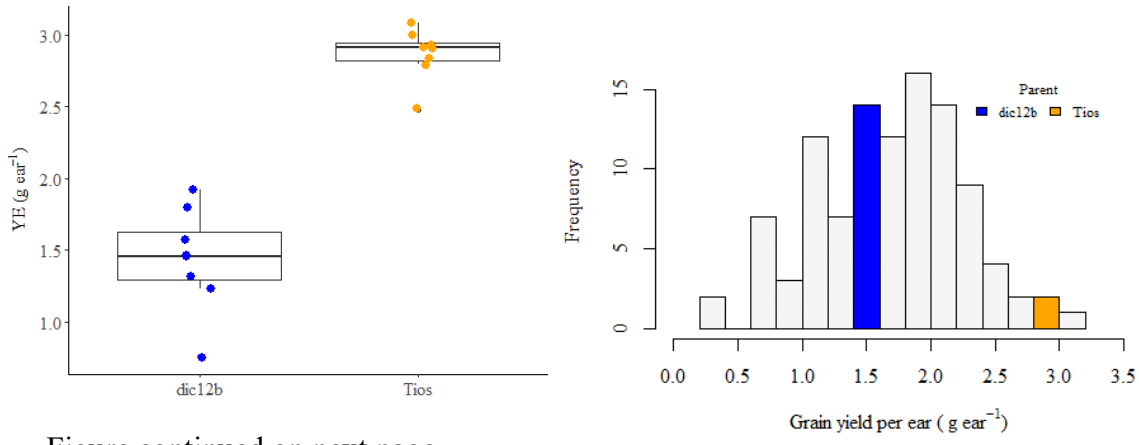

Figure continued on next page.

q).

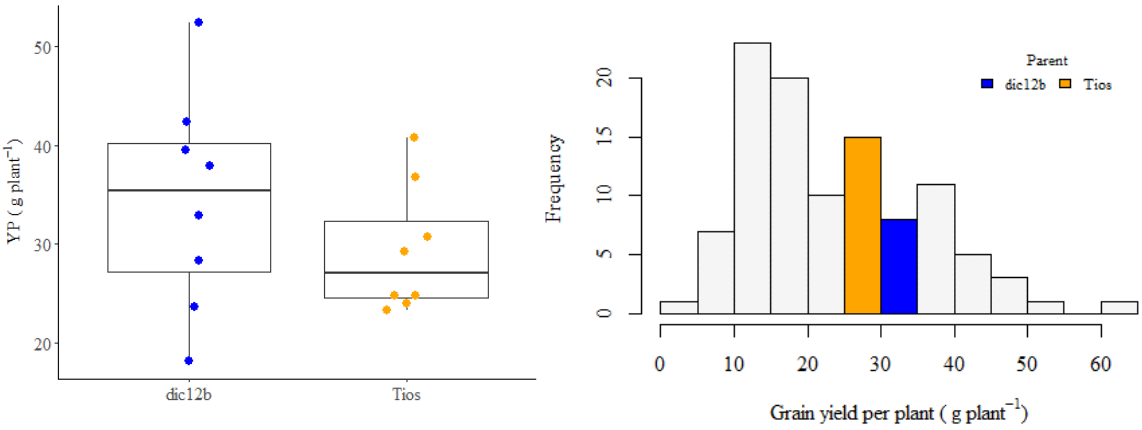

Figure 3-9 – Two graphs are shown for each of the 17 physiological markers recorded in the *PS1* field trial: a) = F_T; b) = FL_L; c) = FL_W; d) = FL_A; e) = E_L; f) = E_{CA}; g) = A_L; h) = FL_{LONG}; i) = FL_{THICK}; j) = S_D; k) = *SLA*; l) = *LDMC*; m) = *RWC*; n) = *Ear No.*; o) = *HI*; p) = *YP*; q) = *YE*. The left-hand graphs show boxplots for the parental lines in the *PS1* field trial for each of the 17 physiological markers, raw data points are overlaid on each boxplot in blue for dic12b and orange for Tios. The median is shown within each boxplot, the lower hinge and upper hinge represent the first and third quartile, respectively. The right-hand graphs show phenotypic frequencies for the 107 individuals of the *PS1* population in the *PS1* field trial for each physiological marker measured. The coloured bins in each of the histograms represent which bin contained the parent mean values (blue for dic12b and orange for Tios).

3.3.1.2 Physiological Marker Correlation.

Correlations between different physiological markers are shown in Figure 3-10 for the *PS1* field trial. As would be expected, *EN* and *HI* were positively correlated with *YP* (Pearson's correlation (*r*) = 0.68 *P* = < 0.001 and *r* = 0.61 *P* = < 0.001, respectively) and a positive correlation was found between *YE* and *YP* (*r* = 0.68 *P* = <0.001). The traits A_L, E_L, E_{CA} and FL_{THICK} were all significantly positively correlated to *YP* (Figure 3-10), whilst only A_L and E_L were correlated with *EN* (*r* = 0.22 *P* = 0.02 and *r* = 0.22 *P* = 0.02, respectively). *YE* was positively correlated with E_L, E_{CA}, FL_{LONG}, and FL_{THICK} (Figure 3-10). No physiological marker was negatively correlated with *YP* or *YE*. However, E_{CA} and FL_W were negatively correlated with *HI*, whilst FL_{LONG} was negatively correlated with *EN* (Figure 3-10).

There were a number of correlations between the traits not directly linked to yield (Figure 3-10), for instance F_T was negatively correlated FL_L and FL_A, but positively correlated with FL_{LONG} (*r* = 0.28 *P* = 0.003) and *SLA* (*r* = 0.28 *P* = 0.007). The trait FL_W was negatively associated with A_L (*r* = -0.21 *P* = 0.03) but positivity correlated with E_L (*r* = 0.32 *P* = 0.001) and E_{CA} (*r* = 0.48 *P* = <0.001), which are characteristics of the Tios parent (Table 3-4). The trait FL_W was also positively associated with FL_{THICK} (*r* = 0.35 *P* = <

0.001). The physiological marker *RWC* was the only physiological marker with no significant relationship to any other trait.

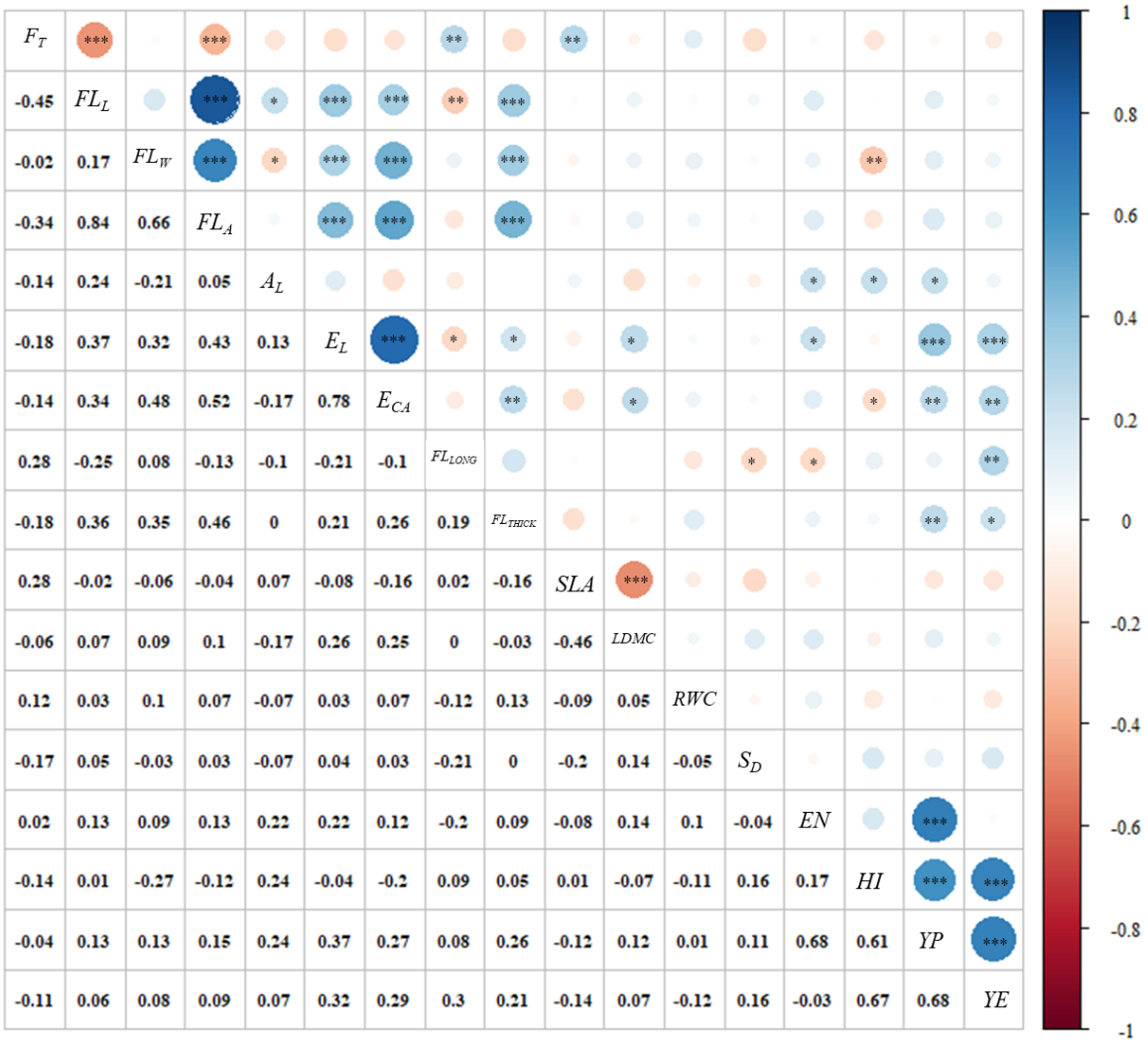

Figure 3-10 – Pearson correlation matrix for the 17 physiological markers measured in the *PS1* field trial. The matrix includes data from the 107 measured *PS1* population individuals and parents (mean values were used for each parent). A list of the acronym meaning for each physiological marker is shown in Table 3-3. The upper right-hand triangle shows a colour heat map of pairwise correlation coefficients and significance thresholds (* *P* < 0.001; ** *P* < 0.01; * *P* < 0.05). The bottom left-hand triangle shows the values of Pearson's correlation coefficients for each paired comparison.**

3.3.1.3 Environment Effect in the *PS1* Field Trial

Germination Heterogeneity

There was strong evidence the trait F_T was influenced by the germination heterogeneity (ANOVA: F = 9.8, P = < 0.01) and weaker evidence that *YE* was influenced (F = 3.2, P = 0.04). There was little evidence to suggest any other traits were influenced by the germination heterogeneity (P = > 0.05). For F_T and *YE*, adjustments for bias were completed using linear regression. The trait data were regressed on the germination scores

and residuals extracted from the model. The residuals were then used as the adjusted trait data for the QTL mapping.

Plot Variation

The parent data were used to test potential variation associated with plot number. A two-way ANOVA was completed for each trait using parent line and plot number as independent variables. There was little evidence to suggest plot number had a significant influence on each of the traits (P = > 0.05). Furthermore, no significant interaction was found between parental line and plot number (P = > 0.05).

3.3.2 Genetic Analysis Results of the *PS1* Population

PS1 Genetic Map

The *PS1* genetic map consisted of 1779 markers along 14 chromosomes, formed from 104 individuals (Figure 3-11).

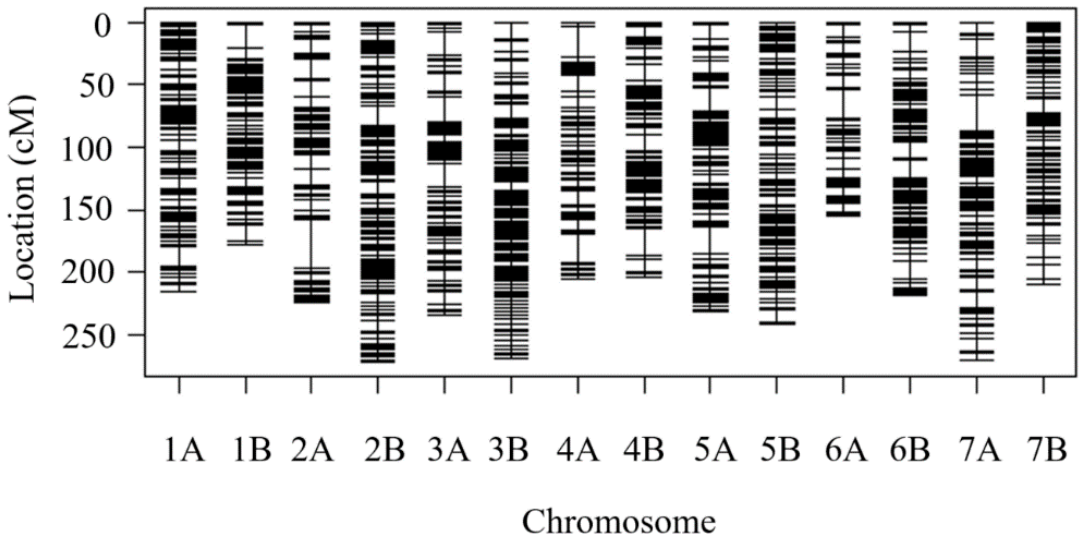

Figure 3-11 - The genetic map created for the *PS1* population showing marker spacing across 14 chromosomes, formed using the packages ASMap and R/QTL in RStudio (V - 3.4.3). The map was created using 1779 SNP markers and 104 individuals. The horizontal line on each chromosome represents the mapped position for each SNP.

The total map length spanned 3126.4 cM with an average spacing of 1.8 cM with the largest spacing of 39.2 cM found on chromosome 2A (Figure 3-11). Chromosome length varied from 154.4 cM (6A) to 271.9 cM (2B, Table 3-9). The lowest frequency of markers was found on the chromosomes 6A and 4A (70 and 95 respectively) and the highest on 3B and 2B (188 and 178 respectively). The lowest density of markers was found on chromosome 2A with an average spacing of 2.3 cM and the highest density on

chromosome 1B with an average spacing of 1.3 cM. In total the B genome had a higher coverage of markers than the A genome with 1006 associated markers across an average spacing of 1.6 cM compared to 773 markers with an average spacing of 2.0 cM.

Table 3-9 – A summary table of the marker distribution across each chromosome in the *PS1* genetic map. The map was formed using the packages ASMap and R/QTL in RStudio (V - 3.4.3). The new map had a total length of 3126.4 cM and was formed using 1779 SNP markers.

Chromosome	Number of Markers	Length (cM)	Average Spacing (cM)	Max Spacing (cM)
1A	113	215.6	1.9	14.9
1B	140	178.4	1.3	19.9
2A	97	224	2.3	39.5
2B	178	271.9	1.5	14.7
3A	111	234.9	2.1	21.2
3B	188	268.4	1.4	12.6
4A	95	204.7	2.2	24.1
4B	103	203.3	2	21.1
5A	143	231.6	1.6	20.7
5B	144	241	1.7	10
6A	70	154.4	2.2	24.2
6B	127	218.6	1.7	15.8
7A	144	270.4	1.9	29.3
7B	126	209.1	1.7	12.3
Total	**1779**	**3126.4**	**1.8**	**39.5**

QTL Mapping

In the *PS1* field trial, 9 candidate QTL were identified for a range of physiological markers across 5 chromosomes (2B, 4A, 5B, 6A and 7B), results are shown in Table 3-10. The percentage phenotypic variation explained by each QTL ranged from 11.7% (A_L, *Q2*) to 33.8% (A_L, *Q3*) and LOD scores ranged from 5.48 (FL_W, *Q1*) to 13.85 (A_L, *Q3*). The second highest LOD score was observed for a QTL mapped for F_T (LOD = 10.1, *Q9*). The -1 LOD support intervals, expanded to the nearest flanking marker, ranged from 3.2 cM for *Q5* (*HI*) to 29.1 cM for *Q7* (S_D). The additive effect for each QTL, shown in Table 3-10, indicated the effect of one dic12b allele (0.5 of BB) to the trait data. There was a positive additive effect of a dic12b allele at the QTL: *Q2* (A_L), *Q3* (A_L), *Q4* (*EN*), *Q6* (FL_W) and *Q7* (S_D). Whereas, there was a negative additive effect of a dic12b allele at the QTL: *Q1* (FL_W), *Q5* (*HI*), Q8 (FL_L) and *Q9* (F_T).

In the *PS1* glasshouse trial, 2 different candidate QTL were identified for FL_L and *LDMC* contributing phenotypic variance of 11.8 and 13.8% and had LOD scores of 6.8 and 8.5,

respectively (Table 3-10). There was a positive additive effect of a dic12b allele at *Q10* (FL_L) and negative at *Q11* (FL_W). For the traits replicated over both trials, no QTL were consistent over the different environments.

Table 3-10 – QTL results from the Composite Interval Mapping (CIM) completed in R/QTL for the *PS1* population from both trials. The interval shown for each QTL is the -1 LOD surpport interval expanded to the flanking markers. Using the R/QTL function 'fitqtl', percentage phenotypic varation explained by QTL (% variation) and additive effects were calculated using multiple model fitting with the QTL identified through the CIM analysis. LOD thresholds are shown at the significance levels of 5% Alpha and 10% Alpha, these were determined through running 5000 permutations within the R/QTL 'CIM' function

QTL	Trait	Chromosome	Map Position (cM)	Closest SNP	LOD	Interval (cM)	Flanking Markers	% variation	Additive*	5% Alpha	10% Alpha	Permutations
PS1 field trial												
Q1	FL_W	2B	146	AX-94583923	5.48	140.4 – 153.6	AX-94443773-AX-94388449	15.1	-0.09	6.04	5.45	5000
Q2	A_L	2B	185	AX-94641030	6.02	173.0 – 189.3	AX-94609519-AX-94769600	11.7	0.89	6.12	5.57	5000
Q3	A_L	4A	34.8	AX-94464899	13.85	33.1– 36.5	AX-94437374-AX-94389361	33.8	1.56	6.12	5.57	5000
Q4	*EN*	4A	96.1	AX-95156879	5.75	91.4 – 103.6	AX-94583235-AX-95084338	14.2	1.38	6.02	5.53	5000
Q5	*HI*	5B	0.0	AX-94836422	5.79	0.0 – 3.2	AX-94836422-AX-94664659	19.2	-0.05	6.17	5.67	5000
Q6	FL_W	5B	203.6	AX-94402018	6.87	200.2 – 206.5	AX-94535421-AX-95105488	18.9	0.04	6.04	5.45	5000
Q7	S_D	6A	79	AX-95149371	6.43	53.2 – 82.3	AX-94961629-AX-94487644	14.5	3.77	6.09	5.54	5000
Q8	FL_L	6A	93	AX-95105228	5.88	89.8 – 99.8	AX-94416968-AX-95111333	17.5	-1.67	6.04	5.55	5000
Q9	F_T	7B	196	AX-94622790	10.10	187.4 – 204.9	AX-94978456-AX-94742020	25.6	-1.40	6.09	5.55	5000
PS1 glasshouse trial												
Q10	FL_L	4A	166.1	AX-95146535	6.84	158.4 – 169.0	AX-95195078-AX-94482431	11.77	1.91	6.43	5.89	5000
Q11	LDMC	6A	142.5	AX-95140962	8.5	141.4 – 151.3	AX-94557166-AX-94407050	13.82428	-9.182	6.58	5.98	5000

*Additive: Additive effect of 0.5 BB genotype (dic12b parent). Trait units: F_T = Days from sowing to flowering (residuals from adjustment shown); FL_L, FL_W, A_L = cm; *SD* = mm^{-2}; *LDMC* = $mg\ g^{-1}$; *EN* = Ear Number.

PS1 Field Trial

Two QTL were identified for A_L (Figure 3-12), the most significant explained 34.0% of phenotypic variation and was located at 35 cM on chromosome 4A (LOD = 13.85). The closest marker to the QTL was AX-94464899, where individuals with the Tios genotype (AA) had a mean A_L of 4.8 ± 0.3 cm, individuals carrying the dic12b genotype (BB) had a mean A_L of 7.9 ± 0.3 cm and heterozygous individuals (AB) had a mean of 6.7 ± 0.4 cm. The second A_L QTL had a lower LOD score (6.02) and was located at 185 cM on chromosome 2B, the QTL only passed the 10% LOD confidence threshold. No significant interactions were found between the two QTL. The QTL with the second highest LOD score in the study, was identified for F_T (Figure 3-12). It explained 25.6% of phenotypic variation (LOD = 10.1) and was located at 196 cM on chromosome 7B. The closest marker was AX-94622790, where the individuals had a mean F_T of 87.3 ± 0.4 s-f if AA genotype, 84.4 ± 0.3 s-f if BB and 85.1 ± 0.6 s-f if AB (taken from unadjusted data).

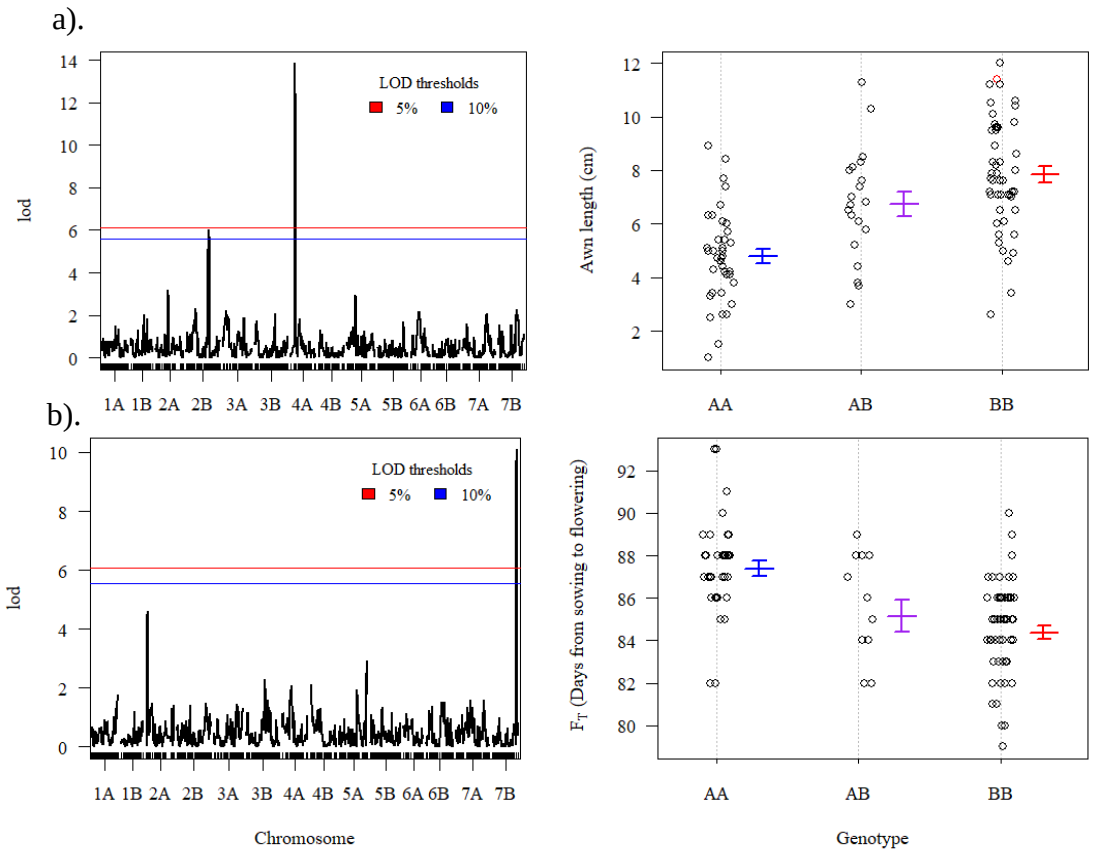

Figure 3-12 – QTL results from the *PS1* field trial for A_L (a) and F_T (b). The left-hand graphs show the LOD scores from the Composite Interval Mapping across all 14 chromosomes. The right-hand graphs show the phenotypes of each allele class (Tios = AA, heterozygote = AB and dic12b = BB) at the peak marker for each trait (a = AX-94464899 and b = AX-94622790), the bars represent phenotypic means and +/- 1 standard error. Points highlighted in red represent imputed genotypes.

One QTL was identified for FL_L that only passed the 10% confidence threshold, the QTL was located on chromosome 6A at 93 cM (LOD = 5.88) which explained 17.5% of phenotypic variation in the population (Figure 3-13). The closest marker to the QTL was AX-95105228, where individuals had a mean FL_L of 25.8 ± 0.7 cm if AA in genotype, 22.5 ± 0.6 cm if BB and 20.0 ± 1.2 cm if AB. Two QTL were found for FL_W, one on chromosome 5B (203.6 cM, LOD = 6.87), which explained 19% of phenotypic variation, and one on 2B (146 cM, LOD = 5.48) which explained 15% (Figure 3-12). The QTL on 2B passed the 10% confidence threshold, but not the 5% threshold. The closest marker to the 5B QTL was AX-94402018, where individuals had a mean FL_W of 1.53 ± 0.03 cm if AA in genotype, 1.65 ± 0.03 cm if BB and 1.81 ± 0.06 cm if AB. The closest marker to the 2B QTL was AX-94583923, where individuals had a mean FL_W of 1.7 ± 0.03 cm if AA in genotype, BB 1.54 ± 0.03 cm if BB and 1.58 ± 0.05 cm if AB. No significant interaction was found between the two QTL.

a).

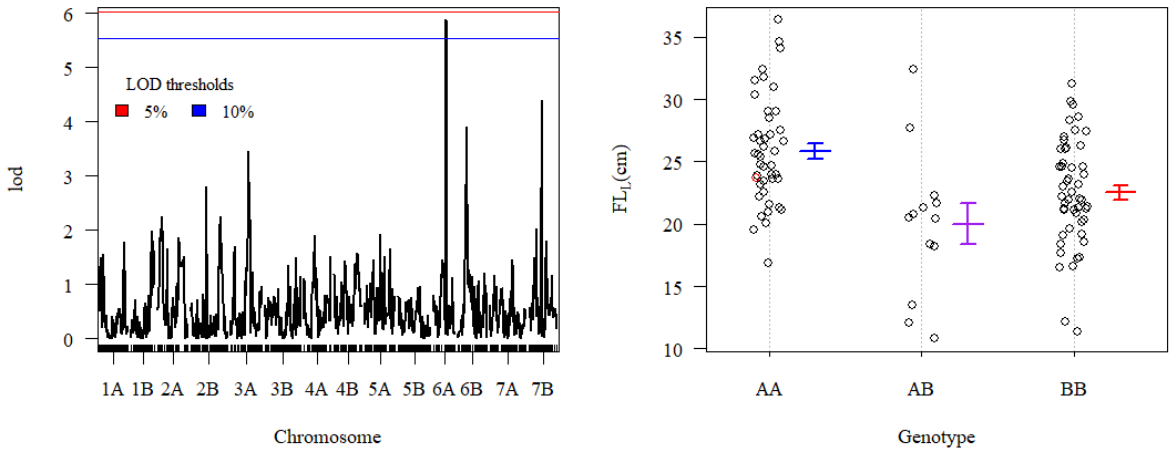

Figure continued on next page.

b).

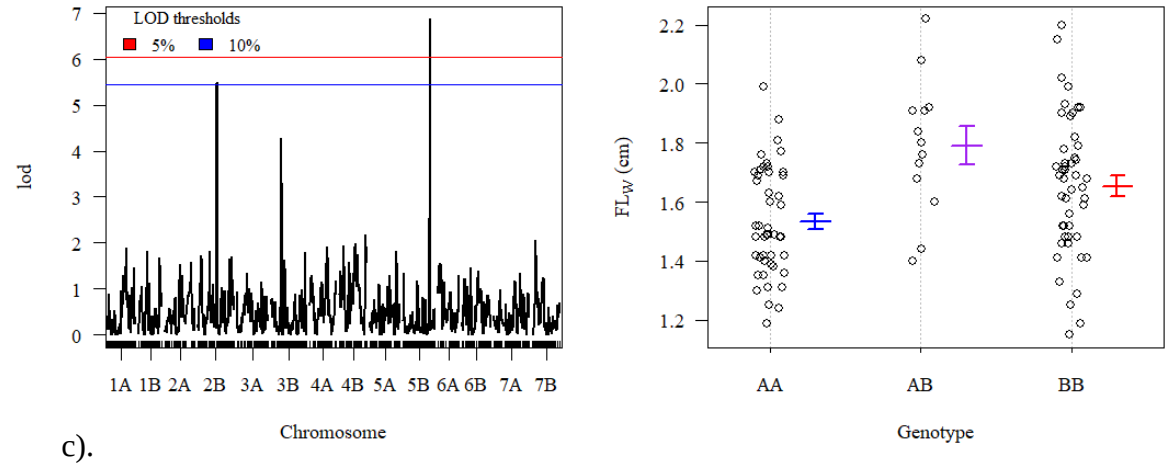

c).

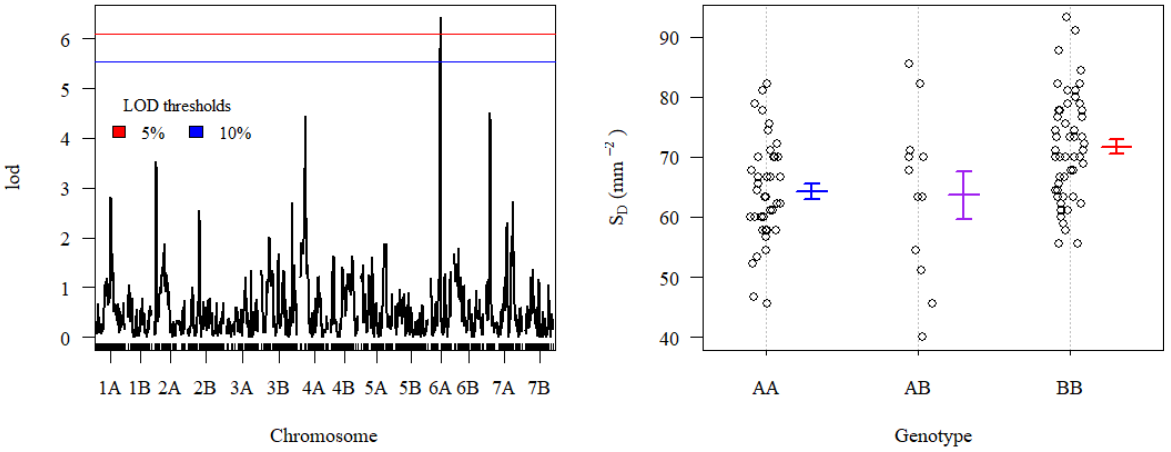

Figure 3-13 – The QTL results from the *PS1* field trial for flag leaf length (a), width (b) and stomatal density (c). The left-hand graphs show the LOD scores from the Composite Interval Mapping across all 14 chromosomes. The right-hand graphs show the phenotypes of each genotype (Tios = AA, heterozygote = AB and dic12b = BB) at the peak marker for each trait (a = AX-95105228, b = AX-94402018 and c = AX-95149371) the bars represent phenotypic means and +/- 1 standard error. Points highlighted in red are imputed genotypes.

One QTL was mapped for S_D to 79 cM on chromosome 6A (LOD = 6.43), which explained 14.5% phenotypic variation (Figure 3-13). The closest marker was AX-95149371, where individuals had a mean S_D of 64.3 ± 1.5 mm^{-2} if AA in genotype, 71.7 ± 1.3 if BB mm^{-2} and 63.7 ± 2.7 if AB mm^{-2}. For the yield related traits, QTL were identified for *EN* and *HI* that only passed the 10% confidence threshold. The QTL for *EN* was mapped to 96.1 cM on chromosome 4A (LOD = 5.75), which explained 14% phenotypic variation (Figure 3-14). The closest marker was AX-95156879, where individuals had a mean ear number of 11.9 ± 0.7 if AA in genotype, 14.7 ± 0.7 if BB and 16.9 ± 1.1 if AB. The QTL for *HI* was mapped to 0.0 cM on chromosome 5B (LOD = 5.8) and explained 19% phenotypic variation (Figure 3-14). The closest marker was AX-

94836422, where individuals had a mean *HI* of 0.52 ± 0.02 if AA in genotype, 0.41 ± 0.02 if BB and 0.38 ± 0.04 if AB. To determine whether the QTL found for *HI* was associated with variation in *YP* or biomass, the phenotype data for two traits were separated into the different allele classes (AA, AB and BB) at the AX-94836422 marker and a Kruskal-Wallis rank sum test was used in RStudio (V - 3.4.3) to test for variation between the two homologous allele groups (AA and BB). Significant variation was found between the allele classes for *YP* (*KW* = 8.4, *df* = 1, *P* = < 0.001) but not biomass (*KW* = 0.74, *df* = 1, *P* = 0.39).

There were QTL mapped for FL_{LONG}, *LDMC* and *SLA* (1B, 6A and 7A respectively). However, ANOVA and Tukey's HSD tests revealed that the AB group contributed to phenotypic variation between the genotypes, suggesting these QTL were false hits and artefacts of noise in the small AB sample size (12.5% of the population).

a).

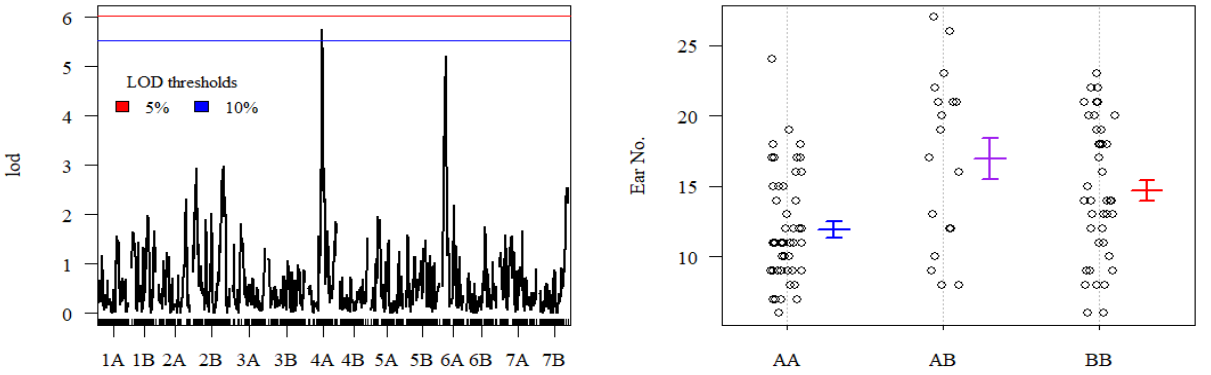

b).

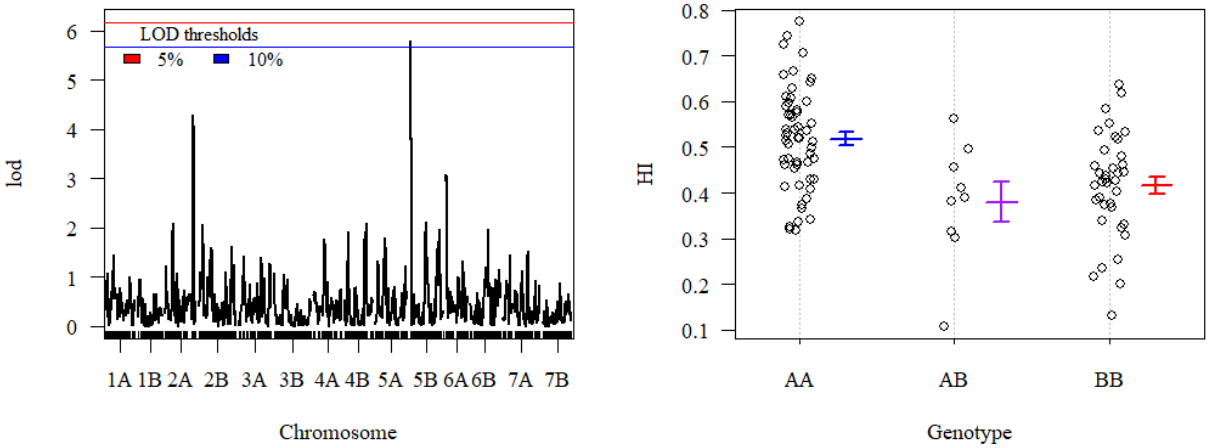

Figure 3-14 - The QTL results from the *PS1* field trial for ear number (a) and harvest index (b). The left-hand graphs show the LOD scores from the Composite Interval Mapping across all 14 chromosomes. The right-hand graphs show the phenotypes of each genotype (Tios = AA, heterozygote = AB and dic12b = BB) at the peak marker for each trait (a = AX-95156879, b = AX-94836422), the bars represent phenotypic means and +/- 1 standard error.

PS1 glasshouse trial

Two QTL were identified in the *PS1* glasshouse trial. The first was for the trait FL_L which explained 11.8% of phenotypic variation located at 166 cM on chromosome 4A (LOD = 6.8). The closest marker to the QTL was AX-95146535, where individuals with the Tios genotype (AA) had a mean FL_L of 23.4 ± 0.9 cm, individuals carrying the dic12b genotype (BB) had a mean FL_L of 27.2 ± 0.8 cm and heterozygous individuals (AB) had a mean of 28.0 ± 1.6 cm. The second QTL was for the *LDMC* trait which explained 13.8% of phenotypic variation and was located at 142.5 cM on chromosome 6A (LOD = 8.5). The closest marker was AX-95140962, where individuals had a mean *LDMC* of 204 ± 3.3 mg g^{-1} if AA in genotype, 185.7 ± 3.6 mg g^{-1} if BB and 197.5 ± 6.5 mg g^{-1} if AB.

Marker Outlook

The information acquired from 'CerealsDB' (Wilkinson et al. 2012) and EnsemblPlant (www.plants.ensembl.org) is shown in Table 3-11. The physical locations of the peak markers taken from EnsemblPlant show mostly correct chromosome assignments, which validated the *PS1* genetic map, excluding the peak markers for *Q1*, *Q2* and *Q5*, which were mapped to the same homoeologous group as their physical location. The physical location for the SNP associated with *Q10* was completely different to the mapped location. To measure the allelic diversity of the markers in the array formation Allen *et al.* (2017) characterised allele frequencies in 1,779 diverse hexaploid accessions from a range of collections. From this an estimate can be made of how common each allele is in hexaploid wheat. Genotypes of a 475 sample are on EnsemblPlant, which is where the minor allele frequencies (MAF) were taken from in Table 3-11.

Table 3-11 - For each of the candidate QTL found in the present study, information was taken from 'CerealsDB' (Wilkinson et al. 2012) and EnsemblPlant release 40 - July 2018 (www.plants.ensembl.org) regarding the closest SNP marker to each identified QTL (Peak SNP). Chromosome and Map Position refer to the mapped positions taken from the *PS1* population map formed in the present study. The 'BA number' for each peak marker is shown under 'Variant ID'.

QTL	Chromosome	Map Position	Peak SNP	Variant ID	Location	Alleles	MAF
Q1	2B	146	AX-94583923	BA00171324	2D:476696204	G/A	0.05
Q2	2B	185	AX-94641030	BA00449529	2A:717882095	T/C	0.15
Q3	4A	34.8	AX-94464899	BA00462181	4A:78025686	C/T	0.16
Q4	4A	96.1	AX-95156879	BA00420988	4B:3861096	G/A	0.08
Q5	5B	0	AX-94836422	BA00273512	5B:10263110	G/A	0.24
Q6	5B	203.6	AX-94402018	BA00114578	5B:671301137	C/A	0.29
Q7	6A	79	AX-95149371	BA00384034	6A:498592894	A/C	0.12
Q8	6A	93	AX-95105228	BA00171166	6A:561436298	A/G	0.25
Q9	7B	196	AX-94622790	BA00362080	7B:13827968	C/T	0.08
Q10	4A	166.1	AX-95146535	BA00370793	7D:18439937	A/G	0.17
Q11	6A	142.5	AX-95140962	BA00343894	6A:609020232	A/C	0.41

Location = Physical location on chromosome in million bases.
Alleles = Reference Alleles (forward strand).
MAF = Highest population minor allele frequency.

3.4 Discussion

3.4.1 The Relevance of the Mapped QTL for Ideotype Breeding.

Leaf Traits

This study has identified phenotypic variation in a novel *T. dicoccum* mapping population for a platform of physiological markers relating to the proposed ideotype (Figure 3-1). The environment of the 2017 field trial was well-watered. Some associations were found between traits directly related to grain yield (*HI*, *YP*, *EN* and *YE*) and physiological markers, which were argued to be promoted by increased selection in a well-watered ideotype. In Figure 3-1, a larger flag leaf is hypothesised to be beneficial in a well-watered environment, either via increased radiation capture or flag leaf CO_2 assimilation. This argument was supported by correlations observed in the 2017 field trial, as increases in *YP* and *YE* were linked to a thicker flag leaf (Figure 3-10). FL_{THICK} was also positively correlated with increased flag leaf size (FL_W, FL_L and FL_A), although no other link was found between leaf area and yield physiological markers. In the classical wheat ideotype (see: Donald 1968), small erect leaves are proposed to be advantageous for improved light distribution through the canopy. While selection for improved leaf angle and architecture does hold potential for increasing radiation use efficiency (Reynolds *et al.* 2009), there are many elite bread wheats that defy this ideotype (e.g. Paragon, Chapter 1). Although no correlation was identified in the *PS1* field trial, a positive relationship was found in Chapter 1 between grain yield and FL_A. These trends suggest that selection for increased source supply from a larger FL_A may predominate over improving flag leaf architecture to reduce shading in the lower canopy. However, the field plots of Chapter 1 and 3 were planted at a considerably lower density than a typical wheat field. Therefore, it is difficult to draw accurate conclusions about canopy effects on grain yield from the present study.

Genetic selection is a conceivable avenue for improving flag leaf morphology (Simón 1999). Although no QTL linked to FL_{THICK} were identified, two QTL were identified for FL_W (Table 3-10), on chromosomes 2B (*Q1*) and 5B (*Q6*). Other studies have identified a considerable number of environmentally stable QTL for FL_A, FL_W and FL_L in hexaploid wheat (Hussain *et al.* 2017; Liu *et al.* 2018). However, there has been limited investigation into QTL linked to flag leaf area in a tetraploid wheat background. In the present study, despite no significant variation between the parents, different QTL were identified for FL_L over both environments. These QTL could be used for selection to

increase or decrease FL_A depending on the ideotype requirements. However, there was an indication that the genetic variance controlling phenotypic variance was low, as no QTL was consistently identified over both environments, variation in FL_A varied between the parents across the environments and moderate H^2 was found in the *PS1* field trial for the leaf area related traits. Greater parent variation in FL_A may have facilitated identification of more stable QTL in this study.

As outlined in the ideotype (Figure 3-1), increased CO_2 supply would be a favourable trait in both environments, but only in the 'well-watered' ideotype would it be appropriate to achieve this via increasing g_s. However, no associations were found with S_D and *YE* or *YP*. In the *PS1* field trial, individuals with the dic12b genotype (BB) at the QTL identified on 6A (*Q7*) had a significantly higher S_D than the Tios genotype individuals (AA, Figure 3-12). In a study using a bread wheat double haploid population, Wang *et al.* (2016) found 40 additive QTL related to stomatal density, width and length across different watering regimes, including QTL identified on chromosome 6A linked to stomatal density. Furthermore, Wang *et al.* (2015) found a QTL relating to transpiration rate on 6A in the same cross population under drought stress. In the present study, only S_D on the abaxial leaf surface was analysed. In a pilot study, Shahinnia *et al.* (2016) found that stomatal traits had greater genetic variability on the adaxial leaf surface. However, they also observed that the stomatal features were highly positively correlated across both surfaces. Genetic variation in the *PS1* mapping population could have been missed by only analysing the abaxial leaf surface and future work could determine if there is greater genetic variability on the adaxial surface. In Chapter 1, $\Delta^{13}C$ was linked to the supply components of photosynthesis and could be used as a proxy for estimating leaf stomatal dynamics. $\Delta^{13}C$ was not determined for this mapped population, but tissue was retained for future work.

Increasing CO_2 supply by promoting higher g_m is warranted in both ideotype environments. However, no significant variation was apparent between the parents for *LDMC*, although a QTL was still identified in the *PS1* glasshouse trial (*Q11*, Table 3-10), where the BB genotype had a negative additive effect on the phenotypic variation. Few QTL have been previously identified for leaf dry matter parameters in wheat. Su *et al.* (2006) found minor QTL for flag leaf weight (dry weight per flag leaf) on seven chromosomes that explained 5.9% to 17.2% of phenotypic variation, however, none were found on 6A where *Q11* was located. The H^2 results (Table 3-7) indicated that the

estimates of *LDMC* were susceptible to error or environmental variance, which could explain the difficulties in identifying QTL for the traits of *SLA* and *LDMC*.

Ear Traits

In both the ideotypes (Figure 3-1), increases in ear size is a trait favoured for improving sink strength. In the *PS1* field trial, E_L and E_{CA} both had a positive association with *YE* and *YP*. No QTL were identified for E_L or E_{CA}, despite the high H^2 observed for E_L. However, QTL have been identified for E_L elsewhere. In a SHW mapping population, Yu *et al.* (2014) mapped 6 QTL for E_L (on: 2D, 3A, 3B, 5A, 6B, 7D). Furthermore, Faris *et al.* (2014) found a QTL on 2A linked to E_L in a tetraploid mapping population. The high H^2 observed in the present study and the multiple QTL observed in other studies, may indicate high polygenetic control of the E_L trait, which could have meant too many QTL were involved for detection through the CIM analysis in the present study. The low H^2 observed for E_{CA} could be linked to the E_W measurements, which was a difficult trait to measure in the field due to the complexity of the organ. A more accurate proxy for E_{CA} needs to be developed, which would improve chances for QTL identification.

Awn presence was not shown to be beneficial to overall grain yield in the majority of the SHW NILs (Chapter 2). However, in the *PS1* field trial increases in A_L were associated with higher *EN*, *HI* and *YP*; conflicting with the hypothesis that investment into awn development is of limited benefit in the absence of water-limitation. Two QTL were identified for A_L, with the largest hit on chromosome 4A (*Q3*). As discussed in Chapter 2, there is a known gene on the short arm of 4A that causes awn shortening and bending, called the *Hd* locus (Rao 1981). In a hexaploid RIL population, Yoshioka *et al.* (2017) identified three major QTL related to awn length which corresponded to the known inhibitor gene locus, including a QTL on 4A corresponding to the *Hd* locus located at 22 cM and explaining 23.1% of the phenotypic variation. Furthermore, Sourdille *et al.* (2002) mapped two QTL relating to awn length which segregated with the *Hd* and *B2* genes. They found no QTL on 5A, suggesting parent lines (Courtot and Chinese Spring) had the same allelic constitution at the *B1* gene. The *B1* gene has been shown to inhibit awn presence in emmer and durum wheat (Goncharov *et al.* 2003). These findings indicate the *PS1* tetraploid parents may possess the same allelic compositions at the *B1* and *B2* locus, but vary at the *Hd* locus. The second QTL linked to A_L was found on chromosome 2B, there is no evidence supported in literature where similar observations have been made. However, Ahmad *et al.* (2014) found marker-trait association located at 66.4 cM on 2A. Furthermore, other studies have identified minor QTL controlling A_L

outside of the known inhibitor gene locus (e.g. Zhang *et al.* 2018). Therefore, QTL were identified for A_L which could be used to promote ear photosynthesis via selection for an increased ear surface area. However, these QTL will probably only be useful in MAS if breeding with awned material.

Plant Traits

Increased photosynthetic duration was hypothesised to be beneficial to grain yield in the 'well-watered' ideotype. Supporting this hypothesis was the correlation between FL_{LONG} and *YE* shown in Figure 3-10. No QTL were found for FL_{LONG} despite moderately high H^2 and significant variation between the parents (Table 3-7). In the *PS1* field trial Tios had a significantly higher FL_{LONG} than dic12b, a trend which was reversed in the glasshouse trial. This indicates that environment and gene interactions may have an important influence on the phenotypic variance, which is supported by the non-normal distribution of the phenotypic population frequencies in both environments, where some post-anthesis disease pressure caused lines to senescence early leading to inaccurate FL_{LONG} measurements. Disease pressure, and other stress factors, can contribute to a decreased FL_{LONG} (Carmo-Silva *et al.* 2017). However, QTL have been successfully identified in other studies using different proxies of the trait (e.g. Shi *et al.* 2017; Yue *et al.* 2006). An improved proxy needs to be established for FL_{LONG} that can distinguish between disease and senescence.

There was no effect of F_T on any of the yield related traits in the *PS1* field trial. It was hypothesised that an earlier flowering time would be most advantageous in a 'water-limited' environment. The genetic control of F_T in wheat is complex and controlled by three signalling pathways: vernalisation (*Vrn* genes), photoperiod response (*Pdp*) and earliness *per se* (*Eps*) (Cockram *et al.* 2007; Langer *et al.* 2014). In the case of spring sown wheat, such as the *PS1* population, there is no vernalisation requirement (Cockram *et al.* 2007). Three genes located on the group 2 chromosomes have been identified and linked to photoperiod response: *Ppd-A1*, *Ppd-B1* and *Ppd-D1* (Kamran *et al.* 2014; Law *et al.* 1978). However, a photoperiod response gene has been mapped to the short arm of 7B in hexaploid wheat, called *Ppd-B2* (Khlestkina *et al.* 2009), this is located at the opposite end of the chromosome to *Q9*. Although, the physical location of the peak marker for *Q9* was towards the start of chromosome 7B (Table 3-11). All genetic control of flowering time outside the pathways of *Vrn* and *Pdp* is termed 'earliness *per se*' (*Eps*) (Hoogendoorn 1985). A considerable number of 'earliness *per se*' QTL have been found in wheat (e.g. Kamran *et al.* 2013; Zikhali *et al.* 2014), suggesting more common

variability in genetic control than the other two pathways (Cockram *et al.* 2007). A QTL for ear heading date, detected over 12 environments, was also mapped to the short arm of chromosome 7B in durum wheat (Maccaferri *et al.* 2008) and heading date can be a trait closely associated with flowering time. In tetraploid wheat, Peng *et al.* (2003) used a tetraploid mapping population to identify four heading date QTL on chromosomes 2A, 4B, 5A, and 6B, which would probably fall into the class of earliness *per se*. It is probable that *Q9* is also a novel earliness *per se* QTL, which could be advantageous in ideotype breeding for environment adaptability, such as promoting earlier development to avoid drought.

The remobilisation of assimilates to the developing grain is a trait favoured for selection in both ideotype environments. Grain yield and *HI* were suggested as suitable proxies for estimating assimilate remobilisation to the developing grain and are traits associated with the overall aim of crop improvement. In other studies, QTL have been found that are linked to yield component traits and overall grain yield in a tetraploid background (Maccaferri *et al.* 2008; Mangini *et al.* 2018; Peng *et al.* 2003). In the present study no QTL were found for *YP* or *YE*, but QTL were identified for *EN* (*Q4*) and *HI* (*Q5*). The parameter *HI* is the proportion of grain yield to biomass and at the locus of the *Q5* individuals with the *AA* genotype had significantly higher *YP* than individuals with the BB in genotype, whereas there was little evidence for variation in biomass. These trends suggests that, although no QTL were found for *YP*, variation in *YP* was linked to the *HI* QTL found on 5B. It has been argued that *HI* is almost optimal in modern wheat (Long *et al.* 2006; Parry *et al.* 2011; Richards 2000), suggesting this trait may already be fixed in a hexaploid background. However, if the QTL was linked to grain yield, it could be profitable in breeding programs, as tetraploid wheat landraces are a genetic reserve for improving yield components in modern varieties (Soriano *et al.* 2018).

Ear number (*EN*) is largely determined by tiller production and survival, which are important components of canopy and yield development (Xie *et al.* 2016). In the Donald (1968) ideotype, it is argued that the model plant should only have a single main tiller to increase per unit area production. Decreasing tiller number has also been associated with increased FL_{LONG} and *HI* (Richards 1988), which is supported by the negative association between *EN* and FL_{LONG} in the present study. Alternatively, in the *PS1* field trial, *EN* was associated with increased *YP*, suggesting the QTL found for *EN* could be used in selection for increased yield. However, yield components were considered on a singular plant basis,

and increased sowing density, typical of a farmer's field or trial plot, may alter the environmental influence on the phenotype.

3.4.2 Ideotype Trait Compensation.

One of the difficulties in ideotype design and trait-based selection are the potential trade-offs or compensations between characteristics (Donald 1968; Martre *et al.* 2015; Rasmusson 1991). This was apparent from a number of negative correlations observed in the *PS1* field trial (Figure 3-10), such as between FL_W and A_L. Trade-offs with awn development were also observed in the SHW NIL analysis (Chapter 2). There were positive correlations reflecting assimilate investment into both the flag leaf and the ear, increases in FL_A were linked to increases in E_{CA}. This combination of large organ size is promising for breeding high yielding lines (Voldeng & Simpson 1967) and shows potential for trait-based selection for increased net photosynthesis by expanding photosynthetic surface area simultaneously in both organs.

Alternatively, trait correlation may indicate genetic linkage between QTL associated with the phenotypic variation. There were QTL linked to FL_W (*Q1*) and A_L on 2B (*Q2*) located 39 cM apart (Table 3-10), where the presence of the BB genotype was linked to higher A_L but lower FL_W. If limited segregation occurred in the offspring in these regions it could explain the negative correlation. To test this, phenotype data at each locus was separated into allele classes for these traits (data not shown), there were no significant differences between the homologous allele classes for FL_W at the *Q1* locus or A_L at the *Q2* locus, suggesting genetic linkage was unlikely. Furthermore, QTL linked to FL_L and S_D were located 14 cM apart and no significant associations were identified between these phenotypes. A number of significant associations were found between F_T and other physiological markers (Figure 3-10). However, despite these significant correlations, no other QTL were identified on chromosome 7B (Table 3-10) suggesting that the link between other traits and F_T, may be a result of physiological or developmental aspects. In a study by Bogard *et al.* (2011), F_T was found to be an important determinant of FL_{LONG}, grain yield and grain protein content. A useful tool in unpicking potential trait compensations could be MAS, which can provide an accurate method for trait selection, although this is dependent on identifying reliable genetic and trait associations.

3.4.3 Transgressive Segregation, Heritability and Environmental Stability.

A considerable amount of transgressive segregation was observed for the majority of physiological markers measured in the *PS1* field trial, indicating the presence of complementary alleles inherited in the progeny from both parents (Tanksley, 1993). Alleles with positive effects were present in each parent for these traits (Hussain *et al.* 2017). This cobination of complementary alleles, leading to progeny with extreme phenotypes, would be useful for trait specific ideotype selection. For the physiological markers E_L and E_{CA}, transgressive segregation only occurred outside the range of dic12b (Figure 3-9), suggesting the presence of few genes and that only positive alleles were contributed from Tios (Sourdille *et al.* 2002).

In the *PS1* field trial, high H^2 was observed for the traits A_L, E_L, S_D and *SLA*. In other studies high heritability has also been observed for A_L, E_L and S_D (Bhagwat & Bhatia 1993; Ebadi-Segherloo *et al.* 2016). For *SLA*, lower H^2 seems to be more commonly observed. For example, de Miguel *et al.* (2012) observed H^2 for *SLA* in *Pinus pinaster* ranging from 0.14 to 0.27 across different watering regimes. In the present study, considerably lower H^2 was observed for the other dry matter analysis traits (RWC and LDMC, Table 3-7).

The traits *LDMC, RWC,* E_{CA} and FL_A appeared to have negative H^2 in the *PS1* field trial. The trait *LDMC* also had a negative H^2 in the glasshouse. The negative H^2 occurred where the environmental variance (V_e: estimated from the replicated parents) was larger than the phenotypic variance (V_p: estimated from variance across the *PS1* individuals for each trait), leading to a negative genetic variance estimate (V_g). This occurred most frequently in traits where there was little evidence of significant variation between the parents, but *S.D* of each parents mean was high (Table 3-4). However, for E_{CA} there is strong evidence of significant variation between the parents, meaning there must have been genetic variation that was not detected to the same degree in the population. Negative H^2 is biologically impossible and is often linked to sampling error (Robinson *et al.* 1955), leading to a lowered bias heritability (Steinsaltz *et al.* 2018). Although interpretations are limited from negative heritability calculations, they should still be reported (Dudley & Moll 1969). It could be argued that negative estimates of heritability are considered close to 0 (Gusmini & Wehner 2007). For the estimate of V_e, the small sample size (n = 8 per parent) would have increased susceptibility to anomalies or measurement error. The physiological markers where H^2 appeared negative were often calculated from formulas involving several traits, which increases the chance of errors influencing the overall

estimate. More parent replicates were included in the *PS1* glasshouse trial, which could explain the higher abundance of positive H^2 estimates, as the impact of outlying data points would have been reduced.

For the traits measured in both the *PS1* field trial and the *PS1* glasshouse trial, no QTL were identified consistently across the environments. For the *PS1* individuals measured over both environments, significant correlation was only found in 4 out of the 8 traits. No correlation was found for *SLA*, *LDMC*, *RWC* and FL_{LONG}, which is another indicator of low heritability and traits which were strongly influenced by environmental conditions. Different growing conditions and environmental pressures are often observed between glasshouse and the field, which can influence results (Limpens *et al.* 2012; Poorter *et al.* 2016). In an effort to mimic conditions across both environments, both trials were irrigated and fertilised. However, despite the supplementary lighting, the plants were grown over the winter in the *PS1* glasshouse trial at considerably lower light levels.

3.4.4 Prospects for MAS.

The use of MAS has been important for transferring wild genes from exotic sources into crops (Nadeem *et al.* 2017). However, difficulties may arise with the direct use of the marker-trait associations, identified in this study, for the introgression of tetraploid diversity into a hexaploid background via MAS. Markers should typically be within 5 cM of the target loci, but poor accuracy in QTL mapping often leads to larger confidence intervals (Collard & Mackill 2008). In the present study, the -1 LOD support intervals were mostly larger than 5 cM (excluding *Q3* and *Q5*), suggesting the accuracy of the QTL mapping may be uncertain. Furthermore, the assumption would have to be made that linkage between the markers and QTL would not break down during the introgression and future generations. Recombination typically occurs between loosely linked markers leading to unusable assays (Sharp *et al.* 2001), which adds further uncertainty to the direct application of the marker-trait associations.

Before direct application could be made using the results in this chapter, a marker validation step would be necessary. Secondly, if the identified desirable alleles linked to targeted traits are already fixed in a modern cultivar background, there would be little profit in the effort of making introgressions. However, some of the peak markers at each loci had very low published MAF (Table 3-11), suggesting that part of the diversity identified in the *PS1* population could be rare in the bread wheat genepool. Using the genotype data, *PS1* individuals could be identified with the greatest combination of

favourable alleles for each ideotype. These lines then could be backcrossed to a hexaploid cultivar with the highest frequency of complementary poor alleles. The resource of 'CerealsDB' (see: Wilkinson et al. 2012) would be useful in identifying these hexaploid cultivars. In the subsequent generations, physiological and genetic markers linked to each QTL would be screened over the different ideotype environments. The flanking markers for each support interval, identified in Table 3-10, would be used to increase precision, ensuring the trait is introgressed as part of a defined interval surrounding the QTL rather than just one marker linked to the QTL (Collard & Mackill 2008). If the alleles vary as predicted with each targeted trait, this would validate the accuracy of the markers for MAS and whether trait improvement is possible in a hexaploid background via tetraploid diversity. If the alleles do not vary as expected in conjunction with the physiological markers, further field trials may be needed to test the environmental stability of the existing identified QTL or to identify more reliable marker-trait associations.

3.5 Conclusion

In a novel tetraploid mapping population, candidate QTL and marker-trait associations have been identified for 8 physiological markers that were suggested for indirect selection for complex targeted traits relating to proposed ideotypes. The marker-trait associations could be developed for MAS, to aid the introgression of diversity from a tetraploid source into modern wheat for trait improvement. However, further work is needed to validate the reliability of these marker-trait associations. Additionally, the ideotype was only tested in a 'well-watered' environment, further analysis is needed to validate the relationship between ideotype traits and yield components in a 'water-limited' environment.

This study has identified genetic diversity for range of traits in two *T. dicoccum* landraces, but may have missed potential diversity capable of improving modern wheat that is monomorphic in a tetraploid background. Further crosses between tetraploid and hexaploid parents could identify diversity lost through domestication, especially if some of the *T. dicoccoides* lines with high photosynthetic rates (identified in Chapter 1) are used as parents.

Chapter Findings Summary.

1. Two ideotypes were outlined that combine a favourable combination of complex traits for two different environments. Based on the findings in the first two chapters and evidence in literature, a collection of physiological markers were

proposed that could be used for secondary selection for the complex ideotype traits.

2. A novel *T. dicoccum* mapping population was created between two landraces that showed variation for the physiological markers of interest. The new population, and parents, were phenotyped in two trials for these physiological markers. Associations were found between yield components and physiological markers that were suggested to be important within a well-watered environment (e.g. grain yield and ear size or flag leaf thickness).
3. The population was genotyped and a new genetic linkage map was created using 1779 single nucleotide polymorphisms (SNPs). Using this map, composite interval mapping was completed to identify 11 candidate QTL for 8 physiological markers located across 5 different chromosomes. However, for the physiological markers measured across both environments, no QTL were consistently identified.
4. Another round of QTL mapping needs to be completed in future analysis, to assess the accuracy of these candidate marker-trait associations.

4 General Discussion and Conclusion.

4.1.1 Conclusion.

This project has evaluated the potential of tetraploid wheat as a source of photosynthetic improvement in modern wheat cultivars. The data presented in the Chapter 1 2016 field trial illustrates the high assimilation rates observed in these progenitor species; if the bread wheat line 'Paragon' possessed the ability to generate the same mean per unit CO_2 assimilation (*A*) observed in the *T. dicoccoides* 'dic71', a 35% increase in flag leaf CO_2 assimilation per leaf would be achieved. Subsequent analysis of the introgressed offspring lines in Chapter 1 highlighted a key problem in harnessing this diversity. If *T. dicoccoides* lines are to be used successfully as donors for improvement, the observed depression of *A* associated with increased leaf area needs to be addressed. Other studies have also observed this compensation across the wheat ploidy continuum (Austin *et al.* 1982; del Blanco *et al.* 2000; Evans & Dunstone 1970). There are two questions to explore in order to address the compensation. Firstly, has *A* rate been inadvertently depressed through domestication due to selection for other favourable characteristics? Secondly, is there a fundamental physiological trade-off, imposing a barrier in incorporating higher *A* across an extended photosynthetic area?

In the present study, there was greater evidence supporting the second hypothesis. Since the initial reports of high photosynthetic rates in progenitor lines (e.g. Dunstone *et al.* 1973; Evans & Dunstone 1970; Khan & Tsunoda 1970), the increased accessibility of tools for dissecting the components of leaf *A* have provided techniques to lay open the individual mechanisms linked to this trade-off, and to some degree this was achieved in the present study. Other authors have highlighted that a larger leaf may lead to a reduction in photosynthetic investment per unit area (e.g. Long *et al.* 2006), which may be linked to a dilution per unit leaf N content (Khan & Tsunoda 1970). However, evidence from Chapter 1 highlighted that the diluted investment into the components of photosynthetic supply imposed the greatest limitation on *A*, evident from the $\Delta^{13}C$ and gas-exchange results. The smaller flag leaf area in the progenitor *T. dicoccoides* reflected increased investment into photosynthetic supply components per unit area (such as stomatal density), a less densely packed mesophyll and higher per unit water expenditure; features

that fuelled higher g_s and g_m. These characteristics were reduced within the cultivated lines with larger flag leaf area, which poses the question: can this high per unit water expenditure linked to productive photosynthetic supply be maintained over a larger surface area? In the hypothetical example above of a leaf with the area of observed in 'Paragon' but with the mean *A* of 'dic71', the leaf would possess a 31% higher transpiration rate than the mean observed in 'Paragon'. In a 'well-watered' environment selection for increased CO_2 supply is favoured, as discussed in Chapter 3. However, increasing transpiration loss could be detrimental to crop improvement in a 'water-limited' environment.

The next direction of investigation should be to assess if this higher per unit investment into CO_2 supply could be incorporated into a larger flag leaf, whilst utilising the diversity available in the *T. dicoccoides* identified in this study. This is where marker assisted selection could be implemented for more accurate selection in breeding populations to maintain high photosynthetic supply whilst sustaining a large leaf area. In Chapter 3, different QTL were identified that were linked to photosynthetic supply components and leaf area traits in a tetraploid background. These QTL may hold potential for marker assisted pre-breeding, but further work is needed to determine the accuracy of the marker-trait associations. Ultimately, if the physiological mechanics of the trade-off between leaf area and *A* can be broken down using the phenotypic or genetic assays developed in this study, *T. dicoccoides* can be used as donors for photosynthetic improvement in modern wheat in a 'well-watered' environment.

Despite the high productivity shown on a per unit leaf basis in *T. dicoccoides*, when considered on a per organ leaf basis; the *T. dicoccoides* individuals had both considerably lower transpiration loss and CO_2 assimilation per leaf, coupled with an extensive investment into awn structure. This evolutionary development for investment into reproductive structure photosynthesis and the organ with the higher drought tolerance (Ding *et al.* 2017; Li *et al.* 2017), reflects adaptation to the more water limited environment of the progenitor's origin and is a promising source of diversity for forming the 'water-limited' ideotype outlined in Chapter 3. However, in Chapter 2 this study evaluated the potential benefits relating to the presence of awns within the 'well-watered' environment of the UK and found there was no substantial advantages to awn presence. As with the analysis in Chapter 1, if these trials were repeated under a 'water-limited' environment, the findings may show an advantage and indicate whether *T. dicoccoides* should be used as a resource for increasing investment into ear photosynthesis.

The present study has used conventional breeding techniques; no avenues of genetically modified organisms were explored. While conventional breeding techniques shaped the first green revolution, genetically modified crops may hold the key to major future advancements in yield (Basu *et al.* 2010). Rather than replacing the techniques of the present study, this technology would complement and advance the prospects of expanding the modern wheat genepool. As shown in Chapter 1, one of the major limitations of crosses with wild wheat is the unintentional linkage drag of undesirable genes. Genetic modification could increase the accuracy of introgression and thus suppress one of the major drawbacks in harnessing diversity from wild wheat.

4.1.2 Study Limitations, Future Work and Plans for Moving Forward.

It became evident early on in the project that the progenitor lines showed a greater degree of stress when grown in the light-limited conditions of the glasshouse compared to the modern varieties. This posed limitations on the number of experiments that could be completed on plants at maturity, as all experiments had to be conducted in field trials. However, conducting the measurements in the field meant observations were made within a more relevant environment to conditions used in breeding programs, and ultimately the farmer's field. The drawback of the field environment was an increase in abiotic and biotic stresses and at times limitations imposed by space restrictions; particularly evident in the 2016 field trial of Chapter 1. Within a nitrogen rich environment, lodging was a risk with the tetraploid lines; plants required individual staking with bamboo support. For some of the progenitor individuals seed stocks were limited. These factors restricted the scale of the field trials and the majority of measurements were completed on replicated single plants within large plots, rather than using replicated plots of individuals. Germination inconsistency was a problem throughout the project, evident from the missed target of 200 individuals in the *PS1* population and the poor germination success when direct sowing was used in the 2017 field trial in Chapter 3. It was for these reasons that plants were transplanted into the field as seedlings, after artificial vernalisation was used to standardise vernalisation requirements. Ultimately, there are limitations imposed by any field study, but measuring the true performance of the plants in a relevant environment is worth the cost.

This project has covered a broad array of different traits and components linked to wheat photosynthesis, using a comprehensive range of different physiological and genetic assays. There are substantial directions for further work to support the hypotheses,

conclusions and answer questions raised through the project. Some of the most pressing are listed below:

1. In every chapter of this project, analyses were completed within the conditions of the UK; a 'well-watered' environment. Future work is needed to test the hypotheses in a 'water-limited' environment and to weigh the potential drought tolerance advantage of awns.
2. If increases in leaf area are associated with limitations to per unit photosynthetic supply components, there may be an evaporative boundary linked to the variation observed across wheat ploidy. Investigation into anatomical aspects of flag leaf water supply in *T. dicoccoides* could pinpoint features to overcome these evaporative limits. Austin et al. (1982) observed a higher vein density in flag leaves of progenitor wheat (including *T. dicoccoides*) in comparison to modern cultivars, which may be indicative of improved leaf hydraulic conductance and thus a higher per unit water expenditure. Conversely, stem shortening through the 'green revolution' may have already improved hydraulic continuity to some degree in modern cultivars (Raven & Griffiths, 2015). Further investigation into traits linked to anatomical leaf water supply could shed light on the observed trade-off between leaf area and *A*.
3. Stable natural isotope partitioning could be used as a tool for deciphering the contribution of the ear, awns and flag leaf to remobilising photo-assimilates to grain filling (Raven & Griffiths 2015). This would involve pulse labelling different photosynthetic organs (ears and flag leaves) of the near isogenic lines from Chapter 2 with an artificially enriched label of the heavier C and N isotopes (^{13}C and ^{15}N). On organs of different plants, this pulse label could be applied as a urea solution or fed as a gas to a closed chamber containing each organ. Half of the labelled organs would be harvested 24 hours later to provide a baseline of how much label was absorbed by the plant. Once the remaining plants are fully mature, the grain ^{13}C and ^{15}N isotope compositions would be informative of which organ had made the largest contribution of remobilising assimilates to the developing grain. There is an ongoing collaboration between the UK and India exploring these techniques (The Cambridge-India Network in Translational Nitrogen, www.niab.com/cintrin).
4. When breeding for improvements in leaf photosynthesis the conditions of the crop canopy should be taken into consideration (Horton 2000). The interactions of leaves within a canopy and the competition of neighbouring plants, were not taken into

consideration within this project and there may be an additional trade-off associated with canopy shading that was not analysed.

5. As discussed in Chapter 3, the candidate QTL and marker-trait associations need to be validated in a second year of field trials. Additionally, in forming a mapping population between two *T. dicoccum* accessions, diversity may have been lost through domestication that is present in *T. dicoccoides*. Forming mapping populations with the *T. dicoccoides* accessions of Chapter 1 and cultivated lines with a lower *A*, may be a more direct approach for identifying marker-trait associations with the desirable photosynthetic traits observed in the wild progenitors.

4.1.3 Closing remark.

This project has been a revisited exploration into the photosynthetic diversity in tetraploid progenitor wheat, using a diverse range of modern techniques to identify some of the underlying mechanisms driving the photosynthetic diversity across ploidy. Donors of beneficial diversity, genetic markers linked to this diversity and key road blocks in accessing that diversity were all identified. Overall, the project has made a contribution towards addressing the bottlenecks in increasing photosynthesis and expanding genetic diversity in modern bread wheat varieties.

5 REFERENCES

Abbad, H., El Jaafari, S., Bort, J., & Araus, J. L. (2004). Comparison of flag leaf and ear photosynthesis with biomass and grain yield of durum wheat under various water conditions and genotypes. *Agronomie*, pp. 19–28.

Abràmoff, M. D., Magalhães, P. J., & Ram, S. J. (2004). Image processing with ImageJ. *Biophotonics International*, **11**(7), 36–41.

Acquaah, G. (2012). *Principles of Plant Genetics and Breeding*, Chichester, UK: John Wiley & Sons, Ltd.

Affymetrix. (2011). Axiom ® Genotyping Solution DataAnalysis Guide, (702961). Retrieved from http://media.affymetrix.com/support/downloads/manuals

AHDB. (2017). Wheat Pocketbook 2017/18. *Agricultural & Horticulture Development Board*, Recommened List.

Ahmad, M. Q., Khan, S. H., Khan, A. S., Kazi, A. M., & Basra, S. M. A. (2014). Identification of QTLs for drought tolerance traits on wheat chromosome 2A using association mapping. *International Journal of Agriculture and Biology*, **16**(5), 862–870.

Ainsworth, E. A., & Long, S. P. (2005). What have we learned from 15 years of free-air CO_2 enrichment (FACE)? A meta-analytic review of the responses of photosynthesis, canopy properties and plant production to rising CO_2. *New Phytologist*, **165**, 351–372.

Allen, A. M., Winfield, M. O., Burridge, A. J., … Edwards, K. J. (2017). Characterization of a Wheat Breeders' Array suitable for high-throughput SNP genotyping of global accessions of hexaploid bread wheat (*Triticum aestivum*). *Plant Biotechnology Journal*, **15**(3), 390–401.

Allwood, J. W., Chandra, S., Xu, Y., … Bowsher, C. G. (2015). Profiling of spatial metabolite distributions in wheat leaves under normal and nitrate limiting conditions. Phytochemistry, **115**(1), 99–111.

Alonso, A., Pérez, P., & Martínez-Carrasco, R. (2009). Growth in elevated CO_2 enhances temperature response of photosynthesis in wheat. *Physiologia Plantarum*, **135**(2), 109–120.

Araus, J. L., Brown, H. R., Febrero, A., Bort, J., & Serret, M. D. (1993). Ear photosynthesis, carbon isotope discrimination and the contribution of respiratory CO_2 to differences in grain mass in durum wheat. *Plant, Cell & Environment*, **16**(4), 383–392.

Austin, R. B., Bingham, J., Blackwell, R. D., … Taylor, M. (1980). Genetic Improvements in Winter-Wheat Yields Since 1900 and Associated Physiological-Changes. *Journal of Agricultural Science*, **94**(JUN), 675–689.

Austin, R., Morgan, C., Ford, M., & Bhagwat, S. (1982). Flag leaf photosynthesis of *Triticum aestivum* and related diploid and tetraploid species. *Annals of Botany*, (1973), 177–189.

Babar, M. A., van Ginkel, M., Reynolds, M. P., Prasad, B., & Klatt, A. R. (2007). Heritability, correlated response, and indirect selection involving spectral reflectance indices and grain yield in wheat. *Australian Journal of Agricultural Research*, **58**(5), 432.

Baker, N. R. (2008). Chlorophyll Fluorescence: A Probe of Photosynthesis In Vivo. *Annual Review of Plant Biology*, **59**(1), 89–113.

Ban, T., & Watanabe, N. (2001). The effects of chromosomes 3A and 3B on resistance to Fusarium head blight in tetraploid wheat. *Hereditas*, **135**(2–3), 95–9.

Barbour, M. M., Bachmann, S., Bansal, U., Bariana, H., & Sharp, P. (2015). Genetic control of mesophyll conductance in common wheat. *New Phytologist*. doi:10.1111/nph.13628

Barbour, M. M., Fischer, R. A., Sayre, K. D., & Farquhar, G. D. (2000). Oxygen isotope ratio of leaf and grain material correlates with stomatal conductance and grain yield in irrigated wheat. *Functional Plant Biology*, **27**(7), 625–637.

Barbour, M. M., Warren, C. R., Farquhar, G. D., Forrester, G., & Brown, H. (2010). Variability in mesophyll conductance between barley genotypes, and effects on transpiration efficiency and carbon isotope discrimination. *Plant, Cell and Environment*, **33**(7), 1176–1185.

Barrs, H. D., & Weatherley, P. E. (1962). A Re-Examination of the Relative Turgidity Technique for Estimating Water Deficits in Leaves. *Australian Journal of Biological Sciences*, **15**(3), 413–428.

Basu, S. K., Dutta, M., Goyal, A., … Prasad, R. (2010). Is genetically modified crop the

answer for the next green revolution? GM Crops, **1**(2), 11–22.

Bates, D., Mächler, M., Bolker, B., & Walker, S. (2014). Fitting Linear Mixed-Effects Models using lme4, **67**(1). doi:10.18637/jss.v067.i01

Beadle, C. L., & Long, S. P. (1985). Photosynthesis — is it limiting to biomass production? *Biomass*, **8**(2), 119–168.

Beddington, J. (2010). Food security: contributions from science to a new and greener revolution. *Philosophical Transactions of the Royal Society of London. Series B, Biological Sciences*, **365**, 61–71.

Beed, F. D., Paveley, N. D., & Sylvester-Bradley, R. (2007). Predictability of wheat growth and yield in light-limited conditions. *Journal of Agricultural Science*, **145**(1), 63–79.

Bell, C. J., & Incoll, L. D. (1990). The redistribution of assimilate in field-grown winter wheat. *Journal of Experimental Botany*, **41**(8), 949–960.

Bellasio, C., Beerling, D. J., & Griffiths, H. (2016). An Excel tool for deriving key photosynthetic parameters from combined gas exchange and chlorophyll fluorescence: Theory and practice. *Plant Cell and Environment*, pp. 1180–1197, pp. 1180–1197.

Bellasio, C., & Griffiths, H. (2014). Acclimation of C_4 metabolism to low light in mature maize leaves could limit energetic losses during progressive shading in a crop canopy. *Journal of Experimental Botany*, **65**(13), 3725–3736.

Bellasio, C., Burgess, S. J., Griffiths, H., & Hibberd, J. M. (2014b). A high throughput gas exchange screen for determining rates of photorespiration or regulation of C_4 activity. *Journal of Experimental Botany*, **65**(13), 3769–3779.

Bender, J., Hertstein, U., & Black, C. R. (1999). Growth and yield responses of spring wheat to increasing carbon dioxide, ozone and physiological stresses: A statistical analysis of "ESPACE-wheat" results. *European Journal of Agronomy*, **10**(3–4), 185–195.

Benjamini, Y., & Hochberg, Y. (1995). Controlling the False Discovery Rate: A Practical and Powerful Approach to Multiple Testing. *Journal of the Royal Statistical Society. Series B (Methodological)*, **57**(1), 289–300.

Berry, P. M., Sylvester-Bradley, R., & Berry, S. (2007). Ideotype design for lodging-

resistant wheat. *Euphytica*, **154**(1–2), 165–179.

Bhagsari, A. S., & Brown, R. H. (1986). Leaf Photosynthesis and its Correlation with Leaf Area. *Crop Science*, **26**, 127–132.

Bhagwat, S. G., & Bhatia, C. R. (1993). Selection For Flag Leaf Stomatal Frequency In Bread Wheat. *Plant Breeding*, **110**(2), 129–136.

Blum, A. (1985). Photosynthesis and transpiration in leaves and ears of wheat and barley varieties. *Journal of Experimental Botany*, **36**(164), 432–440.

Bock, D. G. (2017). The genetics of contemporary evolution in an invasive perennial sunflower. PhD Thesis, The University of British Columbia (Vancouver).

Boesgaard, K. S., Mikkelsen, T. N., Ro-Poulsen, H., & Ibrom, A. (2013). Reduction of molecular gas diffusion through gaskets in leaf gas exchange cuvettes by leaf-mediated pores. *Plant, Cell and Environment*, **36**(7), 1352–1362.

Bogard, M., Jourdan, M., Allard, V., … Le Gouis, J. (2011). Anthesis date mainly explained correlations between post-anthesis leaf senescence, grain yield, and grain protein concentration in a winter wheat population segregating for flowering time QTLs. *Journal of Experimental Botany*, **62**(10), 3621–3636.

Borlaug, N. E. (1968). Wheat Breeding and its Impact on World Food Supply. In *Third International Wheat Genetics Symposium*, Mexico: CIMMYT, 1–36.

Brennan, J. P., Condon, A. G., Van Ginkel, M., & Reynolds, M. P. (2007). Paper presented at international workshop on increasing wheat yield potential, CIMMYT, Obregon, Mexico, 20-24 March 2006: An economic assessment of the use of physiological selection for stomatal aperture-related traits in the CIMMYT wheat breeding programme. *Journal of Agricultural Science*, **145**(3), 187–194.

Broman, K. W. (2010). Genetic map construction with R/qtl. *Department of Biostatistics & Medical Informatics Technical Report* **214**, 1-41.

Broman, K. W., & Sen, S. (2009). *A Guide to QTL Mapping with R/qtl*, New York, NY: Springer New York. doi:10.1007/978-0-387-92125-9

Carmo-Silva, E., Andralojc, P. J., Scales, J. C., … Parry, M. A. J. (2017). Phenotyping of field-grown wheat in the UK highlights contribution of light response of photosynthesis and flag leaf longevity to grain yield. *Journal of Experimental Botany*. doi:10.1093/jxb/erx169

Carmo-Silva, E., Scales, J. C., Madgwick, P. J., & Parry, M. A. J. (2015). Optimizing Rubisco and its regulation for greater resource use efficiency. *Plant, Cell and Environment*, **38**(9), 1817–1832.

Carver, B. F., Johnson, R. C., & Rayburn, A. L. (1989). Genetic analysis of photosynthetic variation in hexaploid and tetraploid wheat and their interspecific hybrids. *Photosynthesis Research*, **20**, 105–118.

Carver, B. F., & Nevo, E. (1990). Genetic diversity of photosynthetic characters in native populations of *Triticum dicoccoides*. *Photosynthesis Research*, **25**, 119–128.

Chanishvili, S. S., Badridze, G. S., Barblishvili, T. F., & Dolidze, M. D. (2005). Defoliation, photosynthetic rates, and assimilate transport in grapevine plants. *Russian Journal of Plant Physiology*, **52**(4), 448–453.

Chapman, V., & Riley, R. (1970). Homoeologous Meiotic Chromosome Pairing in *Triticum aestivum* in which Chromosome 5B is replaced by an Alien Homoeologue. *Nature*, **226**(5243), 376–377.

Chaudhary, H. K., Kaila, V., Rather, S. A., … Mahato, A. (2014). Wheat. In: *Alien Gene Transfer in Crop Plants, Volume 2*, New York, NY: Springer New York, pp. 1–26.

Civáň, P., Ivaničová, Z., & Brown, T. A. (2013). Reticulated origin of domesticated emmer wheat supports a dynamic model for the emergence of agriculture in the fertile crescent. *PLoS ONE*, **8**(11), 1–11.

Cockram, J., Jones, H., Leigh, F. J., … Greenland, A. J. (2007). Control of flowering time in temperate cereals: Genes, domestication, and sustainable productivity. *Journal of Experimental Botany*, **58**(6), 1231–1244.

Collard, B. C. Y., & Mackill, D. J. (2008). Marker-assisted selection: an approach for precision plant breeding in the twenty-first century. *Philosophical Transactions of the Royal Society B: Biological Sciences*, **363**(1491), 557–572.

Collard, B. C. Y., Jahufer, M. Z. Z., Brouwer, J. B., & Pang, E. C. K. (2005). An introduction to markers, quantitative trait loci (QTL) mapping and marker-assisted selection for crop improvement: The basic concepts. *Euphytica*, **142**, 169–196.

Condon, A. G., Richards, R. A., & Farquhar, G. D. (1987). Carbon Isotope Discrimination is Positively Correlated with Grain Yield and Dry Matter Production in Field-Grown Wheat. *Crop Science*, **27**(5), 996.

Condon, A. G., Richards, R. A., Rebetzke, G. J., & Farquhar, G. D. (2004). Breeding for high water-use efficiency. *Journal of Experimental Botany*, **55**(407), 2447–2460.

Cox, T. S. (1997). Deepening the Wheat Gene Pool. *Journal of Crop Production*, **1**(1), 1–25.

Curtis, T., & Halford, N. G. (2014). Food security: the challenge of increasing wheat yield and the importance of not compromising food safety. *Annals of Applied Biology*, **164**(3), 354–372.

Dawson, T. E., Mambelli, S., Plamboeck, A. H., Templer, P. H., & Tu, K. P. (2002). Stable Isotopes in Plant Ecology. *Annual Review of Ecology and Systematics*, **33**, 507–559.

De Miguel, M., Sánchez-Gómez, D., Cervera, M. T., & Aranda, I. (2012). Functional and genetic characterization of gas exchange and intrinsic water use efficiency in a full-sib family of *Pinus pinaster* Ait. in response to drought. *Tree Physiology*, **32**(1), 94–103.

del Blanco, I. A., Rajaram, S., Kronstad, W. E., & Reynolds, M. P. (2000). Physiological Performance of Synthetic Hexaploid Wheat-Derived Populations. *Crop Science*, **40**(1982), 1257.

Denćić, S. (1994). Designing a Wheat Ideotype with Increased Sink Capacity. *Plant Breeding*, **112**(4), 311–317.

Dhiman, S. D., Sharma, H. C., & Singh, R. P. (1980). Association between flag leaf area and grain yield in wheat. *Indian Journal of Plant Physiology*. **23**(3), 282-287.

Ding, H., Liu, D., Liu, X., … Wang, G. (2017). Photosynthetic and stomatal traits of spike and flag leaf of winter wheat (*Triticum aestivum* L.) under water deficit. *Photosynthetica*, **55**(X), 1–11.

Diouf, J. (2009). FAO's Director-General on How to Feed the World in 2050. *Population and Development Review*, **35**(4), 837–839.

Doerge, R. W. (2002). Mapping and analysis of quantitative trait loci in experimental populations. *Nature Reviews Genetics*, **3**(1), 43–52.

Donald, C. M. (1968). The breeding of crop ideotypes. *Euphytica*, **17**(3), 385–403.

Drake, B. G., Gonzàlez-Meler, M. A., & Long, S. P. (1997). More efficient plants: A Consequence of Rising Atmospheric CO_2 ? *Annual Review of Plant Physiology and*

Plant Molecular Biology, **48**(1), 609–639.

Drewry, D. T., Kumar, P., Long, S., Bernacchi, C., Liang, X. Z., & Sivapalan, M. (2010). Ecohydrological responses of dense canopies to environmental variability: 1. Interplay between vertical structure and photosynthetic pathway. *Journal of Geophysical Research: Biogeosciences*, **115**(4), 1–25.

Driever, S. M., Lawson, T., Andralojc, P. J., Raines, C. A., & Parry, M. A. J. (2014). Natural variation in photosynthetic capacity, growth, and yield in 64 field-grown wheat genotypes. *Journal of Experimental Botany*, **65**(17), 4959–4973.

Dudley, J. W., & Moll, R. H. (1969). Interpretation and Use of Estimates of Heritability and Genetic Variances in Plant Breeding. *Crop Science*, **9**(3), 257.

Dunstone, R. L., & Evans, L. T. (1974). Role of Changes in Cell Size in the Evolution of Wheat. *Functional Plant Biology*, **1**(1), 157–165.

Dunstone, R. L., Gifford, R. M., & Evans, L. T. (1973). Photosynthetic charecteristics of modern and primitive wheat species in relation to Otogeny and Adaption to light. *Aust. J. Biol. Sci*, **26**(August 1972), 295–307.

Dvorák, J., Terlizzi, P., Zhang, H. B., & Resta, P. (1993). The evolution of polyploid wheats: identification of the A genome donor species. *Genome*, **36**(1), 21–31.

Ebadi-Segherloo, A., Mohammadi, S. A., Sadeghzadeh, B., & Kamrani, M. (2016). Study of Heritability and Genetic Advance of Agronomic Traits in Barley (*Hordeum vulgare L.*) and Graphic Analysis of Trait Relations by Biplot. *Jordan Journal of Agricultural Sciences*, **12**(1), 299–310.

Edwards, G. E., & Baker, N. R. (1993). Can CO_2 assimilation in maize leaves be predicted accurately from chlorophyll fluorescence analysis? *Photosynthesis Research*, **37**(2), 89–102.

Ergen, N. Z., Thimmapuram, J., Bohnert, H. J., & Budak, H. (2009). Transcriptome pathways unique to dehydration tolerant relatives of modern wheat. *Functional and Integrative Genomics*, **9**(3), 377–396.

Evangelista, D., Hotton, S., & Dumais, J. (2011). The mechanics of explosive dispersal and self-burial in the seeds of the filaree, *Erodium cicutarium* (Geraniaceae). *Journal of Experimental Biology*, **214**(4), 521–529.

Evans, J. R. (1983). Nitrogen and Photosynthesis in the Flag Leaf of Wheat (*Triticum*

aestivum L.). *Plant Physiology*, **72**, 297–302.

Evans, J. R. (1989). Photosynthesis and nitrogen relationship in leaves of C3 plants. *Oecologia*, **78**, 9–19.

Evans, J. R., Kaldenhoff, R., Genty, B., & Terashima, I. (2009). Resistances along the CO_2 diffusion pathaway inside leaves. *Journal of Experimental Botany*, **60**(8), 2235–2248.

Evans, J. R., & Poorter, H. (2001). Photosynthetic acclimation of plants to growth irradiance: The relative importance of specific leaf area and nitrogen partitioning in maximizing carbon gain. *Plant, Cell and Environment*, **24**(8), 755–767.

Evans, J. R., & Von Caemmerer, S. (1996). Carbon Dioxide Diffusion inside Leaves. *Plant Physiology*, **110**(2), 339–346.

Evans, L. T., Bingham, J., Jackson, P., & Sutherland, J. (1972). Effect of awns and drought on the supply of photosynthate and its distribution within wheat ears. *Annals of Applied Biology*, **70**(1), 67–76.

Evans, L. T., & Dunstone, R. L. (1970). Some Physiological Aspects of Evolution in Wheat. *Australian Journal of Biology Science*, **23**, 725–742.

Evans, L. T., Evans, L. T., Peacock, W. J., & Frankel, O. H. (1981). Wheat Science - Today and Tomorrow, Cambridge: Cambridge University Press.

Evans, L. T., & Fisher, R. A. (1999). Yield potential: Its definition, measurement, and significance. *Crop Science*, **39**(6), 1544–1551.

Falconer, D. S. (1960). *Introduction to Quantitative Genetics*, Edinburgh and London: Oliver and Boyd.

FAO. (1996). Rome Declaration on World Food Security and World Food Summit Plan of Action. In *World Food Summit*, Rome: FAO.

FAO. (2018a). *Crop Prospects and Food Situation. Quarterly Global Report. Global Information and Early Warning System on Food and Agriculture.*, Rome. Retrieved from http://www.fao.org/3/i8764en/I8764EN.pdf

FAO. (2018b). FAO Cereal Supply and Demand Brief. Retrieved from http://www.fao.org/worldfoodsituation/csdb/en/

FAO, IFAD, UNICEF, WFD and WHO (2017). *The State of Food Security and Nutrition in the World 2017. Building resilience for peace and food security.*, Rome, FAO.

Retrieved from http://www.fao.org/state-of-food-security-nutrition/en/

Faris, J. D., Zhang, Z., Garvin, D. F., & Xu, S. S. (2014). Molecular and comparative mapping of genes governing spike compactness from wild emmer wheat. *Molecular Genetics and Genomics*, **289**(4), 641–651.

Farquhar, G. D., Ehleringer, J. R., & Hubick, K. T. (1989). Carbon Isotope Discrimination and Photosynthesis. *Annual Review of Plant Physiology and Plant Molecular Biology*, **40**, 503–537.

Farquhar, G. D., & Richards, R. A. (1984). Isotopic Composition of Plant Carbon Correlates With Water-Use Efficiency of Wheat Genotypes. *Functional Plant Biology*, **11**(6), 539–552.

Farquhar, G. D., von Caemmerer, S., & Berry, J. A. (1980). A biochemical model of photosynthetic CO_2 assimilation in leaves of C3 species. *Planta*, **149**(1), 78–90.

Farquhar, G., O'Leary, M., & Berry, J. (1982). On the Relationship Between Carbon Isotope Discrimination and the Intercellular Carbon Dioxide Concentration in Leaves. *Australian Journal of Plant Physiology*, **9**(2), 121.

Feldman, M., Liu, B., Segal, G., Abbo, S., Levy, A. A., & Vega, J. M. (1997). Rapid elimination of low-copy DNA sequences in polyploid wheat: A possible mechanism for differentiation of homoeologous chromosomes. *Genetics*, **147**(3), 1381–1387.

Ferrão, L. F. V., Benevenuto, J., Oliveira, I. de B., … Munoz, P. (2018). Insights Into the Genetic Basis of Blueberry Fruit-Related Traits Using Diploid and Polyploid Models in a GWAS Context. *Frontiers in Ecology and Evolution*, **6**. 1-16.

Fischer, R. A., Bidinger, F., Syme, J. R., & Wall, P. C. (1981). Leaf Photosynthesis, Leaf Permeability, Crop Growth, and Yield of Short Spring Wheat Genotypes Under Irrigation. *Crop Science*, **21**, 367–373.

Fischer, R. A., Rees, D., Sayre, K. D., Lu, Z. M., Condon, A. G., & Larque Saavedra, A. (1998). Wheat yield progress associated with higher stomatal conductance and photosynthetic rate, and cooler canopies. *Crop Science*, **38**(6), 1467–1475.

Fleischer, W. E. (1935). The Relation Between Chlorophyll Content and Rate of Photosynthesis. *The Journal of General Physiology*, **18**, 573–597.

Flexas, J., Barbour, M. M., Brendel, O., … Warren, C. R. (2012). Mesophyll diffusion conductance to CO_2: an unappreciated central player in photosynthesis. *Plant*

Science : An International Journal of Experimental Plant Biology, **193**–**194**, 70–84.

Flexas, J., Díaz-Espejo, a., Berry, J. a., … Ribas-Carbó, M. (2007). Analysis of leakage in IRGA's leaf chambers of open gas exchange systems: Quantification and its effects in photosynthesis parameterization. *Journal of Experimental Botany*, **58**(6), 1533–1543.

Flexas, J., Ribas-Carbó, M., Diaz-Espejo, A., Galmés, J., & Medrano, H. (2008). Mesophyll conductance to CO_2: Current knowledge and future prospects. *Plant, Cell and Environment*, **31**, 602–621.

Flexas, J., Scoffoni, C., Gago, J., & Sack, L. (2013). Leaf mesophyll conductance and leaf hydraulic conductance: An introduction to their measurement and coordination. *Journal of Experimental Botany*, **64**(13), 3965–3981.

Fortineau, A., & Bancal, P. (2018). An innovative light chamber for measuring photosynthesis by three-dimensional plant organs. *Plant Methods*, **14**(1), 1–12.

Foulkes, M. J., Slafer, G. A., Davies, W. J., … Reynolds, M. P. (2011). Raising yield potential of wheat. III. Optimizing partitioning to grain while maintaining lodging resistance. *Journal of Experimental Botany*, **62**(2), 469–486.

Franks, P. J., Drake, P. L., & Beerling, D. J. (2009). Plasticity in maximum stomatal conductance constrained by negative correlation between stomatal size and density: An analysis using Eucalyptus globulus. *Plant, Cell and Environment*, **32**(12), 1737–1748.

Fulton, T., Chunwongse, J., & Tanksley, S. (1995). Microprep protocol for extraction of DNA from tomato and other herbaceous plants. *Plant Molecular Biology …*, **13**(3), 207–209.

Gaju, O., DeSilva, J., Carvalho, P., … Foulkes, M. J. (2016). Leaf photosynthesis and associations with grain yield, biomass and nitrogen-use efficiency in landraces, synthetic-derived lines and cultivars in wheat. *Field Crops Research*, **193**, 1–15.

Galmés, J., Flexas, J., Keys, A. J., … Parry, M. A. J. (2005). Rubisco specificity factor tends to be larger in plant species from drier habitats and in species with persistent leaves. *Plant, Cell and Environment*, **28**(5), 571–579.

Gardner, K. A., Wittern, L. M., & Mackay, I. J. (2016). A highly recombined, high-density, eight-founder wheat MAGIC map reveals extensive segregation distortion and genomic locations of introgression segments. *Plant Biotechnology Journal*,

14(6), 1406–1417.

Garnier, E., Shipley, B., Roumet, C., & Laurent, G. (2001). A standardized protocol for the determination of specific leaf area and leaf dry matter content. *Functional Ecology*, **15**(5), 688–695.

Gebbing, T., & Schnyder, H. (2001). Labeling kinetics of sucrose in glumes indicates significant refixation of respiratory CO2 in the wheat ear. *Australian Journal of Plant Physiology*, **28**(10), 1047–1053.

Genty, B., Briantais, J.-M., & Baker, N. R. (1989). The relationship between the quantum yield of photosynthetic electron transport and quenching of chlorophyll fluorescence. *Biochimica et Biophysica Acta (BBA) - General Subjects*, **990**(1), 87–92.

Gilbert, M. E., Zwieniecki, M. a., & Holbrook, N. M. (2011). Independent variation in photosynthetic capacity and stomatal conductance leads to differences in intrinsic water use efficiency in 11 soybean genotypes before and during mild drought. *Journal of Experimental Botany*, **62**(8), 2875–2887.

Gillon, J., Borland, A., Harwood, K., Roberts, A., Broadmeadow, M. S., & Griffiths, H. (1998). Carbon isotope discrimination in terrestrial plants: carboxylation and decarboxylations. In H. Griffiths, ed., *Stable Isotopes integration of biological, ecological and geochemical processes*, Oxford: Bios Scientific Publishers, pp. 111–131.

Glover, N. M., Redestig, H., & Dessimoz, C. (2016). Homoeologs: What Are They and How Do We Infer Them? *Trends in Plant Science*, **21**(7), 609–621.

Goncharov, N. P., Mitina, R. L., & Anfilova, N. A. (2003). Inheritance of awnlessness in tetraploid wheat species. *Russian Journal of Genetics*, **39**(4), 463–466.

Grassini, P., Eskridge, K. M., & Cassman, K. G. (2013). Distinguishing between yield advances and yield plateaus in historical crop production trends. *Nature Communications*, **4**, 1–11.

Griffiths, A. J. F., Gelbart, W. M., Miller, J. H., & Lewontin, R. C. (1999). Inheritance of Organelle Genes. In *Modern Genetic Analysis*, New York, NY: W. H. Freeman.

Gu, J., Yin, X., Stomph, T. J., Wang, H., & Struik, P. C. (2012). Physiological basis of genetic variation in leaf photosynthesis among rice (Oryza sativa L.) introgression lines under drought and well-watered conditions. *Journal of Experimental Botany*,

63(14), 5137–5153.

Guitman, M. R., Arnozis, P. A., & Barneix, A. J. (1991). Effect of source-sink relations and nitrogen nutrition on senescence and N remobilization in the flag leaf of wheat. *Physiologia Plantarum*, **82**(2), 278–284.

Guo, Z., & Schnurbusch, T. (2016). Costs and benefits of awns. *Journal of Experimental Botany*, **67**(9), 2533–2535.

Gupta, P. K., Langridge, P., & Mir, R. R. (2010). Marker-assisted wheat breeding: Present status and future possibilities. *Molecular Breeding*, **26**(2), 145–161.

Gusmini, G., & Wehner, T. C. (2007). Heritability and genetic variance estimates for fruit weight in watermelon. *HortScience*, **42**(6), 1332–1336.

Haggard, J. E., Johnson, E. B., & St. Clair, D. A. (2013). Linkage Relationships Among Multiple QTL for Horticultural Traits and Late Blight (*P. infestans*) Resistance on Chromosome 5 Introgressed from Wild Tomato *Solanum habrochaites*. *G3. Genes|Genomes|Genetics*, **3**(12), 2131–2146.

Hall, D. O., & Rao, K. K. (1994). *Photosynthesis*, Cambridge: Cambridge University Press.

Harley, P. C., Loreto, F., Di Marco, G., & Sharkey, T. D. (1992). Theoretical Considerations when Estimating the Mesophyll Conductance to CO_2 Flux by Analysis of the Response of Photosynthesis to CO_2. *Plant Physiology*, **98**(4), 1429–36.

Haudry, A., Cenci, A., Ravel, C., … David, J. (2007). Grinding up Wheat: A Massive Loss of Nucleotide Diversity Since Domestication. *Molecular Biology and Evolution* , **24**(7), 1506–1517.

Hetherington, A. M., & Woodward, F. I. (2003). The role of stomata in sensing and driving environmental change. *Nature*, **424**(6951), 901–908.

HGCA. (2013). Wheat Pocketbook 2013/14. *HGCA Recommended List*.

Hill, W. G. (2010). Understanding and using quantitative genetic variation. *Philosophical Transactions of the Royal Society B: Biological Sciences*, **365**(1537), 73–85.

Hoogendoorn, J. (1985). The Physiology of Variation in the Time of Ear Emergence Among Wheat Varieties from Different Regions of the Worls. *Euphytica*, **34**, 559–571.

Horton, P. (2000). Prospects for crop improvement through the genetic manipulation of photosynthesis: morphological and biochemical aspects of light capture. *Journal of Experimental Botany*, **51**(1), 475–485.

Hospital, F., & Charcosset, A. (1997). Marker-assisted introgression of quantitative trait loci. *Genetics*, **147**(3), 1469–1485.

Hospital, F., Moreau, L., Lacoudre, F., Charcosset, A., & Gallais, A. (1997). More on the efficiency of marker-assisted selection. *Theoretical and Applied Genetics*, **95**(8), 1181–1189.

Huang, X., & Han, B. (2014). Natural Variations and Genome-Wide Association Studies in Crop Plants. *Annual Review of Plant Biology*, **65**(1), 531–551.

Hughes, J., Hepworth, C., Dutton, C., … Gray, J. E. (2017). Reducing Stomatal Density in Barley Improves Drought Tolerance without Impacting on Yield. *Plant Physiology*, **174**(2), 776–787.

Hussain, W., Stephen Baenziger, P., Belamkar, V., … Poland, J. (2017). Genotyping-by-Sequencing Derived High-Density Linkage Map and its Application to QTL Mapping of Flag Leaf Traits in Bread Wheat. *Scientific Reports*, **7**(1), 1–15.

International Wheat Genome Sequencing Consortium (IWGSC). (2014). A chromosome-based draft sequence of the hexaploid bread wheat (*Triticum aestivum*) genome. *Science (New York, N.Y.)*, **345**(6194), 1251788.

IWGSC. (2018). Shifting the limits in wheat research and breeding through a fully annotated and anchored reference genome sequence. *Science*, **7191**. doi:10.1126/science.aar7191

Jackson, P., Robertson, M., Cooper, M., & Hammer, G. (1996). The role of physiological understanding in plant breeding; From a breeding perspective. *Field Crops Research*, **49**(1), 11–37.

Jahan, E., Amthor, J. S., Farquhar, G. D., Trethowan, R., & Barbour, M. M. (2014). Variation in mesophyll conductance among Australian wheat genotypes. *Functional Plant Biology*, pp. 568–580.

James, S. a, & Bell, D. T. (2000). Influence of light availability on leaf structure and growth of two *Eucalyptus globulus* ssp. *globulus provenances*. *Tree Physiology*, **20**(15), 1007–1018.

JIC, WISP, & DFW. (2018). The AE Watkins bread wheat landrace collection and the diverse Core Set. Retrieved from http://wisplandracepillar.jic.ac.uk

Joggi, D., Hofer, U., & Nosberger, J. (1983). Leaf area index, canopy structure and photosynthesis of red clover (*Trifolium pratense* L.). *Plant, Cell and Environment*, **6**(8), 611–616.

Johnson, R. C., Kebede, H., Mornhinweg, D. W., Carver, B. F., Rayburn, A. L., & Nguyen, H. T. (1987a). Photosynthetic Differences Among *Triticum* Accessions At Tillering. *Crop Science*, **27**(5), 1046–1050.

Johnson, R. C., Mornhinweg, D. W., Ferris, D. M., & Heitholt, J. J. (1987b). Leaf photosynthesis and conductance of selected *Triticum* species at different water potentials. *Plant Physiology*, **83**(4), 1014–7.

Jones, H., Civá, P., Cockram, J., … Brown, T. A. (2011). Evolutionary history of barley cultivation in Europe revealed by genetic analysis of extant landraces. *BMC Evolutionary Biology*, **11**(1). doi:10.1186/1471-2148-11-320

Kabbaj, H., Sall, A. T., Al-Abdallat, A., … Bassi, F. M. (2017). Genetic Diversity within a Global Panel of Durum Wheat (*Triticum durum*) Landraces and Modern Germplasm Reveals the History of Alleles Exchange. *Frontiers in Plant Science*, **8**(July), 1–13.

Kamran, A., Iqbal, M., & Spaner, D. (2014). Flowering time in wheat (*Triticum aestivum* L.): A key factor for global adaptability. *Euphytica*, **197**(1), 1–26.

Kamran, A., Iqbal, M., Navabi, A., Randhawa, H., Pozniak, C., & Spaner, D. (2013). Earliness *per se* QTLs and their interaction with the photoperiod insensitive allele *Ppd-D1a* in the Cutler × AC Barrie spring wheat population. *Theoretical and Applied Genetics*, **126**(8), 1965–1976.

Kenney, A. M., Mckay, J. K., Richards, J. H., & Juenger, T. E. (2014). Direct and indirect selection on flowering time, water-use efficiency (*WUE*, $\delta^{13}C$), and *WUE* plasticity to drought in *Arabidopsis thaliana*. *Ecology and Evolution*, **4**(23), 4505–4521.

Khaliq, I., Irshad, A., & Ahsan, M. (2008). Awns and Flag Leaf Contribution Towards Grain Yield in Spring Wheat (*Triticum aestivum* L.). *Cereal Research Communications*, **36**(1), 65–76.

Khan, M. A., & Tsunoda, S. (1970). Evolutionary trends in leaf photosynthesis and related leaf characters among cultivated wheat species and its wild relatives.

Japanese Journal of Breeding, **20**(3), 133–140.

Khazaei, H., Monneveux, P., Hongbo, S., & Mohammady, S. (2009). Variation for stomatal characteristics and water use efficiency among diploid, tetraploid and hexaploid Iranian wheat landraces. *Genetic Resources and Crop Evolution*, **57**(2), 307–314.

Khlestkina, E. K., Giura, A., Röder, M. S., & Börner, A. (2009). A new gene controlling the flowering response to photoperiod in wheat. *Euphytica*, **165**(3), 579–585.

Khush, G. S. (1995). Modern varieties? Their real contribution to food supply and equity. *GeoJournal*, **35**(3), 275–284.

Khush, G. S. (2001). Green revolution: the way forward. *Nature Reviews. Genetics*, **2**(October), 815–822.

Knoppik, D., Selinger, H., & Ziegler-Jöns, A. (1986). Differences between the flag leaf and the ear of a spring wheat cultivar (*Triticum aestivum* cv. Arkas) with respect to the CO_2 response of assimilation, respiration and stomatal conductance. *Physiologia Plantarum*, **68**(3), 451–457.

Koebner, R. M. D., & Summers, R. W. (2003). 21st century wheat breeding: Plot selection or plate detection? *Trends in Biotechnology*, **21**(2), 59–63.

Konvalina, P., Capouchová, I., Stehno, Z., & Moudrý, J. (2011). Variation for carbon isotope ratio in a set of emmer (*Triticum dicoccum* Schrank) and bread wheat (*Triticum aestivum* L .) accessions. *African Journal of Biotechnology*, **10**(21), 4450–4456.

Kromdijk, J., Griffiths, H., & Schepers, H. E. (2010). Can the progressive increase of C_4 bundle sheath leakiness at low PFD be explained by incomplete suppression of photorespiration? *Plant, Cell and Environment*, **33**(11), 1935–1948.

Kumar, N., & Rustgi, S. (2014). Agronomically Relevant Traits Transferred to Major Crop Plants by Alien Introgressions. In A. Pratap & J. Kumar, eds., *Alien Gene Transfer in Crop Plants, Volume 1: Innovations, Methods and Risk Assessment*, New York, NY: Springer New York, pp. 211–245.

Langer, S. M., Longin, C. F. H., & Würschum, T. (2014). Flowering time control in European winter wheat. *Frontiers in Plant Science*, **5**(October), 1–11.

Law, C. N., Sutka, J., & Worland, a. J. (1978). A genetic study of day-length response in

wheat. *Heredity*, **41**(2), 185–191.

Lawlor, D. W., & Cornic, G. (2002). Photosynthetic carbon assimilation and associated metabolism in relation to water deficits in higher plants. *Plant, Cell & Environment*, **25**(Evans 1998), 275–294.

Lawson, T., & Blatt, M. R. (2014). Stomatal Size, Speed, and Responsiveness Impact on Photosynthesis and Water Use Efficiency. *Plant Physiology*, **164**(4), 1556–1570.

Lawson, T., Kramer, D. M., & Raines, C. A. (2012). Improving yield by exploiting mechanisms underlying natural variation of photosynthesis. *Current Opinion in Biotechnology*, **23**(2), 215–220.

Lawson, T., Simkin, A. J., Kelly, G., & Granot, D. (2014). Mesophyll photosynthesis and guard cell metabolism impacts on stomatal behaviour. *New Phytologist*, **203**(4), 1064–1081.

Leigh, F. J., Mackay, I., Oliveira, H. R., … Brown, T. a. (2013). Using diversity of the chloroplast genome to examine evolutionary history of wheat species. *Genetic Resources and Crop Evolution*, **60**, 1831–1842.

Leister, D. (2012). How Can the Light Reactions of Photosynthesis be Improved in Plants? *Frontiers in Plant Science*, **3**(August), 1–3.

Li-Cor. (2012). *Manual*. *Using the LI-6400/Version 6*, 6th edn, Nebraska: LI-COR Biosciences, Inc. Retrieved from www.licor.com

Li, H., Ye, G., & Wang, J. (2007). A Modified Algorithm for the Improvement of Composite Interval Mapping. *Genetics*, **175**(1), 361–374.

Li, J., Wan, H. S., & Yang, W. Y. (2014). Synthetic hexaploid wheat enhances variation and adaptive evolution of bread wheat in breeding processes. *Journal of Systematics and Evolution*, **52**(6), 735–742.

Li, L., Zhang, X., & Zhao, H. (2012). eQTL. In S. A. Rifkin, ed., *Quantitative Trait Loci (QTL): Methods and Protocols*, Totowa, NJ: Humana Press, pp. 265–279.

Li, X., Wang, H., Li, H., … Lin, J. (2006). Awns play a dominant role in carbohydrate production during the grain-filling stages in wheat (*Triticum aestivum*). *Physiologia Plantarum*, **127**(4), 701–709.

Li, Y. P., Li, Y. Y., Li, D. Y., Wang, S. W., & Zhang, S. Q. (2017). Photosynthetic response of tetraploid and hexaploid wheat to water stress. *Photosynthetica*, **55**(3),

1–13.

Limpens, J., Granath, G., Aerts, R., … Xu, B. (2012). Glasshouse vs field experiments: Do they yield ecologically similar results for assessing N impacts on peat mosses? *New Phytologist*, **195**(2), 408–418.

Lin, M. T., Occhialini, A., Andralojc, P. J., Parry, M. A. J., & Hanson, M. R. (2014). A faster Rubisco with potential to increase photosynthesis in crops. *Nature*, **513**(7519), 547–550.

Lincoln, S. E., & Lander, E. S. (1992). Systematic detection of errors in genetic linkage data. *Genomics*, **14**(3), 604–610.

Liu, K., Xu, H., Liu, G., … Du, J. (2018). QTL mapping of flag leaf-related traits in wheat (*Triticum aestivum* L.). *Theoretical and Applied Genetics*. **131**(4), 839-849.

Liu, T., Huang, R., Cai, T., Han, Q., & Dong, S. (2017). Optimum Leaf Removal Increases Nitrogen Accumulation in Kernels of Maize Grown at High Density. *Scientific Reports*, **7**, 1–10.

Long, S. P., & Bernacchi, C. J. (2003). Gas exchange measurements, what can they tell us about the underlying limitations to photosynthesis? Procedures and sources of error. *Journal of Experimental Botany*, **54**(392), 2393–2401.

Long, S. P., Farage, P. K., & Garcia, R. L. (1996). Measurement of leaf and canopy photosynthesic CO_2 exchange in the field. *Journal of Experimental Botany*, **47**(304), 1629–1642.

Long, S. P., Zhu, X.-G., Naidu, S. L., & Ort, D. R. (2006). Can improvement in photosynthesis increase crop yields? *Plant, Cell and Environment*, **29**(3), 315–330.

Lopes, M. S., El-Basyoni, I., Baenziger, P. S., … Vikram, P. (2015). Exploiting genetic diversity from landraces in wheat breeding for adaptation to climate change. *Journal of Experimental Botany*, **66**(12), 3477–3486.

Loreto, F., Harley, P. C., Di Marco, G., & Sharkey, T. D. (1992). Estimation of Mesophyll Conductance to CO_2 Flux by Three Different Methods. *Plant Physiology*, **98**(4), 1437–1443.

Loriaux, S. D., Avenson, T. J., Welles, J. M., … Genty, B. (2013). Closing in on maximum yield of chlorophyll fluorescence using a single multiphase flash of sub-saturating intensity. *Plant, Cell and Environment*, **36**(10), 1755–1770.

Lucas, S. J., Salantur, A., Yazar, S., & Budak, H. (2017). High-throughput SNP genotyping of modern and wild emmer wheat for yield and root morphology using a combined association and linkage analysis. *Functional and Integrative Genomics*, **17**(6), 667–685.

Luo, M. C., Yang, Z. L., You, F. M., Kawahara, T., Waines, J. G., & Dvorak, J. (2007). The structure of wild and domesticated emmer wheat populations, gene flow between them, and the site of emmer domestication. *Theoretical and Applied Genetics*, **114**(6), 947–959.

Lupton, F. G. H., & Ali, M. A. M. (1966). Studies on photosynthesis in the ear of wheat. *Annals of Applied Biology*, **57**(2), 281–286.

Maccaferri, M., Sanguineti, M. C., Corneti, S., … Tuberosa, R. (2008). Quantitative trait loci for grain yield and adaptation of durum wheat (*Triticum durum* Desf.) across a wide range of water availability. *Genetics*, **178**(1), 489–511.

Mach, J. (2015). Domesticated versus wild rice? Bring it awn!: *The Plant Cell*, **27**(7), 1818–1818.

Mackay, I. J., Bansept-Basler, P., Barber, T., … Howell, P. J. (2014). An Eight-Parent Multiparent Advanced Generation Inter-Cross Population for Winter-Sown Wheat: Creation, Properties, and Validation. *G3. Genes|Genomes|Genetics*, **4**(9), 1603–1610.

Makino, A. (2011). Photosynthesis, Grain Yield, and Nitrogen Utilization in Rice and Wheat. *Plant Physiology*, **155**(1), 125–129.

Mangini, G., Gadaleta, A., Colasuonno, P., … Blanco, A. (2018). Genetic dissection of the relationships between grain yield components by genome-wide association mapping in a collection of tetraploid wheats. *PLOS ONE*, **13**(1), e0190162.

Marais, G. F., Pretorius, Z. A., Wellings, C. R., McCallum, B., & Marais, A. S. (2005). Leaf rust and stripe rust resistance genes transferred to common wheat from *Triticum dicoccoides*. *Euphytica*, **143**(1–2), 115–123.

Martinez-Perez, E., Shaw, P., Aragon-Alcaide, L., & Moore, G. (2003). Chromosomes form into seven groups in hexaploid and tetraploid wheat as a prelude to meiosis. *Plant Journal*, **36**(1), 21–29.

Martins, S. C. V, Galmés, J., Molins, A., & Damatta, F. M. (2013). Improving the estimation of mesophyll conductance to CO_2: On the role of electron transport rate

correction and respiration. *Journal of Experimental Botany*, **64**(11), 3285–3298.

Martre, P., Quilot-Turion, B., Luquet, D., Memmah, M.-M. O.-S., Chenu, K., & Debaeke, P. (2015). Model-assisted phenotyping and ideotype design. In *Crop Physiology*, Second Edi, Elsevier, pp. 349–373.

Maxwell, K., & Johnson, G. N. (2000). Chlorophyll fluorescence—a practical guide. *Journal of Experimental Botany* , **51**(345), 659–668.

Maydup, M. L., Antonietta, M., Graciano, C., Guiamet, J. J., & Tambussi, E. A. (2014). The contribution of the awns of bread wheat (*Triticum aestivum* L.) to grain filling: Responses to water deficit and the effects of awns on ear temperature and hydraulic conductance. *Field Crops Research*, **167**, 102–111.

McClendon, J. H. (1962). The Relationship Between the Thickness of Deciduous Leaves and their Maximum Photosynthetic Rate. *American Journal of Botany*, **49**(4), 320.

McFadden, E., & Sears, E. (1946). The origin of *Triticum spelta* and its free-threshing hexaploid relatives. *Journal of Heredity*. Retrieved from http://jhered.oxfordjournals.org/content/37/4/107.extract

Mcintosh, R., Dubcovsky, J., Rogers, W. J., Morris, C. ., Appels, R., & Xia, X. C. (2013). Catalogue of Gene Symbols for Wheat. In *12th International Wheat Genetics Symposium*, Yokohama, Japan.

McKenzie, H. (1972). Adverse Influence of Awns on Yield of Wheat. *Canadian Journal of Plant Science*, **52**(1), 81–87.

Mellers, G., & Wright, T. (2017). Unlocking the photosynthetic potential of wheat. *NIABTAG Landmark*, **September**(31), 12–13.

Merchuk-Ovnat, L., Barak, V., Fahima, T., … Saranga, Y. (2016a). Ancestral QTL Alleles from Wild Emmer Wheat Improve Drought Resistance and Productivity in Modern Wheat Cultivars. *Frontiers in Plant Science*, **7**(April), 452.

Merchuk-Ovnat, L., Fahima, T., Krugman, T., & Saranga, Y. (2016b). Ancestral QTL alleles from wild emmer wheat improve grain yield, biomass and photosynthesis across enviroinments in modern wheat. *Plant Science*, **251**, 23–34.

Milach, S. C. K., & Federizzi, L. C. (2001). Dwarfing genes in plant improvement. In *Advances in Agronomy*, Vol. 73, pp. 35–63.

Miralles, D. J., & Slafer, G. A. (2007). Paper Presented at International Workshop on

Increasing Wheat Yield Potential, CIMMYT, Obregon, Mexico, 20-24 March 2006. Sink limitations to yield in wheat: How could it be reduced? *Journal of Agricultural Science*, **145**(2), 139–149.

Mitchell, R. A. C., Black, C. R., Burkart, S., … Van Oijen, M. (1999). Photosynthetic responses in spring wheat grown under elevated CO_2 concentrations and stress conditions in the European, multiple-site experiment "ESPACE-wheat." *European Journal of Agronomy*, **10**(3–4), 205–214.

Monteith, J. L., & Moss, C. J. (1977). Climate and the Efficiency of Crop Production in Britain [and Discussion]. *Philosophical Transactions of the Royal Society B: Biological Sciences*, **281**(980), 277–294.

Moose, S. P., & Mumm, R. H. (2008). Molecular Plant Breeding as the Foundation for 21st Century Crop Improvement. *Plant Physiology*, **147**(3), 969–977.

Mu, X., Chen, Q., Chen, F., Yuan, L., & Mi, G. (2016). Within-Leaf Nitrogen Allocation in Adaptation to Low Nitrogen Supply in Maize during Grain-Filling Stage. *Frontiers in Plant Science*, **7**(May), 1–11.

Mujeeb-Kazi, A., Kazi, A. G., Dundas, I., … Farrakh, S. (2013). *Genetic diversity for wheat improvement as a conduit to food security*. *Advances in Agronomy*, 1st edn, Vol. 122, Elsevier Inc.

Murchie, E. H., & Lawson, T. (2013). Chlorophyll fluorescence analysis: A guide to good practice and understanding some new applications. *Journal of Experimental Botany*, **64**(13), 3983–3998.

Murchie, E. H., Pinto, M., & Horton, P. (2009). Agriculture and the new challenges for photosynthesis research. *The New Phytologist*, **181**(3), 532–52.

nabim. (2018). *Wheat Guide 2018*, National Association of British & Irish Millers, London.

Nadeem, M. A., Nawaz, M. A., Shahid, M. Q., … Baloch, F. S. (2017). DNA molecular markers in plant breeding: current status and recent advancements in genomic selection and genome editing. *Biotechnology & Biotechnological Equipment*, **2818**, 1–25.

Nesbitt, M., & Samuel, D. (1996). From staple crop to extinction? The archaeology and history of the hulled wheats. *Proceedings of the First International Workshop on Hulled Wheats*, **4**(July), 41–100.

Nevo, E. (2014). Evolution of wild emmer wheat and crop improvement, **52**(6), 673–696.

Nevo, E., Carver, B. F., & Beiles, a. (1991). Photosynthetic performance in wild emmer wheat, *Triticum dicoccoides*: ecological and genetic predictability. *Theoretical and Applied Genetics*, **81**, 445–460.

Nevo, E., & Chen, G. (2010). Drought and salt tolerances in wild relatives for wheat and barley improvement. *Plant, Cell and Environment*, **33**(4), 670–685.

Nevo, E., Gorham, J., & Beiles, A. (1992). Variation for ^{22}Na Uptake in Wild Emmer Wheat, *Triticum dicoccoides* in Israel: Salt Tolerance Resources for Wheat Improvement. *Journal of Experimental Botany*, **43**(4), 511–518.

Nevo, E., Korol, A. B., Beiles, A., & Fahima, T. (2002). *Evolution of Wild Emmer and Wheat Improvement*, Berlin, Heidelberg: Springer Berlin Heidelberg.

Nobel, P. S. (2005). *Physicochemical and Environmental Plant Physiology*, Third Edit, United States: Burlington, MA: Elsevier.

Ober, E. S., Bloa, M. Le, Clark, C. J. A., Royal, A., Jaggard, K. W., & Pidgeon, J. D. (2005). Evaluation of physiological traits as indirect selection criteria for drought tolerance in sugar beet. *Field Crops Research*, **91**(2–3), 231–249.

Occhialini, A., Lin, M. T., Andralojc, P. J., Hanson, M. R., & Parry, M. A. J. (2016). Transgenic tobacco plants with improved cyanobacterial Rubisco expression but no extra assembly factors grow at near wild-type rates if provided with elevated CO_2. *The Plant Journal*, **85**(1), 148–160.

Oguchi, R., Hikosaka, K., & Hirose, T. (2003). Does the photosynthetic light-acclimation need change in leaf anatomy? *Plant, Cell and Environment*, **26**(4), 505–512.

Olugbemi, L. B., Austin, R. B., & Bingham, J. (1976a). Effects of awns on the photosynthesis and yield of wheat, *Triticum aestivum*. *Annals of Applied Biology*, **84**(2), 241–250.

Olugbemi, L. B., Bingham, J., & Austin, R. B. (1976b). Ear and flag leaf photosynthesis of awned and awnless Triticum species. *Annals of Applied Biology*, **84**(2), 231–240.

Orr, D., Alcântara, A., Kapralov, M. V, Andralojc, J., Carmo-Silva, E., & Parry, M. A. J. (2016). Surveying Rubisco diversity and temperature response to improve crop photosynthetic efficiency. *Plant Physiology*, **172**(October), 707-717.

Ouellette, L. A., Reid, R. W., Blanchard, S. G., & Brouwer, C. R. (2018).

LinkageMapView-rendering high-resolution linkage and QTL maps. *Bioinformatics*, **34**(2), 306–307.

Özkan, H., Brandolini, A., Schäfer-Pregl, R., & Salamini, F. (2002). AFLP Analysis of a Collection of Tetraploid Wheaats Indicates the Origin of Emmer and Hard Wheat Domestication in Southeast Turkey. *Molecular Biology and Evolution*, **19**(10), 1797–1801.

Parker, M. L., & Ford, M. A. (1982). The structure of the mesophyll of flag leaves in three *Triticum* species. *Ann. Bot.*, **49**, 165–176.

Parmar, A. (2015). Exploiting resource use efficiency and resilience traits in ancient wheat species, University of Nottingham, HGCA Student Report No . 29.

Parry, M. A. J., Andralojc, P. J., Scales, J. C., … Whitney, S. M. (2013). Rubisco activity and regulation as targets for crop improvement. *Journal of Experimental Botany*, pp. 717–730.

Parry, M. A. J., Madgwick, P. J., Carvalho, J. F. C., & Andralojc, P. J. (2007). Prospects for increasing photosynthesis by overcoming the limitations of Rubisco. *Journal of Agricultural Science*, **145**(1), 31–43.

Parry, M. A. J., Reynolds, M., Salvucci, M. E., … Furbank, R. T. (2011). Raising yield potential of wheat. II. Increasing photosynthetic capacity and efficiency. *Journal of Experimental Botany*, **62**(2), 453–467.

Pask, A.J.D., Pietragalla, J., Mullan, D.M. and Reynolds, M.P. (Eds.) (2012) Physiological Breeding II: A Field Guide to Wheat Phenotyping. Mexico, D.F., CIMMYT.

Peleg, Z., Fahima, T., Abbo, S., … Saranga, Y. (2005). Genetic diversity for drought resistance in wild emmer wheat and its ecogeographical associations. *Plant, Cell and Environment*, **28**(2), 176–191.

Peleg, Z., Fahima, T., Korol, A. B., Abbo, S., & Saranga, Y. (2011). Genetic analysis of wheat domestication and evolution under domestication. *Journal of Experimental Botany*, **62**(14), 5051–5061.

Peleg, Z., Fahima, T., Krugman, T., … Saranga, Y. (2009). Genomic dissection of drought resistance in durum wheat x wild emmer wheat recombinant inbreed line population. *Plant, Cell and Environment*, **32**(7), 758–779.

Peng, J. H., Sun, D. F., Peng, Y. L., & Nevo, E. (2012). Gene discovery in *Triticum dicoccoides*, the direct progenitor of cultivated wheats. *Cereal Research Communications*, **1**(1), 1–22.

Peng, J. H., Sun, D., & Nevo, E. (2011). Domestication evolution, genetics and genomics in wheat. *Molecular Breeding*, **28**, 281–301.

Peng, J., Korol, A. B., Fahima, T., … Nevo, E. (2000). Molecular Genetic Maps in Wild Emmer Wheat,. *Genome Research*, 1509–1531.

Peng, J., Ronin, Y., Fahima, T., … Korol, A. (2003). Domestication quantitative trait loci in *Triticum dicoccoides*, the progenitor of wheat. *Proceedings of the National Academy of Sciences*, **100**(5), 2489–2494.

Peng, S., Khush, G. S., Virk, P., Tang, Q., & Zou, Y. (2008). Progress in ideotype breeding to increase rice yield potential. *Field Crops Research*, **108**(1), 32–38.

Petersen, G., Seberg, O., Yde, M., & Berthelsen, K. (2006). Phylogenetic relationships of *Triticum* and *Aegilops* and evidence for the origin of the A, B, and D genomes of common wheat (*Triticum aestivum*). *Molecular Phylogenetics and Evolution*, **39**(1), 70–82.

Poorter, H., & Evans, J. R. (1998). Photosynthetic nirtogen-use efficiency of species that differ inherntly in specific leaf area. *Growth (Lakeland)*, 26–37.

Poorter, H., Fiorani, F., Pieruschka, R., … Postma, J. (2016). Pampered inside, pestered outside? Differences and similarities between plants growing in controlled conditions and in the field. *New Phytologist*, **212**(4), 838–855.

Preece, C., Livarda, A., Christin, P. A., … Osborne, C. P. (2017). How did the domestication of Fertile Crescent grain crops increase their yields? *Functional Ecology*, **31**(2), 387–397.

Price, A. L., Patterson, N. J., Plenge, R. M., Weinblatt, M. E., Shadick, N. A., & Reich, D. (2006). Principal components analysis corrects for stratification in genome-wide association studies. *Nature Genetics*, **38**(8), 904–909.

Prins, A., Orr, D. J., Andralojc, P. J., Reynolds, M. P., Carmo-Silva, E., & Parry, M. a J. (2016). Rubisco catalytic properties of wild and domesticated relatives provide scope for improving wheat photosynthesis. *Journal of Experimental Botany*, **67**(6), 1827–1838.

R Core Team. (2017). R: A Language and Environment for Statistical Computing, Vienna, Austria. Retrieved from https://www.r-project.org/

Raines, C. A. (2003). The Calvin cycle revisited. *Photosynthesis Research*, **75**, 1–10.

Rajabi, A., Ober, E. S., & Griffiths, H. (2009). Genotypic variation for water use efficiency, carbon isotope discrimination, and potential surrogate measures in sugar beet. *Field Crops Research*, **112**, 172–181.

Rao, M. V. P. (1981). Telocentric mapping of the awn inhibitor gene *hd* on chromosome 4B of common wheat. *Cereal Research Communications*, **9**(4), 335–337.

Rao, S. D. (1992). Flag leaf a selection criterion for exploiting potential yields in rice. *Indian. J. Plant. Physio.*, **25**(3), 265–268.

Rasmusson, D. C. (1991). A plant breeder's experience with ideotype breeding. *Field Crops Research*, **26**(2), 191–200.

Raven, J. A., & Griffiths, H. (2015). Photosynthesis in reproductive structures: costs and benefits. *Journal of Experimental Botany*, **66**(7), 1699–1705.

Rawson, H. (1970). Spikelet Number, Its Control and Relation to Yield Per Ear in Wheat. Australian Journal of Biological Sciences, **23**(1), 1-15.

Ray, D. K., Mueller, N. D., West, P. C., & Foley, J. A. (2013). Yield Trends Are Insufficient to Double Global Crop Production by 2050. *PLoS ONE*, **8**(6). doi:10.1371/journal.pone.0066428

Read, J., & Farquhar, G. (1991). Comparative Studies in *Nothofagus* (Fagaceae). I. Leaf Carbon Isotope Discrimination. *Functional Ecology*, **5**(5), 684.

Rebetzke, G. J., Bonnett, D. G., & Reynolds, M. P. (2016). Awns reduce grain number to increase grain size and harvestable yield in irrigated and rainfed spring wheat. *Journal of Experimental Botany*, **67**(9), 2573–2586.

Rebetzke, G. J., Condon, A. G., Richards, R. A., & Read, J. J. (2001). Phenotypic variation and sampling for leaf conductance in wheat (*Triticum aestivum* L.) breeding populations. *Euphytica*, **121**, 335–341.

Rebetzke, G. J., Read, J. J., Barbour, M. M., Condon, A. G., & Rawson, H. M. (2000). A hand-held porometer for rapid assessment of leaf conductance in wheat. *Crop Science*, **40**, 277–280.

Remigereau, M. S., Lakis, G., Rekima, S., … Robert, T. (2011). Cereal domestication

and evolution of branching: Evidence for Soft Selection in the *Tb1* orthologue of Pearl Millet (*Pennisetum glaucum* [L.] R. Br.). *PLoS ONE*, **6**(7).

Reynolds, M. ., Delgado B, M. ., Gutiérrez-Rodríguez, M., & Larqué-Saavedra, A. (2000). Photosynthesis of wheat in a warm, irrigated environment. *Field Crops Research*, **66**(1), 37–50.

Reynolds, M., Bonnett, D., Chapman, S. C., … Parry, M. A. J. (2011). Raising yield potential of wheat. I. Overview of a consortium approach and breeding strategies. *Journal of Experimental Botany*, **62**(2), 439–452.

Reynolds, M., Foulkes, J., Furbank, R., … Slafer, G. (2012). Achieving yield gains in wheat. *Plant, Cell and Environment*, **35**(10), 1799–1823.

Reynolds, M., Foulkes, M. J., Slafer, G. A., … Angus, W. J. (2009). Raising yield potential in wheat. *Journal of Experimental Botany*, **60**(7), 1899–1918.

Ribaut, J. M., William, H. M., Khairallah, M., Worland, A. J., & Hoisington, D. (2001). Genetic Basis of Physiological Traits. In M. P. Reynolds, J. I. Ortiz-Monasterio, & A. McNab, eds., *Application of Physiology in Wheat Breeding.*, Mexico D.F: CIMMYT, pp. 29–47.

Richards, R. A. (2000). Selectable traits to increase crop photosynthesis and yield of grain crops. *Journal of Experimental Botany*, **51** (1), 447–458.

Richards, R. A. (1988). A tiller inhibitor gene in wheat and its effect on plant growth. *Australian Journal of Agricultural Research*, **39**(5), 749–757.

Richards, R. A., & Condon, A. G. (1995). The use of Carbon Isotope Discrimination Analysis in Plant Improvement. In H. Skerrit J & R. Appels, eds., *New Diagnostics in Crop Sciences*, CAB International, pp. 319–332.

Richards, R. A., Rebetzke, G. J., Watt, M., Condon, A. G., Spielmeyer, W., & Dolferus, R. (2010). Breeding for improved water productivity in temperate cereals: Phenotyping, quantitative trait loci, markers and the selection environment. *Functional Plant Biology*, **37**, 85–97.

Righetti, T. L., Vasconcelos, C., Sandrock, D. R., Ortega-Farias, S., Moreno, Y., & Meza, F. J. (2007). Assessments of CO_2 assimilation on a per-leaf-area basis are related to total leaf area. *Journal of the American Society for Horticultural Science*, **132**(2), 230–238.

Rimbert, H., Darrier, B., Navarro, J., … Paux, E. (2018). High throughput SNP discovery and genotyping in hexaploid wheat. *PLoS ONE*, **13**(1), 1–19.

Robinson, H. F., Comstock, R. E., & Harvey, P. H. (1955). Genetic variances in open pollinated varieties of corn. *Genetics*, **40**, 45–60.

Rodeghiero, M., Niinemets, Ü., & Cescatti, A. (2007). Major diffusion leaks of clamp-on leaf cuvettes still unaccounted: How erroneous are the estimates of Farquhar et al. model parameters? *Plant, Cell and Environment*, **30**(8), 1006–1022.

Rosyara, U. R., De Jong, W. S., Douches, D. S., & Endelman, J. B. (2016). Software for Genome-Wide Association Studies in Autopolyploids and Its Application to Potato. *The Plant Genome*, **9**(2), 0.

Salamini, F., Özkan, H., Brandolini, A., Schäfer-Pregl, R., & Martin, W. (2002). Genetics and geography of wild cereal domestication in the near east. *Nature Reviews Genetics*, **3**(6), 429–441.

Sanchez-Bragado, R., Molero, G., Reynolds, M. P., & Araus, J. L. (2014). Relative contribution of shoot and ear photosynthesis to grain filling in wheat under good agronomical conditions assessed by differential organ $\delta^{13}C$. *Journal of Experimental Botany*, 1–13.

Sarlikioti, V., De Visser, P. H. B., Buck-Sorlin, G. H., & Marcelis, L. F. M. (2011). How plant architecture affects light absorption and photosynthesis in tomato: Towards an ideotype for plant architecture using a functional structural plant model. *Annals of Botany*, **108**(6), 1065–1073.

Schapendonk, A. H. C., Spitters, C. J., & Groot, P. (1989). Effects of water stress on photosynthesis and chlorophyll fluorescence of five potato cultivars. *European Association of Potato Research*, **32**, 17–32.

Scharen, A. L., Krupinsky, J. M., & Reid, D. A. (1983). Photosynthesis and yield of awned versus awnless isogenic lines of winter barley. *Canadian Journal of Plant Science*, **63**(2), 349–355.

Seibt, U., Rajabi, A., Griffiths, H., & Berry, J. A. (2008). Carbon isotopes and water use efficiency: Sense and sensitivity. *Oecologia*, **155**(3). 441–454.

Semagn, K., Babu, R., Hearne, S., & Olsen, M. (2014). Single nucleotide polymorphism genotyping using Kompetitive Allele Specific PCR (KASP): Overview of the technology and its application in crop improvement. *Molecular Breeding*, **33**(1), 1–

14.

Sen, S., & Churchill, G. A. (2001). A statistical framework for quantitative trait mapping. *Genetics*, **159**(1), 371–87.

Shahinnia, F., Le Roy, J., Laborde, B., … Fleury, D. (2016). Genetic association of stomatal traits and yield in wheat grown in low rainfall environments. *BMC Plant Biology*, **16**(1), 1–14.

Sharkey, T. D., Bernacchi, C. J., Farquhar, G. D., & Singsaas, E. L. (2007). Fitting photosynthetic carbon dioxide response curves for C3 leaves. *Plant, Cell and Environment*, **30**, 1035–1040.

Sharma, S. N., Sain, R. S., & Sharma, R. K. (2003). Genetics of spike length in durum wheat. *Euphytica*, **130**(2), 155–161.

Sharp, P. J., Johnston, S., Brown, G., … Jones, M. G. K. (2001). Validation of molecular markers for wheat breeding. *Australian Journal of Agricultural Research*, **52**(12), 1357.

Sharwood, R. E. (2017). Engineering chloroplasts to improve Rubisco catalysis: prospects for translating improvements into food and fiber crops. *New Phytologist*, **213**(2), 494–510.

Sharwood, R. E., Ghannoum, O., & Whitney, S. M. (2016). Prospects for improving CO_2 fixation in C3-crops through understanding C_4-Rubisco biogenesis and catalytic diversity. *Current Opinion in Plant Biology*, **31**, 135–142.

Shavrukov, Y., Kurishbayev, A., Jatayev, S., … Langridge, P. (2017). Early Flowering as a Drought Escape Mechanism in Plants: How Can It Aid Wheat Production? *Frontiers in Plant Science*, **8**(November), 1–8.

Shearman, V. J., Scott, R. K., & Foulkes, M. J. (2005). Crop Physiology and Metabolism. Physiological Processes Associated with Wheat Yield Progress in the UK. *Crop Science*, **185**(January 2005), 175–185.

Shi, S., Azam, F. I., Li, H., Chang, X., Li, B., & Jing, R. (2017). Mapping QTL for stay-green and agronomic traits in wheat under diverse water regimes. *Euphytica*, **213**(11), 1–19.

Shibles, R. M., & Weber, C. R. (1966). Interception of Solar Radiation and Dry Matter Production by Various Soybean Planting Patterns. *Crop Science*, **6**, 55–59.

Shiferaw, B., Smale, M., Braun, H. J., Duveiller, E., Reynolds, M., & Muricho, G. (2013). Crops that feed the world 10. Past successes and future challenges to the role played by wheat in global food security. *Food Security*, **5**, 291–317.

Silva, M. D. A., Jifon, J. L., Da Silva, J. A. G., & Sharma, V. (2007). Use of physiological parameters as fast tools to screen for drought tolerance in sugarcane. *Brazilian Journal of Plant Physiology*, **19**(3), 193–201.

Simmonds, J. R., Fish, L. J., Leverington-Waite, M. A., Wang, Y., Howell, P., & Snape, J. W. (2008). Mapping of a gene (*Vir*) for a non-glaucous, viridescent phenotype in bread wheat derived from *Triticum dicoccoides*, and its association with yield variation. *Euphytica*, **159**, 333–341.

Simón, M. R. (1999). Inheritance of flag-leaf angle, flag-leaf area and flag-leaf area duration in four wheat crosses. *Theoretical and Applied Genetics*, **98**(2), 310–314.

Simons, K. J., Fellers, J. P., Trick, H. N., … Faris, J. D. (2006). Molecular characterization of the major wheat domestication gene *Q*. *Genetics*, **172**(1), 547–555.

Skovmand, B., Reynolds, M. P., & Delacy, I. H. (2001). Searching Genetic Resources fo Physiological Traits with Potential for Increasing Yield. In M. P. Reynolds, J. I. Ortiz-Monasterio, & A. McNab, eds., *Application of Physiology in Wheat Breeding.*, Mexico D.F: CIMMYT, pp. 17–28.

Slafer, G. A., & Savin, R. (1994). Postanthesis green area duration in a semidwarf and a standard-height wheat cultivar as affected by sink strength. *Australian Journal of Agricultural Research*, **45**(7), 1337–1346.

Slaton, M. R., & Smith, W. K. (2002). Mesophyll Architecture and Cell Exposure to Intercellular Air Space in Alpine, Desert, and Forest Species. *International Journal of Plant Sciences*, **163**(6), 937–948.

Sood, S., Kuraparthy, V., Bai, G., & Gill, B. S. (2009). The major threshability genes soft glume (*sog*) and tenacious glume (*Tg*), of diploid and polyploid wheat, trace their origin to independent mutations at non-orthologous loci. *Theoretical and Applied Genetics*, **119**(2), 341–351.

Soriano, J. M., Villegas, D., Sorrells, M. E., & Royo, C. (2018). Durum Wheat Landraces from East and West Regions of the Mediterranean Basin Are Genetically Distinct for Yield Components and Phenology. *Frontiers in Plant Science*, **9**(February), 1–

9.

Sourdille, P., Cadalen, T., Gay, G., Gill, B., & Bernard, M. (2002). Molecular and physical mapping of genes affecting awning in wheat. *Plant Breeding*, **121**(4), 320–324.

South, A. (2011). rworldmap: A New R package for Mapping Global Data. *The R Journal*, **3**, 35–43.

Srinivasan, V., Kumar, P., & Long, S. P. (2017). Decreasing, not increasing, leaf area will raise crop yields under global atmospheric change. *Global Change Biology*, **23**(4), 1626–1635.

Steinsaltz, D., Dahl, A., & Wachter, K. W. (2018). Statistical properties of simple random-effects models for genetic heritability. *Electronic Journal of Statistics*, **12**(1), 321–358.

Stich, B., Möhring, J., Piepho, H. P., Heckenberger, M., Buckler, E. S., & Melchinger, A. E. (2008). Comparison of mixed-model approaches for association mapping. *Genetics*, **178**(3), 1745–1754.

Su, J. Y., Tong, Y. P., Liu, Q. Y., … Li, Z. S. (2006). Mapping quantitative trait loci for post-anthesis dry matter accumulation in wheat. *Journal of Integrative Plant Biology*, **48**(8), 938–944.

Summers, R. W., & Brown, J. K. M. (2013). Constraints on breeding for disease resistance in commercially competitive wheat cultivars. *Plant Pathology*, **62**(S1), 115–121.

Tambussi, E. A., Nogués, S., & Araus, J. L. (2005). Ear of durum wheat under water stress: Water relations and photosynthetic metabolism. *Planta*, **221**(3), 446–458.

Tambussi, E. A, Bort, J., Guiamet, J. J., Araus, J. L., & Nogu, S. (2007). The Photosynthetic Role of Ears in C3 Cereals: Metabolism , Water Use Efficiency and Contribution to Grain Yield. *Critical Reviews in Plant Sciences*, **26**(1), 1–16.

Tanksley, S. D. (1993). Mapping Polygenes. *Annual Review of Genetics*, **27**(1), 205–233.

Tanksley, S. D., & McCouch, S. R. (1997). Seed banks and molecular maps: unlocking genetic potential from the wild. *Science (New York, N.Y.)*, **277**(5329), 1063–1066.

Tanksley, S. D., & Nelson, J. C. (1996). Advanced backcross QTL analysis: A method for the simultaneous discovery and transfer of valuable QTLs from unadapted

germplasm into elite breeding lines. *Theoretical and Applied Genetics*, **92**(2), 191–203.

Taylor, J. (2017). Efficient linkage map construction using R / ASMap. *Statistics for the Australian Grains Industry Technical Report Series*. Retrieved from https://cran.r-project.org/web/packages/ASMap/vignettes/asmapvignette.pdf

Taylor, J., & Butler, D. (2017). R Package ASMap: Efficient Genetic Linkage Map Construction and Diagnosis. *Journal of Statistical Software; Vol 1, Issue 6 (2017)*. Retrieved from https://www.jstatsoft.org/v079/i06

Tazoe, Y., Von Caemmerer, S., Badger, M. R., & Evans, J. R. (2009). Light and CO_2 do not affect the mesophyll conductance to CO_2 diffusion in wheat leaves. *Journal of Experimental Botany*, **60**(8), 2291–2301.

Teare, I. D., Law, A. G., & Simmons, G. F. (1972a). Stomatal Frequency and Distribution on the Inflorescence of *Triticum aestivum*. *Canadian Journal of Plant Science*, **52**(1), 89–94.

Teare, I. D., & Peterson, C. J. (1971). Surface Area of Chlorophyll-containing Tissue on the Inflorescence of *Triticum aestivum* L.1. *Crop Science*, **11**(5), 627.

Teare, I. D., Sij, J. W., Waldren, R. P., & Goltz, S. M. (1972b). Comparative Data on the Rate of Photosynthesis, Respiration, and Transpiration of Different Organs in Awned and Awnless Isogenic Lines of Wheat. *Canadian Journal of Plant Science*, **52**(6), 965–971.

Terashima, I., Miyazawa, S.-I., & Hanba, Y. T. (2001). Why are Sun Leaves Thicker than Shade Leaves? — Consideration based on Analyses of CO_2 Diffusion in the Leaf. *Journal of Plant Research*, **114**(1), 93–105.

Thilakarathne, C. L., Tausz-Posch, S., Cane, K., Norton, R. M., Tausz, M., & Seneweera, S. (2013). Intraspecific variation in growth aand yield response to elevated CO_2 in wheat depends on the differences of leaf mass per unit area. *Functional Plant Biology*, **40**, 185–194.

Tholen, D., Boom, C., & Zhu, X. G. (2012). Opinion: Prospects for improving photosynthesis by altering leaf anatomy. *Plant Science*, **197**, 92–101.

Thorne, G. N. (1974). Physiology of Grain Yield of Wheat and Barley. *Rothamsted Experimental Station Report For 1973*, **2**(Part 2), 5–25.

Tilman, D., Balzer, C., Hill, J., & Befort, B. L. (2011). From the Cover: Global food demand and the sustainable intensification of agriculture. *Proceedings of the National Academy of Sciences*, **108**(50), 20260–20264.

Tomás, M., Flexas, J., Copolovici, L., … Niinemets, Ü. (2013). Importance of leaf anatomy in determining mesophyll diffusion conductance to CO_2 across species: Quantitative limitations and scaling up by models. *Journal of Experimental Botany*, **64**(8), 2269–2281.

Tomás, M., Medrano, H., Brugnoli, E., … Flexas, J. (2014). Variability of mesophyll conductance in grapevine cultivars under water stress conditions in relation to leaf anatomy and water use efficiency. *Australian Journal of Grape and Wine Research*, **20**(2), 272–280.

Turner, A., Beales, J., Faure, S., Dunford, R. P., & Laurie, D. A. (2005). Botany: The pseudo-response regulator *Ppd-H1* provides adaptation to photoperiod in barley. *Science*, **310**(5750), 1031–1034.

Uauy, C. (2017). Wheat genomics comes of age. *Current Opinion in Plant Biology*, **36**, 142–148.

van Oeveren, A. J. (1991). A comparison between single seed descent and early cross selection in wheat breeding. *Euphytica*, **58**(3), 275–287.

Vile, D., Garnier, É., Shipley, B., … Wright, I. J. (2005). Specific leaf area and dry matter content estimate thickness in laminar leaves. *Annals of Botany*, **96**(6), 1129–1136.

Visscher, P. M., Hill, W. G., & Wray, N. R. (2008). Heritability in the genomics era - Concepts and misconceptions. *Nature Reviews Genetics*, **9**(4), 255–266.

Voldeng, H. D., & Simpson, G. M. (1967). The relationship between photosynthetic area and grain yield per plant in wheat. *Canadian Journal of Plant Science*, **47**(4), 359–365.

von Caemmerer, S. (2000). Biochemical models of leaf photosynthesis. *Techniques in Plant Sciences*, **53**(9), 1689–1699.

von Caemmerer, S., & Farquhar, G. D. (1981). Some relationships between the biochemistry of photosynthesis and the gas exchange of leaves. *Planta*, **153**(4), 376–387.

Wang, S. G., Jia, S. S., Sun, D. Z., … Ma, G. (2015). Genetic basis of traits related to

stomatal conductance in wheat cultivars in response to drought stress. *Photosynthetica*, **53**(2), 299–305.

Wang, S., Jia, S., Sun, D., Fan, H., Chang, X., & Jing, R. (2016). Mapping QTLs for stomatal density and size under drought stress in wheat (*Triticum aestivum* L.). *Journal of Integrative Agriculture*, **15**(9), 1955–1967.

Wang, S., Wong, D., Forrest, K., … Akhunov, E. (2014). Characterization of polyploid wheat genomic diversity using a high-density 90 000 single nucleotide polymorphism array. *Plant Biotechnology Journal*, **12**(6), 787–796.

Warren, C. (2006). Estimating the internal conductance to CO_2 movement. *Functional Plant Biology*, **33**(5), 431–442.

Warren, C. R., & Adams, M. A. (2006). Internal conductance does not scale with photosynthetic capacity: implications for carbon isotope discrimination and the economics of water and nitrogen use in photosynthesis. *Plant, Cell & Environment*, **29**(2), 192–201.

Watkins, A. E., & Ellerton, S. (1940). Variation and genetics of the awn in *Triticum* . *Journal of Genetics*, **40**(1), 243–270.

Watson, D. J. (1958). The dependence of net assimilation rate on leaf-area index. *Annals of Botany*, **22**(85), 37–54.

Weyhrich, R. A., Carver, B. F., & Martin, B. C. (1995). Photosynthesis and water-use efficiency of awned and awnletted near-isogenic lines of hard red winter wheat. *Crop Science*, **35**(1), 172–176.

Wilkinson, P. A., Winfield, M. O., Barker, G. L. A., … Edwards, K. J. (2012). CerealsDB 2.0: an integrated resource for plant breeders and scientists. *BMC Bioinformatics*, **13**(1).

Winfield, M. O., Allen, A. M., Burridge, A. J., … Edwards, K. J. (2016). High-density SNP genotyping array for hexaploid wheat and its secondary and tertiary gene pool. *Plant Biotechnology Journal*, **14**(5), 1195–1206.

Wong, S. C., Cowan, I. R., & Farquhar, G. D. (1979). Stomatal conductance correlates with photosynthetic capacity. *Nature*, pp. 424–426.

Wu, Y., Bhat, P. R., Close, T. J., & Lonardi, S. (2008). Efficient and accurate construction of genetic linkage maps from the minimum spanning tree of a graph. *PLoS Genetics*,

4(10). doi:10.1371/journal.pgen.1000212

Xie, Q., Mayes, S., & Sparkes, D. L. (2016). Optimizing tiller production and survival for grain yield improvement in a bread wheat × spelt mapping population. *Annals of Botany*, **117**(1), 51–66.

Xie, W., & Nevo, E. (2008). Wild emmer: Genetic resources, gene mapping and potential for wheat improvement. *Euphytica*, **164**(3), 603–614.

Xu, Y. (2010). *Molecular Plant Breeding*, Illustrate, CABI. Retrieved from https://books.google.co.uk/books?id=PRGM-iHuJcMC

Yoshioka, M., Iehisa, J. C. M., Ohno, R., … Takumi, S. (2017). Three dominant awnless genes in common wheat: Fine mapping, interaction and contribution to diversity in awn shape and length. *PLoS ONE*, **12**(4), 1–21.

Yu, J., Pressoir, G., Briggs, W. H., … Buckler, E. S. (2006). A unified mixed-model method for association mapping that accounts for multiple levels of relatedness. *Nature Genetics*, **38**(2), 203–208.

Yu, M., Chen, G., Zhang, L., … Zheng, Y. (2014). QTL Mapping for Important Agronomic Traits in Synthetic Hexaploid Wheat Derived from *Aegiliops tauschii* ssp. *tauschii*. *Journal of Integrative Agriculture*, **13**(September), 1835–1844.

Yue, B., Xue, W.Y., Luo, L.J., & Xing, Y.Z. (2006). QTL Analysis for Flag Leaf Characteristics and Their Relationships with Yield and Yield Traits in Rice. *Acta Genetica Sinica*, **33**(9), 824–832.

Zadoks, J. C., Chang, T. T., & Konzak, C. F. (1974). A decimal code for the growth stages of cereals. *Weed Research*, **14**(6), 415–421.

Zhai, H., Feng, Z., Li, J., … Sun, Q. (2016). QTL Analysis of Spike Morphological Traits and Plant Height in Winter Wheat (*Triticum aestivum* L.) Using a High-Density SNP and SSR-Based Linkage Map. *Frontiers in Plant Science*, **7**(November), 1–13.

Zhang, C., JunTao, J. J., Feng, J., Cui, Z., Xu, X., & DaoJie1, S. (2018). QTL Identification for Awn Length Based on 90K Array Mapping in Wheat. *Scientia Agricultura Sinica*, **51**(1), 17–25.

Zhang, H., Turner, N. C., & Poole, M. L. (2010). Source-sink balance and manipulating sink-source relations of wheat indicate that the yield potential of wheat is sink-limited in high-rainfall zones. *Crop and Pasture Science*, **61**(10), 852–861.

Zhou, B., Sanz-Sáez, Á., Elazab, A., … Araus, J. L. (2014). Physiological traits contributed to the recent increase in yield potential of winter wheat from Henan Province, China. *Journal of Integrative Plant Biology*, **56**(5), 492–504.

Zhou, B., Serret, M. D., Elazab, A., … Sanz-Saez, A. (2016). Wheat ear carbon assimilation and nitrogen remobilization contribute significantly to grain yield. *Journal of Integrative Plant Biology*, **58**(11), 914–926.

Zikhali, M., Leverington-Waite, M., Fish, L., … Griffiths, S. (2014). Validation of a 1DL earliness *per se* (*eps*) flowering QTL in bread wheat (*Triticum aestivum*). *Molecular Breeding*, **34**(3), 1023–1033.

Zohary, D., & Hopf, M. (2000). *Domestication of Plants in the Old World: The Origin and Spread of Cultivated Plants in West Asia, Europe, and the Nile Valley*, Oxford: Oxford University Press.

6 APPENDICES

APPENDIX 1: CONTROL AND METHODOLOGY VALIDATION (CHAPTER 1 - IDENTIFYING DESIRABLE FLAG LEAF PHOTOSYNTHETIC TRAITS IN PROGENITOR SPECIES.

The 2016 field trial (field vs. laboratory measurement analysis).

On the 6th of July, during the 2016 field trial (Chapter 1), a comparison was completed to test for variation between measurements made in the field and those made in the laboratory after cutting the tillers. Five Paragon plants from the buffer rows were selected at the start of anthesis (around GS61). Measurements were completed using a LI-COR-6400XT with a Leaf Chamber Fluorometer (LCF), chamber conditions were: leaf fan set to fast, gas flow rate set to 300 µmol s^{-1}, block temperature was controlled at 25 ºC, a photosynthetic photon flux density (PPFD) of 1500 µmol m^{-2} s^{-1} and a CO_2 reference of 400 µmol mol^{-1} was set. Relative humidity was controlled at 60 ± 5%. On flag leaves of each plant, measurements were taken in the field, then the same leaves were individually measured back in the laboratory using the tiller cutting technique and the same LI-COR conditions. Before each measurement was taken, plants were left to acclimatise until *A* and g_s had stabilised. It should be noted that the plants took longer to acclimatise in the laboratory than the field. Measurements were completed between 10:00 and 15:00. A paired t-test was used in RStudio to identify potential significant differences. No significant difference was observed between *A* in the field and the laboratory (field: mean = 23.9 µmol CO_2 m^{-2} s^{-1} and *S.D* = 3.0, laboratory: 22.4 and *S.D* = 0.88); t (4) = 1.23, P = 0.29. Furthermore, no significant difference was observed between g_s in the field and the laboratory (Field: mean = 0.26 mol H_2O m^{-2} s^{-1}, *S.D* = 0.05 and Laboratory: 0.25, *S.D* = 0.03); t (4) = 0.57, P = 0.60.

Light Curves 2016 field trial.

Light curves of flag leaves from Robigus (GS53) and Paragon (GS61) were completed using the same LI-COR setup as Chapter 1, to determine a near-saturating PPFD to complete A/C_i curves at and insure light intensity was not a limiting factor during the measurements:

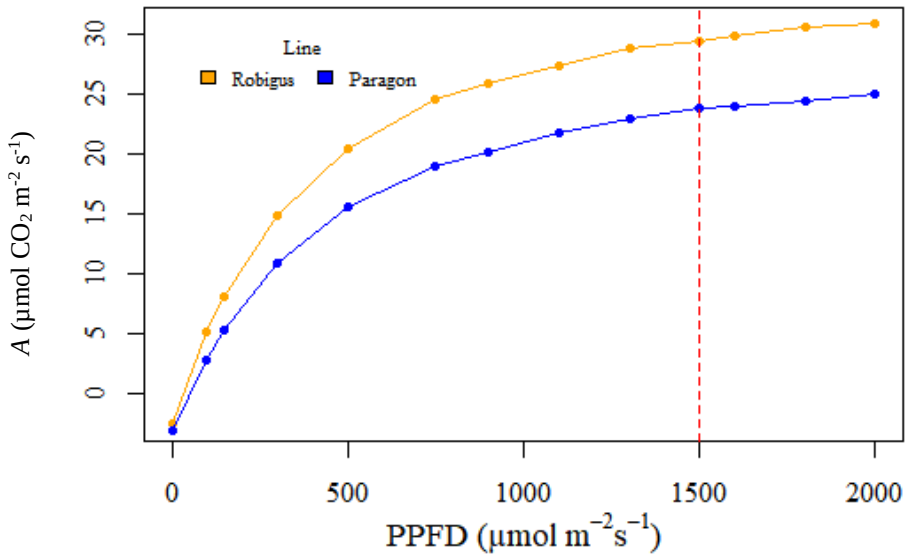

Figure 6-1 - Light response curves from the 2016 field trial of Chapter 1, where *A* was plotted against a range of light intensities. The plot was used to determine a near-saturating PPFD intensity to complete *A/Ci* curves at. Flag leaves of bread wheat lines Robigus (GS53) and Paragon (GS61) were used.

APPENDIX 2: CONTROL AND METHODOLOGY VALIDATION (CHAPTER 2 - THE PHOTOSYNTHETIC CONTRIBUTION OF AWNS).

NILs field trial (Chamber acclimatisation).

Acclimatisation logs were made on the 22nd of May 2017 on the main tillers of a pair of SHW NILs (Pair 1) at GS59. Logs were recorded every 10 seconds after the organ had been placed in the LI-COR CC, until *A* and g_s had stabilised. From these plots it was clear that 3 minutes would be a suitable acclimatisation time for each measurement.

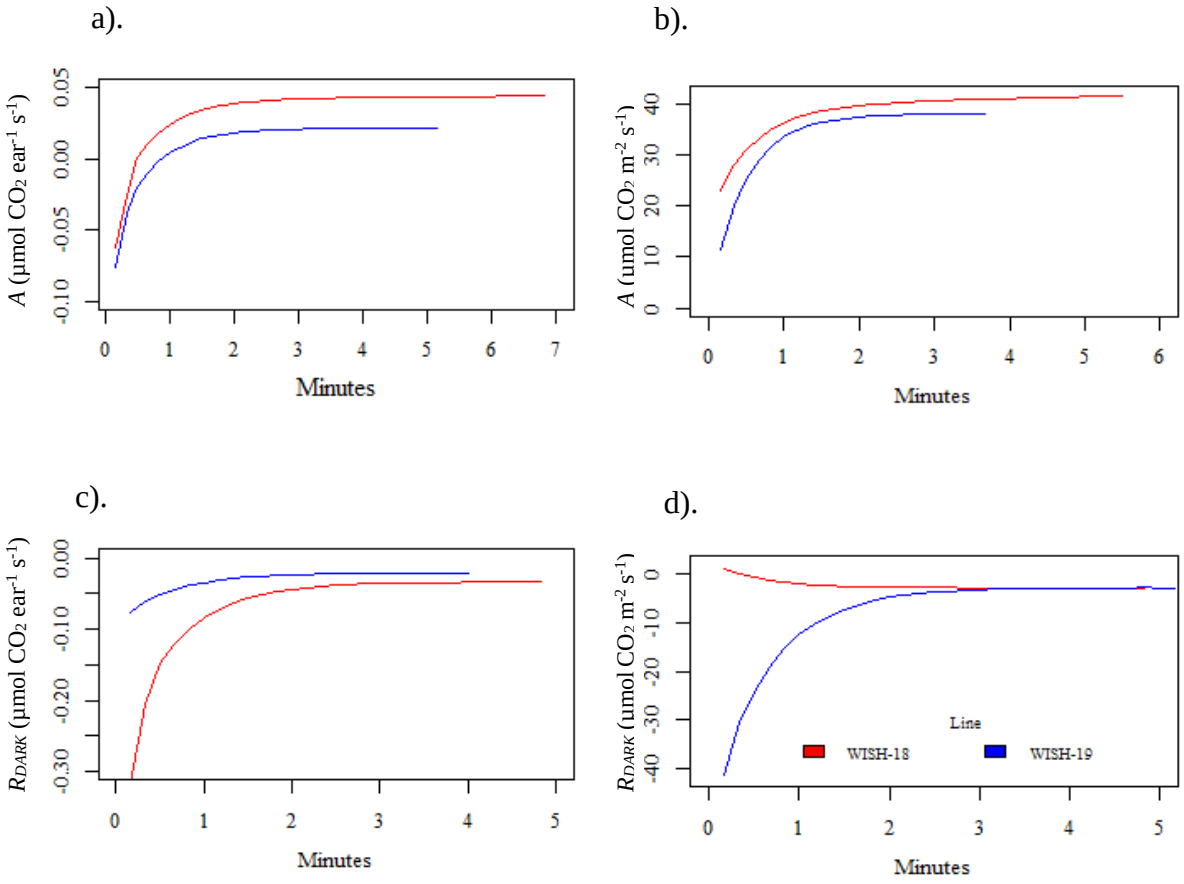

Figure 6-2 - Acclimatisation logs of WISH-18 and 19 (Pair 1) showing organ photosynthesis and respiration chamber responses. Logs were taken during the NILs field trial using a LI-COR CC. Logs were recorded every 10 seconds from when the organ was enclosed in chamber, until *A* and g_s had fully stabilised. Using these plots, 3 minutes was selected as a suitable acclimatisation time.

APPENDIX 3: CONTROL AND METHODOLOGY VALIDATION (CHAPTER 3 - IDEOTYPE FORMATION AND QTL MAPPING.

FL_A estimation

The accuracy of the FL_A estimation method was compared to the more time consuming method of measuring FL_A through image analysis using *ImageJ* (V - 1.51) and showed strong positive correlation; linear regression was used to identify a significant model (F (1, 4) = 133.3, P = < 0.001) with an adjusted R^2 of = 0.96.

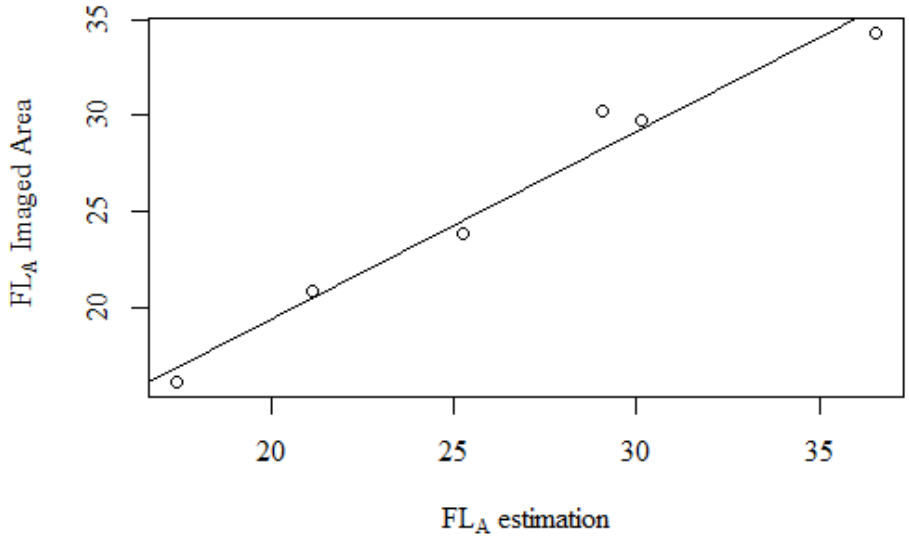

Figure 6-3 - Two methods for estimating Flag Leaf Area (FL_A). 'FL_A estimation' was calculated using the Teare & Peterson (1971) equation and 'FL_A Imaged Area' was calculated from the same leaves using image analysis in ImageJ. The six flag leaves were taken from glasshouse grown dic12b lines at anthesis.

Grain yield proxy.

A validation test for using 3 ears to estimate overall grain yield per plant (*YP*) is shown Figure 6-4, where the remaining ears from 10 *PS1* individuals were threshed and weighed. Linear regression was used to test the relationship between the estimated *YP* and the actual measured *YP*, a significant model was found (F (1, 8) = 60.0, P = < 0.001), with an adjusted R^2 of 0.85: indicating the estimation method was a suitable proxy.

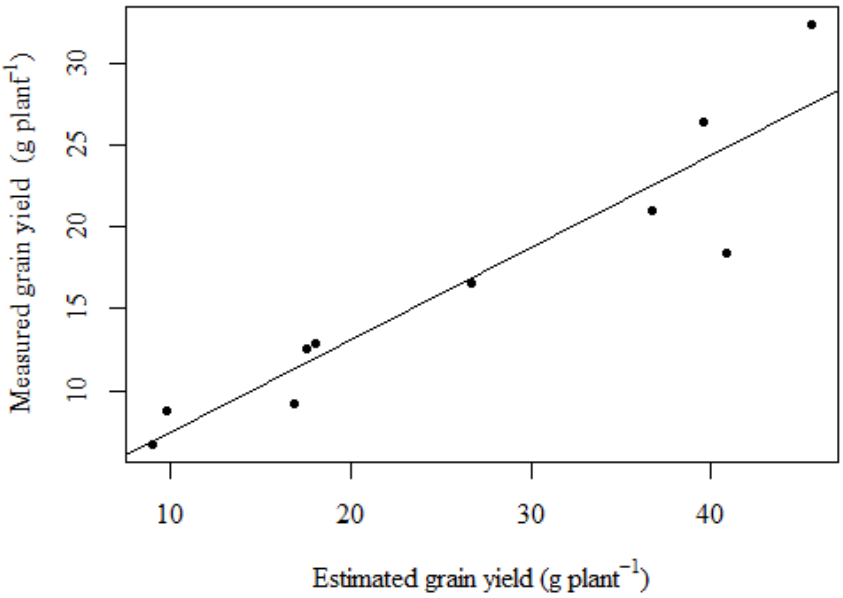

Figure 6-4 – A comparison using 10 *PS1* individuals to show if estimating grain yield of plants in the 2017 *PS1* field trial is a valid proxy for actual grain yield. 'Estimated grain yield' was determined by threshing only three ears to calculate an average seed number per ear and then multiplying this by ear number. For 'measured grain yield', all ears were threshed for each plant and a total seed weight was taken.

APPENDIX 4: ADDITIONAL MATERIAL.

Growth stage guide.

Table 6-1 - The 'Zadoks decimal code' for growth stages used in this study. Adapted from Zadoks et al. (1974). The 2-digit code corresponds to the growth stages referenced in this study (e.g. GS61).

2-digit code	General description		Feekes' scale	Additional remarks on wheat, barley, rye, and oats
	Inflorescence emergence			
50	First spikelet of inflorescence just visible	N	10·1	N = non-synchronous crops; S = synchronous crops — see text
51		S		
52	¼ of inflorescence emerged	N	10·2	
53		S		
54	½ of inflorescence emerged	N	10·3	
55		S		
56	¾ of inflorescence emerged	N	10·4	
57		S		
58	Emergence of inflorescence completed	N	10·5	
59		S		
	Anthesis			
60	Beginning of anthesis	N	10·51	Not easily detectable in barley. In rice: usually immediately following heading
61		S		
62	—			
63	—			
64	Anthesis half-way	N		
65		S		
66	—			
67	—			
68	Anthesis complete	N		
69		S		
	Milk development			
70	—			
71	Caryopsis water ripe		10·54	
72	—			
73	Early milk			
74	—			
75	Medium milk		11·1	Increase in solids of liquid endosperm notable when crushing the caryopsis between fingers
76	—			
77	Late milk			
78	—			
79	—			

Table 6-2 - Flowering time (F_T), flag leaf longevity (FL_{LONG}), awn length (A_L) and calculated ear area (E_{CA}) from the 2017 field trial of Chapter 1. The collection includes the tetraploid parents, hexaploid parents and the offspring individuals. Measured using the same methodology as described in Chapter 3 for each trait.

Line Name	F_T		FL_{LONG}		A_L		E_{CA}	
	Mean	S.D	Mean	S.D	Mean	S.D	Mean	S.D
31_07K	69.3	0.5	34.3	3.9	4.6	1.0	48.6	4.2
31_07L	65.5	2.6	41.0	3.6	1.2	0.4	61.0	6.3
31_12K	69.0	0.8	37.5	1.0	1.6	0.3	75.5	6.2
32_16E	65.0	0.0	37.5	1.0	7.2	0.3	47.1	2.4
32_21C	63.8	1.5	35.8	2.6	0.6	0.1	49.9	4.8
32_23D	65.5	1.7	34.5	2.1	8.6	0.9	39.5	4.5
32_23E	68.3	1.5	32.8	3.0	1.4	0.6	45.9	3.2
32_23G	66.3	1.3	19.0	1.4	5.1	1.3	46.1	7.0
32_23I	65.0	0.8	36.3	2.2	8.3	0.3	43.3	2.5
dic12b	68.8	0.5	26.3	1.7	9.1	0.4	27.3	2.8
dic71	63.8	1.0	22.3	2.6	15.1	0.9	23.7	6.1
dic72	64.3	0.5	22.0	2.9	14.1	2.0	25.8	2.6
Paragon	69.0	0.0	38.8	1.0	0.8	0.3	65.6	3.7
Robigus	70.3	1.5	40.3	2.2	1.0	0.1	55.8	3.0
Tios	77.0	0.0	27.8	2.1	5.4	0.5	60.6	3.8

Trait units: F_T = Days from sowing to flowering; FL_{LONG} = Days from flowering to 80% senescence; A_L = cm; E_{CA} = cm^2.

APPENDIX 5: TRIAL WEATHER CONDITIONS.

Table 6-3 – Weather conditions for the 2016 field trial period. Data were taken from the NIAB, Cambridge Met Office weather station (https://www.metoffice.gov.uk). The average values shown reflect the maximum and minimum temperature and daily precipitation over the entire trial period.

Date	24 hour max temperature (°C)	24 hour min temperature. (°C)	Daily precipitation (mm)
05/06/2016	20.1	9.9	0
06/06/2016	24	6.9	0
07/06/2016	24.8	9.1	0
08/06/2016	22.3	14.8	0
09/06/2016	22	10.1	0
10/06/2016	23	10.8	0
11/06/2016	21.3	12.6	0
12/06/2016	19.2	14.7	NA
13/06/2016	17.9	14.3	NA
14/06/2016	19.6	12.9	NA
15/06/2016	21.2	10.3	NA
16/06/2016	18.4	10.7	NA
17/06/2016	17.6	12.3	NA
18/06/2016	16.6	11.4	NA
19/06/2016	20.6	10.7	NA
20/06/2016	21.6	15	NA
21/06/2016	20.9	12.9	0
22/06/2016	21.7	13.2	2.8
23/06/2016	23.1	15.5	13.6
24/06/2016	21.5	12.7	6.2
25/06/2016	19.6	9.5	0.6
26/06/2016	20.6	11.1	1
27/06/2016	19.8	13.5	0
28/06/2016	20.2	7.8	3
29/06/2016	17.8	10.2	2
30/06/2016	21.4	10.7	0.8
01/07/2016	19.6	14.6	0
02/07/2016	19.1	9.3	1
03/07/2016	21	9.7	0
04/07/2016	22.4	7.9	0
05/07/2016	20.6	14.2	0
06/07/2016	20.5	7.9	0
07/07/2016	21.6	12.7	0.2
08/07/2016	23.7	14.4	0
09/07/2016	23.4	14.2	0
10/07/2016	22.7	16.8	0.2
11/07/2016	22.2	14.4	0
Average	**20.91**	**11.88**	**1.12**

Table 6-4 - Weather conditions for the 2017 field trial period. Data were taken from the NIAB, Cambridge Met Office weather station (https://www.metoffice.gov.uk). The average values shown reflect the maximum and minimum temperature and daily precipitation over the 5 days of May shown and the whole of June and July.

Date	24 hour Max temperature (°C)	24 hour Min temperature. (°C)	Daily participation (mm)
27/05/2017	26.1	12.2	0.2
28/05/2017	22.7	10.9	5.6
29/05/2017	19.9	14.2	1.6
30/05/2017	20.1	14.6	0
31/05/2017	21.9	12.7	0
Average (May)	**22.14**	**12.92**	**1.48**
01/06/2017	24.3	13.3	0
02/06/2017	23	11.6	7
03/06/2017	19.6	13.7	0
04/06/2017	18.5	9.1	0
05/06/2017	18.8	10.6	3.2
06/06/2017	14.9	10.3	14.2
07/06/2017	18.1	10.1	1.2
08/06/2017	18.1	11.7	0.2
09/06/2017	20.5	11.3	0.2
10/06/2017	24.3	12.3	0
11/06/2017	22.5	16.4	0
12/06/2017	18.8	10.8	0
13/06/2017	21.7	10.2	0
14/06/2017	24.8	12.3	0
15/06/2017	22.7	12.1	0
16/06/2017	22.3	11.5	0
17/06/2017	28	15.2	0
18/06/2017	30.1	14.4	0
19/06/2017	30.8	16.5	0
20/06/2017	29	16	0
21/06/2017	30.1	13.2	0
22/06/2017	21.4	17.6	0
23/06/2017	20.7	12	0
24/06/2017	24	16.9	0
25/06/2017	21.2	13.8	0
26/06/2017	20.6	7.8	0
27/06/2017	17.5	13.7	NA
28/06/2017	14.4	13.4	NA
29/06/2017	17.2	11.1	0
30/06/2017	19.4	9.2	0.2
Average (June)	**21.91**	**12.60333333**	**0.935714286**

Table continued on next page.

01/07/2017	21.3	13.5	0
02/07/2017	21.4	13.5	0
03/07/2017	23.40	11.70	0.00
04/07/2017	22.9	11.8	0
05/07/2017	25.7	11.6	0
06/07/2017	26.4	14.5	11.6
07/07/2017	25.6	15.9	0
08/07/2017	23.4	15.9	0
09/07/2017	25.9	14.5	0
10/07/2017	23.2	15.8	0.4
11/07/2017	19.5	13.1	14.2
12/07/2017	19.1	13.4	0
13/07/2017	21.3	8.4	0
14/07/2017	19	13.8	0
15/07/2017	21.9	12.1	0.2
16/07/2017	22.9	15.9	2.4
17/07/2017	24.8	9.3	0
18/07/2017	25.6	13.9	10.8
19/07/2017	23.8	16	5.4
20/07/2017	19.8	15.6	0
21/07/2017	22.7	10.7	3.2
22/07/2017	20.2	13.3	4.4
23/07/2017	18.9	11.8	14.4
24/07/2017	15.4	12.7	2.2
25/07/2017	21.4	13.1	0
26/07/2017	22.6	13.7	1
27/07/2017	21.1	12.2	2.2
28/07/2017	21.5	13	1.4
29/07/2017	20.5	13.8	20
30/07/2017	21.4	13.2	1
31/07/2017	22.5	11.6	0
Average (July)	**22.1**	**13.20322581**	**3.058064516**

APPENDIX 6: PROJECT CONTRIBUTORS.

1. With guidance from Dr. Fiona Leigh, I selected the lines included in Chapter 1 based on: glasshouse work conducted by Angie White and Fiona Leigh (unpublished), preliminary analysis that I had completed at the start of the project and the availability of diverse material in ongoing research projects at NIAB.

2. The majority of the crossing and parent selection to form the *PS1* population was conducted by Dr. Fiona Leigh. However, I assisted with some of the pollinations and sowed the seed for the plants. After the initial crosses, I was responsible for advancing the population. Sophie Bates and Maxime Kadner assisted with some of the generation advancement sample processing.

3. Dr. Phil Howell created, selected and provided the WISH SHW material. Dr. Phil Howell and Dr. Fiona Leigh provided the genotype data for Chapter 2. I selected the lines included in the ploidy field trial (dic71, dic72, Paragon and Robigus), based on observations in Chapter 1.

4. Maxime Kadner assisted with the 2017 field trial phenotyping and sample processing (Chapter 1 and 3).

5. Emma Deeks assisted with some of the threshing and microscope slide analysis of Chapter 1 and 3.

6. The KWS (Thriplow, UK) Research and Development team grew and mechanically harvested the field material in Chapter 2.

7. The yield in Chapter 2 (excluding the 2017 NILs field trial) was provided by the WISH project. The WISH project was supported by the BBSRC Follow-On Fund, (BB/K020269/1) and the plant breeders KWS UK Ltd, Limagrain UK Ltd and RAGT Seeds Ltd.

8. Material studied in this program was developed in the BBSRC funded projects WISP (Wheat Improvement Strategic Program), DFW (Designing Future Wheat) and WISH (Wheat Improvement from Synthetic Hexaploids).